UNIVERSITY OF SOUTHAMPTON

FACULTY OF ENGINEERING AND THE ENVIRONMENT

Aerodynamics and Flight Mechanics Group

Experimental Evaluation of Hydrogen Peroxide Catalysts for Monopropellant Attitude Control Thrusters

by

Matthew James Palmer

Thesis for the degree of Doctor of Philosophy

September 2014

UNIVERSITY OF SOUTHAMPTON

ABSTRACT

FACULTY OF ENGINEERING AND THE ENVIRONMENT

Aerodynamics and Flight Mechanics Group

Doctor of Philosophy

Experimental Evaluation of Hydrogen Peroxide Catalysts for Monopropellant Attitude Control Thrusters

by Matthew James Palmer

Currently the space community relies on propellants such as hydrazine and its derivatives in propulsion systems aboard satellites and spacecraft. However their highly toxic and carcinogenic nature results in significant costs in handling, storage and transport compared to less toxic propellants. It is due to this benefit that there is a renewed interest in 'green' or less toxic propellants. One such green propellant is hydrogen peroxide. This liquid propellant must be catalytically decomposed into steam and oxygen within the thruster.

The current PhD is charged with advancing the state of hydrogen peroxide heterogeneous catalysts and associated thruster hardware. To this end a range of assessment techniques have been employed to develop solid catalysts based on metallic gauze, metallic foam and ceramic pellets. In all cases these catalysts must be suitable for the decomposition of up to 99% hydrogen peroxide concentration by mass. This work assesses these catalysts under both laboratory and fully representative conditions using 87.5% hydrogen peroxide concentration by mass.

This thesis contains a detailed literature review into heterogeneous catalysts and catalyst supports. This has resulted in the procurement and manufacture of thirty-eight candidate catalysts from all three support types. A selection of these catalysts have undergone physical assessment using a range of surface characterisation techniques in an attempt to understand their performance.

The results of a review into experimental hardware have led to the development of two laboratory-based apparatus designed to measure initial performance and catalyst longevity. The results have been described and used to down-select from thirty-eight candidate catalysts to a final selection of four.

Additional testing of these four catalysts has been conducted within a highly instrumented catalyst bed to provide performance data under fully representative conditions. With their performance verified an engineering bread-board (EBB) thruster has been developed to investigate the effect of various changes to thruster hardware such as injector and catalyst bed geometry, pre-heating methodology and effect of anti-channelling baffles.

Table of Contents

List of Figures

List of Tables

Academic Thesis: Declaration of Authorship

I, Matthew Palmer declare that this thesis entitled *Experimental Evaluation of Hydrogen Peroxide Catalysts for Monopropellant Attitude Control Thrusters* and the work presented in it are my own and have been generated by me as the result of my own original research.

I confirm that:

1. This work was done wholly or mainly while in candidature for a research degree at this University;

2. Where any part of this thesis has previously been submitted for a degree or any other qualification at this University or any other institution, this has been clearly stated;

3. Where I have consulted the published work of others, this is always clearly attributed;

4. Where I have quoted from the work of others, the source is always given. With the exception of such quotations, this thesis is entirely my own work;

5. I have acknowledged all main sources of help;

6. Where the thesis is based on work done by myself jointly with others, I have made clear exactly what was done by others and what I have contributed myself;

7. Parts of this work have been published as given in the List of Publications

Signed: ……

Date:……

List of Publications

Palmer, M.J., Musker, A.J., Roberts G.T., Ponce-de-Leon, C., *"A Method of Ranking Candidate Catalysts for the Decomposition of Hydrogen Peroxide"* Space Propulsion 2010, San Sebastian, May 2010

Palmer, M.J., Musker, A.J., Roberts G.T., Ponce-de-Leon, C., *"Manufacture, Assessment and Down-Selection of Catalysts for the Decomposition of Hydrogen Peroxide"* 4th European Conference for Aerospace Sciences, Saint Petersburg, 2011

Palmer, M., Musker, A., Roberts, G. *"Experimental Assessment of Heterogeneous Catalysts for the Decomposition of Hydrogen Peroxide"* 47th AIAA Joint Propulsion Conference, San Diego, July 2011, AIAA 2011-5695

Palmer, M.J., Roberts G.T., Musker, A.J., *"Design, Build and Test of a 20N Hydrogen Peroxide Monopropellant Thruster"* 47th AIAA Joint Propulsion Conference, San Diego, July 2011, AIAA 2011-5695

Acknowledgments

I would like to take this opportunity to thank all those individuals who have helped and supported me in my work over the last few years.

Firstly, I would like to thank my supervisors from the University of Southampton, Dr. Graham Roberts and Dr. Carlos Ponce de León Albarrán. Without their continued support and guidance, especially from Graham, I would not have been able to see this project through to completion. A special thanks also goes to Professor Antony Musker. His valued expertise and contributions have been indispensible and without which much of this work could not have been undertaken. A special mention also goes to Anne Musker, who provided valuable sustenance during many a cold days testing.

Secondly, thanks go to my colleagues and friends from the 'Aerodynamics and Flight Mechanics group', especially to Robert-Jan Koopmans for all your helpful advice and suggestions, which have proved invaluable, and for your good humour. I would also like to thank Agi Kourmatzis, Andy Ju, Sina Heari, Kangping Zhang, Man Zhang and Yu Zhao, with whom I shared an office for many years. All of their support, good humour and distractions were most welcome. On a personal note, a special thanks also goes to my friends, too numerous to mention, who have on many occasion saved me from insanity. They have been there for me during difficult times and can always be relied upon to act as drinking buddies, confidants and generally lighten the mood.

Thanks also goes to all those who have provided employment when times were getting a little tight. I have learnt invaluable lessons from them all and wish all my co-workers every success. Special mention should also be made to my current employers, SSTL, who have been very supportive and understanding throughout my write-up. Their assistance during this time is much appreciated.

Finally, I would like to thank my parents and family for their enduring support and encouragement. Without them I fear I may not have had the motivation to continue with the project and see it through to completion. My parents have helped me get to where I am today and for that I will always be eternally grateful. Last but not least, an enormous thank you to my better half, Gaynor, for her love, patience, and support throughout the years. I have no doubt that I have put her through hell on so many occasions but she never gave up on me. Her constant encouragement, although sometime frustrating, in retrospect is greatly appreciated.

Many thanks to you all.

Nomenclature

Symbols

A	Area	[m^2]
A_P	Pre-exponential factor	
c	effective exit velocity	[m/s]
C^*	Characteristic velocity	[m/s]
C_d	Coefficient of discharge	
C_F	Coefficient of thrust	
d	Diameter	[m]
E_A	Activation Energy	[kJ/mol]
F	Thrust	[N]
f	Frequency	[Hz]
g_0	Acceleration due to gravity (9.81 m/s^2)	[m/s^2]
γ	Ratio of specific heats of exhaust gas	
I_{sp}	Specific Impulse	[s]
k	Rate constant	
k'	Specific rate constant	
M	Mach number	
M	Average molecular mass of the gas	[g/mol]
m	Mass	[kg]
$\dot{m}$	Mass flow rate of propellants	[kg/s]
No	Number of moles	
P	Pressure	[Pa]
Q	Volume flow rate	[l/min]
ρ	Density	[kg/m^3]
R	Universal gas constant	[J/mol*K]
R	Specific gas constant	[J/kg*K]
R_{PC}	Chamber pressure roughness	[%]
T	Temperature	[K]
t	Time	[s]
t_{90}	Time to 90% steady-state temperature	[s]
t_{90P}	Time to 90% steady-state pressure	[s]
V	Nozzle exit velocity	[m/s]
V	Volume	[m^3]
η	Efficiency	[%]
ρ	Density	[kg/m^3]

Abbreviations

AFM	Atomic force microscope	
AIT	Auto-ignition temperature	
BEI	Backscattering electron image	
BET	Brunauer Emmett Teller surface area analysis	
Conc	Concentration	
CBL	Catalyst bed loading	[kg/s/m^2]
CSA	Cross sectional area	
DAQ	Data Acquisition	
DC	DELTACAT Ltd.	
DM	Demonstration model	
DOT	Department of Transport	
EBB	Engineering breadboard	
EDX	Energy dispersive X-ray	
ESA	European Space Agency	
EU	European Union	
FCV	Flow Control Valve	
F/O	Fuel to oxidiser ratio	
GRASP	GReen Advanced Space Propulsion	
hICB	highly Instrumented Catalyst Bed	
HTP	High test peroxide	
IARC	International Agency for Research on Cancer	
LC_{50}	Lethal concentration for 50% of the population	[mg/m^3]
LD_{50}	Lethal dose for 50% of the population	[mg/kg]
L/D	Length to diameter ratio	
LTML	Lifetime Mass Loss apparatus	
MMH	Mono-methyl hydrazine	
MnO_x	Oxides of manganese (unknown phases)	
MON	Mixed oxides of nitrogen	
MIB	Minimum impulse bit	
NASA	National Aeronautics and Space Administration	
NI	National Instruments	
NTO	Nitrogen tetroxide	
O/F	Oxidiser to fuel ratio	
OSHA	US Occupational Safety and Health Administration	
pICB	preliminary Instrumented Catalyst Bed	
PEL	Peak Exposure Limit	[ppm]
ppi	Pores per inch	
RATO	Rocket assisted take-off	
RCS	Reaction control system	

REACH	Regulation, Evaluation, Authorization and Restriction of Chemicals
R-Phrases	Risk phrases
S_{BET}	Surface area calculated using the BET technique
SCAPE	Self Contained Atmospheric Protective Ensemble
SG	Specific Gravity
SEM	Scanning electron microscope
SR	Sealed Reactor apparatus
STDV	Standard deviation
S.T.P	Standard temperature and pressure
TRL	Technology Readiness Level
TWA	Time weighted average
UDMH	Un-symmetrical di-methyl hydrazine
UK	United Kingdom
UN	United Nations
UoS	University of Southampton
USA	United States of America
USAF	United States Air Force
WSA	Wetted surface area
XPS	X-ray photoelectron spectroscopy
XRD	X-ray diffraction

Subscripts

amb	Ambient
c	Combustion/decomposition chamber
cat	Catalyst
CC	Calcined control
CI	Impregnated control
e	Exit
HTP	High test peroxide
i	Injector
ideal	Theoretical ideal
Min	Minimum
Max	Maximum
n	Nozzle
PRESS	Pressure
prop	Propellant
SC	Calcined sample
SI	Impregnated sample
sol	Solution
t	Throat

tank	Propellant tank
TEMP	Temperature
TH	Thermal
TOT	Total

Miscellaneous

wt%	Percentage with respect to weight
At%	Percentage with respect to atomic content
Δ	Delta, change in

Appendix A - Symbols

D_d	Overall gauze disc diameter	[cm]
a_d	Overall gauze disc area	[cm]
V_d	Overall gauze disc volume	[cm]
ρ_m	Metal density	[g/cm^3]
δs	Gauze section	
l_s	Length of gauze section	[cm]
w_s	Width of gauze section	[cm]
d_s	Depth of section	[cm]
δV_s	Total volume of section	[cm^3]
Hs	Hole Size	[cm]
D_w	Wire diameter	[cm]
C_w	Wire circumference	[cm]
CS_w	Wire cross sectional area	[cm^2]
δA_w	Surface area of wire in section	[cm^2]
A_d	Total surface area of wire in gauze disc	[cm^2]
δV_w	Volume of wire in section	[cm^3]
V_s	Total volume of wire in gauze disc	[cm^3]
v_w	Volume of wire per cm^3 of packed gauze	
a_w	Surface area of wire per cm^3 of packed gauze	[cm^{-1}]
ρ_g	Gauze density	[g/cm^3]
a_g	Surface area per gram of gauze	[cm^2/g]
δV_f	Free (open area) volume in section	[cm^3]
V_o	Total free volume in gauze disc	[cm^3]
v_f	Free volume of wire per cm^3 of packed gauze	
v_o	Free volume per gram of gauze	[cm^3/g]
$v_f : v_w$	Ratio of free volume to wire volume per cm^3 of packed gauze	

Preface

I have always had a passion for understanding how things work, so it felt like a natural progression to pursue a career in engineering. After studying aerospace engineering at the University of Southampton for four years, I was given the opportunity to work within the field of space propulsion. I have come to the personal realisation that if an object does not produce fire, smoke or noise then it just doesn't excite me! Over the duration of my PhD my belief in hydrogen peroxide as a viable rocket propellant has grown considerably. I am now able to take with me these valuable lessons learnt, and use them to enrich my future career, with the aim of pursuing hydrogen peroxide for rocket applications. Although I still have much to learn, working towards achieving my PhD has been a great first step on the ladder, and one for which I will be forever grateful. This experience certainly has ignited my passion for propulsion.

Matthew James Palmer

Southampton, September 2014

1 Introduction

Liquid propellants are widely used in both bi-propellant and mono-propellant rocket thrusters. Their application is widespread from primary propulsion, such as Earth ascent vehicles, to secondary propulsion used for spacecraft orbit insertion and attitude control. Hydrogen peroxide is one such liquid propellant. The report will focus solely on secondary propulsion since it is here that hydrogen peroxide will most likely provide a viable alternative to current technology.

The industrial manufacture of hydrogen peroxide can be traced back to the work done by L. J. Thenard in 1818. Thenard produced low concentrations of aqueous hydrogen peroxide by reacting barium peroxide with nitric acid [1]. A succession of improvements in the manufacturing technique eventually led to large scale production of 100% concentration with respect to weight (wt%) hydrogen peroxide. High concentration hydrogen peroxide above approximately 80% is more commonly known as high test peroxide or HTP. It would be more than 100 years after its initial discovery before its potential as a propellant was recognised.

Helmuth Walter was the first to develop hydrogen peroxide into a propellant. He started a company, Walterwerke, in 1934 which designed and produced engines using high concentration HTP. His initial work focused on submarine propulsion but his major success came with the rocket engines he designed for powering the Messerschmitt Me 163 type aircraft. The first of these; the ‘cold’ R11, 203 B engine was designed for the Me 163A in 1941 [2]. This monopropelant engine relied on the decomposition of 80 wt% HTP by manganese salts to provide thrust. On 2 October 1941 the Me 163A achieved a speed of over 1000 kph, a speed elusive to jet fighters even in the immediate post war world record flights [3]. With this success Walter continued on to develop the ‘hot’ engine used to power the Messerschmitt ME 163B. This used an 80%HTP oxidiser in combination with a hydrazine hydrate and methanol hypergolic fuel (C-stoff) [2]. Helmuth Walter also developed the power plant for the V1 catapult and the V2 turbo-pump gas generator which used 80% hydrogen peroxide catalysed by a potassium permanganate solution.

In the immediate aftermath of the war the German stockpile of 80% peroxide was shipped to the UK and USA. In the UK work began on using hydrogen peroxide in rocket assisted take-off (RATO) systems. This culminated in the development of the Sprite (monopropellant) and the Super Sprite (HTP/kerosene bi-propellant) rockets [4]. The initial design of the Sprite relied on similar liquid catalysts that had proven so successful for the Germans. However, it was soon realised that liquid catalysis had several drawbacks. They served to increase the complexity and mass of the design requiring the need for additional storage tanks and feed lines. They also reduced performance; the catalyst lowered the peak temperature within the reaction chamber

and was then ejected out the nozzle which served to lower the specific impulse. In further refinements to the Sprite rocket design a solid catalyst comprising silver plated nickel gauze was used, this was first demonstrated in April 1952 aboard the Sprite 2 (DSpr.2) [1].

These programs were eventually discontinued but the lessons learned were not completely lost. With the onset of the cold war the British government wanted a rocket that could be used to deliver missiles anywhere in the world. To facilitate this they needed to test various components including the re-entry nose that would protect the payload. In 1955 the development of the Black Knight rocket began with Armstrong Siddeley beginning work on designing the Gamma 201 engine; a 85wt% hydrogen peroxide/kerosene bi-propellant thruster. The Black Knight used four Gamma 201 engines each producing ~17.8kN of thrust. The propellant was supplied by individual turbo pumps and each engine was independently swivelled to provide flight control. These were later updated to Gamma 301 engines which provided a total of just over 96 kN of thrust. The hydrogen peroxide was decomposed using silver deposited on nickel screens [5]. These were pre-treated with a solution of Samarium Nitrate to improve performance [6]. The precise mechanism by which the improvement was achieved is still the subject of much debate and will be discussed later in this project. The decomposition gases were then combined with kerosene at a fuel/oxidiser ratio of 1:8.2; these gases were hot enough to cause the auto-ignition of kerosene [7]. The Gamma engine technology probably remains the highest performing hydrogen peroxide engines ever put into production [8]. Out of twenty-two launches only seven would not have delivered a satellite into orbit; this is considered a good record for one of the world's first modern bi-propellant liquid rockets [9]. The project was eventually cancelled in favour of the Black Arrow rocket. This was a three stage rocket designed to deliver a satellite into low Earth orbit. Four completed launches were made with the last of these delivering a 66kg [10] satellite called Prospero to Low Earth Orbit. The first stage was powered by the Gamma 8 engine developing 222kN of thrust at sea level. The Gamma 8 engine used 8 rocket motors arranged in 4 pairs of 2 which were gimbled to provide vehicle control. The peroxide was provided by two turbo-pumps and the fuel to oxidiser ratio was maintained at 1:8.2 [11]

At the same time as the Black Knight project, research and testing of hydrogen peroxide rocket engines was being conducted by the USA. Although some work was done on bi-propellant peroxide thrusters the majority of the work was focused on mono-propellants. Testing had begun on mono-propellant HTP thrusters which were to be used in reaction control systems (RCS) in a range of vehicles. This culminated in the production of RCS thrusters that were used most notably on the Mercury spacecraft and the X-1 and X-15 space planes. The X-1B used hydrogen peroxide decomposed over a silver catalyst. These were silver coated stainless steel screens, inter-dispersed with non-coated screens to add additional support. For maximum performance all RCS thrusters were preheated with a small, continuous flow of HTP. This

reduced start-up time which was measured at 0.2s from pilot input to full thrust; 0.1s was the delay in the catalyst bed itself as the peroxide was decomposed [12].

The Soviet Union developed hydrogen peroxide systems throughout the cold war era. Little is known about the progress made due to the Iron Curtain which made information transfer between the East and West almost impossible. What is known is that the work resulted in the use of hydrogen peroxide in the Soyuz launch vehicle. It continues to be used to drive the RCS thrusters and main engine turbine pump with over 1700 launches successfully completed [13].

Although research into hydrogen peroxide had shown promising results, its use in the European and American space industries began to cease in the 1970's and 1980's. With the onset of the cold war it became clear that higher performance propellants were wanted, with little regard given to toxicity or cost. Hydrazine had been identified as one such propellant but it was not until a new catalyst, Shell 405, was developed in 1966 that its use became widespread [14]. Monopropellant designs utilising hydrazine quickly emerged followed by bi-propellant applications using hydrazine derivatives, such as monomethyl hydrazine (MMH) and unsymmetrical dimethyl hydrazine (UDMH). These bipropellants used nitrogen tetroxide (NTO) or Mixed Oxides of Nitrogen (MON) as oxidisers. The bipropellant combinations were hypergolic with low freezing points and high specific impulse. At the same time several publications had been produced attacking the viability of hydrogen peroxide as a propellant [15,16]. These mainly focused on, amongst others, difficulties with storage, self-decomposition and poor physical properties such as a high freezing point (-11°C for 90% HTP and -0.5°C for 100% HTP). Although in later years these problems were rebuked by the likes of Musker [13] the damage had already been done. For over 40 years hydrazine and its derivatives have been the mainstay storable propellants of the space industry and as a result have an impressive heritage which can be matched by no other non-cryogenic propellant.

1.1 The need for green propellants

Hydrazine has proven to be an excellent monopropellant in terms of its performance with a theoretical specific impulse of 230s [17] (obtained from real performance data); however, its biggest drawback is its toxicity. This section will show that despite its performance the space community has recognised that the increased costs associated with handling hydrazine, and its derivatives, may out way the loss in performance offered by some green propellant alternatives. The main features of a green propellant are to reduce costs, complexity and environmental pollution. The definition of a green propellant that appears to have been accepted by the ESA [18] is given below with a more detailed description being provided in [17]:

"A green propellant is one that has the potential to have reduced adverse impact (i.e. toxicity), either to the environment (planetary body) or to personnel with whom it may come into contact, whilst still having the performance to meet mission requirements."

A range of green propellants have been identified by the space community, of which hydrogen peroxide is one. Others include ADN (an ionic liquid), nitrous oxide and electric propulsion in generality. The performance of ADN is greater than that of hydrazine with an Isp of 251s [17]. This value was calculated using the NASA CEA code originally created by Gordon and McBride [19]. It is based on a 10barA chamber pressure, chemical equilibrium frozen in the throat and a nozzle expansion ratio of 40. However, ADN does suffer from some drawbacks including; higher propellant and thruster costs compared to hydrazine systems, a limited supply chain (manufactured under license by a single European supplier) and limited flight heritage. However, the high system cost is offset by significant savings in the ground handling of this low toxicity propellant resulting in a cheaper system overall when compare to hydrazine. Nitrous oxide can achieve a theoretical performance of 198s [17], calculated using the NASA CEA code based on the conditions described above. Again the reduced performance is offset by the reduced system cost. However the high decomposition temperature of 1640°C has resulted in significant challenges in developing viable catalysts. To date nitrous oxide has no heritage as a rocket propellant. A variant of nitrous oxide, NOFBX™ (a nitrous oxide fuel blend) has a claimed Isp of 325s [20] but again no flight heritage. Finally, electric propulsion can provide exceptionally high specific impulse. There are various types of electric propulsion but generally they work by generating an ionized gas which is accelerated by an electric field. The QinetiQ T6 ion thruster can achieve an Isp of 4120s at 143mN [21]. However they are very expensive and require a significant amount of electrical energy (~4.5kW) [21] which has major impact on spacecraft design. The low thrust means it must operate for extended periods of time and makes it unsuitable for some manoeuvres such as debris avoidance. Although each of these green alternatives have their own advantages the drawbacks identified have made them unsuitable for further investigation within this project. With the flight heritage identified in the introductory remarks hydrogen peroxide is still seen by this author as one of the most viable green propellants.

As with many of the green alternatives hydrogen peroxide has a performance lower than that of hydrazine; 90wt% HTP can achieve a theoretical specific impulse of 145s and 100wt% HTP 161s. Again these values were calculated using the NASA CEA code based on the conditions described above. However, it will be shown that hydrogen peroxide is much less toxic. Toxicity data can be split into two main categories. The first is referred to in [17] as *acute toxicity data*. This covers unexpected spills and human contact, considered to be unlikely in a normal working environment. The second is referred to as *working toxicity data;* this is much more relevant to

industry as it covers exposure limits, protective equipment, storage and transport. The literature has shown that the precise toxicity values can vary between sources due to inconsistencies in the methods used to collect the data. However, the general trends in propellant ranking are considered to be similar in all cases.

The limits placed on human exposure are based on the assessment of several parameters including European Union (EU) risk phrases, LD_{50} and LC_{50}. The Risk phrases (R-phrases) were initially defined by the European Union and can be found in Annex III of European Union Directive 67/548/EEC [22]. They give a now internationally recognised method of assessing toxicity. These are separated in [17] into eight categories identifying the most serious toxic effects. These categories are defined as follows:

- **R23-R28** Toxic or very toxic if swallowed, inhaled or in contact with skin
- **R39** Danger of very serious irreversible effects
- **R48 and R68** Danger of serious damage to health, possible risk of irreversible effects
- **R45 and R49** May cause cancer with or without inhalation
- **R46** May cause heritable genetic damage
- **R60 and R61** May impair fertility or cause harm to the unborn child
- **R50-R53** Harmful or very toxic to aquatic life
- **R54-R59** Toxic to flora and fauna, dangerous to the o-zone layer

Table 1-1 shows how these categories relate to three propellants, namely hydrogen peroxide (a candidate green propellant), hydrazine and one of the hydrazine derivatives MMH. If a propellant has any R phrases under a given category the table cell is given a binary 1 entry otherwise it receives zero. In principle, it is possible for a propellant to score a total of 8. In practice however the highest score was found to be 3.

	Hydrogen Peroxide	**Hydrazine**	**MMH**
R23-R28	0	1	1
R39	0	0	0
R48 and R68	0	0	0
R45 and R49	0	1	1
R46	0	0	0
R60 and R61	0	0	0
R50-R53	0	1	0
R54-R59	0	0	0
Total	0	3	2

Table 1-1: R-phrase categories for hydrogen peroxide, hydrazine and MMH

As can be seen from the table hydrazine and MMH are shown to be significantly more toxic than hydrogen peroxide. Hydrogen peroxide does cause burns to the skin, but short contact causes no lasting damage and any signs of the burn would have normally disappeared within 24 hours. There is little data on hydrazine's effect on humans due to the tight controls over its use. However, on the few occasions that accidental exposure has occurred the effects are severe. One individual after being exposed to hydrazine for an unknown amount of time at unknown concentrations suffered vomiting, fever, diarrhoea, heart muscle degeneration, liver and kidney damage which finally lead to his death [23].

The dangers of these propellants limit testing to animals and rodents. One such set of tests identifies the toxicity of the propellant according to the concentration required to kill 50% of an exposed population within two weeks of exposure. The chemicals can be administered in one of three ways; LD_{50} refers to oral or dermal exposure while LC_{50} refers to exposure through inhalation over a four hour period. The EU uses hazard statements, such as the one shown in Table 1-2 to more clearly identify cases of extreme toxicity.

	Category 1	**Category 2**	**Category 3**	**Category 4**	**Category 5**
LD_{50} Oral (mg/kg)	< 5	< 50	< 300	< 2000	≥ 2000
LD_{50} Dermal (mg/kg)	< 50	< 200	< 1000	< 2000	≥ 2000
LC_{50} Inhalation (mg/m^3/4hr)	< 500	< 2000	< 10000	< 20000	≥ 20000

Table 1-2: EU hazard statement [17]

The table shows that the higher the category the less toxic it is considered to be. The results of this assessment for the propellants of interest are shown in Table 1-3, the raw data is given with the associated category being placed in brackets. Also included is the vapour pressure which is used to give context to the LC_{50} values.

	Hydrogen Peroxide	**Hydrazine**	**MMH**
LD_{50} Oral (mg/kg)	>805 (4)	60 – 200 (3)	33 (2)
LD_{50} Dermal (mg/kg)	2000 (5)	91 – 290 (2)	183 (3)
LC_{50} Inhalation (mg/m^3/4hr)	4000 (3)	430 (1)	140 (1)
Vapour pressure (Pa)	670	1295	6526

Table 1-3: Exposure toxicity data for propellants of interest [17]

The data given must be used cautiously, in some cases the animals used are not from the same species and this can skew the results. It is also important to place the LC_{50} values in context. Even a very low LC_{50} value can be considered to have a relatively low toxicity if the vapour pressure is also low. This benefits hydrogen peroxide which already has a high value of LC_{50}

but when combined with its low vapour pressure, is shown to be significantly safer than both hydrazine and MMH.

The result of this assessment shows that the EU considers hydrazine and MMH to be some of the most toxic chemicals in use. This is a sentiment echoed by the United States of America (USA) and provides the reason behind a decision taken by the USA government in 2008. At this time the USA had lost control of a reconnaissance satellite which would result in its uncontrolled re-entry to Earth and possible impact with the ground. The decision was taken to destroy the satellite in orbit to avoid the risk of human contact with the hydrazine fuel on board. General James Cartwright (2008) was quoted as saying the satellite "could release much of 1,000lb (454kg) plus of its Hydrazine fuel as a toxic gas" adding "there was enough of a risk for the President [of the USA] to be quite concerned about human life" [24]. General Cartwright went on to say that exposure to Hydrazine would be similar to that of inhaling Chlorine or Ammonia; with a burning sensation in the lungs and, if in high enough concentrations, even death.

It is due to these hazards that governments around the world have placed strict controls on the handling of propellants such as hydrazine and MMH. The space industry, although wary of environmental pollution, does not use this as the main driver in selecting their propellants. Instead their focus is on performance and cost with a significant proportion of the costs being associated with the ground handling of propellants. The acute toxicity data helps put into context the stringent guidelines placed on handling these propellants, which is referred to in [17] as *working toxicity data*.

The US Occupational Safety and Health Administration (OSHA) provide a Permissible Exposure Limit (PEL). This is the time weighted average (TWA) concentration based on an 8-hour working day and 40-hour working week. This value must not be exceeded. This limit constrains the use of personal protective equipment and also influences the storage and transport of these chemicals. Table 1-4 summarises the findings of [17] for hydrogen peroxide, hydrazine and MMH.

	Hydrogen peroxide	Hydrazine	MMH
OSHA PEL (ppm)	1	0.03	0.2
Eye protection	PVC or vinyl face mask	Goggles that protect from liquid chemicals, gases or vapours	Goggles that protect from liquid chemicals, gases or vapours
Skin protection	Rubber or neoprene gloves	Appropriate gloves to prevent skin exposure.	Appropriate gloves to prevent skin exposure.
Required clothing	Wear PVC or vinyl apron/protection suit	Appropriate clothing to prevent skin exposure.	Appropriate clothing to prevent skin exposure.
Respirators	NIOSH approved self contained breathing apparatus if more than 10ppm	Full hood negative pressure respirator with self-contained breathing apparatus	Full hood negative pressure respirator with self-contained breathing apparatus
Storage instructions	Stored in clean, vented, passivated, aluminium tanks.	Stored in a cool, well sealed, DOT* approved container. Suggested to be stored under nitrogen	Stored in a cool, well sealed, DOT* approved container. Only open in an inert atmosphere such as nitrogen

* Department of Transport

Table 1-4: Summary of working toxicity data for propellants of interest

It can be seen that the precautions required for hydrazine and MMH are significantly more stringent than those for hydrogen peroxide. As a result special SCAPE (Self Contained Atmospheric Protective Ensemble) suits are required by personnel that handle hydrazine-based propellants and fill spacecraft. Not only does this affect the personnel in direct contact with hydrazine it also has a negative impact on other technicians working around the spacecraft. When hydrazine is being loaded no other technicians are allowed within the vicinity and this slows the preparation of the spacecraft for launch. In an industry where time is such a critical factor the added time delay and stringent handling and storage precautions results in a substantial cost to the manufacturers.

It is due to these severe safety concerns that Hydrazine was added to the European Commission's REACH (Registration of Evaluation Authorisation and Restriction of Chemicals) in 2011 as a substance of very high concern. Although it is likely that it will be exempt for space uses the risk that hydrazine will be prohibited or restricted in the near- to mid-term remains. Due to these directives and the costs associated with handling toxic propellants, green propellants are once again being considered as attractive alternatives especially for small satellite manufactures, where the costs of propulsion systems using toxic propellants such as hydrazine do not scale down proportionally with satellite size [25]. The European Space Agency and EADS ST have recognized the use of 'green' propellants as having the potential to save a substantial amount of money in the manufacturing and ground handling of spacecraft [26]. This potential financial saving has caused a surge in interest in green propellants. Kappenstein [27]

has shown this in Figure 1-1 which illustrates the growth in publications related to green propellants between 1994 and 2007.

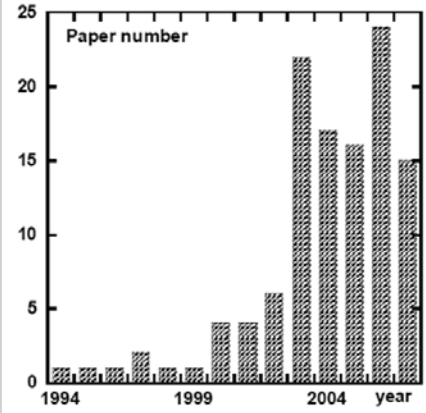

Figure 1-1: Number of papers presented in relation to green propellants 1994-2007

The ESA have indicated that some loss of performance is acceptable if the other goals are achieved. This has a significant influence on green propellant research, as the majority of propellants investigated have some loss of performance when compared to hydrazine. This leads to what is commonly referred to by authors [28] as the 80/20 rule. Thought to have initially been coined by the USAF it provides the criteria by which new propellants are assessed. According to this "rule" new propellants should have at least 80% of the performance for at most 20% of the cost of the existing propellant it is designed to replace. Whether this goal can be achieved with the use of green propellants is, at present, debatable.

1.2 The GRASP Consortium

It is due to the possible benefits associated with green propellants that the European Union was keen to fund research into this area. As a result funding was found in the Seventh Framework Programme, commonly known as FP7, to support a three year research program called GRASP. GRASP, standing for GReen Advanced Space Propulsion, was tasked with advancing the knowledge in green propellants and pushing the technology forward to the point needed to prove that they are feasible and competitive. GRASP, initiated in 2008, consisted of a consortium of eleven companies and research institutions combining some of the world leaders in green propulsion research.

The aim of GRASP was to provide a systematic down-selection of available green propellants and implement the most promising of these in demonstrator propulsion systems. Besides the development of propulsion systems, another general objective was to produce a comprehensive database of the physical characteristics and pertinent properties of green propellants. At all times the following issues were addressed [17]:

- Similar or better performance than those propellants used currently
- System advantages
- Detailed investigation of the storage and handling properties
- Compatibility with existing hardware
- Likelihood of reduced costs in the long-term

These were important if the space community was going to be convinced of the advantages of green propellants over current, much more widely used propellants. To help achieve this, the final propulsion systems developed within GRASP had a TRL of between 3 and 5. TRL's, or Technology Readiness Levels, are a method of categorising the current state of new technology and are widely used throughout the world by governments and companies alike. TRL's 3 to 5 are briefly defined as follows, for a more detailed explanation see The Los Almos National Laboratory website [29]:

TRL 3: Proof of concept validation through active research and development using representative data in analytical and experimental studies to show technical feasibility.

TRL 4: Prototype validation in laboratory environment with full scale problems or data sets.

TRL 5: System, subsystem and component validation in a relevant environment with prototype implementations conforming to target environment and interfaces.

To accomplish the aims set out in GRASP the work had been split into a number of individual tasks known as work packages. Each work package had associated documentation and manufacturing deliverables. This helped to keep the project moving forward at a sensible speed. The first of these deliverables, known as the general assessment, which has already been referenced in this document [17], was tasked with down-selecting the wide range of green propellants according to a range of criteria including toxicity and performance. Many of these deliverables have had a direct impact on the direction of the PhD research, which was partially funded by the GRASP program.

1.3 Research Objectives

This PhD works closely with the GRASP consortium to help achieve some of the aims listed above. There were two main goals of this PhD, these were;

1. To develop and assess, experimentally, a range of catalysts suitable for decomposing >95wt% hydrogen peroxide.

2. To develop an experimental thruster to assess various hardware design features such as injector and bed geometries, location and size of anti-channelling baffles and pre-heating methodology.

In order to achieve the first goal it was necessary to develop a range of novel catalyst substrate and active phase combinations in three distinct forms, namely; metallic gauze, ceramic pellets and metallic foams. These catalysts should aim to replace silver (a commonly used hydrogen peroxide catalyst) since at this concentration the temperature of the decomposition products are higher than the melting point of silver. The process used to manufacture these catalysts was refined using the results from a range of characterisation techniques with the resulting combinations being tested in two laboratory-based experiments. These novel pieces of apparatus helped down-select the most viable catalysts for testing within an instrumented catalyst bed under representative conditions. Post-firing catalyst characterisation gave an indication of catalyst degradation with extended exposure to HTP. This combination of data allowed conclusions to be drawn on the suitability of these catalysts for hydrogen peroxide thrusters.

The second goal was achieved through the development of a mono-propellant EBB (Engineering Breadboard) thruster with a TRL of between 3 and 4. As well as allowing further assessment of catalyst performance the bolt-up design allowed interchangeable injectors and catalyst bed geometries to be tested. Through the use of pressure, temperature, thrust and mass flow-rate measurements the effect of hardware changes could be quantified and optimised.

1.4 Research Methodology

The development of catalysts for hydrogen peroxide is a far-reaching subject. It will be seen in Chapter 3 that many authors use different combinations of catalyst substrates and active phase. It was not possible with the resources available to test all possible combinations thoroughly. Consequently a methodology was put in place which focused resources on catalysts which showed high performance when exposed to hydrogen peroxide. Figure 1-2 provides a flow chart to guide the reader through this methodology.

Following this approach minimised the number of catalysts which were subject to resource intensive process such as catalyst characterisation and catalyst bed testing. Some preliminary characterisation was required after the catalysts had been manufactured to help refine the procedure used to produce subsequent batches. Further characterisation was only conducted after the catalysts had been successfully down-selected through experimental testing within the laboratory. The first laboratory apparatus; the sealed reactor was used to assess preliminary performance. Catalysts that failed to decompose peroxide were rejected and subject to no further assessment. The second piece, the life-time mass loss apparatus, was used to verify performance

over an extended period of time. A combination of catalyst characterisation and experimental results were then used to identify the highest performing catalysts of each of the three forms assessed. Final testing of these catalysts was conducted within the highly instrumented catalyst bed (hICB) and the EBB thruster. To provide the design parameters for the EBB thruster a preliminary instrumented catalyst bed (pICB) was developed and tested in parallel with the laboratory assessment. After a successful test campaign the catalyst were characterised again to identify what, if any, damage had occurred as a result of their use within the beds.

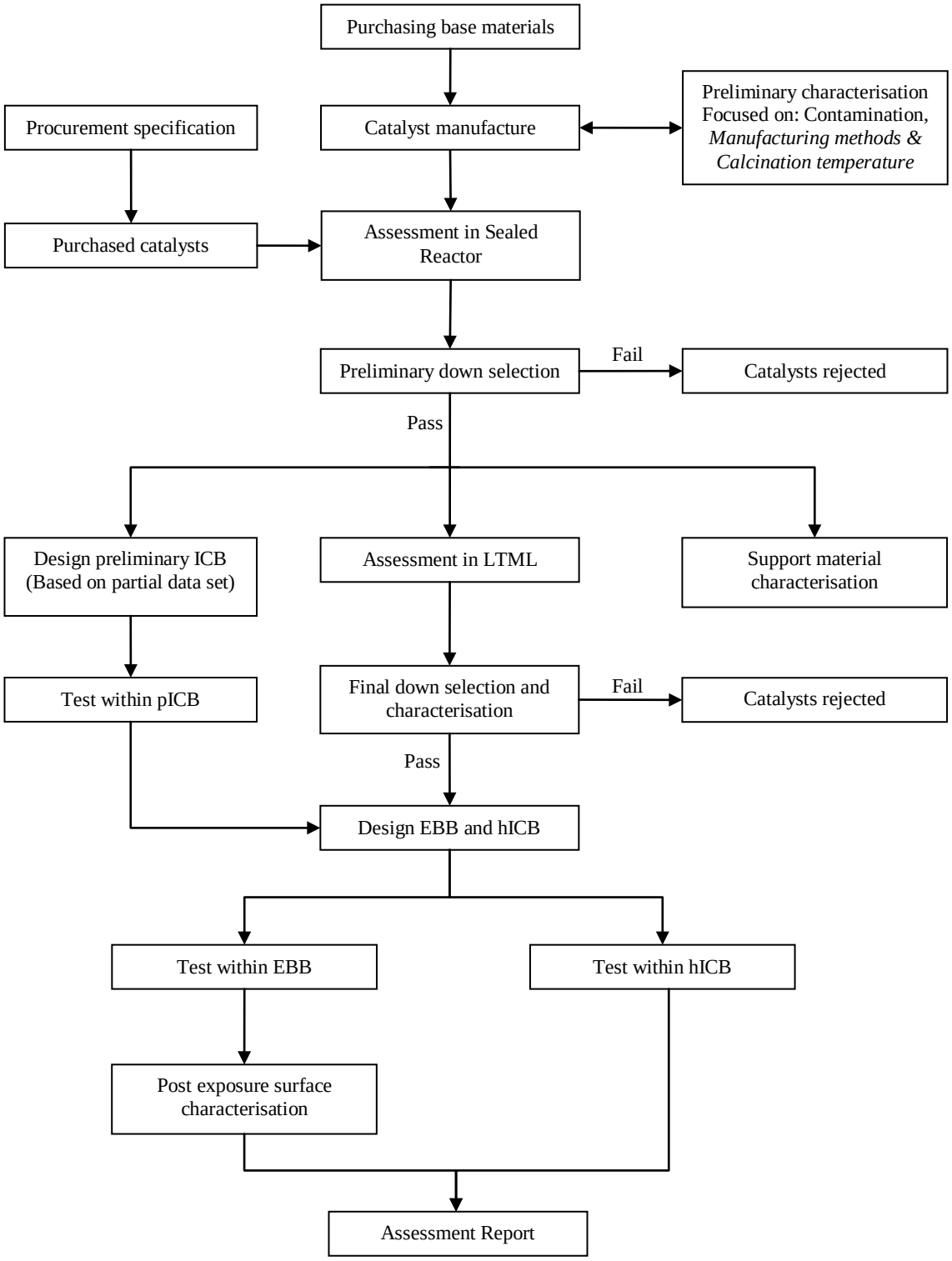

Figure 1-2: Research methodology flow chart

2 Rocket Fundamentals and Definitions

Both in the research and experimental work references to catalyst bed and thruster performance are made. This section will provide the reader with some of the information required for a deeper understanding of rocket thruster design. Using [30] some basic equations on rocket propulsion are given in an effort to define the performance parameters of a rocket engine.

Within a chemical rocket the propellant(s) enter a combustion chamber where they react (either in the form of combustion or decomposition) producing high temperature exhaust products, normally gases, which are expanded through a nozzle generating a thrust force, F:

$$\mathrm{F} = \dot{\mathrm{m}} V_e + A_e[P_e - P_{\mathrm{AMB}}] \qquad \text{(Eq. 2-1)}$$

Where $\dot{\mathrm{m}}$ is the propellant mass flow rate, $\mathrm{V_e}$ is the propellant exhaust velocity, A_e the nozzle exit area, P_e is the exhaust pressure at the nozzle exit and P_{AMB} is the ambient pressure. The last term in this equation can be considered zero for spacecraft attitude control thrusters where the nozzle expansion ratio is set such that $P_e \approx P_{AMB}$.

The nozzle exhaust velocity, V_e, can be calculated using equation 1-2 below:

$$V_e = \sqrt{\frac{2\gamma}{\gamma - 1}\frac{\boldsymbol{R}T_c}{\mathbf{M}}\left[1 - \left(\frac{P_e}{P_c}\right)^{\gamma-1/\gamma}\right]} \qquad \text{(Eq. 2-2)}$$

Here γ is the ratio of specific heats, **R** is the universal gas constant and **M** is the average molecular weight of the exhaust gases. The equation shows that the exhaust velocity can be increased by increasing the chamber temperature, reducing the average molecular weight of the exhaust gasses (by using lighter gases such as hydrogen) or increasing the pressure ratio P_e/P_c. The result of these equations is that for a fixed chamber pressure and nozzle geometry, as P_{AMB} reduces, the thrust will increase. This is why vacuum thrust is greater than sea-level thrust. To allow for an over or under expanded nozzle as a result of difference between exit and ambient pressures an effective exhaust velocity, *c*, can be defined:

$$\mathrm{c} = V_e + \frac{A_e[P_e - P_{\mathrm{amb}}]}{\dot{\mathrm{m}}} \qquad \text{(Eq. 2-3)}$$

It can be seen that for a perfectly expanded nozzle i.e. $P_e = P_{amb}$ the effective exhaust velocity equals the actual exhaust velocity.

The specific impulse for steady state operation can now be defined as the ratio of the thrust, F, to the weight flow rate of propellant, $\dot{m}g_0$ where g_0 is the gravitational acceleration at sea level (9.81 ms^{-2}):

$$I_{SP} = \frac{\mathrm{F}}{\dot{m}g_0} \qquad \text{(Eq. 2-4)}$$

I_{SP} is a measure of the energy content of the propellant and how effectively it is converted into thrust. It is considered one of the key performance parameters by which a thruster is assessed. In a chemical rocket it can be calculated using the chamber temperature,T_c, and the average molecular weight of the exhaust gases, **M**, as follows:

$$I_{SP} = \frac{\mathrm{c}}{g_0} = \frac{1}{g_0}\left(\sqrt{\frac{2\gamma}{\gamma-1}\frac{\boldsymbol{R}T_c}{\mathbf{M}}\left[1-\left(\frac{P_e}{P_c}\right)^{\gamma-1/\gamma}\right]} + \frac{A_e[P_e - P_{\mathrm{amb}}]}{\dot{m}}\right) \qquad \text{(Eq. 2-5)}$$

Here γ is the ratio of specific heats, **R** is the universal gas constant and P_c is the chamber pressure. It is assumed the velocity within the combustion chamber is approximately zero. For a perfectly expanded nozzle, $P_e = P_{AMB}$, the final term $A_e[P_e - P_{\mathrm{amb}}]/\dot{m}$ cancels. Again it can be seen that in a vacuum the specific impulse is larger than at sea-level conditions.

Specific impulse describes the effective generation of thrust per unit mass of propellant. For small volume constricted spacecraft, like those where hydrogen peroxide may have the greatest benefit, another term become important; the density specific impulse. This describes the generation of thrust per unit volume of propellant by multiplying the specific impulse by the specific gravity, SG, of the propellant.

$$\rho_{I_{SP}} = \frac{\mathrm{F}}{\dot{m}g_0}\ \mathrm{SG} \qquad \text{(Eq. 2-6)}$$

When comparing specific impulse, as has already been noted, hydrazine significantly outperforms 90wt% hydrogen peroxide (230s vs. 166s). However, if density specific impulse is considered the values are almost identical; 232s vs. 230s. This makes hydrogen peroxide particularly attractive to volume limited spacecraft designers.

The specific impulse is closely linked to the velocity change, ΔV. This is a space vehicle design parameter and can be shown using the Tsiolkovsky or ideal rocket equation:

$$\Delta V = g_0\, I_{SP} \ln\left[\frac{m_{tot}}{m_{tot} - m_{prop}}\right] \qquad \text{(Eq. 2-7)}$$

Where m_{tot} is the total vehicle mass (i.e. with propellant) and m_{prop} is the propellant mass. For a given delta V as set out by mission requirements a propulsion system with a high I_{SP} reduces the amount of propellant required.

The thrust coefficient, C_F, is defined as the thrust, F, divided by the chamber pressure, P_c and throat area, A_t. It can also be defined in terms of the specific impulse and characteristic velocity, C^*, as Equation 2-8 shows.

$$C_F = \frac{F}{A_t P_c} = \frac{I_{SP}\, g_0}{C^*} \qquad \text{(Eq. 2-8)}$$

The characteristic velocity is a measure of the energy available from the combustion (or decomposition) process and the efficiency of the conversion into high-velocity exhaust gas. It is given by:

$$C^* = \frac{P_c A_t}{\dot{m}_{prop}} \qquad \text{(Eq. 2-9)}$$

It can be seen that C^* characterises the combustion chamber and C_F characterises the nozzle performance. The product of these is the effective exhaust velocity. Therefore these performance parameters can completely parameterise the thruster and are often specified when a propulsion system is needed for a mission.

For the work being reported in this thesis several other terms will be used; the description of these terms follows. When developing thrusters many authors often compare the true performance to the theoretical ideal performance. One such example is the C* efficiency and is given by:

$$\eta_{C^*} = \frac{C^*}{C^*_{ideal}} \qquad \text{(Eq. 2-10)}$$

Where C* is the true characteristic velocity and C^*_{ideal} is the theoretical ideal characteristic velocity calculated using the ideal decomposition temperature, T_{ideal}. By replacing T_{ideal} with T_c an alternate method for calculating the measured C* can also be found.

$$C^*_{ideal} = \frac{\sqrt{\gamma \boldsymbol{R} T_{ideal}}}{\gamma \sqrt{\left(2/\gamma + 1\right)^{\frac{\gamma+1}{\gamma-1}}}} \qquad \text{(Eq. 2-11)}$$

Another term often encountered is the decomposition efficiency, η_{TH} which is defined as:

$$\eta_{TH} = \frac{T_c - T_{amb}}{T_{ideal} - T_{amb}} \quad \text{(Eq. 2-12)}$$

Where T_{amb} is the ambient temperature. For a homogenous chamber temperature, i.e. where T_c is fully representative of the combustion chamber η_{C^*} and η_{TH} are directly proportional. The decomposition efficiency should be used with care since it is dependent on two unrelated phenomena. The first is the reaction's thermal efficiency; a measure of the catalyst's ability to successfully decompose the peroxide. A poor catalyst will release the energy liberated from the decomposition slowly. This will be absorbed by the remaining liquid peroxide limiting the temperature rise. The second parameter is thermal losses either to the catalyst material itself or to the walls of the catalyst bed.

Over the life of a thruster catalyst degradation can lead to the formation of voids within the catalyst bed. Direct assessment through the use of X-rays can quantify this damage however many thruster manufacturers also use an indirect method of assessing thruster health [31]. One such parameter is to measure the chamber pressure roughness (R_{Pc}); this tends to increases during thruster operational lifetime as the catalyst material begins to move within the bed. Different approaches can be used but the equation listed below is generally accepted by the propulsion community. This term is normally expressed as a percentage.

$$R_{Pc} = \left(\frac{P_{cMax} - P_{cAVERAGE}}{P_{cAVERAGE}}\right) \times 100 \quad \text{(Eq. 2-13)}$$

Where P_{cMAX} is the maximum chamber pressures and $P_{cAVERAGE}$ is the average chamber pressure measured over the same time period. Testing of Aerojet's MR-106L 22N hydrazine thruster gave an average chamber pressure roughness of 18% after being exposed to a cumulative total of 166kg of propellant (~356kN-s total impulse) [32]

For an attitude control thruster in addition to the specific impulse another term becomes important. This is the minimum impulse bit (MIB); it is mission specific and defined as the smallest change in momentum required to allow for fine attitude or orbit control of a spacecraft. Typical values for a 1N monopropellant hydrazine thruster are 0.01-0.043Ns [33]. It is feasible for a poor performing catalyst to still have a small MIB. For a fixed pulse width a poor catalyst would generate a low chamber pressure and therefore thrust. It is for this reason that MIB is often quoted alongside specific impulse. Only a high performing thruster would generate a small MIB while still achieving relatively high specific impulse. MIB is also heavily influenced by thruster design. A large combustion chamber volume or significant 'dead space' can result in a low MIB (due to low thrust build up) but is also highly detrimental to specific impulse. Dead spaces are volumes downstream of the flow control valve (FCV) which must be filled with propellant but do not help in the decomposition process or generation of thrust.

In addition to the performance parameters described, two design parameters are also often quoted. These are the catalyst bed loading and the wetted area loading. These are used along with the length-to-diameter ratio, L/D, to dimensionalise the catalyst bed. The catalyst bed loading or cross sectional area catalyst bed loading (CBL_{CSA}) is defined as the mass flow rate of propellant per unit cross sectional area (CSA):

$$CBL_{CSA} = \frac{\dot{m}_{prop}}{Catalyst\ bed\ CSA} \quad \text{(Eq. 2-14)}$$

Meanwhile the catalyst bed wetted area loading (CBL_{WSA}) is defined as the mass flow rate of propellant per unit wetted surface area (WSA) of catalyst:

$$CBL_{WSA} = \frac{\dot{m}_{prop}}{Catalyst\ WSA} \quad \text{(Eq. 2-15)}$$

It will be seen later in this thesis that a low value of either of these two terms increases the catalyst bed life by reducing the quantity of peroxide each unit area of catalyst has to decompose. However, this leads to a large thruster increasing mass and reducing MIB performance.

3 Hydrogen Peroxide and its Catalysis

This PhD focuses solely on the development of catalysts and hardware for use with hydrogen peroxide. This chapter provides some background information on hydrogen peroxide as well as the methods and catalysts used by other authors to decompose peroxide for rocket applications.

3.1 Hydrogen Peroxide

3.1.1 Uses and production

Hydrogen peroxide is widely used in range of industries at varying concentrations. As Figure 3-1 shows its primary use is in the pulp and paper manufacturing industry which accounts for over half the world's consumption. In this application concentrations of between 30-50wt% are used to prepare peroxyacids for use in the MILOX (Milieu Pure Oxidative) pulping and bleaching process [34].

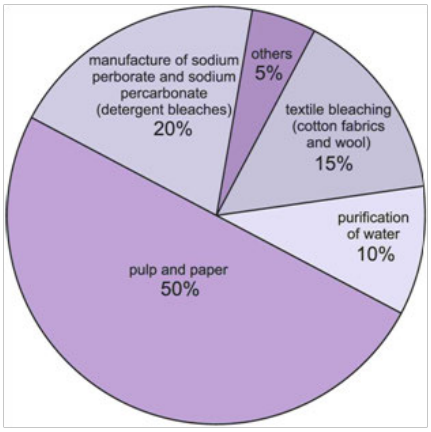

Figure 3-1: Uses of hydrogen peroxide [35]

Its highly diverse uses results in annual worldwide production of over 3.8 million tonnes (100wt%) with 1.3 million tons being produced in Europe [35]

3.1.2 Types of hydrogen peroxide

There is a wide range of hydrogen peroxide concentrations available with varying levels of stabilisers. This section will not describe all of them but focus specifically on three which are referenced regularly in the research and are used in the experimental section of this work.

Perdrogen is a low concentration (30wt%) hydrogen peroxide with a low stabiliser content normally used by authors to calculate catalyst reaction rates. A low stabiliser content is important as it minimises the poisoning effects of stabilisers on catalysts. Perdrogen is chosen as its low concentration limits the temperature rise due to decomposition. As will be seen in later

in this chapter this is important as temperature change can significantly affect the resultant decomposition rates calculated.

The majority of the experimental work conducted in this thesis uses 87.5wt% concentration HTP provided by Evonik Industries. PROPULSE™875 as it is commercially referred to, is used by a large number of referenced sources when assessing the performance of their catalysts. A variation of this product, PROPULSE™825, an 82.5wt% concentration HTP is used in the Soyuz launch vehicle to drive the main engine propellant turbo pumps.

Many critics of hydrogen peroxide make reference to problems with long term storage as a reason for it not being more widely adopted by the space community [15,16]. One possible solution to this is the use of highly stabilised hydrogen peroxide or HSHP. This contains significantly higher concentrations of stabilisers in an effort to avoid self-decomposition. Although some work has been conducted into HSHP this has normally been limited to homogenous catalysis due to the poisoning effects of stabilisers on heterogeneous catalyst beds [36,37,38]. Therefore a batch of HSHP was specially made to order by Evonik with an increased phosphate stabiliser content.

The three products described are detailed below with their relative stabiliser contents. Stabilisers with concentrations below 0.5 mg/l are not given. It can be seen that HSHP has phosphate stabiliser content 2000 times greater than its commercially available equivalent.

Commercial Name	Perdrogen [39]	PROPULSE™875	HSHP*
Concentration (wt%)	30	87.5	87.5
Density at 25°C (kg/m^3)	1099	1368	1368
Stabiliser / impurity (mg/l)			
Sodium nitrate ($NaNO_3$)	*Unknown*	12.0 – 20.0	12.0 – 20.0
Tin (Sn)	*Unknown*	5.00 – 9.00	5.00 – 9.00
Phosphate (as PO_4)	≤1.01	≤ 0.50	1000
Sulphate (as SO_4)	≤1.01	≤ 5.00	≤ 5.00
Chloride (Cl)	≤0.51	≤ 2.00	≤ 2.00
Aluminium (Al)	≤0.51	≤ 1.00	≤ 1.00
Carbon (C)	*Unknown*	≤ 1.00	≤ 1.00

* HSHP is not a commercially available product

Table 3-1: Hydrogen peroxide product details

3.1.3 Storability

The storability, or lack thereof, has been debated by various parties for many years. Some authors maintain that hydrogen peroxide is not a storable propellant [15,16], however other authors argue the contrary. Musker *et al* and Ventura *et al* both cite examples of successful long term storage both on the ground and in orbit [13,40]. It was found that after storing for 17 years (in vented containers) at ambient conditions in Texas the concentration had reduced from 90-91wt% to 84wt%. A second vented container was stored at 5°C over the same period and was found to have increased in concentration from 90wt% to 90.5wt%. Proof of storability on orbit was also provided by the Early Bird satellite which stored 5.45lb of hydrogen peroxide propellant for 5 years in the 1960's. These examples along with a 10 month study conducted by Ventura [41] all argue that hydrogen peroxide is a storable propellant. They also suggest that storability is improved with increasing concentration and it is the presence of water in dilute solutions that helps initiate decomposition.

The University of Southampton has conducted a much longer storability study. The mass of two vented aluminium storage containers were monitored over 53.5 months (~4.5years). One contained HTP and the other HSHP; both containers were stored in a fridge between 3-10°C. The results shown in Figure 3-2 suggest that HSHP is more stable over the longer term; however the standard HTP had a negligible mass change of 0.37%. It is unclear why the mass has increased instead of decreasing as would be expected if decomposition was occurring and oxygen was being released. However, the hydroscopic nature of hydrogen peroxide may have absorbed atmospheric water through the vented flask. In any case these small mass changes indicate that little to no decomposition has occurred over this time period, consistent with the findings of other authors.

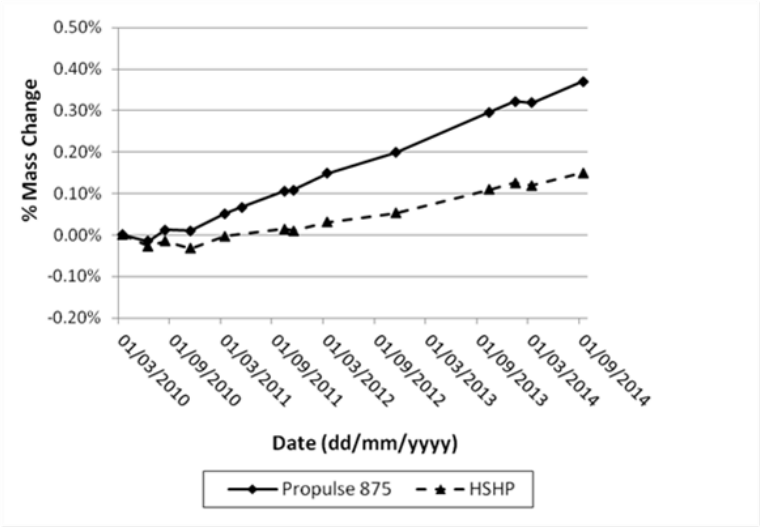

Figure 3-2: Hydrogen peroxide storage data

3.2 Hydrogen Peroxide Catalysts

3.2.1 Types of hydrogen peroxide decomposition

It is not the aim of this work to provide a detailed investigation into the types of decomposition and associated reaction rates. Throughout this project the development and testing of catalysts is focused on final application so 87.5%HTP is used throughout and assessment is based on demonstrable physical changes such as temperature and pressure rises. However, this short introduction does provide some background on the chemical process used to transform hydrogen peroxide into its decomposition products.

Hydrogen peroxide decomposes in one of two ways; either thermally or catalytically. With either method hydrogen peroxide is converted into steam and oxygen in the form of a redox reaction:

$$H_2O_2 \xrightarrow{k} H_2O + \frac{1}{2}O_2 \qquad \text{(Eq. 3-1)}$$

The enthalpy of formation for this reaction, $\Delta_f H^0{}_{gas}$ is -136.11 KJ/mol [42], shows the reaction to be highly exothermic. The rate constant, k, quantifies the speed at which the decomposition occurs and can be described using the Arrhenius equation [43]:

$$k = A_P e^{\left(\frac{-E_A}{\mathbf{R}T}\right)} \qquad \text{(Eq. 3-2)}$$

In the Arrhenius equation A_P is the pre-exponential factor, E_A is the activation energy, **R** is the universal gas constant and T is the temperature. E_A and **R** are constant for a given chemical reaction and catalyst but A_P is also dependent on the temperature. As a result it can be seen that the rate constant has a strong dependence on the temperature at which the reaction occurs.

3.2.2 Thermal decomposition

It is known above a certain temperature thermal decomposition is the primary form of decomposition. Several authors have suggested the mechanisms for this and although there is general agreement over the first few steps; Equations 2-3 and 2-4, author's opinions tend to vary on the steps required to reach completion [44,45]. Equations 2-5 and 2-6 are proposed by Giguère *et al.* It is generally agreed that this is a first order reaction meaning the reaction rate is directly proportional to the concentration of HTP.

$$H_2O_2 = OH + OH \qquad \text{(Eq. 3-3)}$$

$$OH + H_2O_2 = H_2O + HO_2 \qquad \text{(Eq. 3-4)}$$

$$HO_2 + HO_2 = H_2O_2 + O_2 \quad \text{(Eq. 3-5)}$$

$$HO_2 + OH = H_2O + O_2 \quad \text{(Eq. 3-6)}$$

Although interesting, to an engineer these steps are of little relevance. However the work conducted in this area, summarised neatly by [46], shows that thermal decomposition dominates at temperatures exceeding 450°C. This is of interest as it could influence catalyst bed lifetime. As long as the catalyst can achieve this critical temperature thermal decomposition can be partially, if not predominately, relied upon to achieve full HTP decomposition.

3.2.3 Catalytic decomposition

Although thermal decomposition can dominate at high temperatures in monopropellant thrusters catalysts are required to initiate the reaction. A catalyst works by reducing the activation energy required to initiate the decomposition; this is shown graphically in Figure 3-3. It is known that the rate of decomposition is highly dependent on temperature (as shown in Eq. 2-2), surface area and the concentration of reactant(s) [47].

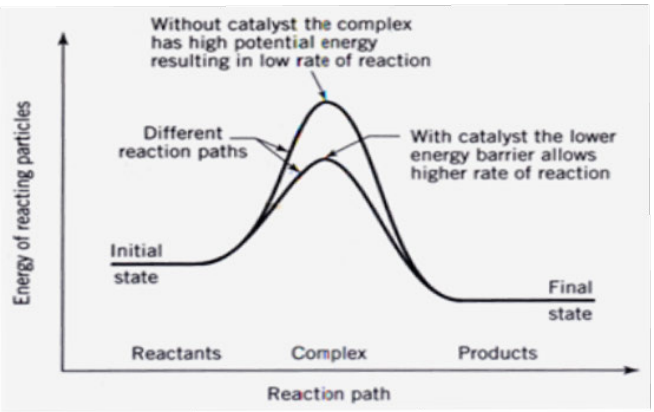

Figure 3-3: Effect of catalyst on activation energy [47]

Pearson *et al* [46] showed the activation energy required for thermal decomposition varied between 188-230kJ/mol however Bonifacio *et al* [48] identified a range of 40-50kJ/mol for catalytic decomposition. The resulting increase in reaction rate leads to a reduction in catalyst bed length. The process of catalyst decomposition is described in generality by Levenspiel [47] but Koopmans [49] focuses specifically on the catalytic decomposition of hydrogen peroxide. He identified seven steps in the catalytic decomposition process and suggested of these seven, absorption and decomposition at the catalyst surface were the most important. The rate of surface decomposition depends on the active phase chosen; this will be further investigated in Section 2.3. Absorption is dependent on the number of active sites available to the peroxide which is maximised by increasing the catalyst percentage loading (this term is described in detail later in this chapter). Interestingly the internal diffusion of the reactant from the surface to the inside of the catalyst was not an important factor. This was due to the generation of gaseous

decomposition products within the catalyst pores. This limited the ability of liquid peroxide to enter the pores setting up an oscillatory behaviour. A study by Oemichen *et al* [50] discussed within this work noted that only 2% of the pore surface area took part in the reaction (this was experimentally validated with 30wt% hydrogen peroxide). The result of this would suggest that surface concentration of catalyst is more important than overall catalyst percentage loading. It will be seen that this assumption is validated later in this work.

3.2.4 Heterogeneous vs. homogenous catalysts

There is a wide range of catalysts that can be used to decompose hydrogen peroxide but only a few that provide the performance required by the space industry. Catalysts can be split into two main categories, namely homogenous (in the same phase as HTP, i.e. liquid) and heterogeneous (in a different phase to HTP, normally solid). Liquid catalysts were used exclusively in the Messerschmitt Me 163 type aircraft [2] and for the Sprite 1 RATO thruster [4]. However it was the British developers of the Sprite 1 that identified serious drawbacks to liquid catalysts. These included additional weight, complexity and reduced performance when compared to equivalent solid catalysts. This was due to the requirement of a second propellant tank and feed system and the decomposition temperature being limited by the presence of an un-reactive fluid, i.e. the catalyst solution. This led to the development of solid catalysts, such as silver gauze which was used successfully on the Sprite 2 and more notably on the British Black Knight rocket. However these brought a different set of issues. The developers of the Black Knight noted that silver dissolved off the upstream gauzes, either being deposited further downstream or ejected out of the rocket completely. This resulted in the bed length having to be increased by over 20% so that even as the upstream catalysts became less active complete decomposition within the bed was still achieved [6]. This has a negative impact on the performance due to the increased thermal mass of the catalyst. More recent research has been conducted into liquid catalysts in an attempt to avoid the problem of exhausting the catalyst bed. Work done by the University of Southampton and DELTACAT Ltd. over a number of years [36-38,51,52] showed that although HTP could be successfully decomposed the complexity problems remained. Precise valve timing was required to stop a build up of HTP before the liquid catalyst was added. If a build-up occurred the resulting sudden decomposition, often referred to as a hard start, can be enough to damage the thruster [37]. Even if the complexity problems were overcome the space industry would most likely not accept liquid catalysts due to the mass increase associated with the additional storage requirements. It would be, in effect, a bipropellant system for a monopropellant application and performance. This is why this project will focus exclusively on solid, heterogeneous catalysts.

3.2.5 Catalyst Literature Review

Catalysis as a general topic, but even more specifically hydrogen peroxide catalysis is an expansive subject. Due to the huge range of catalyst supports, active phases and attachment and post-attachment techniques the matrix of possible catalyst combinations quickly becomes overwhelming. For this reason this review is restricted to a limited selection of publications. As a result of the literature review it was found that the majority of authors have very different approaches to catalyst design, manufacture and assessment. This makes direct comparison between sources difficult. The review has been separated into three sections based around the three main types of catalyst support, namely ceramics, metallic gauzes and metallic foams.

At first the requirement of the catalyst support seems simple: to provide a base for the active phase. However, as well as providing a secure fixing which stops the active phase from being ejected out of the thruster the catalyst support must fulfil several other criteria. These include:

- High surface area to facilitate the decomposition of hydrogen peroxide in the shortest length. This is important for minimising catalyst bed length.
- High thermal shock resistance to reduce the possibility of the substrate failing due to the thermal loads that take place within the support. This is facilitated by high thermal conductivity and a thermal coefficient of expansion similar to that of the active phase deposited on it.
- A chemically inert support that does not react with the peroxide in such a way as to compromise the carrier itself or have a detrimental effect on the catalytic properties of the active phase.
- A high mechanical strength that is able to resist damage caused by the highly energetic and turbulent flow. This can be assessed using the physical properties of the support such as ultimate tensile strength or tested experimentally within a representative bed. In the case of ceramic pellets high strength is also needed since the pellets can vibrate and impact each other.

3.2.5.1 Ceramic supported catalysts

Ceramic supports are at the forefront of hydrogen peroxide catalyst development. They have shown good promise in decomposing high concentration hydrogen peroxide (>90%) due to their high melting temperature. They can also have an exceptionally high surface area, exceeding $200 m^2/g$, with good thermal shock resistance. They can be found primarily in two different forms; monoliths and pellets. There are various advantages and disadvantages to each design.

Monoliths are usually extruded, single ceramic catalyst supports containing internal channels through which the HTP flows and is decomposed. The advantages stated by Kappenstein [53]

include; low pressure drop, better thermal shock and attrition resistance, uniform flow distribution and high surface-to-volume ratio. A low pressure drop was verified by Scharlemann *et al* [54] who showed a combined pressure drop of 0.2 – 0.3bar for a 13.6mm long catalyst bed and injector plate. This equates to only 2.1-3.2% of the steady-state inlet pressure. The catalyst support had a rectangular cross-section of 10.2x10.3mm^2 which was separated into 36 square channels. The catalyst was impregnated with a precursor solution of sodium permanganate resulting in the formation of a Mn_xO_y active phase. Mn_xO_y is used to describe the formation of a range of manganese oxides where x and y take different values, for example MnO_2 or Mn_2O_3. The reduced attrition rates compared to ceramic pellets are due to the catalysts monolithic structure. Ceramic pellets can move relative to each other within the bed leading to mechanical abrasion and possible structural failure. Structural failure leads to the formation of voids which act to further exacerbate the problem. Uniform flow results from an even distribution of propellant through each monolith channel. This avoids the phenomenon of channelling; a serious concern with non-monolithic catalyst beds. Channelling occurs when reaction products (normally gases) result in a local increase in pressure. This causes any peroxide that has not decomposed to disperse in all directions; with large parts of the flow radiating outwards. Here the peroxide runs along the outer walls of the catalyst bed in only minimal contact with the catalyst. As a result the HTP relies more on thermal decomposition instead of catalytic decomposition, tending to move the decomposition plane further down the bed. The high surface area to volume relates to the Euclidean surface area rather than the BET surface area. BET surface area, S_{BET}, is described later in this chapter but is the total surface area (internal and external) as measured by a gas absorption technique. If the catalyst geometry given in [54] is extrapolated for the pICB, details provided in Appendix D, and compared to the Euclidean surface area of the pellet catalyst used, there is an increase in surface area of 500%.

The significant advantages are partially offset by some of the drawbacks associated with using monoliths. Results from [54] show a relatively low temperature rise of ~45°C/s for a bed loading of only 3.6kg/s/m^2 and tests conducted by Bonifacio *et al* [55] show poor performance at bed loadings above 10kgs/m^2. This is much lower than pellet catalyst beds that can exceed 900kg/s/m^2 [56], although typically values of 50-100kg/s/m^2 are used (see Chapter 9). The low loading requires a much larger diameter catalyst bed, increasing thruster weight and volume. Few reasons are given for this but it s likely this is a combination of effects. Firstly, the straight channels result in the HTP passing through the bed very quickly; limiting the time the propellant is in contact with the catalyst. Secondly, the decomposition at the catalyst surface creates a layer of gaseous products which limits the contact between the un-decomposed HTP liquid and the catalyst. This creates a core flow of liquid HTP down the centre of each channel which takes longer to decompose. Finally, the support structure has a very low S_{BET} surface area ($<< 1m^2/g$) requiring the addition of a washcoat. A washcoat is a porous layer (such as γ-alumina) that is

bound to the surface of the catalyst support. This is then impregnated with the active phase and acts to significantly improve the surface area. Kappenstein showed the resultant surface area to be significantly improved at up to 19.6m^2/g [53], although this is still much lower than ceramic pellets which tend to exceed 200m^2/g. The washcoating process can be a difficult one as the bond between not only the washcoat and active phase, but also between the washcoat and carrier, must be strong enough to avoid failure in the energetic confines of the thruster. Although monolithic catalysts show good promise at decomposing HTP at this time they are still an emerging technology. The technology required to produce monoliths and washcoats is currently unavailable to the author of this thesis and for this reason ceramic monoliths will not be investigated further.

Experimental work into other ceramic based catalysts for decomposing HTP has been carried out since the 1990's. Early work was conducted by Rusek at the Edwards Air Force Base who chemically assessed a range of high surface area ceramic spheres and cylindrical extrudes [57]. He assessed alumina ($S_{BET} \approx 200m^2/g$), zeolite molecular sieves ($S_{BET} = 900m^2/g$) and silica-derived compounds (S_{BET} = 300-500 m^2/g). All the bases had been dried overnight at 300°C to remove volatiles before being impregnated for 4 hours with 0.96 molar concentration precursor solutions. After drying at 80°C for 15 hours the catalysts underwent a calcination treatment for a further 15 hours to transition the active phase to the oxide species of interest. Calcination is a thermal treatment process to bring about phase transition or removal of volatiles. The result were catalysts with the following active phases; Ag_2O, RuO_2, MnO_2, Mn_2O_3, PbO, V_2O_5 and Mn_xO_y (from potassium permanganate).

When the completed catalysts were gravimetrically assessed the resultant loadings (percentage of the catalyst mass attributed to the active phase) varied by a factor of 180 with Mn_xO_y on alumina catalyst giving the highest loading at 3.68%. This variation is associated with the differing absorption characteristics of the metal ions with respect to the catalyst bases. The reaction rates were calculated on the basis of experimental results with 70wt% HTP. They showed the following reactivity ranking: $Mn_xO_y > RuO_2 > MnO_2 > Mn_2O_3 > V_2O_5 > Ag_2O >$ PbO. It can be seen that MnO_2 outperformed Mn_2O_3 indicating that efforts should be made to avoid the transition from MnO_2 to Mn_2O_3 which occurs at 535°C. Silver oxide performed poorly, but silver is known to be a very high performing catalyst suggesting that it is silver not silver oxide that should be used for HTP decomposition. Rusek's findings provide a significant insight into high performing catalysts; however no assessment was made of the longevity or survivability of any of the catalysts he fabricated and tested.

More recently similar work has been carried out by Romeo *et al* [58]. He experimented with two different ceramic supports; 0.6mm diameter alumina spheres ($S_{BET} = 170m^2/g$) and 0.6mm

diameter alumina-silica (70:30 wt%) spheres (S_{BET} = 401 m^2/g). After drying under vacuum the base materials were impregnated with a range of precursor solutions (not specified) to achieve active phases consisting of either: Pd, Pt, Ag, Mn_xO_y, Ru or Ru_xO_y. Six different manufacturing methods were used with varying impregnation temperatures, either 20°C or 140°C, and calcination procedures. After impregnation all catalysts were dried under vacuum, some catalysts were then calcined for 2-4hrs in air between 400-800°C or reduced under hydrogen at 130°C for 2hrs. Catalyst loading was identified using an SEM (Scanning Electron Microscope) with combined EDX (Energy Dispersive X-ray). The resulting percent atomic content varied between the highest, silver on alumina at 9.54% to the lowest, ruthenium on alumina at 0.06%. No explanation is given for the large variations in loading.

Romeo *et al* [58] conducted 50 consecutive batch tests using 30wt% hydrogen peroxide (Perdrogen). The activity rankings were as follows; Pt > Ag > Ru > Mn_xO_y > Pd > Ru_xO_y. The performance of silver was equivalent to platinum however after 15 runs the performance dropped suddenly and significantly. It was found that the silver had leached from the alumina base due to a weak binding between the silver and alumina substrate. Of interest is that changes in the drying temperature between 400 and 800°C did not seem to affect performance of Mn_xO_y catalysts. This is contrary to the results gathered by Rusek [57] who showed that Mn_2O_3 performed worse than MnO_2; Mn_2O_3 forms above a transition temperature of 535°C. One possible reason for the results gathered by Romeo could be the short time (2 hrs) that the catalysts were held at the elevated temperature of 800°C. This may not have been long enough for complete transition to occur. Ruthenium as a metal performed well; however Ru_xO_y performed poorly indicating that it is the metal not the oxide that is catalytic. The ruthenium results also showed the importance of catalyst loading and surface area. The performance increased as the catalyst loading increased from 0.06 At% to 0.31 At%. There was also a considerable improvement when the base material was changed from alumina to alumina-silica, increasing the surface area.

A significant quantity of work has been focused on assessing catalyst longevity in representative monopropellant thrusters. Such work has been conducted by Kappenstein *et al* [59] who compared manganese oxide supported on 1.2-1.6 mm spherical alumina (S_{BET} = 250m^2/g), and silver on 1.4-2.8 mm spherical alumina (S_{BET} = 170m^2/g) to standard silver gauze (surface area ≈ 40cm^2/g). Very little data is provided on the manufacturing or testing of the manganese oxide catalysts. Kappenstein does indicate the catalyst performed consistently well within an instrumented catalyst bed achieving decomposition temperatures of 650°C with 89wt% HTP, 63°C below the ideal adiabatic decomposition temperature. He does not identify any poisoning of the catalyst over the duration of the runs. However, much more focus is placed on supported silver versus silver gauze. The supported silver is made by impregnating the ceramic base with

silver nitrate and then reducing this at 300°C for 1 hour, the ceramic base had previously been calcined at 600°C for 5hrs to drive off any volatiles and impurities. From a cold start silver gauze failed to decompose the HTP with a temperature increase limited to 100°C, while silver pellets showed an immediate reaction reaching a temperature of 550°C. However when the bed was pre-heated (with short pulses of HTP) to between 100-200°C the silver gauze out-performed silver pellets with decomposition temperatures reaching 600°C and 500°C (thermal efficiency, η_{TH} = 83.9% and 69.6%) respectively. It was hypothesized that water trapped within the pores of the support, as a result of the preheating pulses, limited the silver pellets' performance. Batch reactor tests using 30% hydrogen peroxide were conducted to help validate the trapped water hypothesis. The results suggested that this was the reason for the relatively poor performance of the pre-heated silver pellets.

Work into iridium catalysts for the decomposition of peroxide has been carried out by the Dalian Institute [60]. Iridium is best known in the space industry as the active phase of Shell 405, a catalyst used to decompose hydrazine in monopropellant thrusters. For that application it is attached to alumina pellets to maximise the available surface area. In experiments conducted by Tian *et al* [60] iridium was again attached to a γ-alumina (S_{BET} = 120m^2/g) support. The active phase was deposited using the wet-impregnation method with a precursor solution of hexachloroiridic acid ($H_2IrCl_6 \cdot 6H_2O$). The impregnated catalyst was then dried in air at 120°C for 12hrs and reduced in hydrogen at 400°C for 2hrs. The resulting catalyst contained 36wt% iridium and 1 wt% chloride. The catalyst was tested in a monopropellant thruster using 85wt% HTP (with unknown stabiliser content) with the aim of assessing performance over a number of 10s start up-shutdown cycles. The results showed a relatively poor chamber temperature of 480°C(η_{TH} = 72.6%) with no explanation given. However by run 25 the performance had dropped significantly with a chamber temperature of only 163°C suggesting the catalyst bed was exhausted. Post testing assessment showed the formation of iridium oxides, a reduction of the active phase and the presence of tin in the catalyst. The tin is most likely from the sodium stannate used to stabilise the HTP. It was concluded that a combination of these three factors led to the loss of performance within the thruster.

The sources identified here are just a small selection of information available on ceramic catalysts. A wide range of ceramic bases, active phases and manufacturing techniques have been employed to produce catalyst of varying quality and survivability. However in the majority of cases the performance of ceramic catalysts is superior to equivalent metallic gauze catalysts.

3.2.5.2 Metallic Gauzes

As can be seen from the flight history given in Chapter 1, metal gauze catalysts have a significant heritage for decomposing hydrogen peroxide. Most notably they were successfully employed on the German V-2 rocket (main engine turbo pump), British Black Knight rocket and NASA's X-1B research plane. Traditionally silver has been used, either as a woven mesh or bonded to the surface of other metal gauzes such as nickel or stainless steel.

Gauzes are normally defined by two parameters; wire size and mesh number. The mesh number relates to the size of the gaps between the wires. The relationship between the gap size and mesh number for woven meshes can be found in [61] and will not be repeated here. It is known that there is a strong link between surface area and rate of reaction for catalysts. As a result the author produced a short mathematical model to calculate the surface area of a known gauze; this can be found in Appendix A. In the model it is assumed that the metal is incompressible and that a Euclidean wire is used; that is, a perfectly cylindrical wire which has not been roughened in any way. The results show that for a silver 20 mesh gauze with a wire diameter of 0.356mm the specific surface area is approximately 10.7cm^3/g; this is several orders of magnitude lower than that of ceramic pellets. In reality however, gauzes are roughened using a variety of methods to increase their surface area. Some of these processes are mentioned later in this section. Even so, the effective surface area is much less than that of ceramic supports.

Britain conducted some of the early work investigating metallic gauze catalysts for use with the Black Knight rocket. Andrews *et al* [7] reports that the gauze catalysts were made in two steps. The first was to deposit a smooth layer of silver onto a nickel support. The support was a 20 mesh nickel gauze with a wire diameter of 0.376mm, the method of attachment has not been given. The first layer provided a good key for the second layer which was also silver. The second layer was much rougher than the first, being described as looking like 'hoar frost' under a microscope. The gauze was activated with samarium nitrate but no details are given on the process. Samarium nitrate, $Sm(NO_3)_3$, is thought to promote the decomposition of HTP however the mechanism is not well understood [62,63]. Seventy silver plated gauzes were compressed into each completed catalyst pack however the level of compression is unknown.

Black Knight testing showed that the 87.5 wt% HTP passed through the first 20 silver plated gauzes with almost no decomposition. However some silver was dissolved from the gauzes and it was this that initiated decomposition, which increased past the 20^{th} gauze and was completed by the 55^{th} gauze. The last 15 gauzes had progressively more involvement in HTP decomposition as the gauze at the bed inlet became less active due to general erosion, poisoning and dissolving of the silver into the HTP. This shifted the decomposition plane downstream, ultimately to the end of the catalyst pack. For a catalyst bed loading of 250 $kg/s/m^2$ (HTP flow

rate divided by the axial cross sectional area of the catalyst bed) the typical pressure drop was 20-30 bar, almost 50% of the bed inlet pressure. They found that pressure drop was proportional to the square of the bed loading but was inconsistent, changing over the life of the catalyst bed and between catalyst beds. The high catalyst bed loading limited catalyst bed life to only 30 minutes which is acceptable for launchers but not for satellite ACS thrusters which require extended operation. Two main causes were identified that limited catalyst bed life. The first was catalyst poisoning; this was due to chlorides, normally chromium chloride found within the HTP. The second was due to the sodium stannate used to stabilize the HTP. This would strip away a significant quantity of silver from the gauze; small amounts of stripping effectively cleaned the silver but large amounts reduced pack life. Initial catalyst bed and peroxide temperatures were also identified as being important. In the temperate climate of Woomera Australia (from where the Black Knight was launched) ambient temperatures could be greater than 30°C. Under such circumstances the full decomposition was achieved in less than 0.05s, but at 0°C the starting delay was 0.5s. At ambient temperatures below -3°C the bed showed no activity.

Significant work was also being conducted by NASA with the main focus being on decomposing 90-98% HTP. Wanhainen [64] investigated the effect of temperature on thrust build-up for two different types of metal gauze catalyst. Although several thrust ranges were investigated the majority of the assessment is focused on the 24lbf (~107N) monopropellant thrusters. The first thruster (configuration 'A') used a catalyst comprising of nickel gauze (20 mesh with a wire diameter of 0.457mm) electroplated with 99% silver and 1% gold. The catalyst bed loading was 230kg/s/m^2 with a total of 102 gauze discs being used. The second thruster (configuration 'B') used silver metal gauze activated with samarium nitrate. This thruster design had a catalyst bed loading of 117kg/s/m^2 and used a silver scroll pre heater. The pre-heater consisted of a silver catalyst which decomposed some of the peroxide warming the propellant before it entered the main catalyst bed. For the 24 lbf (~107N), configuration 'B' thruster the gauze size varied along the bed. The upstream part of the bed was filled with 70 discs of 20 mesh gauze (wire diameter of 0.356mm) with the remainder of the bed filled with approximately 7 discs of 10 mesh gauze (wire diameter of 0.660mm) All tests were conducted with 90 wt% HTP.

The results show at ambient temperatures of 4.4°C the initiation delay (defined as the time taken to reach 90% of steady state pressure) varied greatly in thruster configuration 'A'. At these temperatures the bed was susceptible to flooding with liquid peroxide being expelled. Thruster 'B' produced much more consistent low temperature responses. It is likely that this is a result of the reduced bed loading and use of a pre-heater in the configuration 'B' thruster. However, at lower temperatures both thrusters showed a significant drop in initial performance after six

minutes of operation. It was shown that at low temperatures, performance was highly dependent on the quantity of HTP the catalyst had been exposed to. A similar relationship was identified in the results gathered in Chapter 9 of this work. At ambient temperatures above 15.5°C both catalysts performed well during start-up but unfortunately no steady state data is provided.

NASA was particularly interested in being able to catalyse high concentration HTP (98 wt%) with silver. The work done by Runckel [65] investigated this problem, he devised 7 catalyst beds; beds 1-3 were used to decompose 90 wt% HTP with beds 4-7 decomposing 98 wt% HTP. The beds were constructed of silver gauze activated with 2% or 10% samarium nitrate [$Sm(NO_3)_3$], anti-channel baffles and stainless steel gauzes were used to structurally support the silver. In all cases the catalysts were packed with a compression pressure of between 70 and 350bar. For bed 3 which had a compression pressure of 152bar, the pressure drop to inlet pressure ratio was 0.2. For bed 6 which had a compression pressure of 352bar the pressure drop ratio was 0.28. Both beds had a similar bed loading (178 and 154kg/s/m^2 respectively) and number of metallic gauzes (81 and 86).

In beds 1-3 between 74% and 78% of the available space was occupied with silver gauzes, these were 20 mesh gauzes with a wire diameter of 0.356mm. They were used to successfully decompose 90% HTP, with an initial delay time of 0.04s when the beds were hot (at the end of an 8 minute testing sequence). Bed 2 performed better when started from cold (1.7°C) than bed 3 even though the same catalyst and thruster configuration was used. The only significant difference being the silver in bed 2 was activated with 10% $Sm(NO_3)_3$ while bed 3 was only activated with 2% $Sm(NO_3)_3$ This suggests that an increase in samarium nitrate concentration improves performance. It was noted that thruster performance improved with continuing use. This trend is again seen in the testing conducted in chapter 8. No deterioration in performance was noted over the 8 minutes of testing.

Catalyst beds 4-7 were tested with 98wt% HTP At this concentration hydrogen peroxide can reach decomposition temperatures of 946°C, however silver melts at approximately 898°C [65]. To minimise the amount of silver that would melt the percentage of the bed filled with silver gauzes was reduced to between 20% and 38%, these were either 20 mesh gauzes (wire diameter = 0.356mm) or 40 mesh gauzes (wire diameter = 0.254mm). The remainder of the bed was filled with nickel gauzes which are only catalytic at high temperature (~400°C). Runckel found that increasing the mesh number from 20 to 40 improved performance by increasing the surface area and reduced the overall volume of silver required, However, in this configuration the pressure drop ratio was the same as bed 6 although the bed compression pressure was less at 276bar. Although some melting was identified these beds were able to successfully decompose

98wt% HTP but a trade-off was required between starting performance and catalyst bed longevity due to melting of the silver.

With the development of good hydrazine catalysts, work at NASA into hydrogen peroxide catalysts reduced significantly. Any work that was focused on HTP decomposition was mainly aimed at ceramic and monolithic catalysts. More recently several other authors have re-visited silver gauze as a baseline comparison for more modern catalysts. The University of Southampton assessed silver alongside a range of ceramic catalysts either impregnated with sodium permanganate or coated in platinum [66]. The silver gauze had a mesh number of 20 and a wire diameter of 0.356mm. The silver was treated with a 10% nitric acid bath for 5 minutes. This etches and roughens the surface increasing the surface area. However, no assessment was made on the change of surface area as a result of this process. Thruster tests were conducted using 87.5% HTP. A temperature of 624°C and 629°C were recorded for γ-alumina and zirconia pellets impregnated with sodium permanganate respectively. These compared favourably with silver which only achieved a decomposition temperature of 605°C.

The effect of etching has been categorised by Lee *et al* [63] whilst assessing a range of catalyst beds using silver gauze. The silver used had a mesh number of 20 and a wire diameter of 0.31mm. To improve the surface area he etched the surface of the silver with 30% nitric acid for 30s, this was shown using SEM images to improve the surface roughness. No measurement of the surface area has been taken. Testing of this roughened silver was conducted in an instrumented catalyst bed with 80wt% and 90wt% HTP. As expected the highest performance measured was with the configuration which used the most silver screens (125). It was noted that performance also increased as the number of stainless steel (SS) gauzes in the downstream section increased. It is hypothesized that thermal mass of the SS gauzes initiated thermal decomposition when the bed was hot while also increasing the residence time of the HTP within the bed. Although testing was also conducted with a combination of silver gauzes upstream and a platinum monolith downstream the performance was poor. The reason for this was the low porosity of the monolith that restricted the flow of HTP and increased the pressure drop across the bed to 19bar, three times that of the highest performing bed.

3.2.5.3 Metallic Foam

Metallic foams have rarely been used in the decomposition of hydrogen peroxide; instead impregnated or coated ceramic foams are much more common. Metallic foams offer several advantages; the surface area is much greater than that of gauzes, they do not vibrate and impact each other like pellets and if catalytically active metals are used there is no need to attach a separate active phase. However, ceramic foams have a greater surface area than metal foams when used in combination with a washcoat. One of the drawbacks of foams relates to the

significant pressure drop that results from the unordered structure. Although the structure facilitates intimate contact between HTP and catalyst, the path the hydrogen peroxide takes is tortuous; therefore the pressure required to force the flow through the bed tends to be greater than for pellets and gauzes.

Work conducted by the University of Southampton [52] investigated catalysts supported on nickel foam (Incofoam^{TM}). Several active phases were attached using a wet impregnation method. Three mass ratios of iron (II) chloride: iron (III) chloride co-catalyst were assessed; 101.5:1, 76.9:1 and 50.3:1. The nickel foam was submerged in each of these solutions for an unknown period of time before being baked at 200°C for 15 minutes. The nickel foam was also impregnated with sodium permanganate following the same procedure but being baked at 600°C for 30 minutes. Qualitative assessment was made by dropping 85% HTP onto the surface of the catalyst and visually assessing the result. Nickel foam impregnated with sodium permanganate was identified as the most viable catalyst. This was then placed within an instrumented catalyst bed for testing. Initial results identified that the porosity of the foam was too low and as a result the peroxide failed to pass through the bed. A modification was made with holes being drilled at alternating positions; either on or off axis. This resulted in a reduced pressure drop across the foam allowing the HTP to flow and giving a peak temperature of 480°C. It was found that the bond between the active layer and support was weak with significant quantities of the active phase being stripped from the support.

More successful work has been conducted by the Russian Scientific Centre [67]. Significant advancement has been made with porous metallic supports and catalysts. One such catalyst, referred to as K-87, is an impregnated porous nickel tablet, 4-5mm in size. The precursor solution is potassium permanganate; this is used instead of sodium permanganate. Both result in the formation of Mn_xO_y but with the presence of either potassium or sodium. Although precise details are not given the author suggests the rejection of sodium permanganate is connected to its high solubility. The manufacturing process is not defined but chemical assessment shows the rate of decomposition to be 40 mol/(min·g). This unusual unit is identified by author of the paper as being more relevant than the standard unit (s^{-1}). The unit refers to the mass of HTP that can be decomposed per unit mass of catalyst in unit time. Therefore 40 mol/(min·g) equates to 1360g of HTP being decomposed by 1g of catalyst in 1 minute. Tests with K-87 show it can successfully decompose peroxide at temperatures as low as -40°C. Several other porous metallic catalysts have been manufactured by the same group [67]. Granular catalysts comprising oxides of copper, manganese and a series of additives have successfully decomposed up to 100wt% HTP. Two forms of this catalyst exist, with (K-85) and without activation by potassium permanganate (K-83). Thrusters have been developed which use combinations of K83, K85,

K87 and K-86 (Silver plated stainless steel gauze) which start from -20°C with a response time to 70% of steady state pressure of no more than 0.5s.

Metallic foams have only had limited use within the space propulsion industry; however they are being increasingly used in power sources such as hydrogen peroxide fuel cells. It may be possible to transfer the technology being developed in this area for use within hydrogen peroxide rocket thrusters. One such power study has been undertaken by Yang [68] who successfully tested silver plated nickel foam. The nickel foam (thickness: 1mm, pore density: 110 pores per inch, or ppi) was first cleaned and etched before the silver was applied. This process involved placing the foam in acetone to remove grease and drying in air. The clean foam was then placed in a 3 molar solution of hydrochloric acid at 25°C for 20 minutes. This removed the oxide layer and etched the surface. Finally the nickel foam was electroplated in a solution containing $50g/l^{-1}$ of potassium silver cyanide at a current density of $5mAcm^{-2}$. The precise time is not given but the resulting coating thickness was 1µm. Yang identifies that the silver 'adheres firmly' to the surface of the nickel foam with no impurities found. The silver plated foam was successfully used in a hydrogen peroxide fuel cell. It is not clear whether this foam could be used successfully inside the much more vigorous confines of a thruster without the silver being stripped from the foam support.

3.3 Summary

This chapter started by providing background information on the uses and types of hydrogen peroxide. Although use by the space community is insignificant the global use of peroxide is high [35]. As a result of the large scale production the price of the propellant is reduced. However, due to the stringent requirements on stabiliser content there is an additional cost in refining the industrial form of this propellant to make it suitable for rocket applications. Work done on the British Black Knight rocket showed that high stabiliser content can be detrimental to performance [7]. This will be verified by experimental work conducted with HSHP (Highly Stabilised Hydrogen Peroxide) discussed later in this thesis. The work conducted by this author also suggests that hydrogen peroxide is a storable propellant with only minor changes in mass over a four and a half year period.

The second part of this chapter investigated the methods used to decompose hydrogen peroxide. For rocket applications it was shown that catalytic decomposition was crucial, however, thermal decomposition at high temperatures could be partially relied upon to decompose HTP [46]. This may help to increase the life of the catalyst bed by reducing the reliance on catalytic decomposition at high temperature.

The literature review conducted in the final part of this chapter has provided a strong case for testing each of the three catalyst support structures discussed. Unfortunately it is not possible to test ceramic monoliths although several authors have identified benefits to using this support type [53,54]. A range of active phases have been impregnated into ceramic pellets with some, such as manganese oxide, platinum and ruthenium showing high performance [57]. These active phases will be the subject of further assessment in this work. Silver metallic gauze has been used extensively for HTP decomposition and will form the base comparator for all other catalysts tested. A range of other metallic gauzes will also be tested. This will allow a comparison of metallic gauzes and ceramic catalysts with the same active phase. Finally the findings of [67] make metallic foams an attractive choice for further study. This work showed some of the highest reactivity, and consistent performance at the lowest temperatures.

4 Experimental Techniques for Catalyst Assessment

It can be seen from Chapter 3 that a great variety of methods exist for assessing catalysts. However, the aim is normally the same and can be split into two key questions: firstly, how effectively is the hydrogen peroxide decomposed? This parameter can be quantified in a range of ways, with peak temperature or pressure, time to reach these peak values or rate of evolution of gas being amongst the many. If the results of this first phase assessment are positive then a second question should be posed: what is the likelihood the catalyst will work with continued exposure to hydrogen peroxide? A catalyst that can effectively decompose HTP is of little use if it structurally fails or is exhausted quickly. These two key questions can be answered in a variety of ways using a wide range of experimental apparatus. To help the author narrow this range the following section reviews the techniques and equipment employed by other researchers in this field. The research has been separated into two main sections. The first, laboratory-based testing requires significantly fewer resources compared to the second; catalyst bed testing. However catalyst bed testing is one of the few ways of testing catalysts under truly representative conditions.

4.1 Approach to Catalyst Assessment

Two main approaches exist when it comes to assessing catalysts. The first, described by this author as the ‘chemical approach’, involves measuring and calculating the reaction rate of the decomposition reaction with a particular catalyst. This can be done using a range of experimental equipment normally in the form of a constant pressure or constant volume reactor. The major advantage of this method is, for a fixed set of conditions, a quantitative analysis which is unambiguous. It was identified in chapter 3 that there is significant inconsistencies in the apparatus and methods used by authors of different work. However the ‘chemical approach’ is independent of the apparatus and method as long as the starting conditions (for example temperature) are consistent. Although it would seem as if this approach is very advantageous, there are some drawbacks. It was shown by the Arrhenius equation in Section 3.2.1 that the rate constant, k, is very dependent on temperature so it is important to maintain a constant temperature if k is to be measured accurately. However, the decomposition of hydrogen peroxide generates a great deal of energy in the form of heat. Even with thermally regulating devices such as water baths it can be difficult to maintain a consistent temperature if that energy is released quickly with a high performing catalyst. As a result experiments are normally conducted with relatively low concentrations of peroxide, such as Perdrogen (30wt%), so as not to generate a significant rise in temperature. The main drawback of this approach is that it fails to assess the catalyst over the full temperature range. It is possible that the catalyst absorbs a

significant quantity of heat limiting the peak temperature that can be reached or, at high temperature the catalyst support may fracture due to the thermal loads placed upon it. A chemical approach makes no attempt to assess the long term performance and survivability of the catalyst. These are key drivers when selecting catalysts for thruster applications.

The second approach to assessing catalysts is termed by this author as the 'engineering approach'. The parameters of assessment are based around the variation of temperature and/or pressure with time. This approach normally utilises either batch reactors or a representative catalysts beds. Unlike the chemical approach the engineering approach does not require the use of reduced concentration hydrogen peroxide. As a result this type of assessment gives a better overview of catalyst performance under more realistic conditions. Not only does it assess catalyst reactivity it can also provide information on both longevity and survivability over a wide operational range. For thruster applications reactivity is only one of several key features that catalysts must fulfil. Start-up characteristics, consistent performance during extended HTP exposure and re-start capabilities are equally important. This approach can assess catalysts over the most demanding operational phase i.e. decomposition of peroxide from ambient temperature, especially when quenched. Quenched is a term used to describe catalyst activity when performance is suppressed by the presence of excess liquid hydrogen peroxide. Energy generated by the decomposition of HTP is absorbed by the bulk liquid limiting the temperature rise. Even more so than the 'chemical approach' there are some significant challenges that are faced with the engineering approach. Many of the parameters used to define performance are open to ambiguous interpretation by authors, resulting in a qualitative assessment of quantitative results. The measurements themselves are not just influenced by catalyst performance. They are also an assessment of the overall design of the assessment apparatus. This means that although comparisons of catalysts can be made within the same equipment these cannot be directly compared to other work unless the same equipment is used. Finally, significantly more resources are required to apply the engineering approach than the chemical approach. However, it is critical that the longevity of the catalyst is assessed before it can be considered for use within a rocket thruster.

The literature review will investigate both of these approaches as many authors use a combination of these approaches in laboratory assessments. Section 4.3 will provide details on various catalyst beds developed for catalyst evaluation. This will be used to influence the design of both the catalyst bed and test programs used in this work. It is not the aim of this review to present the findings of these authors, only identify the methods and apparatus used to generate their results.

4.2 Review of Laboratory Catalyst Assessment Techniques

One author that has already been identified as contributing significantly to the advancement of modern hydrogen peroxide catalysts is Rusek [57]. He used two distinct approaches, both chemical and engineering to assess a range of catalysts. The first of these used a constant pressure batch reactor. The reactor was a 50ml flask containing 20ml of 70% HTP constantly agitated at an unknown temperature. At a time, t = 0 a known weight of solid catalyst (not given) was added to the flask with the associated temperature rise being measured using a thermocouple. It is clear that this method does not maintain a constant temperature, however this is not critical. Instead of inferring the rate constant by measuring parameters such as the products of the reaction a direct method is applied. This method requires small samples (40µl) being withdrawn at specified time intervals and the concentration being analysed using a refractive index. By plotting the change in concentration against time and measuring the resulting gradient the rate constant, *k*, could be calculated. The rate constant was then divided by the catalytic loading to give the specific rate constant, *k'*, and the results compared. This parameter is independent of catalyst loadings and allows direct comparison of catalyst reactivity. There are several advantages to this process; the apparatus is simple and the direct measurement method applied does not require a constant temperature to be maintained. This allows the temperature profile to be recorded and assesses the catalyst over a wider range of temperatures. One of the possible problems that may have been encountered, but is not discussed, is difficulty in recording enough samples to ascertain the gradient. A fast acting catalyst can decompose 20ml of hydrogen peroxide in only a few seconds, making sample extraction and accurate time keeping difficult.

The second experimental test used a batch reactor with the assessment criteria being based upon the temperatures recorded. In these experiments 20ml of a 30% hydrogen peroxide solution is placed within 100ml spherical reactor. The solution is initially at ambient temperature and continually stirred. At timer is started when 3.2ml of solid catalyst is added to the reactor and the variation in temperature recorded. The catalysts are assessed according to two parameters; peak temperature and time to peak temperature. The peak temperature is affected by thermal losses to the surroundings; however these losses are constant for all the catalysts tested so a comparative assessment is still possible. Rusek also defines a new parameter, activity, which is the inverse of the time to maximum temperature (h^{-1}). No reason is given for choosing this parameter however it may be to provide consistency for the reader since the units for the rate constant are s^{-1}. The constant catalyst volume assessment is as, if not more, important than constant mass assessment. A low density catalyst can fill a larger volume for the same catalyst mass; however this increase in volume will result in a larger and therefore heavier thruster. Catalyst volume has a much greater influence on overall mass than the catalyst mass itself and is therefore of much more interest to rocket designers. Due to the low concentrations of

peroxide used in these tests the effect of temperature on the performance and survivability of the catalyst is not assessed. One of the main drawbacks to the work conducted by Rusek is that no catalyst bed or thruster testing was conducted. As a result the survivability of the catalyst is not assessed.

Russo-Sorge *et al* [69] also assessed catalysts using a chemical approach. In her work a constant pressure batch reactor was used to directly measure the mass flow rate of oxygen produced (one of the decomposition products). A 200 ml flask was partially filled with 100ml of either 50% or 70% hydrogen peroxide which was continuously stirred. At a known time 100mg of solid catalyst was added and the reaction monitored. An electronically controlled water bath was used to maintain a constant reaction temperature. The apparatus is shown in Figure 4-1.

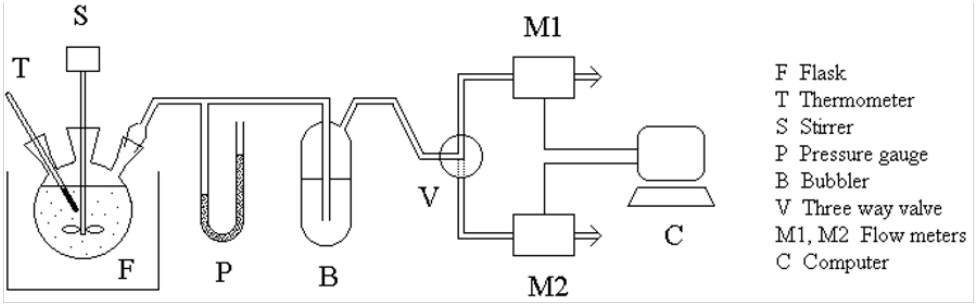

Figure 4-1: The apparatus used by Russo-Sorge et al

A range of instruments were used to monitor the reaction. A thermocouple was used to monitor the reaction temperature and mass flow meters measured the rate of oxygen production. Two flow meters were used with different ranges; $10Lh^{-1}$ and $100Lh^{-1}$. The flow was first passed through a bubbler to remove any water or peroxide vapour that may have been caught in the oxygen stream. The reaction was conducted at two temperatures; 40°C and 70°C. Few results were gathered at 70°C since the reaction was more vigorous and led to an increase in the reaction temperature, affecting the rate constant measured. Russo-Sorge indicated that it is not possible to measure the initial production of oxygen accurately. This is due to an initial high rate of oxygen production which causes the pressure within the system to rise. Only when the production rate reduces to an almost constant value can the flow of oxygen be measured accurately and the rate constant, *k*, calculated according to Equation 4-1;

$$-\frac{\Delta n}{\Delta t} = k\frac{V_{cat}}{V_{sol}}n_0 \qquad \text{(Eq. 4-1)}$$

Here V_{cat} and V_{sol} is the volume of catalyst and solution respectively, n_0 is the number of moles of H_2O_2, Δt is the change in time and Δn is the change in the number of moles of hydrogen peroxide. This value is calculated by converting the number of moles of oxygen generated (according to the mass flow measurements) to the equivalent number of moles of hydrogen peroxide decomposed.

The work conducted by Russo-Sorge makes several assumptions in order for the reaction rate to be calculated. It is assumed that the concentration of peroxide is almost constant throughout the duration of the test due to the high volume of peroxide compared to the small quantity that is decomposed. This allows n_0/V_{sol} to be considered constant. She also assumes after the initial transient that the decomposition rate $-\Delta n/\Delta t$ can also be considered constant. These assumptions will affect her results but no effort has been made to assess the uncertainty that is generated. The method of assessment is not as direct as that used by Rusek, where no assumptions were required in order to calculate the reaction rate. In the introduction to this section it was identified that low peroxide concentrations are required to limit the change in the reaction temperature. However, Russo-Sorge has successfully assessed the reaction constant for 70% hydrogen peroxide with no significant temperature increase. The reason for this is due to the very small quantities of catalyst used. The value of 100mg was for supported catalysts of loadings varying between 2-11%. This indicates that the quantity of active phase was at most 11mg. This had two effects; firstly, the peroxide decomposed slowly so the concentration of peroxide changed very little during the experiment. Secondly, the slow decomposition released only small amounts of energy that was absorbed by the relatively large quantity of peroxide resulting in a very little temperature rise. It was for this reason that the rate constant could be measured. Again, this work does not asses the longevity of the catalyst or their performance over a range of temperatures.

Extensive testing has been conducted at the University of Poitiers; this has covered the assessment of both monolithic and non-monolithic catalysts. One such piece of work by Pirault-Roy *et al* [70] used a combination of constant pressure and constant volume reactors to assess the effect of hydrogen peroxide stabiliser content on peroxide decomposition. The details of the constant volume reactor are unavailable but details are provided on the constant pressure reactor. This apparatus consisted of a double walled reactor with an internal volume of 40ml within which there was 10ml of hydrogen peroxide solution constantly agitated using a magnetic stirrer. The catalyst (10-400mg) was added by inverting a sample tube containing the catalyst which then fell into the peroxide solution. The internal pressure of the reactor was kept constant by displacing water in two burettes with volumes of 10ml and 50ml, the pressure was monitored using a pressure gauge to ensure it remained constant. To allow direct measurement of the reaction rate it was necessary to maintain a constant temperature. This was achieved in two ways; the first was to use low concentration peroxide which varied between 1.6-4.7wt%. The second required a temperature-regulated water flow at 20°C to be circulated between the two walls of the reactor.

The apparatus measured the rate of oxygen generation by the quantity of water displaced in the two burettes over time. The low temperature ensured that no gaseous water or peroxide could be

evolved. The results were used to not only identify the rate constant but also assess the order of the reaction. This is the power to which the concentration is raised in the rate equation. In order to compare reactions with the same order the rate constant was divided by the mass of catalyst used to give *k'*. The apparatus used is relatively simple with no expensive instrumentation. However, the drawback to such a set-up is that the displaced volume was assessed visually resulting in a reduced degree of accuracy compared to a conventional oxygen flow meter. Neither the constant pressure nor constant volume (not described) reactors assessed the longevity of the catalyst when exposed to high concentration peroxide. The constant volume reactor reached a peak temperature of 104°C with 50wt% peroxide, so no assessment was made over the full temperature range the catalyst would be expected to work at within a thruster.

Hydrogen peroxide has also been studied in some detail by Lim *et al* in Korea, where they were attempting to develop a HTP gas generator [71]. Experiments were conducted with both a constant volume reactor and catalyst bed. The constant volume reactor is shown in Figure 4-2 and worked by releasing an unknown quantity of weighted catalyst into a receptacle containing 20g of 80% concentration hydrogen peroxide. The catalyst was weighted to ensure it was fully submersed in the peroxide. A pressure supply of approximately 0.1bar was used to release the catalyst but this was sufficiently low to be undetectable in the results. Pressure and temperature were recorded throughout the experiment. However performance was only assessed using pressure, as temperature measurements showed an uneven behaviour.

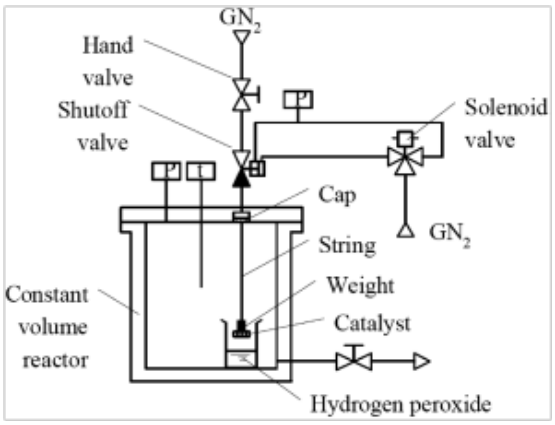

Figure 4-2: Constant volume reactor used by Lim *et al* [71]

The catalyst bed developed utilised a hollow cone spray injector to distribute hydrogen peroxide over a 25mm diameter monolithic catalyst bed. In order for the spray pattern to fully develop the catalyst material was located 25mm downstream of the injector exit plane. In all cases the catalyst material had a length of 50mm. This bolt up assembly was used to assess five catalysts. Results show that although three of these catalysts showed good initial performance within 10s the chamber pressure had dropped significantly, indicating the catalyst reactivity had decayed.

Work conducted by Alta S.p.A and DELTACAT Ltd. used a combination of batch reactor and instrumented thruster tests to assess a range of candidate catalysts. These experiments are reported in [72] with more details of the mathematical model being used to assess the batch reactor results being given in [73]. As well as these methods [73] makes use of 'ad-hoc' experiments for assessing metallic wires. In this context an ad-hoc experiment is one in which no data is collected, with only a visual assessment being made. These ad-hoc experiments consisted of 150mm of 0.1mm diameter metal being shaped into coils with a 5mm diameter. 1ml of peroxide was then dropped onto the coils and the results visually assessed. Tests were conducted both at room temperature and at 50°C. The advantage of such tests is that they are simple, quick and require few resources to conduct. They are a good pre-cursor to more detailed testing and identify candidate catalysts that show no indication of decomposing hydrogen peroxide and hence are not worthy of further investigation.

The constant pressure reactor utilised consisted of a 100ml graduated flask in which was placed 0.85g of the catalyst material, this was then placed within a larger 2L flask. At a known time 5ml of 30% concentration hydrogen peroxide at ambient temperature was placed within the graduated flask. The temperature of both the gas and liquid mixtures were measured continually throughout the experiment. The decomposition products consisting of gaseous peroxide, water and oxygen then passed through a condenser removing the water and peroxide, with the oxygen flow rate being measured using a flow meter. The reaction products were then removed and the apparatus returned to the initial thermal conditions. Liquid temperatures of almost 100°C were recorded. This experiment was repeated 50 times to investigate the variation in catalyst performance over time. The results allowed for several forms of assessment. The first was the time to peak temperature and the variation in temperature over consecutive runs; this provided some indication on both the comparative catalytic reactivity and the longevity of the catalyst. The rate constant was also calculated. This apparatus does not maintain a constant temperature so it was not possible to directly measure the rate constant from the mass flow results. Instead the mathematical model derived in [73] was used to estimate the rate constant. This consisted of initial guesses of the variables *A* and *B* shown in Equation 4-2.

$$k = Ae^{\left(\frac{-B}{RT}\right)} \qquad \text{(Eq. 4-2)}$$

By integrating the 7 differential equations provided by the mathematical model using a 3rd order Runge-Kutta method, a profile for the liquid temperature was generated. An iterative process was then used to match this profile to the measured liquid temperature results and provide the rate constant. The resultant values of *k* compared well to the time to peak temperature for the catalysts tested. Unlike the work conducted by Russo-Sorge and Rusek, the rate constant is indirectly calculated from the liquid temperature profiles. Since the mass flow rate results, although recorded, formed no part of the calculation of the reaction rate, the problems of

pressure variations identified by Russo-Sorge are not encountered. An attempt is made to measure longevity of the catalysts through repeated testing; however this is only done using 30% hydrogen peroxide. This concentration is not high enough to identify mechanical failure due to thermal loads. The effect of catalyst exhaustion may also be accelerated at higher temperature ranges. The second set of experiments used a 5N and 25N instrumented monopropellant thruster [74], the design of these thrusters will be discussed in the following section. Upon testing it was found that the highest performing catalysts from the batch reactor tests failed mechanically when placed within the catalyst bed.

Significant work has been conducted using both “chemical” and “engineering” approaches to assess a range of catalyst characteristics. The chemical approach often results in a straightforward comparative assessment. However, the experimental process can be fraught with difficulties, with care needed to maintain constant experimental conditions often requiring the use of low concentration hydrogen peroxide [70]. Failure to maintain these conditions can lead to rejected results in the case of [69] or the use of complicated mathematical models to calculate the rate constant [73]. Batch reactors are a good form of primary assessment with special note being made of Rusek’s work with a constant catalyst volume batch reactor [57]. The use of ‘ad-hoc’ experimentation has been shown to be an effective way of screening proposed catalysts while requiring minimal resources [73]. However, the lack of quantitative data makes peer assessment difficult relying solely on the interpretation of the results by the author. Positive batch reactor results do not necessarily correlate to good performance in catalyst beds as shown by [71] and [73]. In both these cases batch reactor tests were unable to provide an indication of catalyst life time, resulting in significant resources being invested into the development of catalyst beds for catalysts that showed little promise.

4.3 Experimental Catalyst Bed Research

Each of the methods discussed above assesses the catalyst under conditions unlike those found within a rocket thruster. True performance data under representative operating conditions can only be ascertained through testing within an instrumented catalyst bed. There are three main phases of interest: start-up characteristics, steady-state operation and restart capability. To be considered effective a catalyst must reach steady-state temperature and pressure quickly, with the time taken often referred to as the initiation delay. Once at steady state the temperature and pressure should be consistently high for extended periods of time; an on-orbit thruster would be qualified to operate for tens of thousands if not hundreds of thousands of seconds. Finally, the third phase of interest is catalyst lifetime and the ability of the thruster to be restarted thousands of times. Over time the performance of the catalyst bed will most likely decrease due to mechanical failure or exhaustion. This can lead to inconsistent re-start profiles. The most

demanding operational phase for a catalyst is when it must decompose peroxide from ambient temperature, especially if the bed is partially exhausted. Each of the researchers discussed in this section have taken various approaches in an attempt to investigate some, if not all, of these areas.

The results of Tian *et al* [60] have already been discussed in Chapter 3; these results were gathered using an instrumented thruster. The thruster had an L/D ratio of 1 and a diameter of 26mm resulting in a bed loading of 27.3kg/s/m^2. This is relatively low with many other authors choosing values between 50-100kg/s/m^2. The temperature was measured in the centre of the catalyst bed with pressure being measured in the settling chamber just upstream of the nozzle. This thruster was designed to measure the re-start capability of the iridium on alumina catalyst. A mass flow rate measuring device was used to record the flow rate of 85% HTP into the bed. The thruster used a computer controlled electromagnetic valve to control the flow of HTP into the bed which opened for 10s before being closed. The bed was then subject to spontaneous cooling to return it to its initial conditions. The parameters of interest in this work were steady state chamber pressure, steady state catalyst bed temperature and the initiation delay. Initiation delay was measured as the time taken to reach 10% of steady state pressure value. The precise meaning of initiation delay or even the phrase itself can vary, with other authors referring to it as the time required to reach 90% or even 100% of the steady state chamber pressure or temperature [54,64]. Although in the initial tests the pressure does reach a steady state there is some variation in temperature indicating that the apparatus as a whole may not have reached a truly steady state. The method employed by Tian *et al* does attempt to test the three regimes of the catalyst bed discussed above. The susceptibility of the catalyst to thermal shock is assessed not only at start-up but also when the bed is quenched. The longevity of the catalyst is measured through a repetitive testing cycle with the start-up and restart characteristics clearly quantified. However, the running time of the catalyst is relatively short, only occurring in periods of 10s. Extended length runs would have given a clearer indication of variation of performance with time.

Lee *et al* [63] assessed the performance of silver using six different catalyst configurations within a single catalyst bed; their findings are reported in Chapter 3. The thruster consisted of four main sections; injector, catalyst bed (split into two sections) and nozzle. Both the upper and lower sections of the catalyst bed had a diameter of 25mm and a length of 21.5mm. Three distribution plates were located upstream, downstream and in the middle of the bed in order to prevent the propellant flow channelling. These were 4mm thick and had an open area of 50%. The catalyst bed could be fitted with one of two injectors with the aim of assessing what effect injector orifice diameter had on performance. For all tests a hydrogen peroxide concentrations of between 80-90% was used. Catalyst bed instrumentation consisted of a thermocouple and

pressure transducer located in the upstream part of the bed between the injector and first distribution plate. A second thermocouple and pressure transducer were located in the settling chamber just downstream of the last distribution plate. A flow meter was used to measure the propellant flow rate into the bed with three more pressure transducers in the propellant delivery rig to measure HTP tank and gas feed pressures. Performance comparisons were made on C* efficiency (see Chapter 2 for details) and pressure drop across the bed. The upstream and downstream temperatures were reported but no assessment was made based on these results. Few details are given of the test program employed; the results that are shown indicate short runs in the order of a few seconds. This seems to be long enough to establish a steady-state pressure but the temperature is seen to still be rising when the thruster is shut down. This may be the reason temperature did not form part of the final assessment. The graphical results indicate multiple tests were conducted on each bed; these were not repetitive tests since some variables were changed between runs. The number of tests seemed to vary for different thruster configurations. The tests seemed to lack a structured test program with no total peroxide exposure time being given, so little can be discerned about the longevity of the catalyst.

Purdue University has conducted extensive research into hydrogen peroxide and its catalysts. One such piece of work assessed the effect on catalyst bed performance of various bed loadings and chamber pressures [75]. The silver catalyst bed used in this research had a length of 2.25 inches (57.2mm) and approximate diameter of 1 inch (25.4 mm, estimated by dividing the mass flow rate by the bed loading). A significant quantity of instrumentation allowed a detailed assessment of the catalyst bed performance. Five pressure transducers were distributed along the catalyst bed; these were located at 0, 0.5, 1.0, 1.5 and 2.25 inches from the injector plate. A sixth pressure transducer was situated in the chamber just upstream of the nozzle; all the transducers could measure up to 5000psi. Eleven K-type thermocouples were located at 0.25 inch increments along the bed with a twelfth located in the chamber just upstream of the nozzle. A pneumatic ball valve was used to adjust the flow of 90% HTP into the bed, which was controlled using a cavitating venturi. From the results that are given the open time of the valve is estimated at 10s which was long enough to indicate steady-state characteristics.

The catalyst bed performance was assessed using a wide range of parameters. These included C* efficiency, steady-state temperature, steady-state pressure, pressure drop across the bed and starting transients of both temperature and pressure. The starting transient was defined as the time taken to increase from 5% to 95% of the steady-state parameter. The detailed temperature profile generated by the thermocouple data also allowed the location of the decomposition plane to be estimated. Some of the results indicated a C* efficiency above 100% and as a result an uncertainty analysis was conducted to give confidence to the results. The work has investigated in detail the start-up and steady-state characteristics of the bed. However, no details have been

given about repeat testing and therefore the re-start capability of the bed. The total throughput of the HTP has also not been given and so it is not possible to assess the longevity of the catalyst. Overall an excellent assessment has been made of the performance of the thruster with all uncertainties having been described in detail. The location of instrumentation has provided a detailed insight into the internal performance of the catalyst bed.

Pasini *et al* developed a 5N thruster for assessing the performance of their platinum pellet based catalysts [74]. The design consisted of an injector plate, catalyst bed, distribution/retainer plate and nozzle. The thruster was designed to be easily taken apart so it could be examined and tested with a range of catalysts. To this end all sections were bolted and not welded together. Thruster weight was not a design driver as its role was to test catalysts not to produce a viable flight thruster. This did mean that thermal losses were significant but also consistent for all catalysts tested so direct comparisons could still be made. To ensure complete decomposition the length to diameter (L/D) ratio was 4 and the catalyst bed loading was a conservative 50kg/s/m^2. The significance of these parameters is described within chapter 9. The use and location of instrumentation was critical for accurate measurements that would provide useful comparisons. To that end, for the 5N thruster, pressure was recorded before and after the catalyst bed to allow the pressure drop across the bed to be assessed. A temperature probe located in the converging section of the nozzle provided details on the peroxide decomposition temperature. Finally, a load cell and flow meter were used to measure thrust and the mass flow rate of hydrogen peroxide respectively. In all tests 87.5% HTP was used. The results of these tests showed that the catalysts which were identified as being most suitable in the batch reactor tests undertaken previously failed mechanically when placed within the bed. No attempt was made to measure temperature or pressure variations along the catalyst bed itself. Had it been attempted it would have helped to show the variation in catalyst performance and may have indicated a correlation between catalyst exhaustion and distance from the injector. Catalyst degradation was identified before the re-start capability of the catalyst could be assessed.

The research has shown the importance of catalyst bed testing as a means of assessment. Work by Pasini *et al* [74] has shown that positive laboratory test results do not necessarily lead to successful catalyst bed firings. However catalyst beds are as much of an assessment of the catalyst bed design as they are of the catalyst themselves, with many authors assessing different characteristics making comparisons difficult [54,60,64]. It has been shown that catalyst bed testing does not necessarily assess the longevity and re-start capabilities of the catalyst [63]. However, when used effectively catalyst bed assessment can provide great insight into the internal workings of a catalyst bed and the performance of the catalyst itself [75].

4.4 Summary

This chapter has shown the wide range of hardware used by researchers both in the laboratory and in the field. From this review the author decided to utilise two types of laboratory based equipment for the present work. The first measures the temperature and pressure within a constant volume reactor. This assesses initial performance of candidate catalysts but provides no indication of lifetime. The second is lifetime assessment as a result of mass loss of hydrogen peroxide in a constant pressure environment. This provides a better indication of long-term catalyst performance while minimising the resources required.

After completing the laboratory work the catalysts will be subject to further testing in an instrumented catalyst bed. The design of this bed will be based on the work done by Purdue University [75] with significant quantities of instrumentation equally distributed along the catalyst bed. However, instead of only measuring axial temperature, thermocouples will be placed close to the catalyst bed wall in an attempt to generate a temperature profile along the wall. The test plan will be similar to that used by Tian *et al* [60] with short repeated runs in an attempt to identify changes in catalyst performance due to repeat exposure.

5 Description of experimental Apparatus

This chapter describes the design and operation of four of the five pieces of apparatus developed for this work; the fifth, the engineering breadboard thruster, will be described in chapter 9. This chapter only details the design of the apparatus and not the results; these will be discussed in chapters 7 and 8. As well as providing details on the design this chapter describes the instrumentation used for each experiment.

5.1 Laboratory Hardware

5.1.1 Sealed Reactor

The sealed, constant volume, reactor examined the rates of reaction in terms of rate of change of pressure and temperature, with particular emphasis on assessing the initiation delay. Initiation delay is the time taken for the decomposition to commence once the HTP comes into contact with the catalyst. For thruster applications it is normally defined in terms of the time taken to reach a percentage of the steady state temperature or pressure. This apparatus has been designed to inject impulsively a small quantity (3 cc) of 87.5wt% HTP into a decomposition vessel which exhausts into a sealed main chamber. The aim was to identify the start-up characteristics of the catalysts and quantitatively assess the catalysts' ability to decompose hydrogen peroxide. The sealed reactor was not designed to capture the true thermodynamic decomposition temperature. The reactor was not insulated in any way and its thermal capacity was very large. Its purpose was to allow performance comparisons to be made between the various candidate catalysts.

The sealed reactor developed was a combination of a bomb calorimeter and batch reactor in both its design and operation. The rig can be separated into four main sections; the injection mechanism, decomposition vessel, main chamber and gas exhaustion. To ensure compatibility with hydrogen peroxide and its products the whole assembly is made from grade 316 stainless steel, and sealed with appropriately sized Viton O-rings.

The injection system comprised a delivery tank for holding the peroxide, a solenoid valve, and an injector plate which was connected to the top of the decomposition vessel. A nitrogen supply was used to force the hydrogen peroxide through the solenoid valve into the vessel. To minimise the delay time between opening the solenoid valve and the peroxide coming into contact with the catalyst the valve was screwed directly onto the injector plate as shown in Figure 5-1. The delivery tank was pressurised with nitrogen to a pressure of 10bar absolute for ceramic pellet and metallic foam supported catalysts, and 1.5barA for metallic gauzes. 10bar

was selected to ensure the complete injection of the peroxide. It was thought that the decomposition products generated by a very reactive catalyst may cause a local increase in pressure. If this was high enough and the injection pressure was too low all the peroxide may not impulsively enter the decomposition vessel affecting the results. The lower delivery pressure used for the gauzes reduced the likelihood of the gauze being displaced within the reactor. The delivery pressure was measured using a pressure transducer (designated tank pressure), and adjusted by use of a needle valve. If a dangerous over-pressurisation did occur a safety valve opened venting the nitrogen gas. Once set, the nitrogen pressure regulator was then closed to stop the nitrogen being replenished. When opened the solenoid valve remained open for the duration of the experiment. In the case of ceramic and foam-based catalysts the test duration was set to 60s however, complete decomposition normally occurred within 15s. Due to the slower reaction of the gauze-based catalysts the test time was extended to 180s.

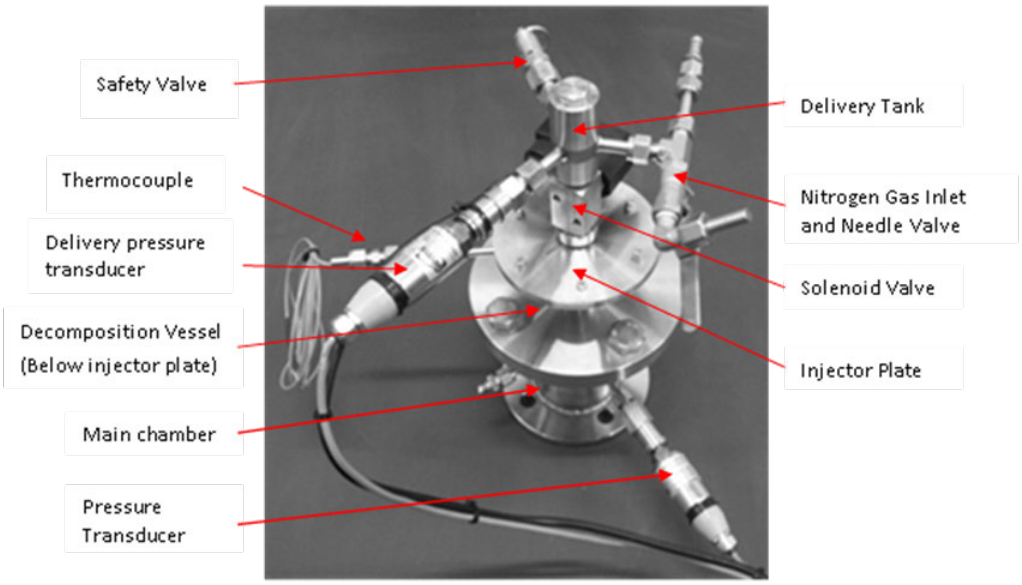

Figure 5-1: Photo of assembled injector plate, decomposition vessel & main chamber

When the solenoid valve opened the HTP settled at the base of a small decomposition vessel containing the catalyst. The decomposition vessel itself had a diameter of 16 mm and a length of 48 mm; this gave a length to diameter ratio of 3. Much thought was given to deciding how best to compare the performance of the ceramic pellets with that of the metallic gauzes and foams. Consideration was placed on normalising all of the results according to the surface area of the catalyst material. However, the BET system for measuring surface area per unit mass does not provide accurate results with very small surface areas such as those associated with metallic gauzes. Moreover, such a method of normalisation disregards the actual volume occupied in a typical catalyst bed. It has been identified by [57] that, from a practical standpoint, this is considered an important parameter for rocket designers. As such this volume was considered by the author to be the relevant control in the context of this investigation. Accordingly, catalyst material was positioned at the bottom of the decomposition vessel to give an equivalent 'occupied bed length' of approximately 3.2 mm.

Initially the void above the pellets and foams was filled with an inert, unimpregnated material which served to mechanically “lock” the catalyst at the bottom of the decomposition vessel. However, it was found that the inclusion of this material led to significant variations in the results gathered. Further investigation identified two problems. Firstly, when injected under pressure, the hydrogen peroxide did not produce a single jet but an atomised spray which coated the walls of the vessel as well as impacting the catalyst. Therefore contact time between the HTP and the active material varied depending on the time taken for the fluid to run down the walls of the reactor. Secondly the inert material (glass beads) acted as a semi permeable barrier between the catalyst and peroxide, and the time taken to pass through the glass beads varied from run to run. A solution to these problems was found in the form of a metallic insert which secured the catalyst and guided the HTP directly to the active material. A schematic of the decomposition chamber can be found in Figure 5-2.

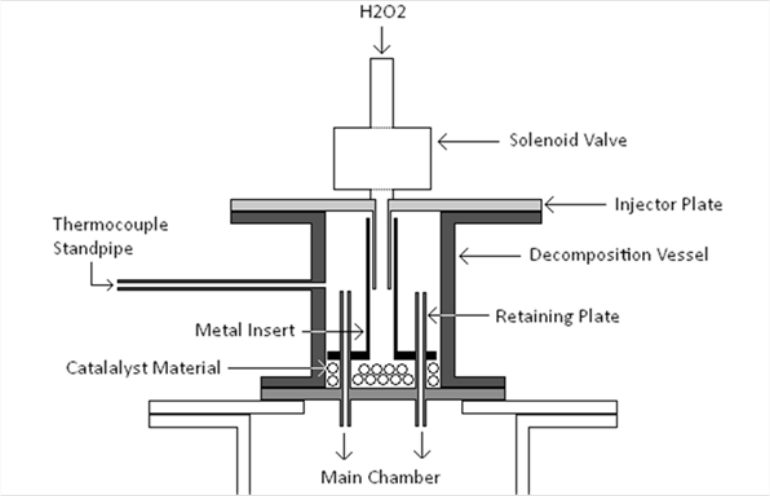

Figure 5-2: Schematic of sealed reactor decomposition vessel

Even with this modification the relatively low temperatures achieved using the gauze catalysts, gave poor and difficult to interpret results. Consequently the metallic insert was removed, the delivery pressure lowered and a flow constrictor added to reduce the velocity of the impinging HTP jet. Visual inspection after these tests indicated that these steps were sufficient to minimise gauze displacement. However, this did mean that direct comparison between gauzes and the other catalysts tested was not possible. The reaction vessel was sealed at the bottom by means of a retainer plate with two stainless steel exhaust tubes; this is shown along with the metal insert in Figure 5-3. In this way the HTP is retained within the decomposition vessel and only the gaseous decomposition products can flow upwards towards the two stainless steel vent tubes and enter the main chamber. The whole assembly was bolted to the main chamber in which pressure measurements were taken.

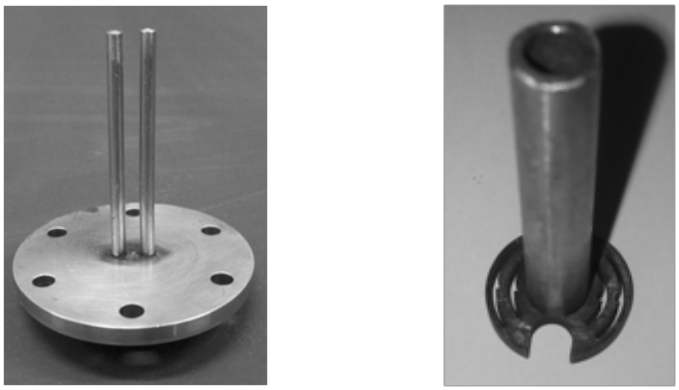

Figure 5-3: Sealed reactor retainer plate and metal insert

The main chamber was a 5 mm thick stainless steel container with an internal diameter of 68mm and an internal length of 132 mm. A mathematical model was generated to identify the maximum pressure the reactor could be exposed to. It was found that there was a safety factor of 10 even if the reactor temperature was 800°C. This was higher than the theoretical maximum decomposition temperature of 87.5wt% HTP. Due to the thermal mass of the system the predicted temperature after decomposition was less than 200°C. Three standpipes were welded to the reactor, one measured pressure (designated reactor pressure) and the second was used to release the exhaust gases through a condenser at the end of the experiment. The third was capped but provided access for additional instrumentation as required.

To return the apparatus to its initial conditions it was necessary to exhaust the gases to atmosphere at the end of the experiment. Due to the high oxygen content of the hot gases there was a concern over material compatibility with the materials used in the manual gas release valve. The introduction of a condenser to cool these gases before they were exhausted removed the material compatibility issue. A stainless steel condensing pipe passed through approximately 1L of water at ambient temperature to cool the gases. It was necessary to minimise the length of the condenser while still cooling the gases to a safe temperature. The gas could enter the condenser while the experiment was in progress so any cooling of the gas resulted in a reduction in overall pressure affecting the results collected. As long as the volume of the pipe was kept small the effect on the measurements were negligible. Heat transfer calculations were undertaken to identify the minimum length and therefore minimum internal volume of the cooling pipe. The calculations showed a pipe with a 2 mm internal diameter and 1.2 m length contained less than 0.8% of the overall volume. This had an insignificant influence on the results gathered while still cooling the gases to almost ambient conditions.

Steps were taken to ensure that the samples to be tested are free of contamination and that all experimentation was repeatable. As well as the procedures laid out in Table 5-1 it was necessary to clean the apparatus carefully before a new sample was tested. The procedure does not include the datum run which was conducted before the main experimentation program began.

Step No.	Description
1	Fill condenser with water ensuring coil is covered
2	Load catalyst
3	Load hydrogen peroxide
4	Pressurise oxidant tank
5	Initiate data acquisition and control software
6	Commence experiment and acquire data
7	Vent gaseous products

Table 5-1: Simplified operating procedure for sealed reactor

5.1.2 Life-Time Mass Loss

The sealed reactor made no attempt to quantify lifetime or survivability; as a result a second set of apparatus was designed to further assess these qualities. To maximise the effectiveness of this rig it was both simple and open, allowing the operator to visually assess the catalyst's structural integrity as well as acquiring data for later quantitative analysis.

The life-time mass loss or LTML equipment measured reactivity and lifetime using a mass loss technique. The apparatus was designed to impulsively introduce a small sample of catalyst, of known dimensions, into a relatively large quantity (10g) of 87.5% HTP within a glass vessel. The result was an increase in peroxide temperature and a reduction in mass as steam, peroxide vapour and oxygen were generated and allowed to escape. An additional aim of this apparatus was to investigate lifetime while utilising the minimum amount of peroxide possible. This was the key driver in deciding both the quantity of HTP and amount of catalyst to be used. Ideally a larger quantity of catalyst would have been assessed to allow for sample variations; however this would have required considerably more HTP in order to see performance degradation in a reasonable number of runs.

The experimental set-up is shown in Figure 5-4. This simple apparatus consisted of a round bottomed flask into which was placed ten grams (± 0.02g) of 87.5% hydrogen peroxide as measured by a mass balance accurate to 0.01g. Preliminary testing was conducted using a conical flask but it was found that towards the end of the experiment the catalyst lost contact with the peroxide.

A thermocouple was also placed within the flask so that its tip lay within the pool of hydrogen peroxide. This was used to record the temperature throughout the run and ensure a consistent start temperature of 22°C ± 0.5°C. In order for the mass results not to be affected the

thermocouple was supported using a retort stand. If the location of the thermocouple was too low the highly energetic decomposition may displace the 0.5mm diameter thermocouple causing it to contact the side of the flask affecting the result.

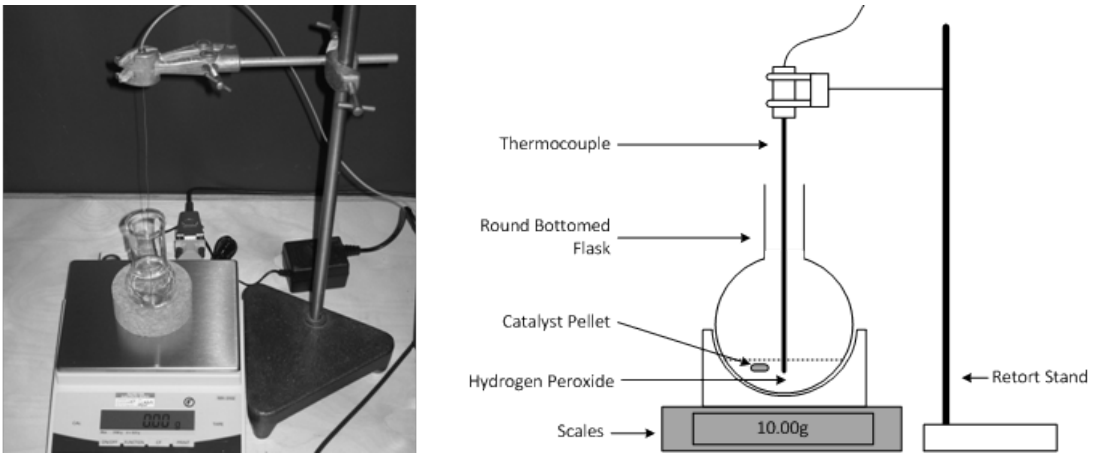

Figure 5-4: LTML experimental set-up, Left: Photograph, Right: Schematic

Much thought was given to the quantity of catalysts to use, due to the additional aims discussed above it was decided the smallest amount possible of catalyst should be used. This meant one ceramic pellet or one rectangle or disc of metallic foam. A fixed mass or smaller volume would have required particles of catalysts to be broken apart, immediately nullifying any structural integrity analysis.

When the experiment was initiated the catalyst was dropped into the flask with the resultant change in mass used to signify the start of the experiment. The experiment was considered to have concluded when one of two criteria was met. The first was whether 90% of the original mass had been lost due to the formation of decomposition products. The target of 90% mass loss was chosen to allow for the added weight of the catalyst and any small droplets of peroxide or water vapour that had condensed around the mouth of the flask and were, therefore, no longer in intimate contact with the catalyst. The second criterion was a time limit of 600s; the experiment was stopped after this time regardless of whether or not the 90% mass loss criterion had been met. After the experiment was completed the catalyst material was removed and allowed to cool in a clean container.

The lifetime of the catalyst was assessed by repeating the above experiment with the same sample of catalyst material until either a run limit of 10 had been reached or the catalyst failed to decompose 10% of the original mass in 600s. If the latter occurred the catalyst was assumed to be exhausted. After each run the catalyst was visually inspected to identify if any structural degradation had occurred; if found, the catalyst was rejected from any further testing.

These two pieces of laboratory apparatus provided an assessment of the whole lifecycle of the catalyst; with the sealed reactor assessing initial performance and the life-time mass loss apparatus providing details on catalyst longevity and structural survivability. The limitations of the hardware have been described but these have mainly been driven by additional requirements negatively influencing the design of the apparatus (such as the catalyst sample size in the LTML hardware).

5.2 Catalyst Bed Hardware

Laboratory testing allowed for the down selection of catalysts but true performance could only be assessed within an instrumented catalyst bed. For this work two beds were developed; the first of these, the preliminary catalyst bed (pICB), was developed early on in the project. This bed was used to provide key design parameters for the Engineering Breadboard thruster discussed in Chapter 9. There were problems with both the catalyst bed design and the test program implemented; as a result the pICB was only subject to very limited testing. Due to its limited use the design of the bed has only been summarised below. Further details can be found in Appendix C or the conference paper detailing this hardware presented at the AIAA Joint Propulsion Conference in July 2011 [76].

The majority of testing was conducted with the second of these catalyst beds; the highly instrumented catalyst bed (hICB). The lessons learnt from the pICB were used to help redesign the hICB to provide large quantities of high quality data. This along with a much more structured test program allowed for better assessment of catalyst performance.

5.2.1 pICB design and instrumentation

The preliminary instrumented catalyst bed was a relatively simple device consisting of an injection assembly, catalyst bed (in which the decomposition occurs), retainer plate and nozzle. The flow of peroxide into the bed was controlled by a solenoid flow control valve (FCV) upstream of the injector plate and measured using a volumetric flow meter. The bed was made from grade 316 stainless steel throughout to avoid any material compatibility issues with either the peroxide or the catalyst samples. The bolt-up design used flanges between the components to facilitate quick assembly and allow multiple catalysts to be tested. As with other experimental apparatus the catalyst bed was passivated with acetone before being placed in a 10% nitric acid bath for 10 minutes to removes any contamination.

The injector assembly consisted of a single 0.5mm hole and connected directly to the solenoid valve upstream. It was designed to maintain a 3 bar pressure drop at a design flow rate of 3.5g/s.

The pressure drop decouples any pressure oscillations due to transient effects inside the catalyst bed from the upstream supply pressure. Without this, pressure spikes could limit the flow of peroxide into the bed and build into high frequency oscillations known as chugging. Sealing between the injector and main chamber was achieved through the use of a Viton O-ring.

The catalyst bed itself had a diameter of 16mm and a length of 104 mm which led to an L/D of 6.5 and a bed loading of 17.6 kg/s/m^2. The low bed loading reduced the likelihood of the catalyst becoming quenched by distributing the peroxide over a larger cross-section. The large L/D reduced the possibility of the catalyst bed becoming depleted by extending its length. This allowed data to be collected over an extended period of time. Chapter 9 includes a more in-depth discussion on these two parameters. Due to the high temperatures at the downstream end of the bed a copper C-ring was used in place of a Viton O-ring to provide sealing between the bed and retainer plate. Pressure and temperature measurements were made using nine standpipes which were located along the length of the catalyst bed. The majority of the temperature measurements were made on the axis but two were made close to the wall of the bed. It was hoped that these radial measurements, could be used to give a deeper insight into the effect of channelling by producing a temperature profile along the wall.

A retainer plate was used to keep all the catalyst within the bed. If any was to break off and clog the nozzle the pressure would increase quickly and could lead to a dangerous over-pressurisation. The maximum open width was limited to 2mm to ensure none of the catalyst particles were able to pass through. The retainer plate was mated to a simple conical nozzle. The throat diameter of 1.6mm was calculated using a mathematical model based on isentropic flow assumptions. Temperature was also measured in the nozzle however since no attempt was made to minimise mass the resultant temperature measured in the settling chamber was significantly lower than can be expected in a real thruster. A schematic of the catalyst bed is provided in Figure 5-5.

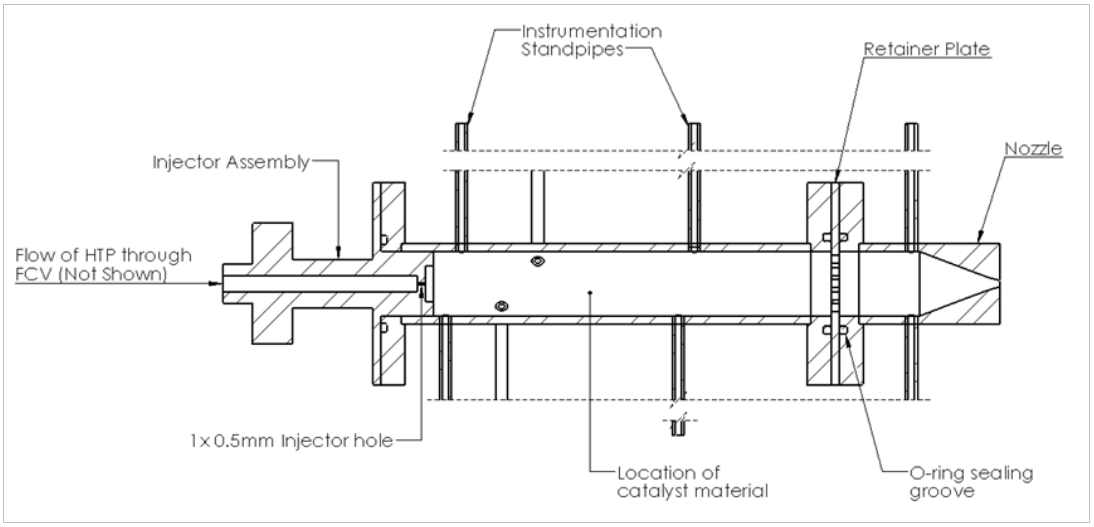

Figure 5-5: Schematic of pICB

After testing significant hardware improvements were identified. Firstly, it was noted that catalyst bed loading was significantly below that of the EBB thruster (17.6 kg/s/m^2 Vs. 50 kg/s/m^2). The low flow rate would reduce quenching and may give an incorrect impression of high catalyst performance. Secondly, the use of a single holed injector was a poor choice but dictated by the required pressure drop and low flow rate. A showerhead injector would have improved the distribution of peroxide into the bed and reduced quenching. Finally, both the location and quantity of instrumentation were not optimised which limited the conclusions that could be drawn from the results. The quantity of instrumentation was dictated by the limited number of available DAQ channels with the optimum location being inferred from laboratory results. From the catalyst performance within the Sealed Reactor it was expected that the majority of decomposition would occur in the upstream half of the catalyst bed so the majority of the instrumentation was placed in this section. However, analyses of the results have shown significant decomposition in the downstream portion of the bed.

In addition to problems with the hardware the test program could also be improved. The limited number of runs conducted within the pICB had not allowed a detailed analysis of start-up characteristics or catalyst lifetime to be made. This problem has been exacerbated by the pre-heating methodology which did not result in uniform initial conditions for all experiments conducted. Finally the variable run time resulted in the catalyst being exposed to differing quantities of HTP as well as not focusing on the most challenging phase of operation; low temperature start-up. In view of these problems the pICB was mothballed in favour of the highly instrumented catalyst bed which attempted to rectify these problems.

5.2.2 Highly instrumented catalyst bed design

The design logic differs slightly to that of the pICB so this section aims to summarise the required design changes. The focus of the hICB design was the location and quantity of instrumentation; this dictated both the injector and retainer plate design. The catalyst bed diameter was maintained at 16mm and the working length reduced to 96mm resulting in an L/D ratio of 6. The bed loading was increased to 70kg/m^2 in an attempt to accelerate catalyst degradation. To achieve this loading a mass flow rate of approximately 14g/s was required. The delivery pressure was adjusted for each catalyst to maintain this flow rate. A total of twenty-one standpipes were attached to the catalyst bed in groups of three located at each L/D value (including an L/D of zero), as shown in Figure 5-6. To facilitate manufacture each set of standpipes was offset by 60° with reference to the previous set to maximise the separation distance between them. At each location axial temperature, pressure and radial temperature (set 1mm in from the wall) were measured. Sealing was achieved at the upstream end using Viton o-rings and at the downstream end with klingersil gaskets. The gaskets were replaced regularly as

the temperatures experienced at that location were above their recommended operating temperature. In order for the standpipes to be welded to the catalyst bed a minimum distance (for the weld head) was required between the standpipes and the flanges used to bolt the catalyst bed to the other thruster components. This has resulted in the need for the injector and retainer assembly to protrude into the bed by 13.5mm at each end.

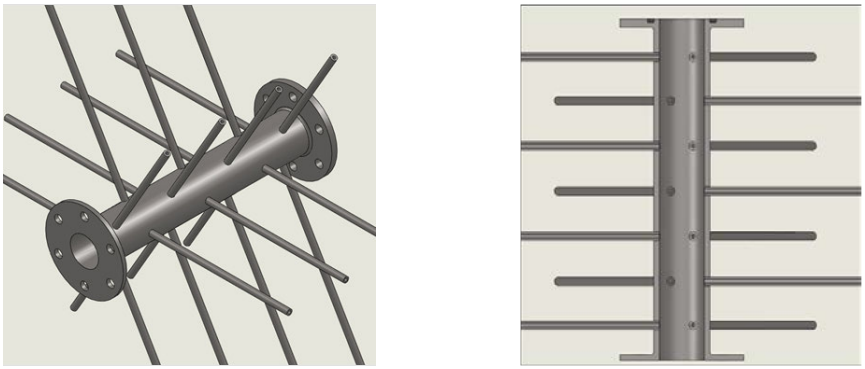

Figure 5-6: CAD model of hICB catalyst bed

The injector assembly consisted of two components; a shower-head type injector plate with 4 holes and an injector manifold. The manifold connected to the upstream propellant delivery rig and also allowed propellant pressure and temperature to be measured. As with the preliminary catalyst bed the injector was designed to induce a minimum pressure drop of 3bar at a 17bar delivery pressure and 14g/s flow rate. The new design and higher flow rate also allowed for a more even distribution of hydrogen peroxide over the surface of the catalyst material by utilising 4-off 0.4mm holes rather than a single 0.5mm hole. This reduced the likeliness of initial catalyst quenching by distributing the HTP more evenly. The injector plate and completed assembly positioned within the catalyst bed can be seen in Figure 5-7. Sealing between the two components was achieved using a Viton O-ring.

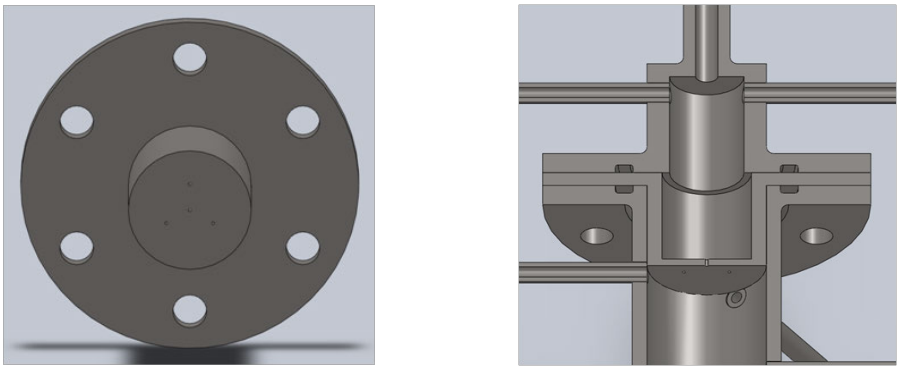

Figure 5-7: CAD model of hICB. Left: injector assembly, Right: injector integration

The retainer plate located at the downstream end of the catalyst bed also needed to be modified to integrate successfully into the new catalyst bed. The slot design was replaced with drilled holes as shown in Figure 5-8; although this reduced open area ratio it simplified and accelerated manufacture. The minimum separation between holes was 1mm to ensure structural integrity.

To maximise the open area the diameter of the central hole was increased to 2.5mm with all other holes having a 1.5mm diameter. Due to the reduced size of the ceria pellets used as a catalyst support, a disc of nickel foam was placed upstream of the retainer to ensure none of the catalyst was ejected from the bed. As with the injector the retainer plate extended 13.5mm into the catalyst bed.

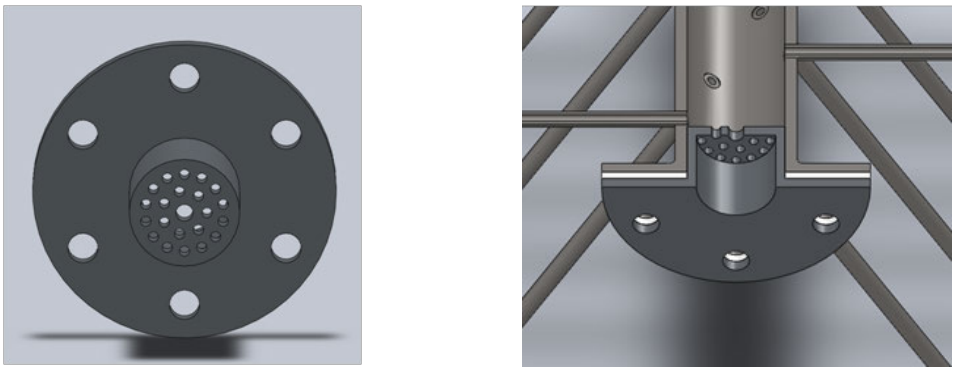

Figure 5-8: CAD model of hICB. Left: retainer plate, Right: Retainer integration

The nozzle only required minor modifications to make it suitable for use within the hICB. Firstly, the original groove for the copper c-ring was removed as sealing would now be achieved with a klingersil gasket. To allow for the increased flow rate the nozzle throat diameter was increased from 1.6mm to 3.55mm, this was calculated using the mathematical model described earlier. The final modification was the addition of a third standpipe to allow both pressure and radial and axial temperature measurements in the nozzle settling chamber. Figure 5-9 provides a schematic of the highly instrumented catalyst bed.

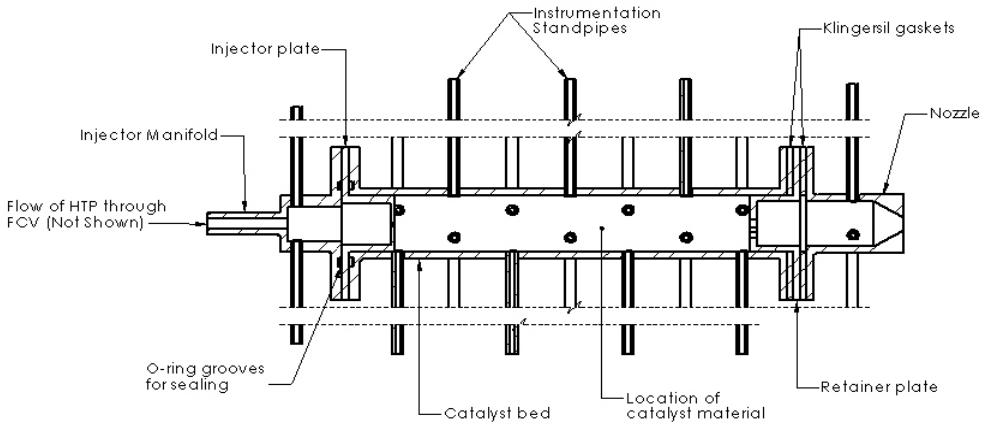

Figure 5-9: Schematic of hICB

The catalyst bed was passivated using the method described for both the sealed reactor and pICB. This ensured no short term material compatibility issues between the catalyst bed and HTP. The testing regime will be discussed in Chapter 8

5.3 Instrumentation and Uncertainty

This section covers the instrumentation used for the various rigs described above. The same types of instrumentation were used throughout; however, the hardware used to capture this data was expanded as the work progressed. The data acquisition (DAQ) hardware was supplied by National Instruments (NI) and based on the CompactDAQ range of products.

The following instrumentation was used throughout the work with the rate of acquisition dependant on the type of experiment and DAQ hardware available.

- Temperature measurements were made using 0.5mm stainless steel sheathed k-type thermocouples. The accuracy was dependent on temperature and varied between ±0.75% at 200°C to ±0.4% at 800°C.
- Pressure measurements were made with GEMS Sensors 0-25barA pressure transducers with a 0-5V output. They have a ±0.25% error of full scale (0.0625bar) and an additional thermal error band of 1.5% between -20°C and 80°C.
- Mass flow rate measurements were made with a Titan 903 volumetric flow. This used a Pelton wheel to generate a pulse frequency proportional to the flow rate with an accuracy of ±1.39%. A formula was then used to convert the flow rate from volume to mass. Since the Pelton wheel must accelerate to match the flow this type of design can struggle to capture short transients, like those associated with pulsed flow.

The remainder of this section describes the acquisition rate and accuracy of the measurements taken with each rig. It will be seen in later chapters that even so some instruments acquire data more rapidly or more accurately than others, in the context of the experiment, they made not provide the most appropriate way of quantifying performance.

5.3.1 Sealed Reactor

The sealed reactor recorded measurements from two pressure transducers and one thermocouple. Both pressure transducers were recorded at 100Hz using a 0-10V NI module with an accuracy of ±0.06%. Due to their location the PT's were not subject to any significant temperature variation so the total error is approximately ±0.068bar. Temperature measurements were acquired by a dedicated thermocouple module with an accuracy of ±1.50°C. For the range of interest (~200°C) the resulting total error was ±3.0°C. Unfortunately the acquisition rate was limited by the DAQ module to only 14Hz. For very high performing catalysts the slow acquisition rate caused the values to vary by over 100°C between successive readings.

5.3.2 Life Time Mass Loss

For the LTML apparatus temperature and mass were recorded. The scales used were Fisher Scientific MH-3102 (supplied by Denver Instruments) with a 3100g capacity and 0.01g accuracy. Due to the limited output rate of the scales the acquisition rate of both the scales and thermocouple was limited to 5Hz.

5.3.3 pICB

In the pICB, as well as recording temperatures, pressures and flow rate the NI hardware controlled the actuation of the FCV. The pICB had a total of eleven instrumentation standpipes; nine were located in the catalyst bed with the other two located in the nozzle. These recorded a combination of temperature and pressure. However data were only collected from ten of these due to a limitation in DAQ inputs. The types and location of the instrumentation are detailed in Table 5-2. The temperature was measured both on axis (axial measurements) and 2mm from the bed wall (radial measurements).

The flow meter was placed approximately 2m upstream of the FCV and as a result there was a time delay between the propellant being detected and it flowing through the FCV. This led to a drop in flow rate before catalyst bed pressure at the end of the run. The pulse train was recorded directly by the DAQ and post-processed into a mass flow rate. It was therefore necessary to set the acquisition rate to at least 400Hz to satisfy the Nyquist criterion. Although pressure and flow rate were recorded at minimum of 400Hz, temperature measurements were limited to 3.5Hz.

Standpipe #	Instrument	Distance from Injector (mm)
SP1	Pressure transducer	10
SP2	Thermocouple - Axial	14
SP3	Thermocouple - Axial	21
SP4	Thermocouple - Axial	24
SP5	Thermocouple - Axial	33
SP6a	Thermocouple - Radial	43
SP6b	Thermocouple - Axial	43
SP7	Thermocouple - Radial	68
SP8	Pressure transducer	72
SP9a	Thermocouple - Axial	124 (located in the nozzle)

Table 5-2: pICB Instrumentation Distribution

5.3.4 hICB

Although the hICB and pICB recorded and controlled the same parameters the quantity of instrumentation within the hICB was significantly greater. The DAQ hardware needed to be expanded to accommodate this increase in instrumentation; the distribution of which is summarised in Table 5-3. In the table, axial thermocouple measurements were those taken on the axis of the bed and radial measurements were taken 1mm from the bed wall. All but the injector thermocouple were connected to a new temperature module which increased the available acquisition rate from 3.5Hz to 50Hz with an accuracy, at 700°C, of ±5.0°C.

To calibrate the ten pressure transducers connected to the hICB, the nozzle was replaced with a blanking plate, essentially turning the catalyst bed into a pressure vessel. The pressure was then incrementally increased with nitrogen gas and the results used to update the equations used to calculate pressure. During testing pressure readings were found to be highly inaccurate. Although post-testing electrical check-out tests were conducted, no failure of the hardware was found. It is thought that localised decomposition within the pressure standpipes caused heating of the PT's stainless steel diaphragm resulting in inaccurate readings. It is likely that the temperature encountered was higher than the maximum operating temperature of the pressure transducer.

To improve the quality of the mass flow rate data the output from the volumetric flow meter was fed into an Omega frequency to voltage converter with ±0.2% accuracy. This was calibrated to a maximum flow rate of approximately 30g/s. One drawback with this hardware was the initial delay in generating data. The converter had to receive between 50 and 100 pulses to calculate the frequency the resulting time delay was shown experimentally to be less than 100ms. The converter allowed the acquisition rate for the flow meter and pressure transducers to be reduced from 500Hz to 200Hz, the thermocouples were limited to 50Hz.

The DAQ hardware controlled both the flow control valve (FCV) and the electrical heating element coiled around the outside of the bed. This allowed for a repeatable run length and consistent initial conditions. Additional manually actuated solenoid valves allowed the system to be made safe if a software failure occurred.

Location	Measurement Type	Position Relative to Injector Face
Propellant delivery rig	Pressure	-
	Mass flow rate	
Injector manifold	Pressure	-27 mm
	Temperature	
Catalyst Bed – L/D 0	Pressure	0 mm
	Temperature – Axial	
	Temperature – Radial	
Catalyst Bed – L/D 1	Pressure	16 mm
	Temperature – Axial	
	Temperature – Radial	
Catalyst Bed – L/D 2	Pressure	32 mm
	Temperature – Axial	
	Temperature – Radial	
Catalyst Bed – L/D 3	Pressure	48 mm
	Temperature – Axial	
	Temperature – Radial	
Catalyst Bed – L/D 4	Pressure	64 mm
	Temperature – Axial	
	Temperature – Radial	
Catalyst Bed – L/D 5	Pressure	80 mm
	Temperature – Axial	
	Temperature – Radial	
Catalyst Bed – L/D 6	Pressure	96 mm
	Temperature – Axial	
	Temperature – Radial	
Nozzle (After retainer plate)	Pressure	126.5 mm
	Temperature – Axial	
	Temperature – Radial	

Table 5-3: hICB Instrumentation Distribution

6 Catalyst Procurement and Manufacture

The research conducted in chapter 3 identified viable catalysts in three main forms, namely ceramic pellets, metallic gauze and metallic foam. All the gauze catalysts and some of the ceramic catalysts have been procured from a range of suppliers. The remainder of the catalysts were manufactured in-house. As well as providing procurement details this chapter describes the development of these catalysts and how chemical characterisation was used to refine the manufacturing methods used.

6.1 Catalyst Procurement

6.1.1 Metallic Gauze Procurement & Preparation

In order to facilitate the procurement the author undertook market research into the three main suppliers of chemicals and chemistry apparatus in the UK. The search was limited to gauzes that have shown some promise in previous investigations; namely silver, palladium, platinum, iridium, ruthenium and nickel [57,58,59]. The results of the market research can be found in Appendix B. The research showed that the gauzes were available in a variety of mesh and wire sizes which made direct comparisons difficult. Two types of catalyst, silver and platinum, were available in a range of different mesh sizes and wire diameters.

Table 6-1 summarises the gauze procurement; as can be seen the silver gauze chosen had a mesh size of 20 and a wire diameter of 0.356mm. This corresponds to gauze specifications used by a number of other authors [7,64,65,66]. The platinum gauze was chosen to be as similar to the silver gauze as possible with a wire diameter sufficiently large to guarantee the structural integrity of the gauze.

Catalyst Name	Metal (wt%)	Supplier Name	Item No.	Mesh size	Wire Ø (mm)
Ag-Gz-20	Ag (99.99)	Alfa Aesar	44449	20	0.3560
Pt-Gz-45	Pt (99.9)	Alfa Aesar	41814	45	0.1980
Pd/Ni-Gz-50	Pd:Ni (95:5)	Alfa Aesar	44698	50	0.1578
Pt/Ir-Gz-150	Pt:Ir (90:10)	Alfa Aesar	40934	150	0.0430
Pt/Rh-Gz-80	Pt:Rh (90:10)	Alfa Aesar	12217	80	0.0760
Pt/Rh/Pd-Gz-80	Pt:Rh:Pd (90:5:5)	Alfa Aesar	12216	80	0.0760

Table 6-1: Summary of gauze procurement

It was not possible to procure gauzes with an identical mesh size and wire diameter. For very fine wire diameters, such as Pt/Ir-Gz-150, structural integrity was a concern. Unfortunately it

was not possible to procure this metal combination in a larger wire diameter. In laboratory experiments which required a fixed volume of catalyst a mathematical model was generated, this can be found in Appendix A. This was used to identify the number of disks required for the chosen volume and the resultant mass and surface area of the catalyst. It was not possible to accurately cut these materials to the specific contours required to fit the sealed reactor detailed in chapter 5. As a result a passivated pair of surgical scissors (placed in a 10% nitric acid bath for 10 minutes) was used to cut the equivalent mass of catalyst to be tested.

The metallic gauzes also underwent a heat treatment to identify what effect, if any, this had on their performance (as measured within the sealed reactor). Detailed assessment of the catalyst would only take place if it was found that the performance of these catalysts were significantly different from the non-heat treated samples. The samples were placed within the furnace at 500°C for two hours and then removed to cool quickly. Mass measurements were taken before and after the sample was placed in the furnace, these results can be found in Table 6-2. The resolution of the balance used was 0.01g

Catalyst Name	Metal	Pre-treatment weight (g)	Post-treatment weight (g)
Ag-Gz-20-HT	Silver	3.22	3.22
Pt-Gz-45-HT	Platinum	4.04	4.03
Pd/Ni-Gz-50-HT	Palladium : Nickel	2.35	2.36
Pt/Ir-Gz-150-HT	Platinum : Iridium	2.52	2.52
Pt/Rh-Gz-80-HT	Platinum : Rhodium	2.48	2.48
Pt/Rh/Pd-Gz-80-HT	Platinum : Rhodium : Palladium	2.53	2.52

Table 6-2: Mass of gauze catalysts before and after heat treatment

It can be seen that the mass changes before and after heat treatment were negligibly small. Visually the palladium/nickel had become much darker with the silver becoming white. This is in accordance with the observations made by Jonker *et* al [77] after a similar heat treatment. No visual change was identified in any of the other catalysts

6.1.2 Ceramic Pellet Procurement

Although a range of ceramic catalysts have been manufactured in-house, a wide range of ceramic catalysts have also been procured for testing. The information provided here gives details of these procured catalysts. The manufacturing procedure is covered in more detail later in this chapter.

Catalyst Name	Description	Supplier	Item No.
0.5%Pd-Al	Palladium on alumina 0.5wt%, 3.2 mm, pellets	Sigma Aldrich	205745
0.5%Ru-Al	Ruthenium on alumina 0.5wt%, 3.2mm, pellets	Sigma Aldrich	206199
2%Ru-Al	Ruthenium on alumina: 2wt%, 3.2mm, pellets	Alfa Aesar	44575
0.5%Pt-Al	Platinum on alumina: 0.5wt%, 3.2 mm, pellets	Sigma Aldrich	206016
1%Pt-Al	Platinum on alumina: 1wt%, 3.2 mm, pellets	Sigma Aldrich	232114
5%Pt-Al	Platinum on alumina: 5wt%, 3.2 mm, pellets	Elemental Microanalysis	03002262
1%Ir-Al	Iridium on alumina: 1wt%, 5 mm, spheres	Alfa Aesar	45570
3%Ag-Al	Silver on alumina: 3-4%, 2-4 mm, spheres	Alfa Aesar	45034

Table 6-3: Summary of pellet procurement

As with the metallic gauzes a market review of ceramic catalysts was undertaken. It was identified that there was a greater consistency in the dimensions of available ceramic catalysts than with gauzes. It was generally found that the ceramic catalysts came in the form of pellets or spheres with little variation from pellet to pellet as can be seen in Table 6-3. The percentage loading is given with respect to the weight of the active phase.

Catalysts have been manufactured using seven different base (catalyst support) materials. Several of these have been tested as part of work done by other authors [52,57,58]. The seven bases are shown in Table 6-4, for ease these will hereafter be referred to by their base name. Two of the materials are alumina in the same form (Al2O3 and Al2O3-γ), one has been identified as being in the gamma phase and the other is of unknown phase. These have been chosen to ascertain if the methods used to manufacture the base materials results in a significant difference to the performance of the impregnated catalyst. Céramiques Techniques Industrielles (CTI) have also provided two forms of their ceria catalyst; both have been manufactured in the same way however CeO2-U has been graded to provide a consistent length.

Base Name	Manufacturer	Product description	Product no.
Al2O3	Alfa Aesar	Aluminium oxide, catalyst support, high surface area	43855
Al2O3-γ	Alfa Aesar	Aluminium oxide, gamma-phase, catalyst support, high surface area, bimodal	43832
ZrO2	Alfa Aesar	Zirconium oxide, catalyst support	43815
TiO2	Alfa Aesar	Titanium (VI) Oxide, catalyst support	44429
CeO2	CTI	Cerium oxide, catalyst support	-
CeO2/U	CTI	Cerium oxide, uniform length	-
Al2O3/Q	CTI	Aluminium oxide, quadrilobed	-

Table 6-4: Details of the catalyst supports used

It was identified that there was some variation in the dimensions of these pellets; both in reference to each other but also when compared to themselves. The average physical dimensions are provided in Table 6-5, with the sample (i.e. n-1 denominator) standard deviation (STDV) being provided to indicate the consistency of the dimensions. A random sample of 10 pellets has been used to provide these dimensions. In all cases the diameter of the pellets shows high consistency; however there is significant variation in the lengths. This high level of variation may result in a reduced packing density when the pellets are packed into the catalyst bed.

Base Name	Average Diameter /mm	Diameter STDV /mm	Average Length /mm	Length STDV /mm
Al2O3	3.06	0.02	3.24	0.59
Al2O3-γ	3.39	0.09	6.27	1.00
ZrO2	3.37	0.05	5.80	1.26
TiO2	1.71	0.02	4.73	0.90
CeO2	1.44	0.02	9.47	1.34
CeO2/U	1.44	0.01	6.12	0.67
Al2O3/Q	1.22	0.40	9.37	1.97

Table 6-5: Physical dimensions of procured catalyst supports

6.1.3 Metallic Foam Procurement

A range of metallic foam catalysts have been assessed, these consisted of two main forms: a silver metal sponge and a nickel foam coated in a catalytic material. The silver metallic sponge has been prepared by the University of Southampton's Chemistry Department. They have produced a self-supporting macroporous silver sponge by dissolving dextran (an organic glucose based substance) in concentrated metallic silver nitrate at different ratios. The resulting viscous liquid mixture is left overnight at room temperature for solidification. Partial reduction of silver occurs during this process. Further heat treatment at 600°C removes any organic material, leaving a monolith structure of the metal in the form of sponge with reasonably good structural properties. The sponge has been characterized by scanning electron microscopy (SEM) and computer tomography (CT) and found to contain micro pores with a diameter of between 1-20 μm.

The second type of metallic foam to be investigated will be coated nickel foams. Of the authors who have evaluated metallic foams the majority have based their catalysts on a nickel foam support [52,67,68]. For this reason the catalysts being manufactured for this work will also use nickel foam. One such supplier, Inco Special Products, an unincorporated business unit of Inco Limited, has been identified as being able to supply this foam. Table 6-6 provides the product information for this material.

Product name	Purity	Thickness	Density	Cell Size
INCOFOAM™	99.9% Nickel	1.2 - 2.0 mm	300 – 600 g/m^2	450 – 800 μm

Table 6-6: Properties of INCOFOAM™

6.2 Catalyst Manufacturing

In total seventeen catalysts have been manufactured following one of five manufacturing procedures, with an eighteenth, procured catalyst, undergoing a heat treatment process. The eighteenth, iridium on alumina, was manufactured in response to the much higher performance of Pt/Ir-Gz-150-HT compared to Pt/Ir-Gz-150 in the sealed reactor. The aim was to identify if heat treated iridium was the driving influence on the improved performance however no pure iridium gauze was available for testing. It was important to maintain a consistent procedure for all batches to assure the quality of the catalysts produced; to this end a range of steps have been taken to avoid sample contamination. These include only handling the catalysts with fresh gloves and cleaning all hardware in a 10% nitric acid bath for 10 minutes (followed by a deionised water rinse) before being used with the catalytic material.

The precise manufacturing procedures are given in Table 6-7; in all cases a control and test sample have been produced. The test samples were impregnated with a precursor solution of sodium permanganate ($NaMnO_4 \cdot H_2O$) resulting in the formation of a MnO_x catalyst after calcination. The control pellets underwent the same processes as the test sample; however, these pellets were only impregnated with distilled water. The control sample provides data on the manufacturing process, such as identification of contamination, as well as allowing a more accurate assessment of catalyst loading.

With weight measurements being taken throughout the manufacturing process it is possible to measure the percentage catalyst loading by mass (%loading). It would be expected that a high catalyst loading in combination with a large surface area would lead to an improved rate of decomposition of hydrogen peroxide. The %loading is calculated using the final measured mass according to equation 6-1, where M_{SI} is the Impregnated sample mass and M_{SC} is the Calcined sample mass.

$$\%loading = (M_{SI} - M_{SC})/M_{SC} \quad \text{(Eq. 6-1)}$$

Two values for the %loading are given, with the corrected value including any mass change due to the control. It is expected that the control samples would return to the post-calcination weight, since the water should be driven off in the drying process (Step 8 in Table 6-7). Any increase in the control weight suggests either the sample has become contaminated or not all the water was removed. Since the processes are identical for the test and control samples it is assumed any increase in mass in the control is also reflected in the test sample. Kappenstein [59] identified residual water as retarding the decomposition process so this result may affect the performance of the catalysts when used within the testing apparatus. The corrected percentage catalyst loading by mass, $\%loading_{C,}$ is calculated using the equation below, where M_{CI} is the Impregnated control mass and M_{CC} is the Calcined control mass.

$$\%loading_C = (M_{SI} - M_{SC})/M_{SC} - (M_{CI} - M_{CC})/M_{CC} \quad \text{(Eq. 6-2)}$$

The %loading values can be found in the catalyst manufacturing summary table (Table 6-8). The table summarises all eighteen batches indicating active phase and base material. The naming convention applied to all manufactured catalysts consists of the active phase, base material and manufacturing procedure. For example; MnO_x-Al-1 indicates an MnO_x active phase on a Al_2O_3 base material manufactured using manufacturing procedure 1. Catalyst batch MnO_x-Ni-2/R is a repeat of MnO_x-Ni-2 with one modification. Whereas MnO_x-Ni-2 is in a rectangular form (approx 8mm by 4mm), MnO_x-Ni-2/R are punched 4mm discs more suited to being packed into a catalyst bed with a higher packing density.

Step	Description				
	Procedure 1	**Procedure 2**	**Procedure 3**	**Procedure 4**	**Procedure 5**
1	*Weigh pellets*				
2	Heat base material before impregnation to 500°C for 2 hours. Remove and allow to cool.				
3	*Weigh pellets*				
4	Mix at a ratio of 3:5 sodium permanganate and distilled water by mass. Agitate the solution using a magnetic stirrer at 60°C, for 1 hour.				
5	Place calcined base material in the solution.				
6	Mix for one hour using a magnetic stirrer.	Mix for 2 hours using a roller mixer.			
7	Remove catalyst, drain excess solution and place in a furnace crucible.				
8	Heat to 500°C for two hours.	Heat to 90°C for 1 hour, increase to 500°C for 2 hours.	Heat to 90°C for 1 hour, increase to 500°C for 2 hours.	Heat to 90°C for 1 hour, increase to 800°C for 2 hours.	Heat to 90°C for 1 hour, increase to 1400°C for 2 hours.
9	Switch off the furnace and allow pellets to cool within the furnace.				
10	*Weigh pellets*				
11			Repeat Steps 2 - 10	Repeat Steps 2 – 10	
12	Using a sieve (1mm aperture) remove any particles (broken pellets, MnO_x powder etc.)				
13	Package in a pristine sample bag labelled with date of manufacture, catalyst I.D. and name. Identify control and test-samples clearly.				

Table 6-7: Manufacturing procedures used to produce all batches

[71]

Catalyst Name	Active Phase	Base Material.	Manufacturing Procedure no.	Test Stages*	%Loading	Corrected %Loading
MnO_x-Al-1	MnO_x	Al_2O_3	1	C / S	14.9	13.0
MnO_x-γAl-1	MnO_x	γAl_2O_3	1	C / S	25.6	24.5
MnO_x-Zn-1	MnO_x	ZnO_2	1	C / S	13.5	11.2
MnO_x-Ti-2	MnO_x	TiO_2	2	C / S	18.9	16.5
MnO_x-Ce-2	MnO_x	CeO_2	2	C / S	22.4	19.1
MnO_x-Ce/U-2	MnO_x	CeO_2/U	2	C / S	9.8	8.8
MnO_x-Ce/U-3	MnO_x	MnO_x-Ce/U-2	3	C / S / P-T	15.9	13.4
MnO_x-Ce/U-4	MnO_x	MnO_x-Ce/U-2	4	C / S	15.7	13.1
MnO_x-QLγAl-2	MnO_x	$QL\gamma Al_2O_3$	2	C / S	57.4	52.3
MnO_x-Al-2	MnO_x	Al_2O_3	2	C / S	21.5	17.3
MnO_x-γAl-2	MnO_x	γAl_2O_3	2	C / S	87.7	83.7
MnO_x-Zn-2	MnO_x	ZnO_2	2	C / S	21.8	20.3
MnO_x/Pt-Al-2	MnO_x / Pt	5% Pl on Al	2	C / S	12.6	11.5
1.0%Ir-Al-HT	Ir	1% Ir on Al	HT	C / S	-	-
Ag-Foam	Ag	-	*Chemistry*	C / S	-	-
MnO_x-Ni-2	MnO_x	Ni Foam	2	C / S	94.0	94.1
MnO_x-Ni-5	MnO_x	Ni Foam	5	C / S	93.8	71.0
MnO_x-Ni-2/R	MnO_x	Ni Foam	2	C / S / P-T	56.8	56.4

*C = Control, S = Sample, P-T = Post-Test Sample (After catalyst bed exposure)

Table 6-8: Catalyst manufacturing summary

[72]

The significance of the change in %loading between corrected and uncorrected values will be discussed in more detail later in this chapter. However with the exception of metallic foam supported catalysts the corrected %loading values have reduced by 5-20%. This is likely due to residual water in the manufacture catalysts which wasn't driven off during the drying process. MnO_x-Ni-2 and MnO_x-Ni-2/R showed very little difference between the corrected and uncorrected %loading, this due to the highly porous structure which allows water to escape more easily. MnO_x-Ni-5 shows the greatest change in %loading. As will be seen the MnO_x-Ni-5 control sample became brittle with a green discoloration consistent with nickel oxidation at high temperature; this was not the case with the impregnated sample. As a result of the oxidation the control sample mass increased considerably which is reflected by the significant drop in the corrected %loading.

6.3 Catalyst Assessment Matrix

In the introduction the approach to catalyst assessment and down-selection was given. With thirty-eight catalysts to assess the approach minimised the resources required to identify the most viable catalysts. The research methodology is summarised below:

1. Catalysts are manufactured or procured.
2. Preliminary characterisation to help improve the manufacturing methodology.
3. Experimental assessment is conducted using the sealed reactor (SR)
4. After preliminary down-selection base material characterisation is conducted.
5. Experimental assessment is conducted using life-time mass loss (LTML) apparatus.
6. A combination of the LTML and SR results are used for final down-selection.
7. Down-selected catalysts are characterised using the equipment specified below.
8. The highest performing catalysts (of each of the three forms assessed) are then tested within the highly instrumented catalyst bed, hICB and the EBB thruster.
9. These catalysts are then subjected to post-testing characterisation.

Table 6-9 shows the completed catalyst assessment matrix. A green cell indicates the catalyst has undergone the assessment phase and a grey cell signifies the catalyst has not (or it is not applicable to that catalyst). The details of the results and the reasoning behind any decisions made are described later in this work.

The first three catalysts manufactured (MnO_x-Al-1, MnO_x-γAl-1, MnO_x-Zn-1) underwent characterisation even though they were later rejected in the experimental phase of the assessment process. This was done to verify the manufacturing technique and ensure no contamination occurred during manufacture.

Catalyst Name	Experimental Assessment					Characterisation			
	SR	LTML	pICB	hICB	EBB	BET	SEM	EDX	Optical Micro.
Pd/Ni-Gz-50									
Pd/Ni-Gz-50-HT									
Pt-Gz-45									
Pt-Gz-45-HT									
Pt/Ir-Gz-150									
Pt/Ir-Gz-150-HT									
Pt/Rh/Pd-Gz-80									
Pt/Rh/Pd-Gz-80-HT									
Pt/Rh-Gz-80									
Pt/Rh-Gz-80-HT									
Ag-Gz-20									
Ag-Gz-20-HT									
0.5%Pd-Al									
0.5%Ru-Al									
2%Ru-Al									
0.5%Pt-Al									
1%Pt-Al									
5%Pt-Al									
1%Ir-Al									
3%Ag-Al									
MnO_x-Al-1									
MnO_x-γAl-1									
MnO_x-Zn-1									
MnO_x-Ti-2									
MnO_x-Ce-2									
MnO_x-Ce/U-2									
MnO_x-Ce/U-3									
MnO_x-Ce/U-4									
MnO_x-QLγAl-2									
MnO_x-Al-2									
MnO_x-γAl-2									
MnO_x-Zn-2									
MnO_x/Pt-Al-2									
1.0%Ir-Al-HT									
Ag-Foam									
MnO_x-Ni-2									
MnO_x-Ni-5									
MnO_x-Ni-2/R									

Table 6-9: Catalyst Assessment Matrix

6.4 Characterisation of manufactured catalysts

At several points throughout this section the author has made reference to identifying changes in the catalyst's physical properties as a result of the manufacturing process. This section describes the equipment that has been used to assess these properties but does not include a description of how the equipment works; these are available in a range of good surface characterisation reference books [78].

6.4.1 Characterisation Equipment

Catalyst loading has already been discussed and was achieved using a self-calibrating mass balance. The scale used was a Mettler AE 240 balance with a resolution of 0.001g. The catalyst was weighed before and after impregnation in order to calculate the percentage mass loading.

To provide information on catalyst distribution, surface formations and surface damage an assessment has been made using an optical macroscope (WILD M420 Makrocsope). Additional images were taken with an Olympus BH2-UMA microscope. Both were attached to computers with integrated cameras.

Further analysis has been provided by a scanning electron microscope (SEM). The SEM used was a JSM-6500F thermal field emission scanning electron microscope which has a magnification of up to 500,000 as shown in Figure 6-1. This is achieved with an accelerating voltage up to 30kV and provides a resolution of 1.5nm at 15kV or 5.0nm at 1kV. The images taken were then recorded for later comparison. A more quantitative assessment was made using the Oxford Inca 300 Energy Dispersive X-Ray microanalysis equipment (EDX). These techniques were employed both before and after the manufacturing process for successful catalysts. The SEM indicates the surface distribution of catalyst and any surface damage on the samples. The EDX examination provides a quantitative measurement of the elements present on the surface of the sample. It is unable to provide data on the oxidation states of the elements present, only the quantity of the elements themselves. EDX also identifies if any contamination of the samples has occurred.

Surface area is another measured parameter; for the catalysts on ceramic supports this is done using a BET measurement technique. BET stands for Brunauer Emmett Teller, the three surnames of the authors who first published an article on BET theory. The BET apparatus used is the Micrometrics Gemini 2375. It can measure surface areas down to 0.01m^2/g depending on the adsorbate gas used. These values have been obtained before and after catalyst attachment and give an indication of whether the attached catalyst blocks some of the pores inside the ceramic supports and reduces the surface area.

Figure 6-1: SEM and EDX hardware

6.4.2 Base Material Characterisation

An assessment was made of suitable (as identified by experimental testing) base materials to see how their surface structure was linked to both surface area and the resulting catalyst percentage loading. The two forms of catalyst support used were ceramic extrudes and metallic foam; these will be investigated separately. The quadrilobed alumina support was not assessed in any detail due to its low mechanical strength which caused failure of the catalyst during both manufacturing and testing.

6.4.2.1 Ceramic Supports

The aim of this work was to identify general trends in physical characteristics of the base materials that may provide further explanation to the experimental results. The BET results showed considerable variation in the surface area depending on the base materials used. In general terms the larger the surface area, the more peroxide can be in contact with the catalyst material, so the higher the expected rate of decomposition. However it is important to understand the significant differences between the BET measurement conditions and the environmental conditions seen by the catalyst both during manufacture and test.

The BET measurement technique assesses surface area through nitrogen gas absorption on the surface of the material. Although it may be possible for the smaller molecules of nitrogen to enter the pores of the substrate in the static conditions of the BET equipment, the same may not be true when the surface of the pellet is exposed to hydrogen peroxide. During testing additional effects need to be considered. For example the gas evolved by the decomposing hydrogen peroxide may itself limit the amount of peroxide that can contact the catalyst surface as suggested by Oemichen *et al* [50]. Nevertheless, it is expected that a catalyst with a higher BET surface area would lead to a high catalyst loading and a more reactive catalyst.

The BET surface area results are shown along with percentage loading of the resulting catalysts in Table 6-10. In all cases the catalysts chosen have been manufactured to the same procedure allowing direct comparisons to be made. The values for the surface area correlate well with work from other authors, with Rusek [57] assessing alumina to have a surface area of ~200m^2/g and Russo-Sorge [69] showing titanium oxide to have a surface area of 120m^2/g.

Base Material / Catalyst	BET Surface Area (Sq.m/g)	Corrected %Loading
ZnO2 / MnO_x-Zn-2	96	20.3
TiO2 / MnO_x-Ti-2	129	16.5
CeO2 / MnO_x-Ce-2	129	19.1
CeO2/U / MnO_x-Ce/U-2	134	8.8
Al2O3 / MnO_x-Al-2	205	17.3
Al2O3-γ / MnO_x-γAl-2	260	83.7
QLγAl2O3 / MnO_x-QLγAl-2	280*	52.3

*As provided by CTI

Table 6-10: Surface area of base materials and catalyst loading of resultant catalysts

Although there is a trend for high BET surface area to result in high catalyst percentage loading there is no direct correlation. This therefore implies that other factors, in addition to the surface area, affect the resulting catalyst loading. Note that although quadrilobed alumina has not had its surface area assessed in the current work a value provided by the manufacturer is included in the above table for completeness. Of particular interest is the significant difference in catalyst loading when CeO2 and CeO2/U are compared. These materials should be identical, and have been shown to have an almost identical surface area so further investigation is required.

Optical investigation conducted with the macroscope shows little variation in the surface topology so much higher magnification, as provided by the SEM, is required. When comparing the two base materials which result in the highest (Al2O3-γ) and lowest (CeO2/U) loading significant differences become apparent. Figure 6-2 shows the external surface of these base materials; Al2O3-γ is shown to be an amalgamation of particles whereas CeO2/U is a single porous structure. A similar composition can be seen in the internal structure of these materials shown in Figure 6-3. This indicates Al2O3-γ has a much more porous structure which may explain why it has the highest catalyst loading.

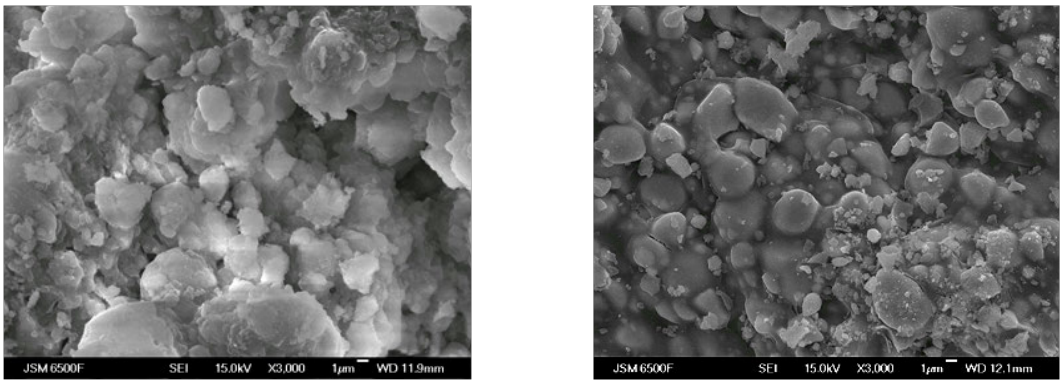

Figure 6-2: External surface (x3000) of Al2O3-γ (Left) and CeO2/U (Right)

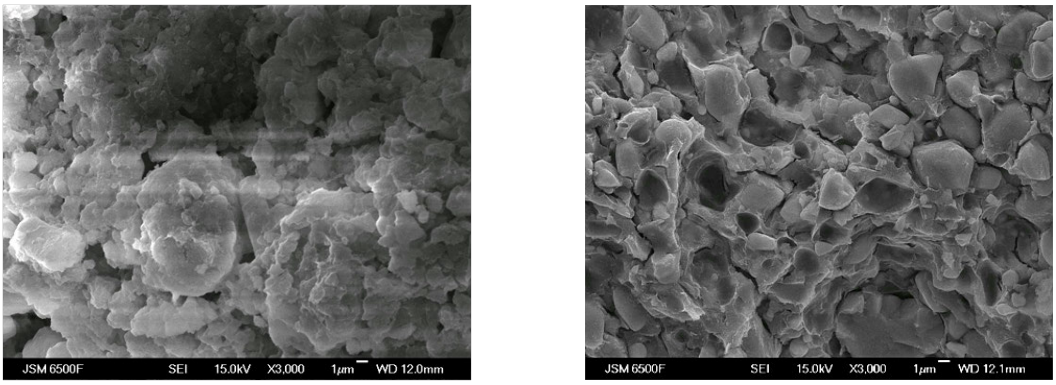

Figure 6-3: Internal surface (x3000) of Al2O3-γ (Left) and CeO2/U (Right)

A similar result can be seen when comparing other base materials. Base Al2O3 and ZrO2 are shown in Figure 6-4 and both have similar porous structures to that of CeO2/U. However the resultant loading is significantly larger in both cases. At a magnification of x3000 their internal structure looks similar, it is not until the magnification is raised to x10,000 that the differences in structure become evident. At this magnification, as shown in Figure 6-5, the internal structure of both Al2O3 and ZrO2 look to be rougher with a greater available surface area for catalyst attachment and is likely responsible for the increase in catalyst loading.

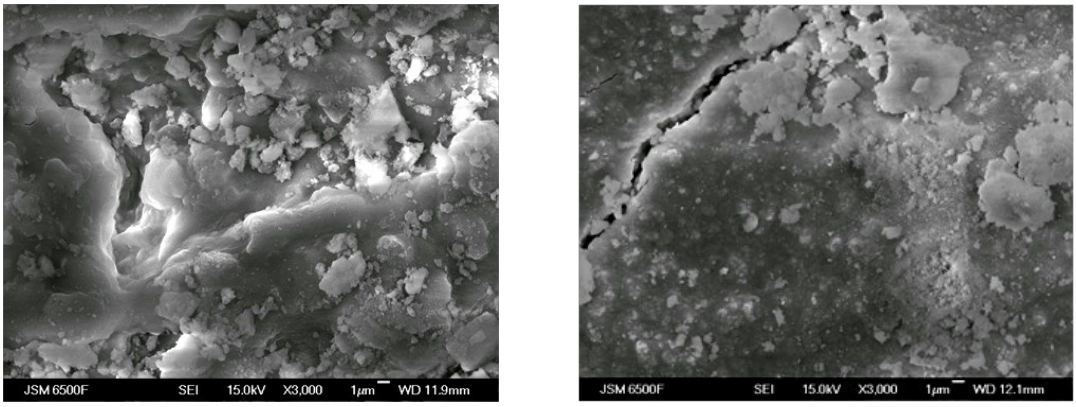

Figure 6-4: External surface (x3000) of Al2O3 (Left) and ZrO2 (Right)

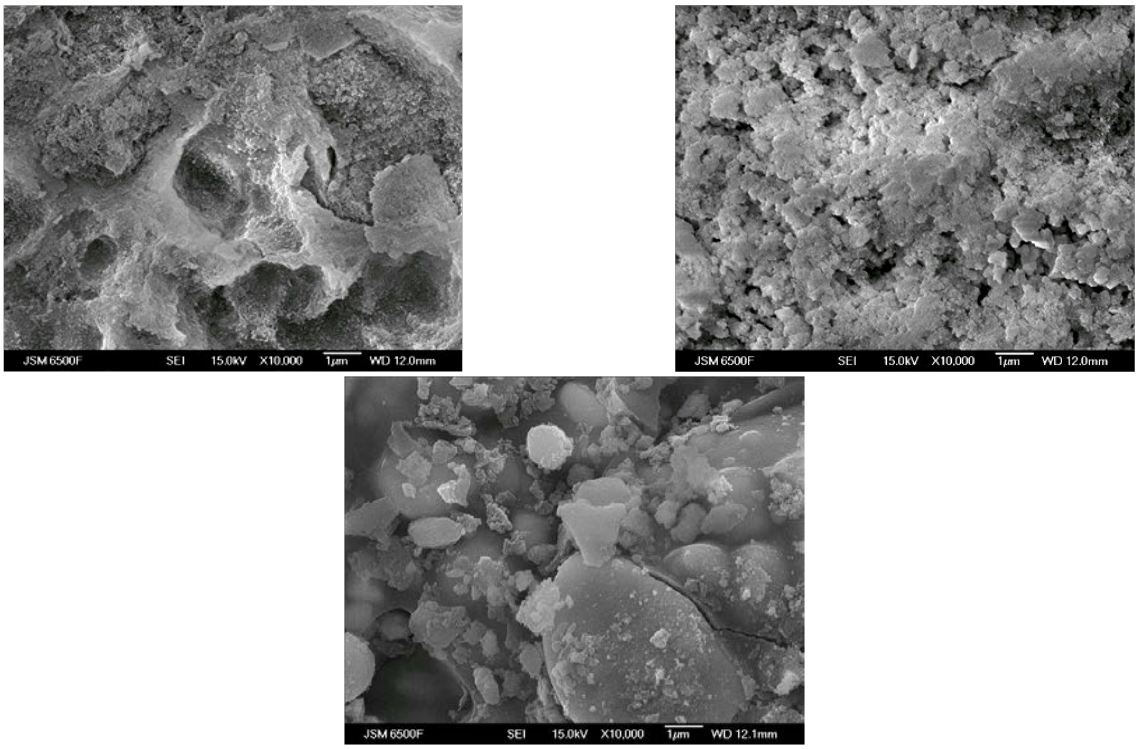

Figure 6-5: Internal surface (x10,000) of Al2O3 (Top left), ZrO2 (Top right) and CeO2/U (Bottom)

The experimental assessment will be covered in greater detail in the following chapter. However, Table 6-11 compares the relative performance of catalysts using the same active phase but differing base materials as assessed within the sealed reactor (SR), along with their percentage catalyst loading. In this table, the overall performance has been compared with the reference sample of the MnO_x-Ce-2 test sample, which had the best performance of the manufactured catalysts with ceramic supports. The table shows that there is little correlation between these values; for example although the catalyst loading of MnO_x-γAl-2 is very high, the performance is relative low. This indicates that high catalyst loading and surface area are not necessarily good performance indicators for highly porous structures. Although the impregnating solution can penetrate deep within the pellet with extended exposure, the hydrogen peroxide in the very violent, short lived exposure to the catalyst does not have time to penetrate below the surface.

Catalyst	Relative performance in the Sealed Reactor	%Catalyst Loading
MnO_x-Ce-2	1.00	19.1
MnO_x-QLγAl-2	0.80	52.3
MnO_x-Zn-2	0.68	20.3
MnO_x-Ti-2	0.62	16.5
MnO_x-Ce/U-2	0.55	8.8
MnO_x-γAl-2	0.41	83.7
MnO_x-Al-2	0.36	17.3

Table 6-11: Experimental results compare to %loading

This was supported by further investigation of the CeO2 and CeO2/U catalyst supports. These two theoretically identical materials resulted in significant differences in both catalyst loading and performance. A comparison of their internal structure (Figure 6-6**)** shows a very similar topology suggesting any variation is likely due to the external surface of the catalysts shown in Figure 6-7. As expected the surface of CeO2 looks more like that of Al2O3-γ than CeO2/U. Since the manufacturing conditions were identical it is hypothesised that the quantity of the active phase deposited on the internal structure is also comparable. Therefore the majority of the difference is likely due to deposits on the external surface which has resulted in a more reactive catalyst as identified by experimentation. The reason for the difference in surface topology is unknown and is likely the result of unknown changes by the manufacturer of the pellets.

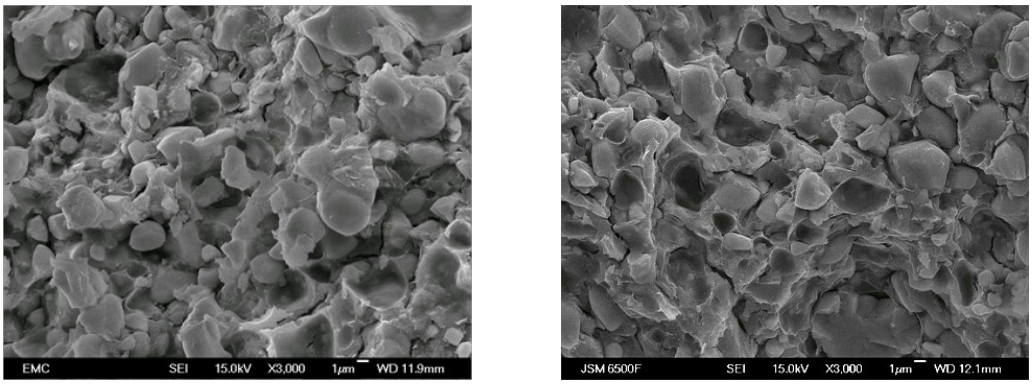

Figure 6-6: Internal surface (x3000) of CeO2 (Left) and CeO2/U (Right)

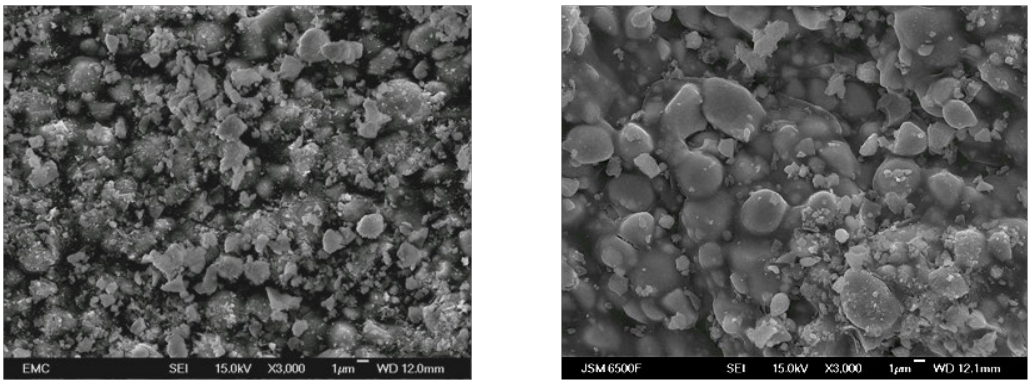

Figure 6-7: External surface (x3000) of CeO2 (Left) and CeO2/U (Right)

The EDX results for the surface of MnO_x-Ce-2 and MnO_x-Ce/U-2 are shown in Figure 6-8. Care must be taken when interpreting these results as many factors affect the accuracy of EDX, so only general trends should to be identified. However as Spectrum 1 in Table 6-12 shows, the trend is for greater concentrations of Mn at the surface of the CeO2 supported catalyst (MnO_x-Ce-2) compared to CeO2/U supported catalysts (MnO_x-Ce/U-2). Spectrum 1 is used as this encompasses the entire assessment area. The presence of additional elements will be discussed later in this chapter.

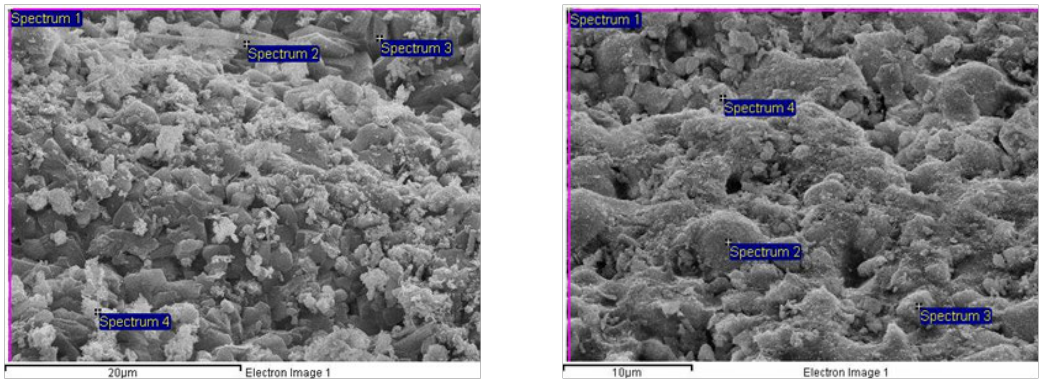

Figure 6-8: EDX images (x3000) of MnO_x-Ce-2 (Left) and MnOx-Ce/U-2 (Right)

	Elements in MnOx-Ce-2 (%)				Elements in MnOx-Ce/U-2 (%)			
Spectrum	**O**	**Na**	**Mn**	**Ce**	**O**	**Na**	**Mn**	**Ce**
Spectrum 1	64.40	4.48	11.61	5.12	36.15	2.20	5.05	49.44
Spectrum 2	74.99	4.27	1.13	4.60	23.79	1.25	1.99	60.43
Spectrum 3	71.87	0.26	1.92	6.39	27.03	1.86	3.75	53.49
Spectrum 4	60.84	3.84	10.54	2.61	34.03	2.15	4.68	46.42

Table 6-12: EDX values for MnO_x-Ce-2 and MnO_x-Ce/U-2

The results of the surface characterisation are inconclusive. That is to say a catalyst with a high surface area or high percentage loading does not immediately equate to an improved performance. It would seem that surface distribution of the catalyst is more important than overall catalyst loading. The current work assumes that the active phase was consistent in all cases for the same manufacturing method. It was not possible in the framework of the current work to assess the phase of the manganese oxide distributed on the surface of the catalyst. However work conducted by Russo-Sorge *et al* [69] would suggest this assumption may not be correct. In this work a range of tests were conducted on manganese dioxide (MnO_2) impregnated titanium dioxide using the wet impregnation method. The catalysts were dried at 120°C and calcined at 500°C (similar to the current work), resulting in catalyst loadings varying between 2.7% and 11% by mass. All catalysts were subject to testing inside a batch reactor. They identified an optimal manganese concentration of 7.3%, after this the rate constant began to fall. Further assessment showed that with increasing manganese concentration not only did the quantity of active phase increase but so did the quantity of Mn_2O_3. The Mn_2O_3 was experimentally found to be less catalytically active and this was the reason suggested for an optimum catalyst loading. This effect may have also been present in the current work and may have affected the experimental results gathered. This will be discussed further in Section 6.4.3.4

6.4.2.2 *Metallic foam supports*

Only one nickel foam substrate was used for all manufacturing; however the temperature was modified for various manufacturing processes. Consequently surface assessment has been conducted on the base material at various temperatures. Due to the low surface area it was difficult to get an accurate BET surface area measurement; although a value of 2.47m^2/g was achieved. This is 50-100 times lower than was measured for ceramic pellets. Figure 6-9 shows the nickel foam taken at magnification of x200 and x800. The structure is highly porous with large pore diameters. It is expected that this much more open structure would allow hydrogen peroxide to penetrate deeper into the catalyst support. The surface is smooth with its grain structure readily identified; this may make catalyst attachment more difficult. EDX measurements show only nickel to be present.

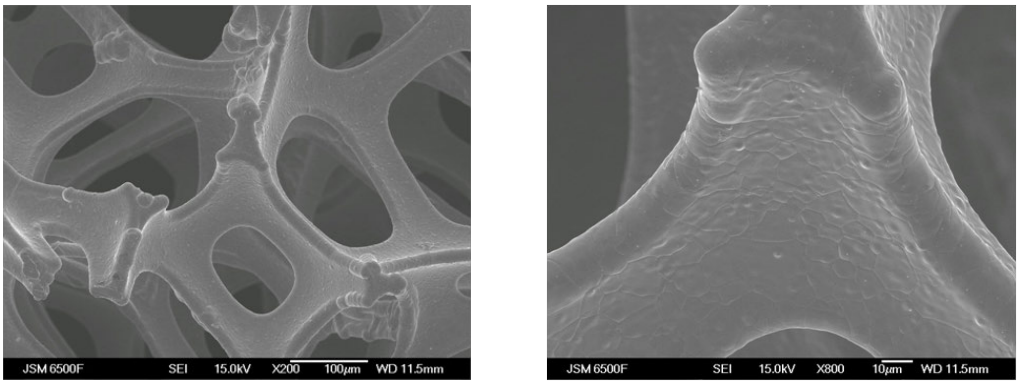

Figure 6-9: External surface at x200 (Left) and x800 (Right)

During manufacturing the baking temperature varied between 500°C and 1400°C and whilst operating within the catalyst bed the temperature can reach 700°C with 87.5wt% hydrogen peroxide. Figure 6-10 and Figure 6-11 shows the nickel foam substrate at 500°C, 700°C, 900°C and 1400°C. As the temperature rises the formation of oxide microstructures on the surface can be seen. It is not the aim of the work to explain these surface formations however a detailed description of these structures can be found in the work done by Peraldi *et al* [79,80].

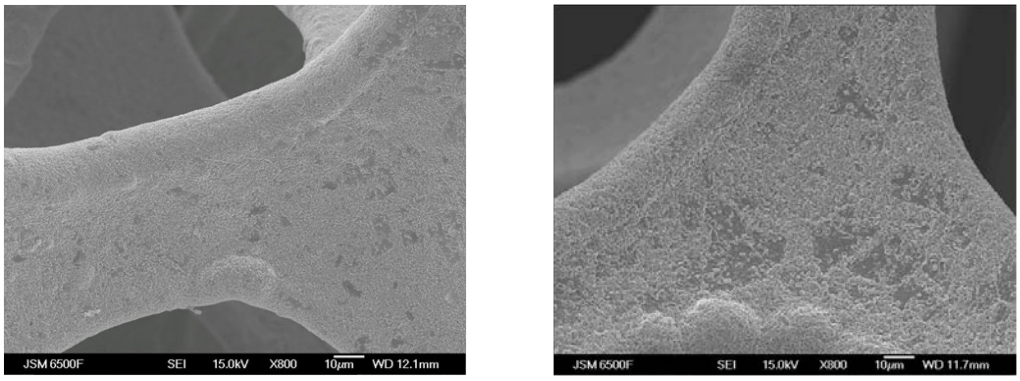

Figure 6-10: Nickel foam (x800) heated to 500°C (left), 700°C (right)

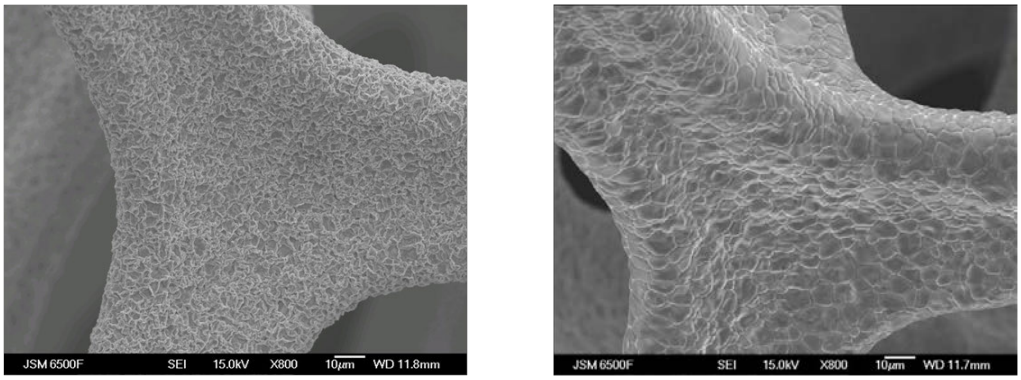

Figure 6-11: Nickel foam (x800) heated to 900°C (left) and 1400°C (right)

The formation of nickel oxide is supported not only by the green colouration of the nickel foam but also the EDX results which show the presence of elements oxygen and nickel. From a catalyst manufacture viewpoint these microstructures may improve attachment between the active phase and the support. However, the increase in temperature also leads to an embrittlement of the nickel foam making it unsuitable as a catalyst due to the increased likelihood of structural failure.

6.4.3 Assessment of manufacturing methodology

One of the main aims of the characterisation is to review and where possible improve the catalyst manufacturing method. As has already been mentioned three catalysts were assessed even though they did not form part of the final down-selection. These catalysts (MnO_x-Al-1, MnO_x-γAl-1 and MnO_x-Zn-1) were the first produced in this work and were used to identify possible contamination and surface damage.

6.4.3.1 Contamination

For every manufactured catalyst a control was also produced for two reasons; to correct the percentage mass loading and identify any contaminates present. The percentage mass loading has already been discussed but the presence of contaminates may affect the performance of the catalyst under test. The control samples for MnO_x-Al-1, MnO_x-γAl-1 and MnO_x-Zn-1 were assessed using EDX. An example of the result for MnO_x-Al-1 is shown in Figure 6-12.

The EDX result shows only contamination by carbon and gold. This is a result of the SEM preparation process. Gold is sputtered onto the surface to improve the conductivity, while carbon strips are used to ground the pellet to avoid the build-up of charge on the top surface. The EDX results do not show any contamination that cannot be accounted for. These results are consistent with all the control samples evaluated using EDX analysis, providing confidence that the manufacturing procedures avoided sample contamination.

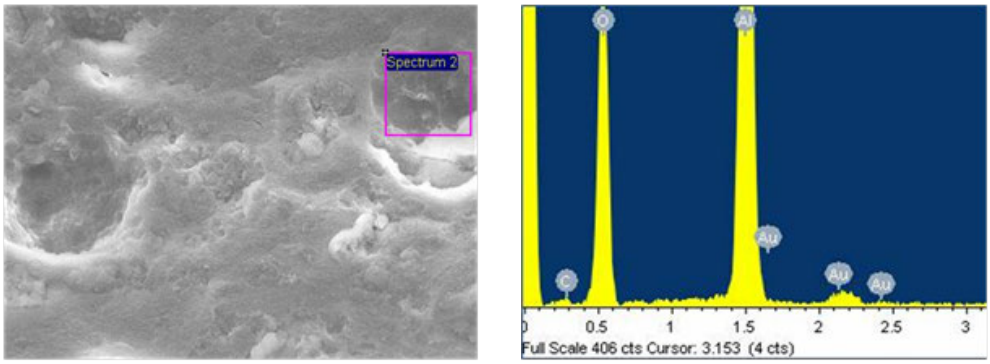

Figure 6-12: EDX analysis of MnOx-Al-1 control

6.4.3.2 Surface Damage

All the catalysts were assessed for surface damage both during manufacture and characterisation. The formation of cracks during manufacture may weaken the catalyst and allow crack propagation over repeated thermal cycles within a catalyst bed. In some cases the base material was delivered with hairline cracks already present, an example is shown in Figure 6-13. Several catalysts showed evidence of this including Al2O3 and ZrO2, this may be partially responsible for the eventual mechanical failure of these supports during laboratory tests.

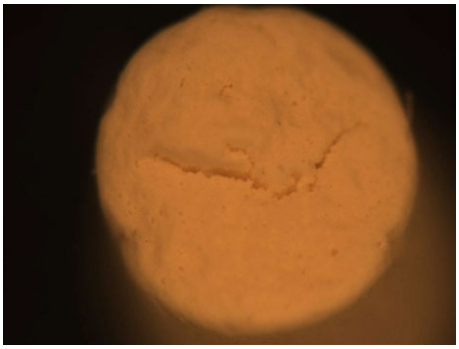

Figure 6-13: Hairline cracks present in CeO2/U

To identify the effect of the manufacturing procedure the control samples were assessed for internal and external defects. It was noted that the BET surface area of these controls had generally reduced after manufacture as shown in Table 6-13. It is unlikely this decrease is due to water retention since the sample must be prepared before being placed within the BET surface area analysis equipment. Part of this preparation requires the pellets to be heated at 200°C, under vacuum, for a minimum of 2 hours until no further weight change can be detected. This should have been enough to drive off any remaining water from within the pellets. The reduction in surface area could be due to pellet damage occurring during the manufacturing process; this may have blocked some of the pores or caused them to collapse completely.

Catalyst	BET Surface Area (m^2/g)		
	Base material	Control sample	Test sample
MnO_x-Al-1	205	206	165
MnO_x-γAl-1	260	249	168
MnO_x-Zn-1	96	75	60
MnO_x-Ti-2	129	95	54
MnO_x-Ce-2	129	126	32
MnO_x-Ce/U-2	129	127	80
MnO_x-Ce/U-3*	80	71	37
MnO_x-Ce/U-4	128	70	34

* The base material was MnO_x-Ce/U-2 (Double impregnated)

Table 6-13: BET measurements for a range of catalysts

In an attempt to minimise this affect the manufacturing method was modified. In manufacturing procedure 1 the base material is mixed with the catalytic solution using a magnetic stirrer. It is likely this caused unnecessary damage to the catalysts. The methodology was then changed to mix the materials using a roller mixer which resulted in a less severe agitation, reducing the likelihood of damage.

It was also identified that the baking process in procedure 1 led to pellets splitting during manufacture, with enough ferocity in some cases to eject them from the furnace crucible. This was attributed to lack of drying before baking. It is hypothesised that the rapid heating of the pellets did not allow all the water to escape the internal pores. This caused the water to boil within the pellets and as a result fracture them. Again the methodology was modified to include a dedicated drying stage below 100°C to minimise this likelihood.

In the majority of cases the high magnification SEM images were ineffective at identifying surface damage so optical macroscope images were relied upon. Generally, little evidence of surface damage was found. However Figure 6-14 does show an example of damage to MnO_x-Ce/U-2 post manufacture. This damage is in the form of small fragments chipped from the edge of the catalyst revealing the lighter colour base material beneath. Damage of this type was rare for the catalysts assessed.

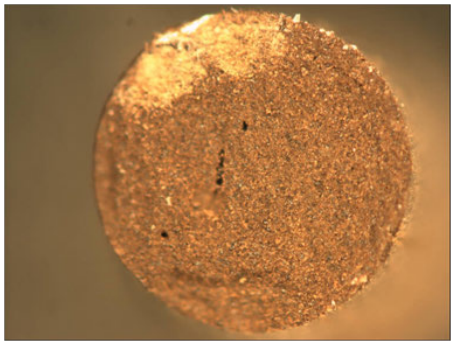

Figure 6-14: Example of post-manufacture surface damage (MnO_x-Ce/U-2, x40)

6.4.3.3 *Effect of impregnation duration and repetition*

Preliminary investigation of MnO_x-Al-1, MnO_x-γAl-1 and MnO_x-Zn-1 showed high percentage catalyst loadings significantly greater than those reported by other authors [57,58,69]. EDX results for the internal surface of MnO_x-γAl-1 are shown in Figure 6-15 and Table 6-14. These indicate the change in elemental composition with increasing distance from the surface of the pellet. Although detected, carbon and gold have been excluded from these results. The unusually high reading for Line Spectrum 1 is likely due to that point being located on an amalgamation of manganese oxide. Nonetheless the general trend of declining manganese concentration with increasing distance from the edge of the pellet is clear. This suggested that the soaking time was insufficient to allow the sodium permanganate to penetrate deeply into the pellet. Subsequent investigation has found that surface concentration of catalyst material is the main driver of performance. However it was anticipated that by increasing the overall mass percentage loading the probability of a high distribution of the catalyst on the surface also increased.

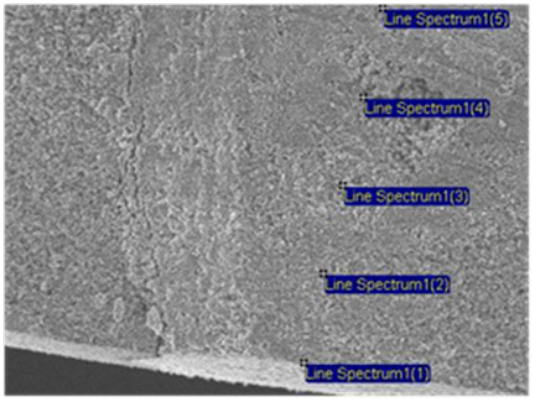

Figure 6-15: EDX image for MnO_x-γAl-1 at x200

Spectrum	O	Na	Al	Mn
1	7.81	1.76	14.55	65.36
2	45.47	6.57	29.41	14.64
3	47.49	5.65	27.41	15.56
4	46.78	4.76	33.47	7.54
5	39.22	4.02	38.20	10.43

Table 6-14: EDX results showing elements by %weight

Increasing the soaking time in manufacturing procedure 2 significantly increased the catalyst percentage loading as can be seen by Table 6-15. Unfortunately MnO_x-Al-2, MnO_x-γAl-2 and MnO_x-Zn-2 were not subject to further investigation since they failed to be down-selected in the performance tests (see chapter 7). So it is not possible to see how the distribution of catalyst within the pellet changed as a result of the manufacturing procedure.

Manufacturing procedure ***(a)***	Corrected percentage catalyst loading (by mass)		
	MnO_x-Al-***(a)***	MnO_x-γAl-***(a)***	MnO_x-Zn-***(a)***
1	21.8	24.5	13.1
2	27.3	83.7	20.3

Table 6-15: % loading using various manufacturing procedures

As well as increasing the impregnation time manufacturing procedure 3 also required a repeat impregnation in an attempt to raise the percentage loading still further. As is shown in Table 6-8 this resulted in an increase in loading from 8.8% to 13.4% for MnO_x-Ce/U-2 and MnO_x-Ce/U-3

respectively. The SEM images for these catalysts show little change. However the EDX results are more revealing: the surface distribution of the catalyst (Figure 6-16 and Table 6-16) shows an increase of Mn present on the surface.

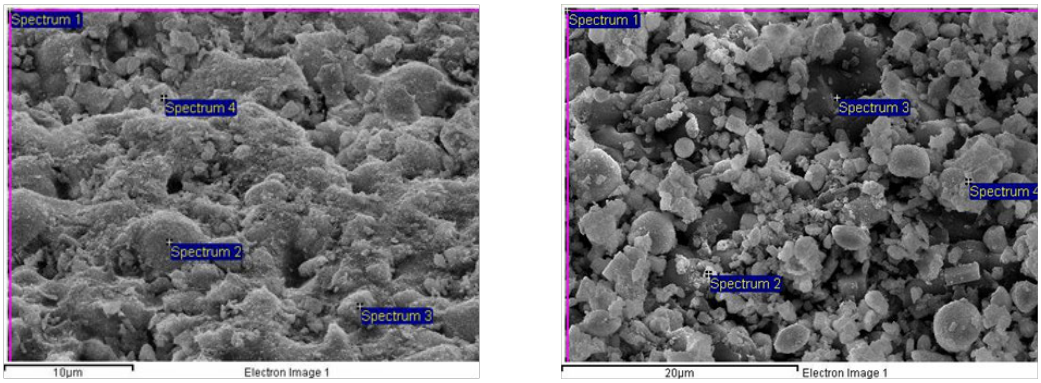

Figure 6-16: EDX images (x3000) of MnO_x-Ce/U-2 (Left) and MnO_x-Ce/U-3 (Right)

	Elements in MnOx-Ce/U-2 (%wt)				Elements in MnOx-Ce/U-3 (%wt)			
Spectrum	**O**	**Na**	**Mn**	**Ce**	**O**	**Na**	**Mn**	**Ce**
Spectrum 1	36.15	2.20	5.05	49.44	49.02	18.01	8.17	14.38
Spectrum 2	23.79	1.25	1.99	60.43	57.38	13.88	1.92	5.13
Spectrum 3	27.03	1.86	3.75	53.49	53.41	24.92	1.38	3.47
Spectrum 4	34.03	2.15	4.68	46.42	34.41	1.67	6.98	46.09

Table 6-16: EDX values for MnO_x-Ce/U-2 and MnO_x-Ce/U-3

The results indicate that there is an advantage to repeat impregnations; this is further supported by experimentation. Both the LTML and SR results showed an improved performance of MnO_x-Ce/U-3 over MnO_x-Ce/U-2.

6.4.3.4 Calcination Temperature

Two manufacturing procedures, 4 and 5, modified the calcination temperature with very different aims. Manufacturing procedure 4 was applied to ceramic catalysts and aimed to quantify the effect of phase transition in MnO_x catalysts, whereas manufacturing procedure 5 was applied to the nickel foam catalysts with the aim of improving the attachment between the base material and active phase.

Many authors have discussed the relative merits of MnO_2 and Mn_2O_3 as effective catalysts, but little agreement has been found [57,58,69] with authors often referring to MnO_x, an unknown combination of the two. Due to the limitation in available characterisation equipment it is not possible to state what phase of manganese oxides is present on the catalysts tested. However,

the transition temperature of MnO_2 to Mn_2O_3 has been identified as between 535°C and 700°C [81]. As a result two batches, MnO_x-Ce/U-3 and MnO_x-Ce/U-4 were produced at calcining temperatures of 500 and 800°C respectively in an attempt to force phase transition. The percentage loading results show a small decrease from 13.4% for MnO_x-Ce/U-3 to 13.1% for MnO_x-Ce/U-4. Since both batches were manufactured together this change could be result of the reduction of MnO_2 to Mn_2O_3 but additional characterisation would be required to verify this. BET surface area analysis shown in Table 6-13 shows a decrease in MnO_x-Ce/U-4 surface area compared to MnO_x-Ce/U-3. No explanation for this can be given, although several of the catalysts display similar behaviour. SEM and EDX images also provide little insight to changes in the catalyst as in both cases the elements Mn and O are detected in varying but similar quantities. Experimental results are similarly inconclusive. Life-time mass loss results show MnO_x-Ce/U-4 outperforming MnO_x-Ce/U-3; however the sealed reactor reverses this result. When the results are combined and normalised, as discussed in chapter 7, MnO_x-Ce/U-3 is shown to perform better overall but the difference remains small. The result of this assessment is inconclusive with the performance of both catalysts similar both in terms of characterisation and experimentation. Further characterisation would be required to confirm the phase of MnO_x on the surface of the catalyst.

Due to the highly porous structure of nickel foam there was a concern over the attachment of the active phase. It was theorised that the wet impregnation caused the active phase to 'fill' the pores and clump to the support material rather than becoming chemically bonded to it. In a macroporous structure this could result in the active phase being washed from the support when exposed to hydrogen peroxide. For ceramics, which have small pores, this was less of a concern. This hypothesis seems to be supported by Figure 6-17 which shows the surface of MnO_x-Ni-2/R. The active phase is seen to be filling some of the voids within the nickel foam support as well as partially attaching to the nickel itself.

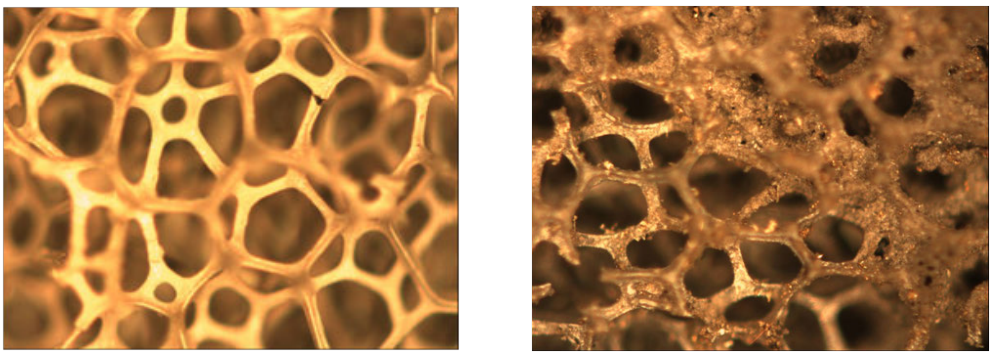

Figure 6-17: Macroscope images (x40) of MnO_x-Ni-2/R control (Left) and Sample (Right)

It has already been shown that high temperatures cause the formation of oxide microstructures on the surface of the nickel, it was hoped these may improve the attachment. MnO_x-Ni-5 was

calcined at 1400°C and is shown in Figure 6-18. The macroscopic images show the active phase still coating the nickel but no longer filling the voids within the foam. Without magnification the catalyst is seen to be significantly more porous than MnO_x-Ni-2/R which may help reduce pressure drop within the catalyst bed.

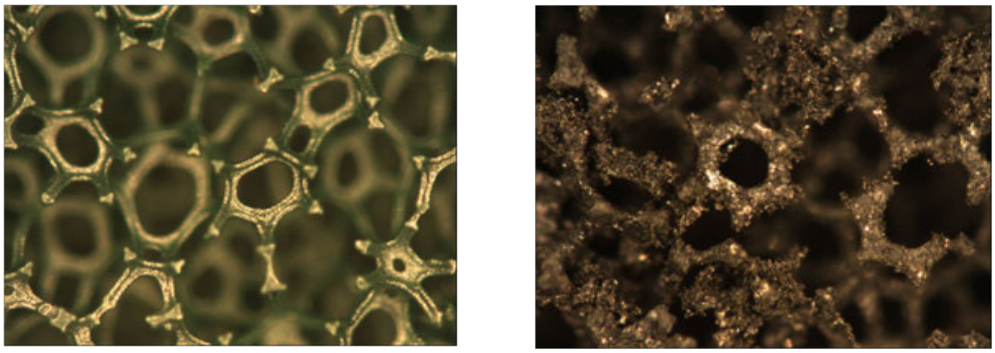

Figure 6-18: Macroscope images (x40) of MnO_x-Ni-5 control (Left) and MnO_x-Ni-5 Sample (Right)

Under the SEM the differences between the two catalysts become even more pronounced. Figure 6-19 shows MnO_x-Ni-2/R and its control. When the two are compared, particles of MnO_x can clearly be seen attached to the nickel. The structure of MnO_x-Ni-5 is shown in Figure 6-20 and seems completely coated in the active phase, with the surface bearing little resemblance to the control. No significant differences were identified when EDX analysis was conducted. Due to the low surface area BET measurements were inconclusive. When tested in the life-time mass loss equipment some residue was identified with MnO_x-Ni-2/R. Although no residue was identified when MnO_x-Ni-5 was tested the support had become brittle and failed quickly.

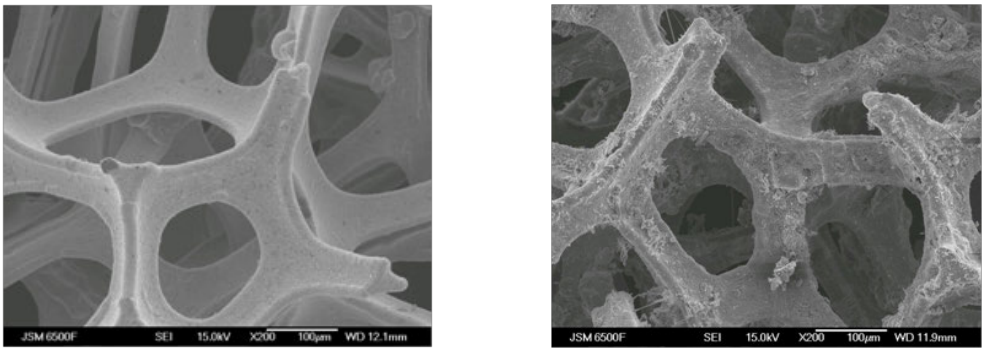

Figure 6-19: SEM (x200) - MnO_x-Ni-2/R control (Left), MnO_x-Ni-2/R Sample (Right)

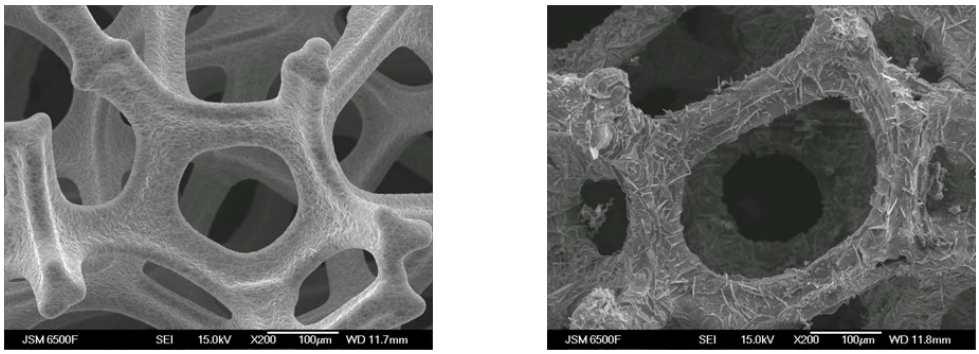

Figure 6-20: SEM (x200) - MnO_x-Ni-5 control (Left), MnO_x-Ni-5 Sample (Right)

6.4.3.5 *Manufacturing consistency*

In the majority of cases the catalysts were manufactured in great enough quantity for additional batches to be unnecessary. It is consequently difficult to make a definitive statement on batch to batch consistency. Three of the catalysts, MnO_x-Al-1, MnO_x-γAl-1 and MnO_x-Zn-1, were manufactured twice. Although no characterisation has been conducted the percentage catalyst loading has been calculated and is shown in Table 6-17. The results show a varying consistency between batches but in all cases the repeat batches have a higher loading. In the case of MnO_x-γAl-1, batch 1 had a loading 21% lower than batch 2. Without additional batches and characterisation it is difficult to provide an explanation for this.

	MnO_x-Al-1	**MnO_x-γAl-1**	**MnO_x-Zn-1**
Batch 1	13.0	24.5	11.2
Batch 2	15.3	31.2	13.1

Table 6-17: Percentage loading for repeat batches

One other catalyst was manufactured twice although the dimensions of the support material were different in each case. After successful testing of MnO_x-Ni-2, a variation of this batch was produced which were in the form of 4mm punched discs instead of the original 8mm by 4mm rectangles; designated MnO_x-Ni-2/R. This was necessary in order to increase the packing density within the catalyst bed and EBB thruster. However, the resulting catalyst loading was significantly different. In both cases the manufacturing procedures were identical; it was theorised that punching the discs had damaged the foam resulting in a lower loading. Initial observations showed that process of punching the discs had crushed the foam, deforming the structure. But subsequent SEM images verified that MnO_x-Ni-2 had a thicker layer of active phase deposited on the nickel foam as can be seen in Figure 6-21. EDX analysis also confirmed a higher quantity of manganese on MnO_x-Ni-2. It has not been possible to identify the reasons for this discrepancy in loading. The difference of 40% is significantly greater than the batch to batch variations noted above. Multiple repeat batches would be needed to investigate this further.

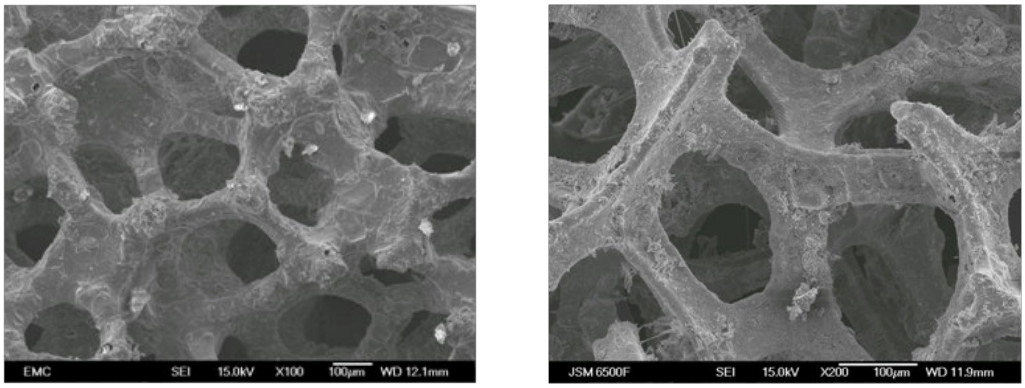

Figure 6-21: SEM images of MnO_x-Ni-2 (Left at x100), MnO_x-Ni-2/R (Right at x200)

6.5 Summary

The literature review conducted in chapter 3 identified a number of materials that are known to effectively decompose hydrogen peroxide. As a result a range of metallic gauzes, foams and ceramic based catalysts have been procured for further assessment. The decisions behind the procurement have been given where applicable.

As well as procured catalysts the manufacturing process for ceramic supported and metallic foam supported catalysts has been provided; this is based on a simple wet impregnation method. At each stage of the manufacturing process the catalyst has been characterised by a range of equipment to identify changes in the base material, effect of the impregnation method and to identify whether any contamination has occurred. The results of this assessment have helped refine the manufacturing methods whilst giving insight into the best parameters to predict catalyst performance.

The influences of impregnation time, repetition and calcination temperatures have all been assessed. It was found, as expected, that increasing impregnation time and repetition improved catalyst loading however this did not always correlate to an improved performance. It is suggested that percentage catalyst loading is not necessarily a good performance indicator in porous structures. This is due to the limited time the hydrogen peroxide has in contact with the catalyst sample stopping the peroxide penetrating below the surface. It is therefore the opinion of this author that BET surface area and catalyst loading should only be used as guide to performance. Instead, where possible, surface content should be used; this has been supported by experimental results. Calcination temperature was found to have little effect on the performance of the catalysts. However, in the case of nickel foam high temperatures resulted in better attachment of the active phase to the support and a more porous structure. Unfortunately, the high temperatures caused embrittlement of the nickel foam resulting in rapid structural failure. Further work is required to see if the embrittlement can be avoided.

An attempt has been made to quantify batch to batch inconsistency which was found to be significant. Repeat batches showed variations in catalyst loading by up to 21%. Greater variation was identified with the nickel foam. However, due to changes in the dimensions of the supporting structure, which resulted in a deformation of the foam, the variation in loading cannot be solely attributed to manufacturing inconsistencies. Considerably more work is required to make a definitive statement on repeatability.

7 Experimental Assessment of Catalysts

Physical characterisation of catalysts, such as that carried out in chapter 6, provides an insight into the effectiveness of the manufacturing technique but can only provide an indication on how the catalyst will perform. True catalyst performance can only be assessed through a detailed experimental program. Two experimental rigs have been developed in an attempt to answer two questions posed in Chapter 4; firstly, how effectively is hydrogen peroxide decomposed? The sealed reactor attempts to answer this question by assessing peak temperature and pressure, and the time taken to reach these peak values. Secondly, what is the likelihood the catalyst will work with continued exposure to hydrogen peroxide? The LTML apparatus investigates this by assessing performance over an extended period of time with the catalysts starting from quenched conditions.

7.1 Sealed Reactor

A full description of the apparatus can be found in Chapter 5; in summary the sealed reactor is a combination of a bomb calorimeter and batch reactor in both its design and operation. 3CC's of HTP is injected under nitrogen gas pressure into a sealed vessel containing a fixed volume of catalyst. The reactor pressure and temperature are monitored over 60s, for ceramic pellets and metallic foams, or 180s for metallic gauzes. The catalysts are assessed based on rates of change of pressure and temperature as well as the maximum values achieved.

7.1.1 Sealed Reactor Results

An initial pellet catalyst datum run was performed with 1% platinum pellets but with no peroxide injected. A similar datum run was conducted for metallic catalysts using silver gauze at the lower nitrogen delivery pressure. These were conducted to ensure that the seals were sound and to record the final state after the nitrogen was released; in this case no additional gas was introduced other than the nitrogen used to inject the peroxide. The reactor pressure recorded in these datum runs were subtracted from the reactor pressure recorded from a "live" run with peroxide injected. This difference in pressure, or relative pressure, is a more sensitive measure of catalyst performance than using the absolute pressure recorded for each live run.

The datum runs can be found in Figure 7-1 and Figure 7-2 for ceramics/foams and gauzes respectively. The time axis is relative to the opening of the solenoid valve signalling the start of the experiment. Figure 7-1 shows that the final equilibrium pressure of 3.23bar absolute being reached in approximately 1s (unless otherwise stated all pressures are in bar absolute). For

gauzes this time is extended to approximately 8s due to the presence of the flow constrictor and lower injection pressure. There is a slight difference of 0.03bar between the tank and reactor pressure in Figure 7-2. This is within the measurement uncertainty of the pressure transducers which is 0.0625bar. The tank and reactor pressure are seen to continue to rise over the full length of the experiment. The reactor pressure increases from 1.13bar to 1.19bar; this is due to the pressure drop induced by the flow constrictor.

A full set of results for all the catalysts tested has been achieved and is available on request. In the majority of cases a minimum of two runs were conducted. However three of the ceramic/metallic foam catalysts were not subjected to repeat testing. MnO_x-QLγAl-2, 1.0%Ir-Al-HT and MnO_x-Ni-5 were identified as either having very poor activity or a loss of structural integrity. These catalysts were subject to additional 'Ad-hoc' dropper tests to verify performance. In these experiments drops of 87.5% hydrogen peroxide was pipetted onto the catalysts and the response visually assessed. These results correlated to the sealed reactor findings. The same methodology was applied to metallic gauzes resulting in only Ag-Gz-20 being subjected to repeat testing. All the other catalysts were found to have unacceptably low performance or were structurally too weak to survive further assessment (Pt/Ir-Gz-150-HT).

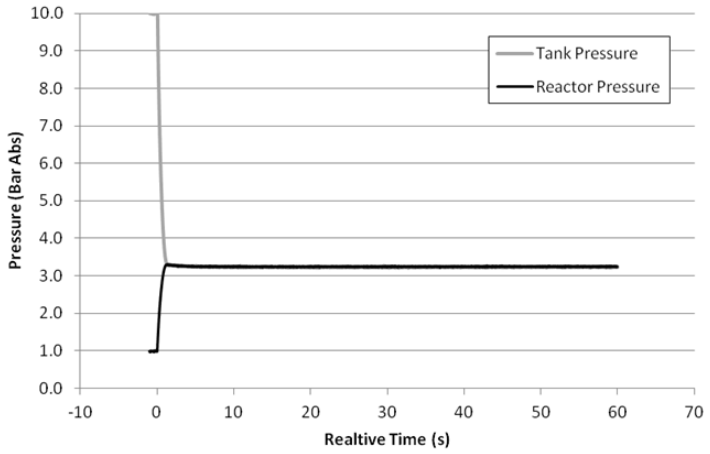

Figure 7-1: Pellet/foam pressure datum

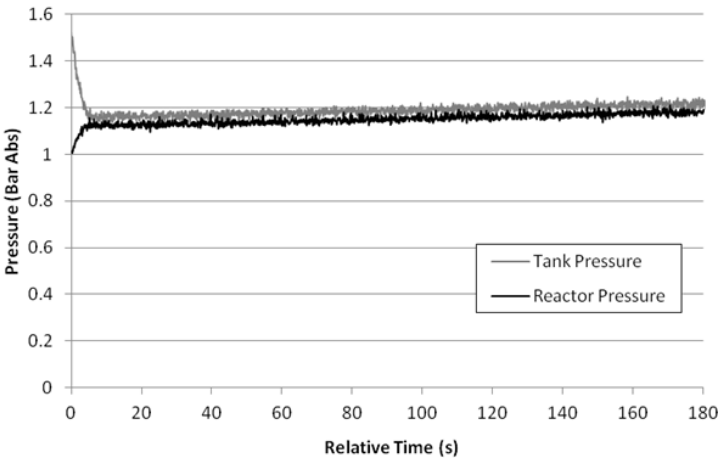

Figure 7-2: Gauze pressure datum

Initial runs were for verification and to assess repeatability and will not be reported here. It is during this phase of testing that the problems with the inert filling material became apparent and the modifications to the decomposition vessel described in chapter 5 were made.

7.1.1.1 Manufactured Ceramic Supported Catalysts

An example of the results obtained with a high performing manufactured ceramic catalyst can be found in Figure 7-3, Figure 7-4 and Figure 7-5. The complete pressure profile for MnO_x-Ce/U-3 is shown in Figure 7-3; this shows a rapid increase in pressure due to the combination of nitrogen injection (from the delivery method) and gas generation from HTP decomposition. This causes the reactor pressure to exceed the datum equilibrium of 3.23bar to an initial spike of approximately 4.9bar. The pressure is seen to then drop slightly before recovering to reach a final pressure of 5.6 and 5.2bar for run 1 and 2 respectively.

A similar profile can be seen in Figure 7-4, which is of the relative pressure, allowing for the influence of the nitrogen injection. The relative reactor pressure is seen to fall initially; this is due to the injection of the hydrogen peroxide at the beginning of the run, which has a much higher density than the nitrogen used in the datum run. The initial spike in pressure is accompanied by a rapid increase in temperature with run 1 and 2 approaching similarly high values of 148°C and 140°C respectively. The slight difference in these values and the rate at which they are achieved is likely the reason for the difference in initial peak pressure values. Thereafter, both the temperature and pressure tend to fall off. This is due to the combined effects of thermal capacity and condensation of the water vapour generated by the reaction. In several cases, such as Figure 7-4, the reduction in pressure is short lived indicating continued decomposition over the life of the experiment, even for the most active of catalysts. This is most likely due to the liquid peroxide being propelled out of contact with the catalytic material, either as a result of atomisation by virtue of the high pressure injection, or the formation of highly energetic gaseous decomposition products on the surface of the catalyst. Over the duration of the experiment the HTP falls back into contact with the catalyst where it decomposes, evolving oxygen and causing a continuous rise in pressure. It would be expected that if the experimental time was extended eventually a drop in pressure due to the cooling of the gases would be seen. Since the sealed reactor was only designed to assess the start-up characteristics of the catalyst the uncertainty over the long duration pressure responses do not affect the assessment.

As can be seen in the figures there is generally good consistency between runs with only small variations visible in the initial stages of the experiment. Any differences will be assessed in more detail in the assessment section and will influence the selection of appropriate criteria.

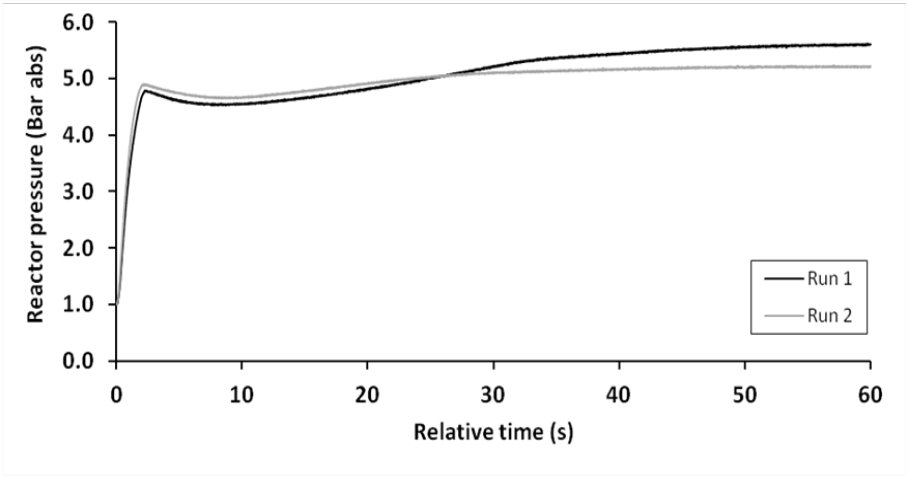

Figure 7-3: Reactor pressure - MnO_x-Ce/U-3

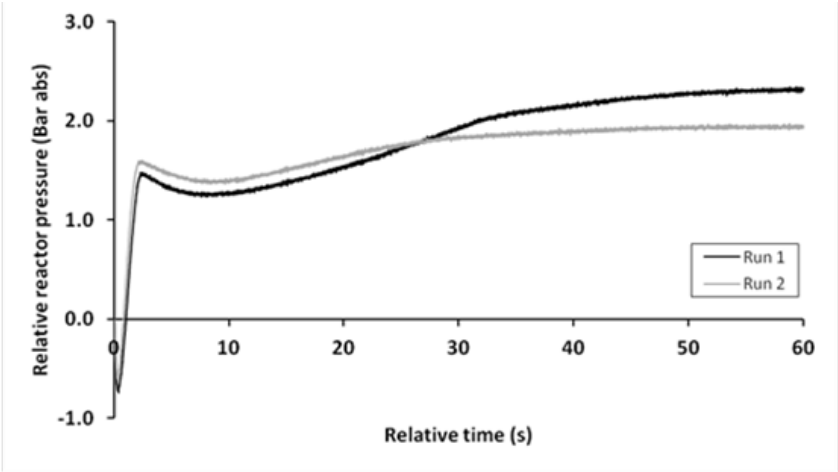

Figure 7-4: Relative reactor pressure - MnO_x-Ce/U-3

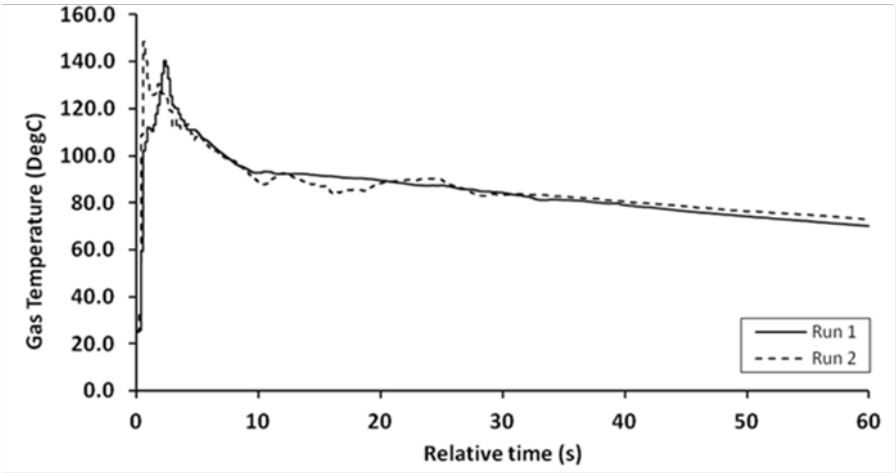

Figure 7-5: Reactor temperature - MnO_x-Ce/U-3

Figure 7-6 gives an example of the worst performing manufactured ceramic catalysts. Similar trends to the figures above can be identified, with a drop in the relative reactor pressure at the start of the run and a continued increase in pressure throughout the run. However, the pressure rise is not accompanied by a significant rise in the reactor temperature. This is a combined result of the slow rate of decomposition and high thermal capacity of the apparatus. Of interest is the magnitude of the initial drop below zero which is closely tied to performance. A poorly

performing catalyst has a long initiation delay slowly decomposing the peroxide with only a slight increase in pressure. This results in a profile with a large minimum value like that demonstrated by 1.0%Ir-Al-HT. This parameter is only appropriate for extremes in performance. Many of the catalysts with similar performance still show small variations in their minimum values. The poor performance of this catalyst was the reason no repeat was conducted. As has already been discussed this poor performance was verified by additional 'Ad-hoc' testing.

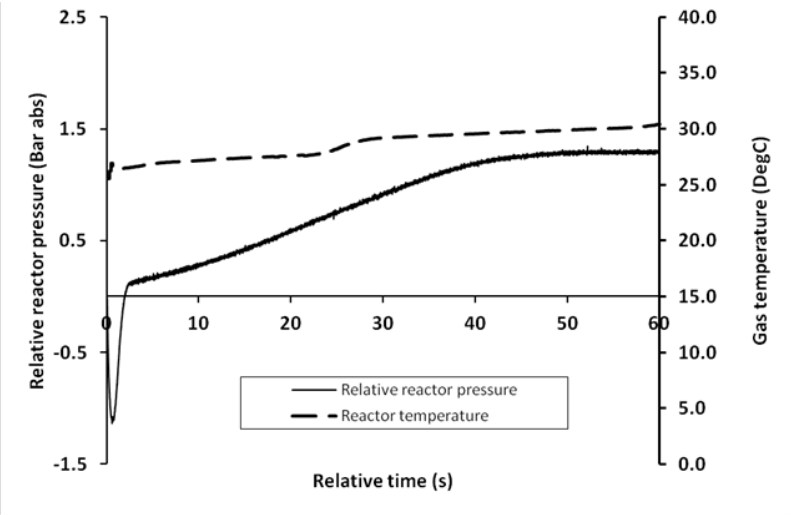

Figure 7-6: Relative reactor pressure and temperature - 1.0%Ir-Al-HT

The results of the sealed reactor allow assessment of some of the manufacturing techniques discussed in chapter 6. Figure 7-7 shows the relative reactor pressure for the four ceria supported catalysts, the values shown are average values over the two runs recorded. Characterisation had shown that the catalyst based on the CeO2 support had a much higher percentage catalyst loading than those based on CeO2/U. Due to the similarities of their internal structure it was suggested that this was due to an improved surface loading. The sealed reactor results corroborate these findings, showing a significantly higher performance of MnO_x-Ce-2 compared to MnO_x-Ce/U-2. They also show that the catalyst based on manufacturing method 3 outperform those based on method 2, as was signified by the increased percentage loading. Finally, the high temperatures used to manufacture MnO_x-Ce/U-4 seemed to have detrimentally affected performance. This would imply that if phase transition from MnO_2 to Mn_2O_3 has occurred this has had a detrimental effect on initial performance, indicating MnO_2 is the superior catalyst. This is in agreement with the findings of Rusek [57].

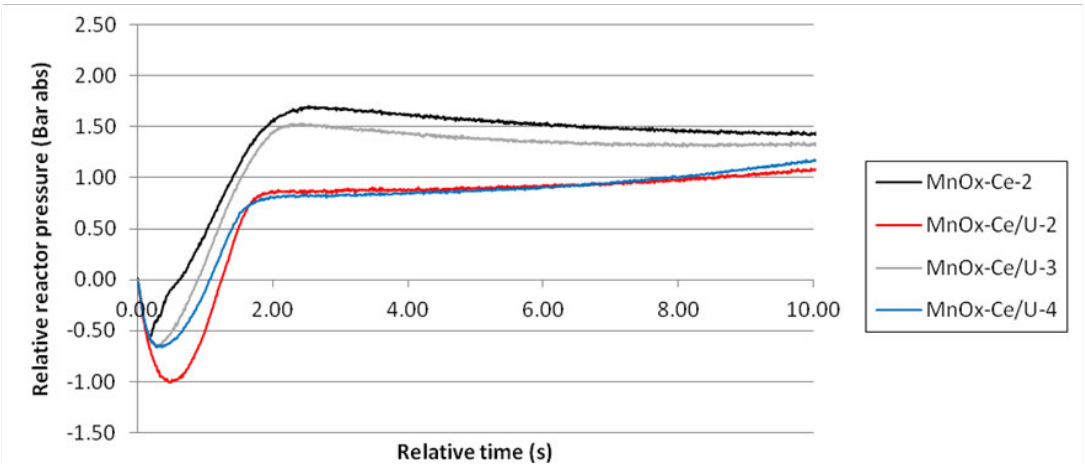

Figure 7-7: Average relative reactor pressure – Ceria supported catalysts

7.1.1.2 Procured Ceramic Supported Catalysts

A summary of all the procured ceramic supported catalysts can be found in Figure 7-8 and Figure 7-9. Again all plots are averaged values over all the repeat runs. Only the first 10 seconds of the run are shown as it is the initial characteristics which this equipment assesses. The step changes shown in the temperature plot are an artefact of the acquisition hardware which has a maximum acquisition rate of 14Hz. The relative pressure results clearly show 5%Pt-Al significantly outperforming the other catalysts. This is not echoed in the temperature plots which show 5%Pt-Al performing well but not best overall. However, the temperature profile does show a rapid climb and a sustained temperature above 100°C indicating any water evolved would be in vapour form. It is likely this is the reason for the high pressure. 5%Pt-Al shows the greatest variance between runs but all the runs show a similar profile and similarly high values.

0.5%Ru-Al shows the fastest rise in temperature, but this is short lived with the temperature dropping quickly before recovering. This suggests the catalyst has become quenched early on in the run. This is evident in the resultant pressure profile which shows a plateau of the pressure at approximately 1.8s before continuing to rise. 0.5%Pd-Al and 1%Ir-Al show similar profiles in both temperature and pressure up until approximately 4s at which point the reactor temperature for the 1%Ir-Al is seen to rise sharply. The results show that although the apparatus has a high thermal capacity there is a good correlation between temperature and pressure profiles.

As was shown for the manufactured catalysts the increase in percentage catalyst loading improves performance. 5%Pt-Al significantly outperforms 1%Pt-Al which only slightly outperforms 0.5%Pt-Al. However this was not the case for ruthenium, the reasons for this are not clear but further assessment in the life-time mass loss equipment (described later in this chapter) may provide additional information.

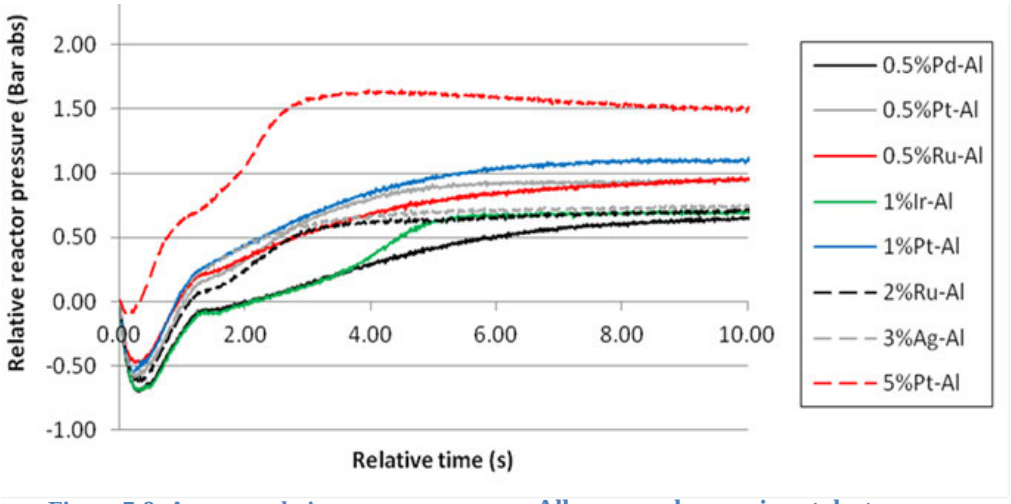

Figure 7-8: Average relative reactor pressure – All procured ceramic catalysts

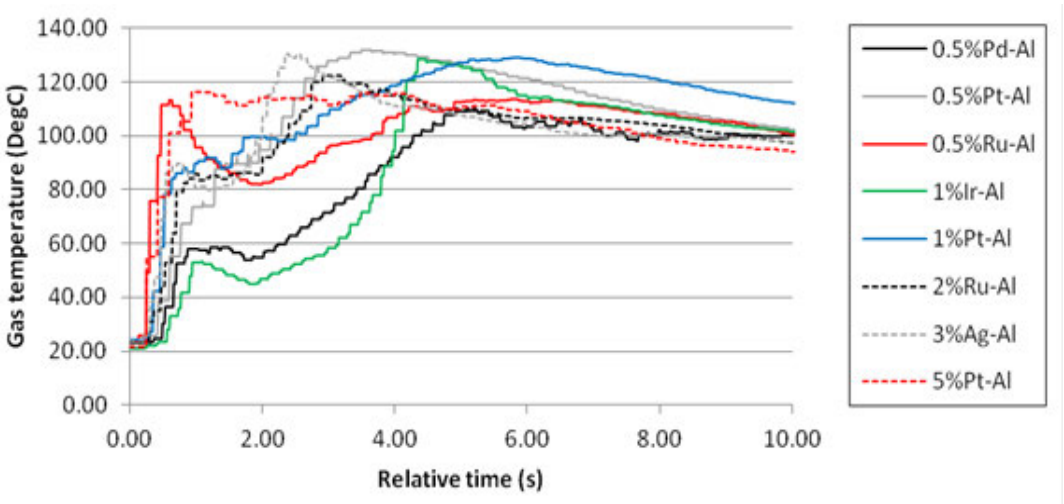

Figure 7-9: Average reactor temperature – All procured ceramic catalysts

7.1.1.3 Metallic Foam Catalysts

By far the highest performing catalysts, with the exception of MnO_x-Ni-5, were those supported on metallic foams. As can be seen in Figure 7-11 reactor temperatures exceeded 200°C with MnO_x-Ni-2 achieving the highest recorded temperature of 258°C. Two of the relative pressure profiles shown in Figure 7-10 do not show an initial drop below zero indicating an exceptionally responsive catalyst. The performance of MnO_x-Ni-5 is poor by comparison, although still excellent when compared to all the other catalysts tested under the same conditions. Subsequent 'ad-hoc' tests showed the presence of active phase residue with MnO_x-Ni-2 and MnO_x-Ni-2/R. This indicates that some of the active phase has been removed from the support and deposited on the bottom of the test beaker. It is thought that this is in part the reason for the high performance as the surface area of this residue is much greater than that of the catalyst itself. However, the removal of active phase may significantly affect catalyst lifetime. During manufacture it was noted that the catalyst loading of MnO_x-Ni-2/R was much lower than MnO_x-

Ni-2 and that this may affect performance. Sealed reactor results would suggest this is not the case, although the equipment makes no attempt to assess lifetime which may be influenced.

Repeat tests were conducted on all the foam materials except MnO_x-Ni-5 which was shown to structurally fail in additional 'ad-hoc' tests. For the most part there was good agreement between the runs. There was significant variance in all the peak temperatures but in all cases the temperatures achieved were significantly higher than the ceramic supported catalysts. However Ag-Foam showed notable differences in the peak pressures achieved. This is attributed to the quenching affect after the initial spike in temperature. In one of the runs the quenching dropped the temperature below 100°C in the decomposition vessel. At this point any water vapour generated would condense to form liquid water thus reducing the reactor pressure.

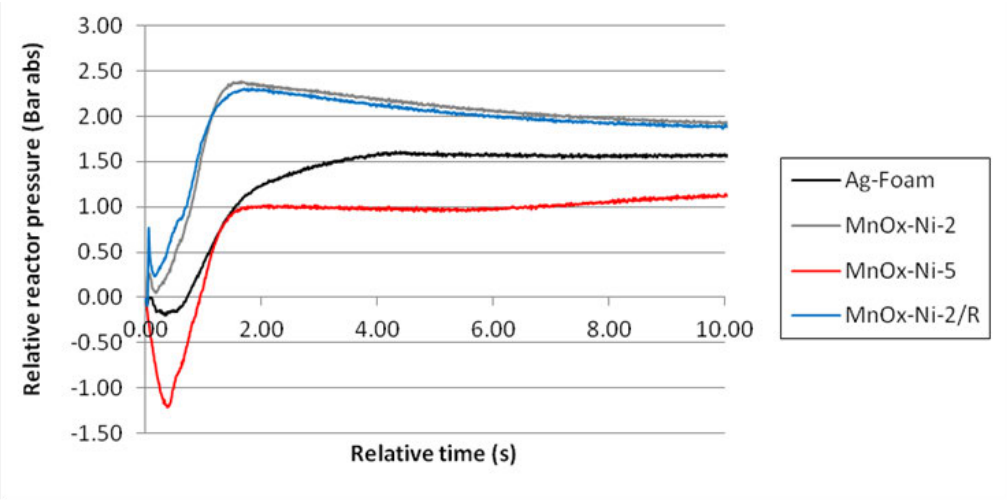

Figure 7-10: Average relative reactor pressure – All metallic foam catalysts

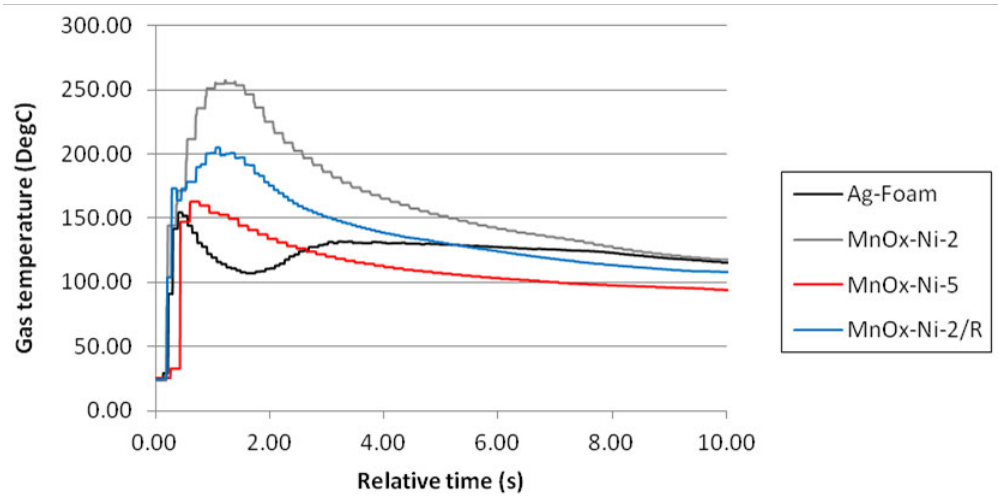

Figure 7-11: Average reactor temperature – All metallic foam catalysts

7.1.1.4 Metallic Gauze Catalysts

The variations in experimental conditions for metallic gauzes, and the reasons why these were necessary, have already been discussed in section 5.1.1. Preliminary experimentation verified the need for these changes and as such those results will not be reported here.

The majority of the metallic gauzes exhibited very poor performance. In some cases the catalytic material was immediately quenched and no decomposition reaction could be identified for the duration of the experiment. The results shown are likely to be slightly skewed due to a variation in catalyst surface area. This is because it was not possible to procure gauzes of different materials with the same mesh size (see chapter 6). Figure 7-12 shows the temperature profiles for a selection of metallic gauzes.

The result for Ag-Gz-20 show the reaction initiating after around 17 seconds with the gas temperature quickly rising reaching a maximum of 134°C after about 18 seconds. As the decomposition reaches completion the temperature is then seen to fall away due to the high thermal capacity of the apparatus. The effect of quenching can clearly be identified in the case of Ag-Gz-20-HT. An initial rise in temperature is seen as the peroxide is injected which is then quenched as the full quantity of fluid enters the decomposition vessel. The injection of peroxide is slower with metallic gauzes due to the lower injection pressure and flow constrictor. Of interest is the significant difference between the heated Pt/Ir-Gz-150-HT, which is shown to perform relatively well compared to the "as supplied" Pt/Ir-Gz-150 which shows a long delay before the reaction initiates. The heat treatment has possibly had one of two effects: firstly it may have chemically altered the composition of iridium or platinum or, secondly, it may have removed surface volatiles improving the reactivity. 1.0%Ir-Al-HT was assessed in an attempt to resolve this question. However the performance was significantly below that of 1.0%Ir-Al indicating heat treatment of iridium was not the source of the improved performance. Heat treatment of platinum gauze did show some improvement but not akin to the difference between Pt/Ir-Gz-150 and Pt/Ir-Gz-150-HT. The cause of these differences in performance due to heat testament therefore at present remains unknown.

The relative reactor pressures are shown in Figure 7-13. Again an initial drop below zero is identified. The results for heated platinum/iridium have had a correction factor applied to remove a 0.8 bar discrepancy in delivery pressure (1.58 bar absolute instead of 1.5 bar). The relative pressure results correlate closely with the associated temperature data and the general trends mirror those of the pellet data. The results show that silver has again performed well; generating a greater pressure than any of the other gauze-based catalysts.

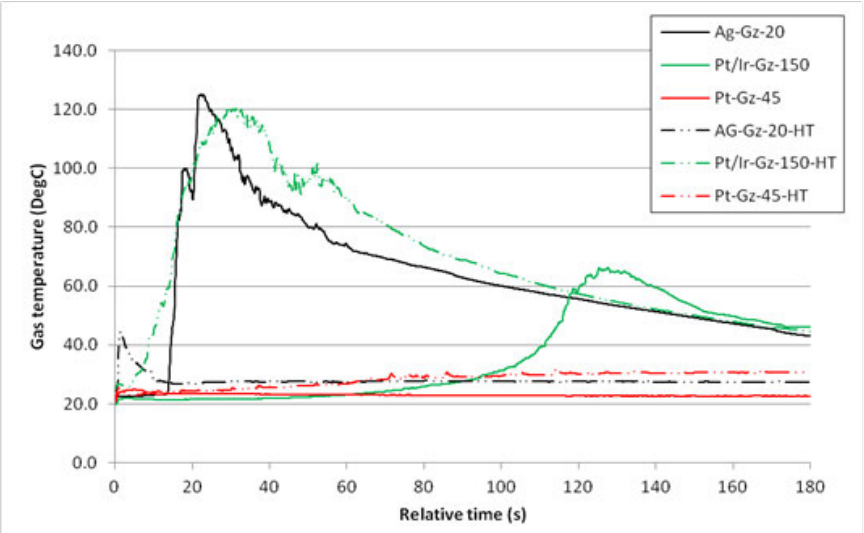

Figure 7-12: Reactor temperature – Metallic gauzes

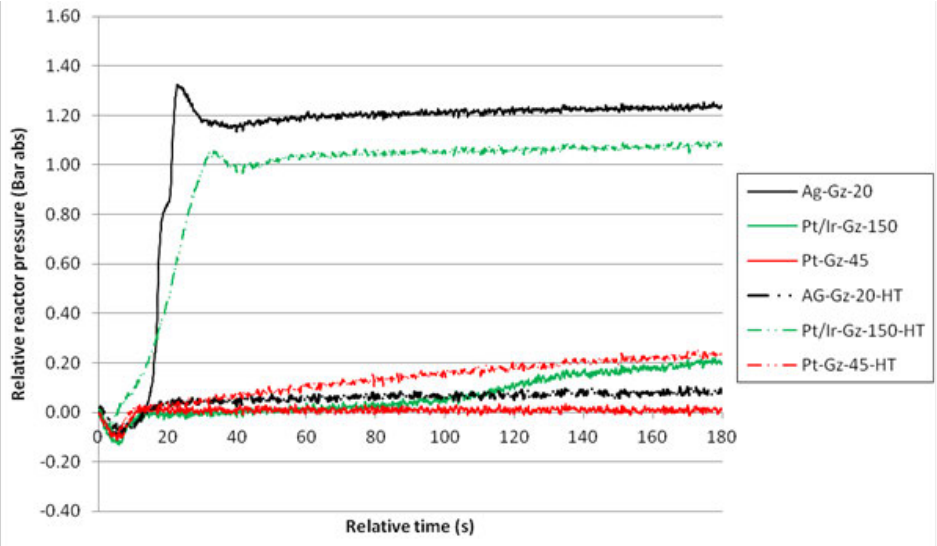

Figure 7-13: Relative reactor pressure – Metallic gauzes

Only silver was subject to repeat tests in response to the good results seen within the sealed reactor. Pt/Ir-Gz-150-HT was not assessed any further due to concerns over its structural integrity which has already been discussed. The repeat test of silver showed the presence of a quenching phase which was not identified in the original run and as a result this delayed the pressure response. The precise reason for this is not clear although previous work has identified the need to preheat silver to avoid this [71,77]. It is therefore likely that silver was close to being quenched in the original run, but this will not significantly affect the results since silver was one of the only gauze catalyst to show good reactivity.

The results for the metallic gauzes are generally disappointing with only silver and heat treated platinum/iridium showing promise. In all cases the metallic gauzes have been outperformed by metallic foam and ceramic supported catalysts.

7.1.2 Sealed Reactor Assessment and Ranking

Due to the variation in the experimental methodology between ceramic/foam and gauze catalysts no direct comparison between the two groups can be undertaken. As a result it was decided to take forward any catalyst that showed promise for further assessment within the life-time mass loss equipment.

The aim of the sealed reactor was to assess the start-up characteristics of the catalysts. In view of this, it has been decided to assess the suitability of the catalysts on the basis of parameters that are more closely related to initial behaviour rather than to the later stages of the reaction.

7.1.2.1 Ceramic and Metallic Foam Supported Catalysts

From the data collected and in view of the appraisal made above the following assessment parameters have been defined:

$\Delta P_{2.5}$: The relative pressure 2.5 seconds after the solenoid valve was opened (bar)

t_{50} : The time taken for the gas temperature to reach 50°C(seconds)

t_{100} : The time taken for the gas temperature to reach 100°C (seconds)

T_{max} : The maximum temperature attained (°C).

Additional investigations found that with liquid water injection and no decomposition products equilibrium pressure was reached in 2s. Accordingly a relative pressure parameter was chosen after this point to be independent of the injection pressure profile. In the majority of cases, the relative pressure was seen to be still increasing 2.5s seconds after initiation, so $\Delta P_{2.5}$ is considered to be a fair measure of overall reactivity with minimal regard to the initial peak activity. If the parameter had been set, say, to 5s, it would not have described the climb towards the peak pressure consistently since all the catalysts showed a peak pressure earlier than 5 seconds. This parameter is considered to be important from the standpoint of catalyst start-up characteristics; a low value would indicate a significant delay in the decomposition reaction, which is undesirable for a thruster. The time taken to reach 50°C (t_{50}) was also chosen for the same reasons. In some cases it was identified that the initial reaction was quickly quenched or there was simply a loss of effectiveness after brief exposure to hydrogen peroxide. A high initial reactivity is of little use if the reaction is subsequently limited by some undesired effect. Therefore a temperature threshold of 100°C was also chosen, which was high enough to have occurred after any quenching effect that may have been experienced. Finally, T_{max} represents the ability of the catalyst to sustain the reaction for long enough to record a significant increase in temperature, despite the high thermal mass of the sealed reactor.

The results show some variation between runs so it was necessary to understand how these affected the assessment parameters chosen. Accordingly Figure 7-14 to Figure 7-17 show graphically the results of the assessment and the population standard deviation due to 'run to run' variations. Differing colours are used to represent the differing forms of the catalyst support structures. Only catalysts that were subject to repeat tests are shown. Ideally, t_{50} and t_{100} should be small, whilst $\Delta p_{2.5}$ and T_{max} should be large.

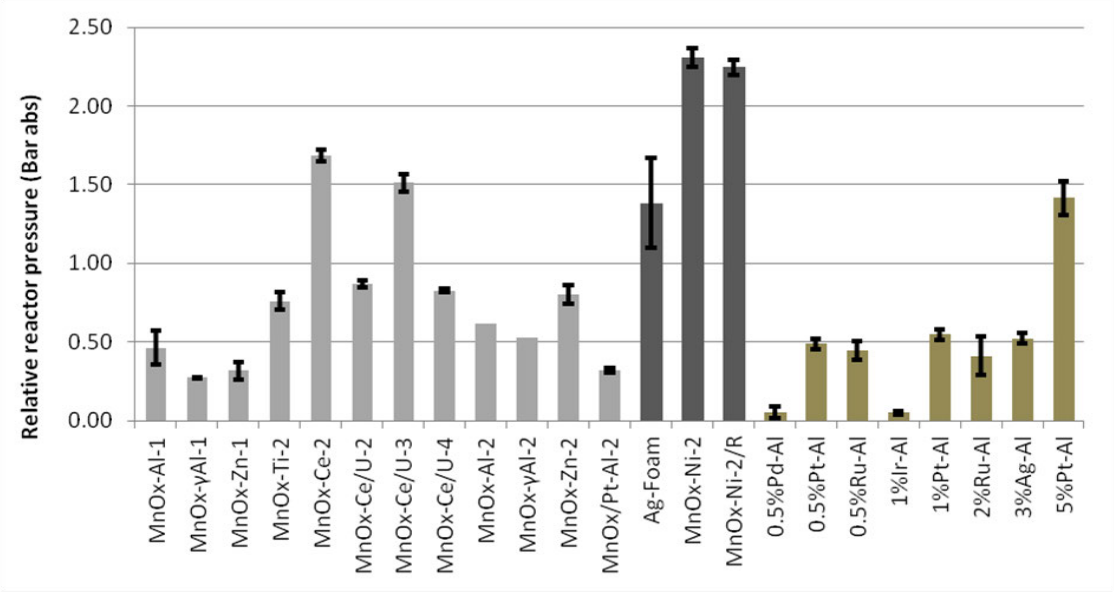

Figure 7-14: Assessment parameter - $\Delta P_{2.5}$

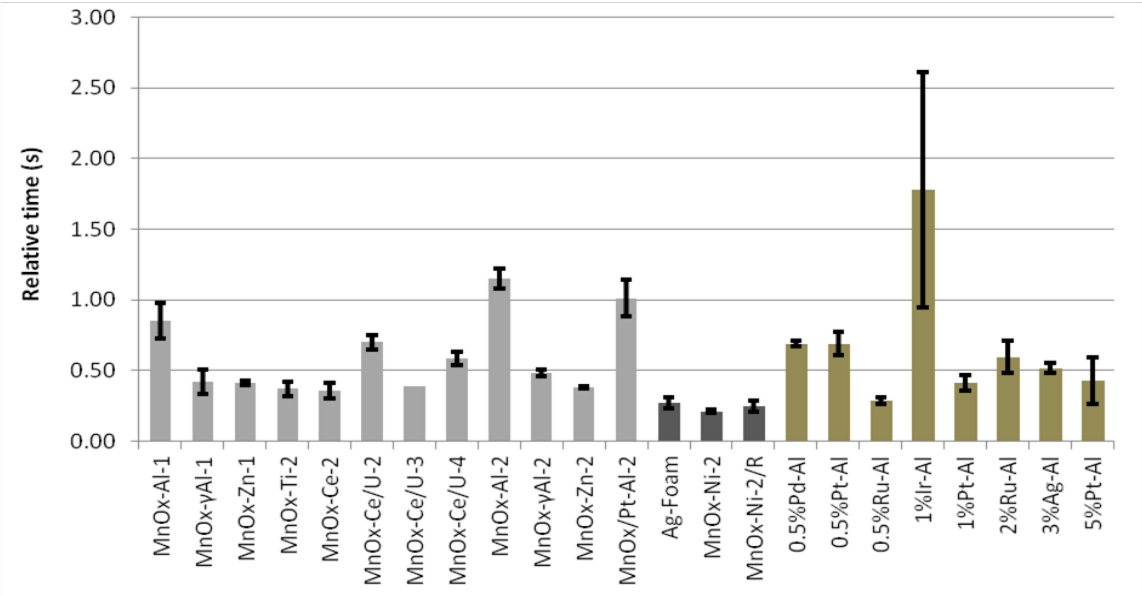

Figure 7-15: Assessment parameter – t_{50}

The significant standard deviation associated with 1%Ir-Al in Figure 7-15 is due to a quenching of the catalyst in the second run, which occurred at a higher temperature than in the first run. Therefore in the second run the parameter refers to the time before the catalyst is quenched and in the first run it is measured after this effect. From these figures the best and worst catalysts are

easily identified. Accordingly these parameters will be used assess the performance of the catalysts within the sealed reactor.

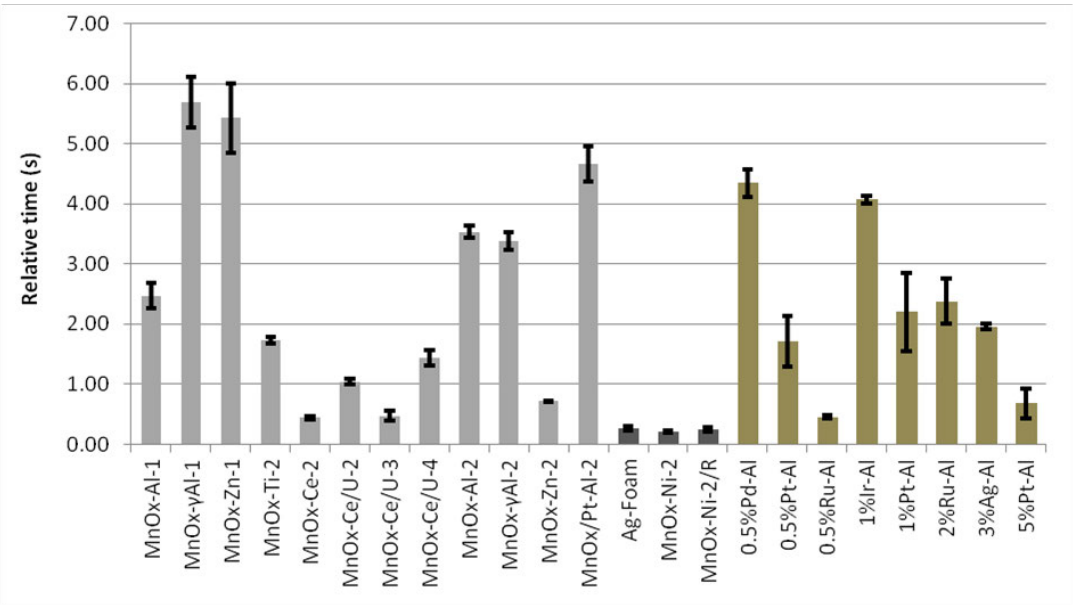

Figure 7-16: Assessment parameter – t_{100}

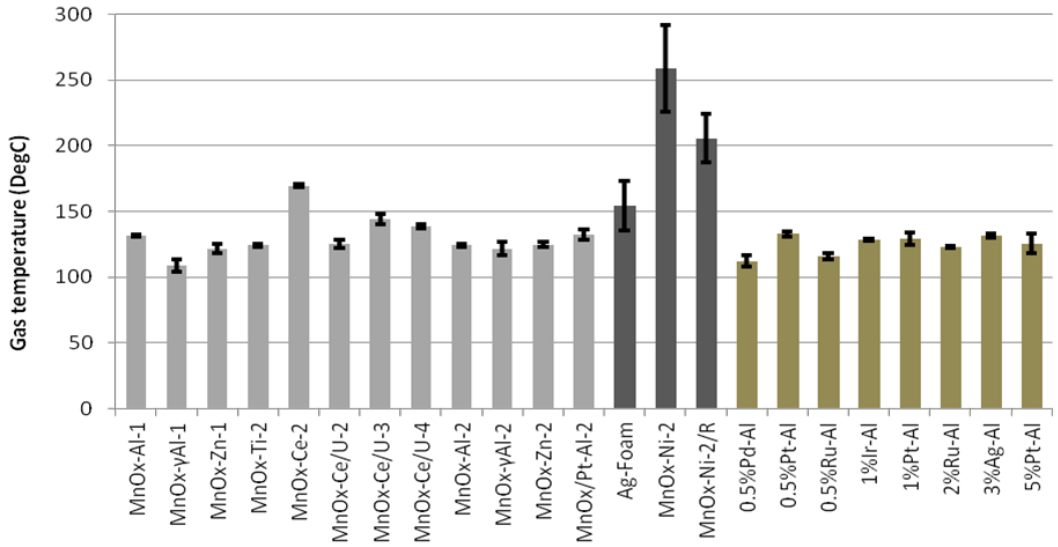

Figure 7-17: Assessment parameter – T_{max}

The above average data are presented in Table 7-1 for the all ceramic and metallic foam based catalysts; significant differences are seen. It is by no means obvious which of these four parameters is the most important from the standpoint of choosing the most appropriate catalyst for a thruster. For example, a high value of T_{max} is of little use if t_{50} is also high, since this combination would be describing a catalyst that is slow to react even though eventually the decomposition temperature is high. Likewise, a low t_{100} in combination with a low $\Delta P_{2.5}$ would indicate rather poor initiation.

Catalysts	$\Delta P_{2.5}$ (bar)	t_{50} (seconds)	t_{100} (seconds)	T_{max} (°C)
MnO_x-Al-1	0.46	0.86	2.47	131.71
MnO_x-γAl-1	0.27	0.42	5.69	108.87
MnO_x-Zn-1	0.32	0.42	5.43	121.66
MnO_x-Ti-2	0.76	0.37	1.73	124.10
MnO_x-Ce-2	1.68	0.36	0.44	169.60
MnO_x-Ce/U-2	0.87	0.70	1.04	125.30
MnO_x-Ce/U-3	1.51	0.39	0.48	144.43
MnO_x-Ce/U-4	0.83	0.59	1.44	138.58
MnO_x-QLγAl-2	1.11	0.42	0.59	143.99
MnO_x-Al-2	0.62	1.15	3.53	124.37
MnO_x-γAl-2	0.53	0.49	3.38	121.70
MnO_x-Zn-2	0.80	0.38	0.72	124.73
MnO_x/Pt-Al-2	0.32	1.01	4.67	132.15
1.0%Ir-Al-HT	0.13	N/A	N/A	30.44
Ag-Foam	1.38	0.27	0.27	154.50
MnOx-Ni-2	2.31	0.21	0.21	258.82
MnOx-Ni-5	1.00	0.44	0.44	162.94
MnOx-Ni-2/R	2.25	0.25	0.25	205.73
0.5%Pd-Al	0.05	0.69	4.35	112.29
0.5%Pt-Al	0.49	0.69	1.71	132.79
0.5%Ru-Al	0.45	0.29	0.46	115.80
1%Ir-Al	0.05	1.78	4.08	128.39
1%Pt-Al	0.55	0.42	2.20	129.07
2%Ru-Al	0.41	0.60	2.38	122.67
3%Ag-Al	0.52	0.52	1.96	131.43
5%Pt-Al	1.42	0.43	0.68	125.60

Table 7-1: Assessment Parameters for HTP Ceramic and Metallic Foam Supported Catalysts

It was decided that at this stage of the assessment no particular weighting should be attached to any one of these parameters. Accordingly the catalysts were ranked with equal weighting according to the values indicated in Table 7-1. The result is shown in Table 7-2 in the form of rankings; where 1 is low and 26 is high (that is to say, 26 indicates desirable reactivity properties). 1.0%Ir-Al-HT failed to meet some of the parameters and is therefore automatically assigned the lowest score. The overall ranking was formed by the sum of each individual score

with a normalised value relative to 1, where 1 is the highest possible score as a result of this assessment.

Catalysts	$\Delta P_{2.5}$ (bar)	t_{50} (s)	t_{100} (s)	T_{max} (°C)	Total	Normalised Total
MnOx-Ni-2	26	26	26	26	**104**	**1.00**
MnOx-Ni-2/R	25	25	25	25	**100**	**0.96**
MnO_x-Ce-2	24	22	22	24	**92**	**0.88**
Ag-Foam	21	24	24	22	**91**	**0.88**
MnO_x-Ce/U-3	23	19	20	21	**83**	**0.80**
MnOx-Ni-5	19	13	22	23	**77**	**0.74**
MnO_x-QLγAl-2	20	15	19	20	**74**	**0.71**
5%Pt-Al	22	14	18	12	**66**	**0.63**
MnO_x-Zn-2	16	20	17	10	**63**	**0.61**
MnO_x-Ce/U-4	17	10	15	19	**61**	**0.59**
MnO_x-Ti-2	15	21	13	8	**57**	**0.55**
0.5%Ru-Al	8	23	21	4	**56**	**0.54**
1%Pt-Al	13	15	11	14	**53**	**0.51**
MnO_x-Ce/U-2	18	6	16	11	**51**	**0.49**
3%Ag-Al	11	11	12	15	**49**	**0.47**
0.5%Pt-Al	10	7	14	18	**49**	**0.47**
MnO_x-Al-1	9	5	9	16	**39**	**0.38**
MnO_x-γAl-2	12	12	8	6	**38**	**0.37**
2%Ru-Al	7	9	10	7	**33**	**0.32**
MnO_x-Al-2	14	3	7	9	**33**	**0.32**
MnO_x/Pt-Al-2	5	4	4	17	**30**	**0.29**
MnO_x-Zn-1	5	15	3	5	**28**	**0.27**
MnO_x-γAl-1	4	15	2	2	**23**	**0.22**
1%Ir-Al	1	2	6	13	**22**	**0.21**
0.5%Pd-Al	1	7	5	3	**16**	**0.15**
1.0%Ir-Al-HT	3	1	1	1	**6**	**0.06**

Table 7-2: Ranking for HTP Ceramic and Foam Catalysts

The majority of these results are as expected with the trends in performance having already being discussed. The change from manufacturing method 1 to method 2 has generally resulted in an improved performance. However MnO_x-Al-1 does not follow this trend but the overall difference between MnO_x-Al-1 and MnO_x-Al-2 is small. Although it is not clear why this is

both have shown relatively poor performance so will not be subjected to a more detailed investigation. The result for ruthenium is also unexpected with 0.5%Ru-Al outperforming 2%Ru-Al, however other authors have identified similar disagreements in performance versus catalyst loading [59,69]. The performance of iridium supported catalysts is contrary to work of authors [60,82]. In both these cases however the percentage catalyst loading was between 3 and 36 times greater than the catalysts used for the current work. It is likely this is the reason for the disagreement.

These results show some agreement with the work of Romeo *et* al [58]. He focused on alumina supported catalysts with various catalyst loadings between 0.06 and 9.54%. Romeo found silver on alumina performed best followed by platinum, ruthenium, manganese oxides and palladium. If only alumina supported catalysts are considered, the current work shows similar results with platinum performing best followed by ruthenium, silver, manganese oxides and palladium. The difference between his work and the current study is limited only to the reactivity of silver on alumina which the present study has found to be relatively low compared to platinum.

7.1.2.2 Metallic Gauze

It was initially hoped to apply the same assessment parameters to the gauzes as were used for the metallic foams and ceramic pellets. However, in light of the results many of the gauze catalysts would not form part of the assessment since the achieved temperatures and pressures were not high enough to meet the assessment criteria. It was therefore necessary to alter these parameters. A trade-off was required; if the criteria were set too high then many of the catalysts would be missed all together. If they were set too low then although more gauze catalysts would meet the criteria the usefulness of the assessment in terms of finding a suitable catalyst for use within a thruster would be brought into question. It was still important to assess the catalysts on the basis of parameters related to short-term behaviour rather than to the later stages of the reaction. Accordingly, the following assessment parameters have been defined:

Δp_{20} : The relative pressure 20 seconds after the solenoid valve was opened (bar)

t_{30} : The time taken for the gas temperature to reach 30 deg C (seconds)

t_{60} : The time taken for the gas temperature to reach 60 deg C (seconds)

T_{max} : The maximum temperature attained (deg C).

The pressures are seen to still be rising in the first 20 seconds after the HTP is injected. This parameter was increased to 20 seconds to allow for the slower injection time (due to the reduced injection pressure and flow constrictor) and the increased initiation delay associated with the gauze catalysts compared to the ceramic-based catalysts. None of the catalysts had reached their peak pressure at this point, so the assessment, Δp_{20}, is independent of the peak pressure. The

first time-related parameter, t_{30}, was based on a relatively low temperature so as to capture gauze catalysts that had become quenched early on in the decomposition. Catalysts such as Ag-Gz-20-HT showed a very short initiation delay time and a significant rate of temperature rise but the reaction quickly became quenched. Although this is a serious concern for catalyst bed applications, several steps can be put in place to reduce the possibility of quenching occurring. A well designed injector, reduced catalyst bed loading and the possibility of pre-heating the bed would all help to mitigate this problem. The second time-related parameter, t_{60}, was also based on a relatively low temperature to allow more of the catalysts to be captured whilst still providing a good indication of the better-performing catalysts. Finally, T_{max} provides an indication of which catalysts can overcome the quenching problem to sustain the reaction for long enough to record a significant increase in temperature.

The metallic gauze data are presented in Table 7-3. As with ceramics and foams it is not obvious which of the four parameters are the most important when choosing a catalyst for thrusters. In cases where the catalyst fails to meet the assessment criteria N/A is put in place of the value.

Gauze Catalysts	ΔP_{20} (bar)	t_{30} (seconds)	t_{60} (seconds)	T_{max}(deg C)
Ag-Gz-20	1.50	15.40	15.60	133.70
Pt-Gz-45	0.01	N/A	N/A	24.90
Pt/Ir-Gz-150	0.02	96.20	120.20	66.40
Pt/Rh/Pd-Gz-80	0.02	N/A	N/A	26.70
Pt/Rh-Gz-80	0.00	N/A	N/A	26.60
Pd/Ni-Gz-50	0.00	N/A	N/A	24.90
Ag-Gz-20-HT	0.05	0.70	N/A	44.30
Pt-Gz-45-HT	0.04	105.30	N/A	31.90
Pt/Ir-Gz-150-HT	0.47	5.40	14.00	120.80
Pt/Rh/Pd-Gz-80-HT	0.04	N/A	N/A	28.20
Pt/Rh-Gz-80-HT	0.04	N/A	N/A	27.10
Pd/Ni-Gz-50-HT	0.03	N/A	N/A	26.20

Table 7-3: Assessment Parameters for HTP Gauze Catalysts

No weighting was attached to any one parameter since it is not clear which is the most important when choosing successful catalysts. The results are shown in Table 7-4 in the form of rankings; where 1 is low and 12 is high (that is to say, 12 indicates desirable reactivity properties). The overall ranking was formed by the sum of each individual score. The catalysts are listed according to their ranking, with the most desirable catalyst at the top of the list. It

should be noted that any catalyst that failed to meet the assessment criteria is automatically assigned the worst score (1). As with ceramic/foam supported catalysts the results have been normalised against the highest possible score as a result of this assessment.

Gauze Catalysts	ΔP_{20}	t_{30}	t_{60}	T_{max}	Total	Normalised Total
Ag-Gz-20	12	10	11	12	**45**	**0.94**
Pt/Ir-Gz-150-HT	11	11	12	11	**45**	**0.94**
Pt/Ir-Gz-150	4	9	10	10	**33**	**0.69**
Ag-Gz-20-HT	10	12	1	9	**32**	**0.67**
Pt-Gz-45-HT	7	8	1	8	**24**	**0.50**
Pt/Rh/Pd-Gz-80-HT	7	1	1	7	**16**	**0.33**
Pt/Rh-Gz-80-HT	7	1	1	6	**15**	**0.31**
Pt/Rh/Pd-Gz-80	4	1	1	5	**11**	**0.23**
Pd/Ni-Gz-50-HT	6	1	1	3	**11**	**0.23**
Pt/Rh-Gz-80	1	1	1	4	**7**	**0.15**
Pt-Gz-45	3	1	1	1	**6**	**0.13**
Pd/Ni-Gz-50	2	1	1	1	**5**	**0.10**

Table 7-4: Ranking for HTP Gauze Catalysts

It can be seen that there is a significant drop in performance after the first two catalysts with Ag-Gz-20 and Pt/Ir-Gz-150-HT placed joint first. The majority of work conducted on gauze based catalysts has previously focused on silver [7,64,65]. The sealed reactor results are in agreement with this research showing that silver is a high performing gauze catalyst. Of interest are the results for platinum; when attached to a ceramic support a high performing catalyst results but in the form of a gauze its performance is poor. This indicates that its performance is highly dependent on the surface area.

7.1.3 Sealed Reactor Summary

A sealed reactor has been developed to test the start-up characteristics of a wide range of catalysts. The results have shown good consistency especially in the early phases of the experiment with the same trends in pressure and temperature being identified in repeat tests. The sealed reactor tests have also confirmed the findings of the catalyst characterisation conducted in chapter 6. Changes to the manufacturing methodology in an attempt to improve performance seemed to have worked with MnO_x-Ce/U-3 outperforming MnO_x-Ce/U-2, with the differences in the ceria base materials being verified by experimental testing. The results have

been used to rank the catalysts in terms of the performance according to four parameters. These parameters have been chosen to focus on the start-up characteristics taking into consideration 'run to run' variations.

Although many of the catalysts have shown similar performance the extremes are clearly identifiable. MnO_x-Ce-2, MnO_x-Ce/U-3 and 5%Pt-Al have been shown to be the best ceramic-based catalysts with MnOx-Ni-2/R and MnOx-Ni-2 the best metallic foam-based catalysts. These have all shown short initiation delay with high peak temperatures and no indication of quenching, key parameters for use within a thruster. At the other end of the spectrum some catalysts have shown very poor performance; with or without heat treatment 1%Ir-Al failed to achieve high temperatures or had an unacceptably long initiation delay. 0.5%Pd-Al showed similarly poor performance.

Generally the gauze catalysts performed poorly in comparison with the ceramic or foam-based catalysts, with the exception of two. Ag-Gz-20 reached high temperatures and pressures but was accompanied by a significant initiation delay; Pt/Ir-Gz-150-HT is worthy of more study due to its high performance and shorter initiation delay, however not in its current structural form. It is possible that its apparent high reactivity is linked to its significantly larger surface area compared to the other gauze catalysts tested.

Some catalysts have been shown to perform well but with additional 'ad-hoc' testing have been shown to be structurally weak. Therefore their continued use within this project would be a waste of resource due to their unsuitability for use within a thruster.

At this time the following catalysts will **not** be subject to further study;

- Pt/Ir-Gz-150-HT
- Pt-Gz-45-HT
- Pt/Rh/Pd-Gz-80
- Pt-Gz-45
- 1%Ir-Al-HT
- MnO_x-QLγAl-2
- Pd/Ni-Gz-50-HT
- Pt/Rh/Pd-Gz-80-HT
- Pt/Ir-Gz-150
- Pd/Ni-Gz-50
- 0.5%Pd-Al
- Ag-Gz-20-HT
- Pt/Rh-Gz-80-HT
- Pt/Rh-Gz-80
- 1%Ir-Al
- MnOx-Ni-5

All the other catalysts will be assessed within the life-time mass loss equipment.

7.2 Life-Time Mass Loss

The Life-time Mass Loss apparatus described in chapter 5 attempts to assess lifetime and survivability; parameters which were not assessed in the sealed reactor. The LTML works by impulsively introducing a small sample of catalyst, of known dimensions, into a relatively large quantity (10g) of 87.5% HTP within a glass vessel. The resulting temperature rise and loss of mass due to the decomposition and release of gaseous products was used to assess catalyst performance. Each catalyst sample was subject to repeat exposure unless the catalyst failed structurally, failed to decompose the peroxide or reached a run limit of ten.

The environment the catalyst saw during this experiment were considered by the author to be the most extreme conditions the catalyst would see during operation, namely a non-preheated thruster which was quenched by the presence of liquid peroxide. A poor catalyst will release the energy liberated from the decomposition slowly. This will be absorbed by the remaining liquid peroxide limiting both the temperature rise and rate of decomposition.

7.2.1 LTML Results

A minimum of two tests have been conducted for each catalyst with a summary of the results shown in Table 7-5. The number of repeats was limited by the available resources. A full set of experimental results has been archived and is available upon request. The results have shown significant variation in the run to run consistency between batches but the catalyst lifetime has generally been shown to be repeatable.

One of the primary aims of this apparatus was to assess structural integrity. There was a concern that the sample size was not large enough to give accurate results. Therefore any catalyst that structurally failed during testing was subject to a minimum of three ‘ad-hoc’ dropper tests to verify the structural integrity over a wider sample range. If no further failure was seen LTML testing was continued. This occurred with both MnO_x-γAl-1 and 0.5%Pt-Al. It is likely that these catalyst samples had a structural defect that caused them to fail.

Catalyst	No. of runs completed and reason for termination*		
	Batch 1	Batch 2	Batch 3
MnO_x-Al-1	1#	1#	2
MnO_x-γAl-1	4#	3	4#
MnO_x-Zn-1	1#	1#	2
MnO_x-Ti-2	2#	2#	
MnO_x-Ce-2	10#	10#	
MnO_x-Ce/U-2	6#	7#	
MnO_x-Ce/U-3	10#	10#	
MnO_x-Ce/U-4	10#	10#	
MnO_x-Al-2	2#	1#	
MnO_x-γAl-2	6#	6#	
MnO_x-Zn-2	1#	1#	
MnO_x/Pt-Al-2	2#	2#	
Ag-Foam	3	2#	2#
MnO_x-Ni-2	10#	10#	
MnO_x-Ni-2/R	6#	5#	5#
0.5%Ru-Al	2#	2#	
2%Ru-Al	1#	2#	
0.5%Pt-Al	7#	1	7#
1%Pt-Al	6#	2	6#
5%Pt-Al	10#	10#	10#
3%Ag-Al	1#	1#	1
Ag-Gz-20	10#	10#	10#

*Green = Completed (>10 runs), Red = Mechanical failure, Grey = Exhausted (<10% mass change)

Table 7-5: Summary of LTML results

The results of the structural integrity assessment are consistent with findings in both this and previous work. During the assessment in chapter 6 it was noticed that ZrO_2, the base material for MnOx-Zn-1 and MnOx-Zn-2, had micro fractures on its surface. It was hypothesised that this may detrimentally affect its structural integrity with this being confirmed through LTML testing. Previous work conducted by the University of Southampton had shown catalyst failure within a 5N HTP thruster using a variant of MnOx-Al-1 [66]. LTML assessment has shown both MnOx-Al-1 and MnO_x-Al-2 do not survive continued exposure to HTP. As catalysts fail the rate of decomposition tends to increase due to an increasing surface area. This results in an

increased rate of mass change in Run 2 compared to Run 1 as shown in Figure 7-18 and Figure 7-19.

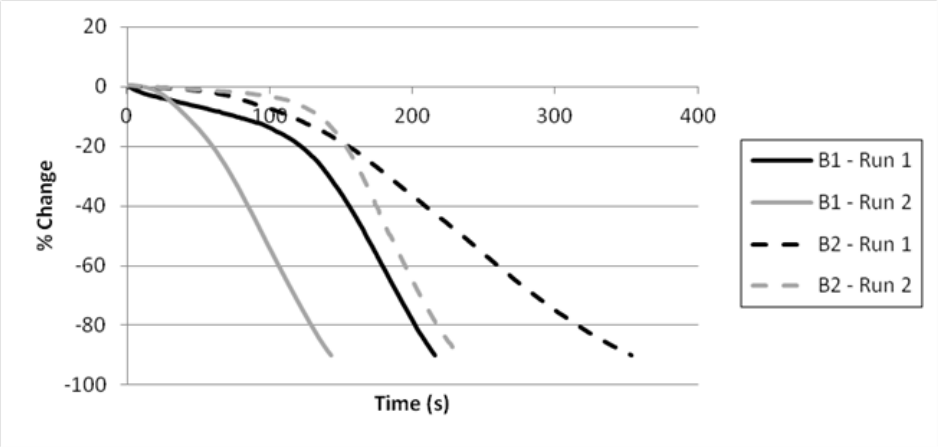

Figure 7-18: MnO_x-Al-2 Test and repeat - % Gradient change

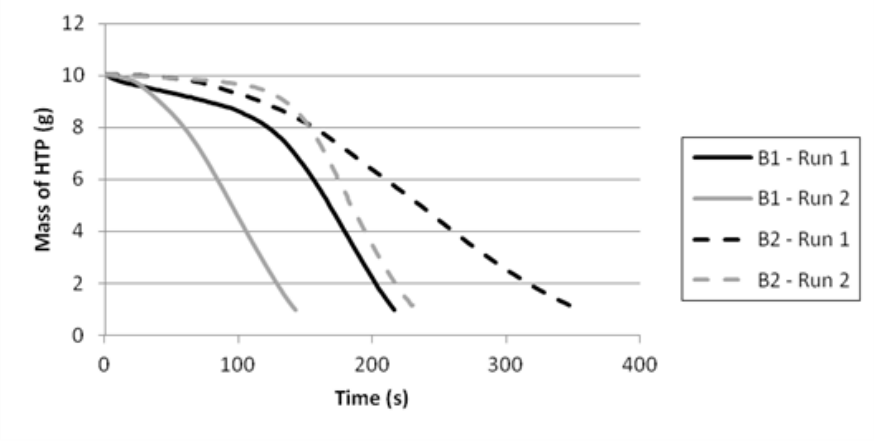

Figure 7-19: MnO_x-Al-2 Test and repeat – Mass change

In order to assess structural integrity the minimum quantity of catalyst was limited to 1 pellet or disc of metallic foam. It was therefore not possible to have consistent catalyst volume (or Euclidean surface area). This variation has undoubtedly had an influence on the catalyst lifetime. It was also not possible to correct for the varying volume as not all the catalysts were taken to exhaustion. Attempting to normalise these results would inevitably lead to errors so care must be taken when interpreting results. For example MnO_x-Ni-2 successfully decomposed 90ml of hydrogen peroxide with complete decomposition being achieved in less than 300s in run 10. However the modified batch MnO_x-Ni-2/R only managed to decompose 35ml of HTP in Run 6. The results for both catalysts can be seen in Figure 7-21 and Figure 7-20 respectively.

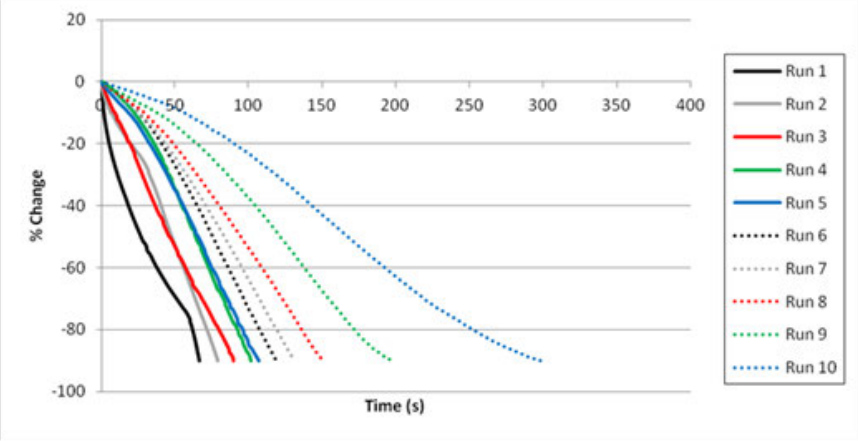

Figure 7-20: MnO_x-Ni-2 Batch 2 Test (Worst Case) – % Gradient Change

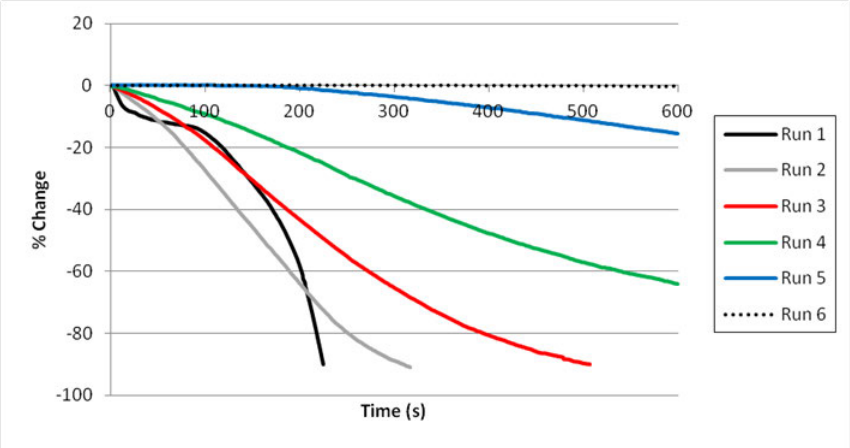

Figure 7-21: MnO_x-Ni-2/R Batch 1 Test (Best Case) – % Gradient Change

Although the performance of MnO_x-Ni-2 looks significantly more active than MnO_x-Ni-2/R its volume was 2.76 times larger. Therefore it cannot be said with confidence that MnO_x-Ni-2 is better than MnO_x-Ni-2/R due to the differences in volume (and resultant Euclidean surface area). However it is likely that some of the performance difference is also associated with variations in the corrected mass loadings reported in chapter 6.

In some cases no interpretation is required. 0.5%Ru-Al was exhausted in two runs as shown in Figure 7-22, decomposing a maximum of 6.22g of HTP. This correlates with previously unpublished work conducted by the University of Southampton and DELTACAT Ltd. They tested 0.5%Ru-Al within a 100N monopropellant thruster. It was found after just one run that the activity of the catalyst had dropped significantly with the test being stopped after four runs due to the expulsion of liquid hydrogen peroxide, indicating little or no decomposition had taken place.

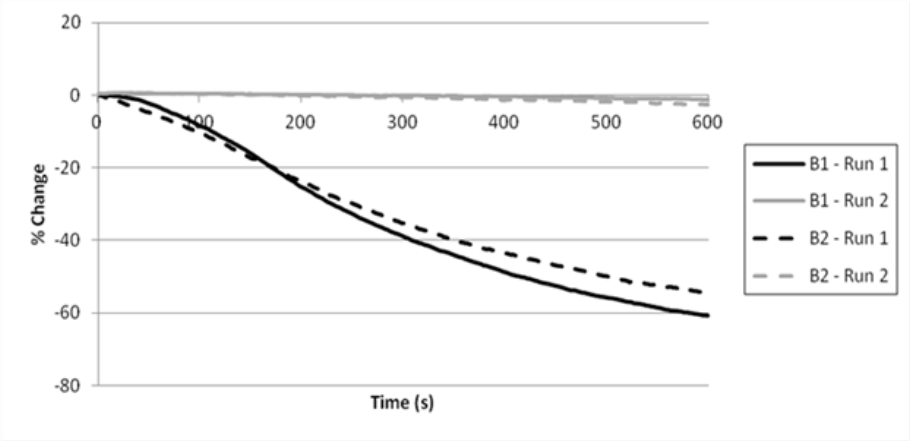

Figure 7-22: 0.5%Ru-Al Test and Repeat - % Gradient change

During testing it was observed that highly reactive catalysts were propelled to the surface of the peroxide solution due to the formation of gaseous decomposition products. As a result the time taken to decompose the HTP solution increased due to the reduced contact area. This did not affect lifetime as the total quantity of HTP decomposed was the same, and as the reactivity decreased the catalysts sank back to the bottom of the flask. However this did influence run to run performance. In addition to this it was noted that at the end of some runs catalytic residue was identified at the bottom of the flask. This was particularly apparent with the manufactured catalysts and led to inconsistent trends in run performance as shown in Figure 7-22 where run 10 is shown to be more active than run 5.

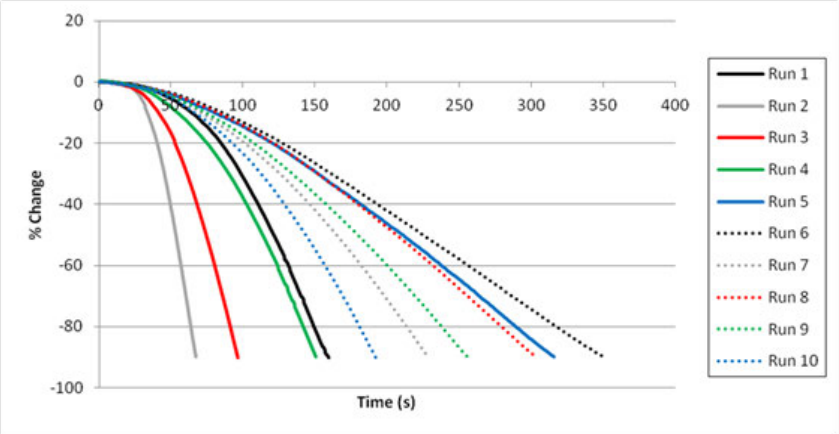

Figure 7-23: MnO_x-Ce/U-4 Batch 1 Test - % Gradient change

This is further exacerbated by high performing catalysts. In these cases, such as above, the performance between runs is already similar so the addition of residue or catalyst movement can appreciably affect the run distribution. The procured catalysts showed less or no residue and as a result the run distribution tended to be linear even for high performing catalysts as can be seen in Figure 7-24.

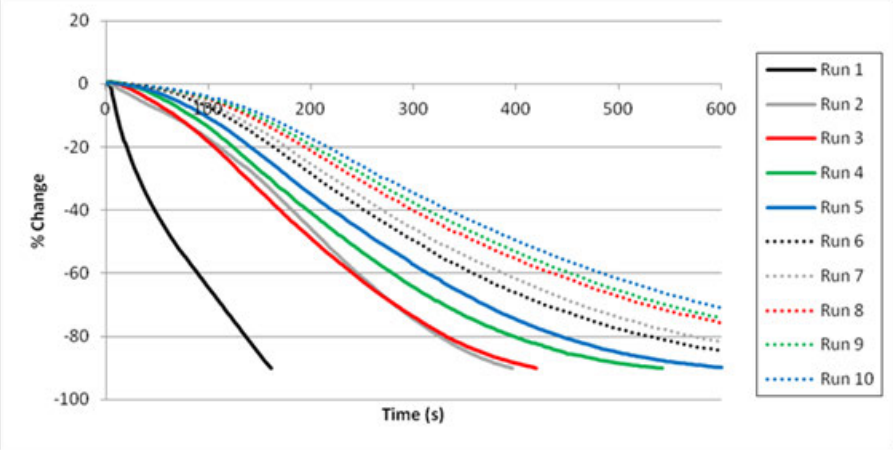

Figure 7-24: 5%Pt-Al 1 Test - % Gradient change

Care must be taken when assessing run to run performance. It would be expected that the formation of residue, and therefore the removal of active phase, would reduce lifetime but, as can be seen in the results, this was not necessarily the case and should not be used as a parameter to reject the catalyst from further investigation.

To this point no mention has been made of the temperature distribution profiles. Figure 7-25 gives a representative example of the temperature distributions.

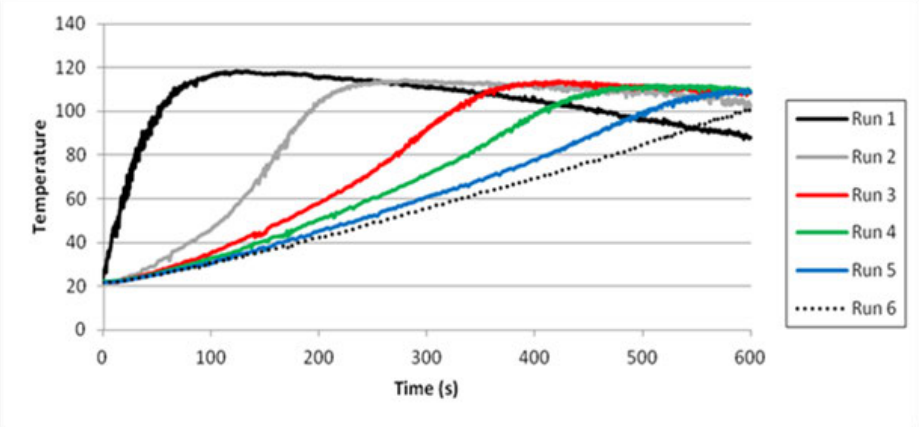

Figure 7-25: 1%Pt-Al Batch 3 Test - Liquid temperature

In all cases the temperature of the liquid did not exceed 120°C which is an indication of the boiling point of the solution. This is low for 87.5wt% hydrogen peroxide which should be approximately 139°C. It is likely this is due a reduced concentration as a result of decomposition in combination with thermal losses. A slow rate of temperature rise and therefore decomposition results in a greater fraction of liquid water reducing the solutions boiling point. As the temperature exceeded 100°C there was a rapid increase in mass loss. At this temperature the reactivity would have increased (according to the Arrhenius equation) but also any water generated would be in a vapour state and allowed to escape. Initially there were concerns that this may alter the results but actually it serves to accentuate the differences between high and low catalyst reactivity. Only those catalysts with good performance will raise the temperature of

the solution beyond 100°C. They are therefore more likely to fulfil the criteria necessary for further testing.

Taking all these factors into consideration there was still good consistency with both the characterisation carried out in chapter 6 and the sealed reactor results. The initial performance of the ceria catalysts assessed on the average time to run 1 completion given in Table 7-6 is equivalent to the sealed reactor results.

Catalyst	Time to run 1 completion
MnO_x-Ce-2	73.3s
MnO_x-Ce/U-2	174.3s
MnO_x-Ce/U-3	118.4s
MnO_x-Ce/U-4	147.5s

Table 7-6: Average time to Run 1 completion for ceria supported catalysts

Since these catalysts had the same support material their volume is similar. Results show MnO_x-Ce/U-2 completed a maximum of 7 runs while all the other catalysts achieved 10. This is in agreement with the reduced percentage catalysts loading identified during manufacture. Unexpectedly MnO_x-Ce/U-4 completed 10 runs with a consistently high performance throughout. This would suggest that the formation of Mn_2O_3 does not have a detrimental effect on lifetime although initial reactivity is lower than MnO_2.

Silver gauze was seen to improve with continued exposure to hydrogen peroxide in the LTML tests, with Figure 7-26 showing a significant improvement in catalyst reactivity after run 2. Previous research discussed in chapter 6 has identified the need to 'activate' this catalyst to maximise performance. This has been associated with a roughening of the surface of silver with exposure to hydrogen peroxide and is consistent with the results seen. Although silver gauze performed well, silver supported on alumina (3%Ag-Al) failed to decompose more than 0.5g in 600s. The reasons for this are unclear but are consistent with the findings of other authors [59].

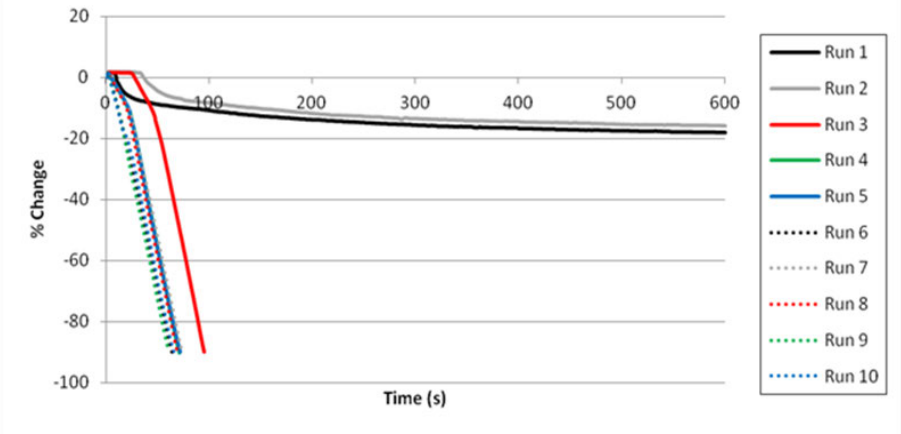

Figure 7-26: Ag-Gz-20 Batch 1 Test - % Gradient change

7.2.2 LTML Assessment and Ranking

As the results have shown, there is significant variation between batches so great care is required when assessing the data. However some parameters do show good repeatability while still offering useful insight into performance. In view of this a total of three assessment parameters have been used to assess the catalysts. Two of these investigate lifetime and survivability while the third investigates catalyst performance;

- M.I.: The mechanical integrity/survivability of the catalyst
- $N_{<10\%}$: Number of runs to <10% Mass loss
- M_{Tot}: The Total mass decomposed over all runs

The first of these is mechanical integrity; this is critically important as a lack of structural integrity will cause catalyst to fragment within the bed leading to increased pressure drop and thruster failure. Any catalysts that fail this criterion after both LTML and 'ad-hoc' testing will be rejected from further assessment.

The second lifetime assessment parameter considered is the number of runs to <10% Mass loss. This criterion was used during testing to identify catalyst exhaustion. Results have shown this parameter has good consistency between batches as Table 7-5 reveals. A catalyst which continues to perform over all 10 runs suggests a good lifetime within a catalyst bed or thruster but makes no attempt to identify high performance.

A catalyst with a long life is of little use if it cannot perform to an acceptable level within a catalyst bed. At the extremes of performance it was possible for a catalyst to complete all 10 runs while only decomposing 1gram in each run, resulting in a total of only 10 out of a possible 90grams of hydrogen peroxide being decomposed. In contrast a catalyst may have only completed 8 runs but decomposed 9grams in runs 1-7 with only 1gram in the final run. This would lead to a total HTP consumption of 64 grams. Therefore only considering the number of runs may lead to an inaccurate placement within the final ranking. The third criterion tries to address this by measuring the total amount of peroxide decomposed over all the runs completed. This is represented graphically in Figure 7-27 with the population standard deviation showing the variation between batches. Colours are used to indicate differing forms of support material. In the majority of cases the variation remains relatively small so the results are considered to be valid.

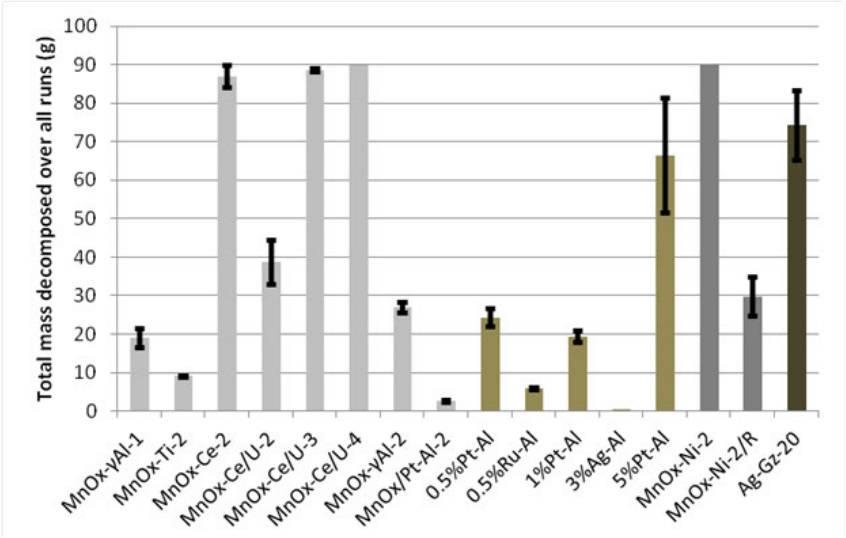

Figure 7-27: Assessment parameter - M_{Tot}

It was initially hoped that the individual run performances could be used to further asses the candidate catalysts. This would have allowed the change in performance to be quantified, making possible a more accurate prediction of catalyst lifetime. The run performance was calculated by placing a linear trend line over the run data and recording the resulting equation, an example of this can be found in Figure 7-28.

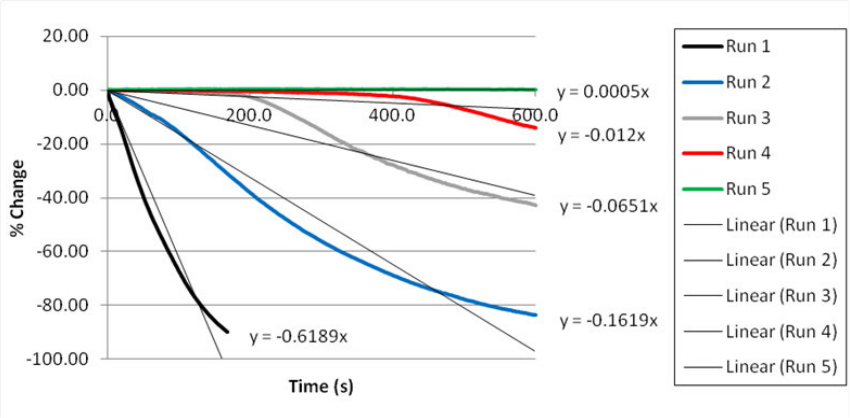

Figure 7-28: Application of linear trend line - MnO_x-Ni-2/R Batch 3

Two approaches were taken; the first was comparing the final run gradients for different catalysts. The second was comparing the change in relative gradients between the first and final runs. In both cases the standard deviation in the results was shown to be unacceptably high. Adjusting the results for the varying catalyst volumes did help reduce this uncertainty but only to an average of 31% and 86% for the two approaches. This was still considered by the author to be too high to allow valid comparisons to be made. The same issue was faced when comparing rate of temperature rise.

The average results of the assessment are summarised in Table 7-7 for all the catalysts tested. For the reasons stated above mechanical integrity has been identified as the most important criterion. The influence of varying catalyst volume has not been taken into consideration. It was identified during the results that normalising any of these parameters against volume could be

misleading as the highest performing catalysts were not exhausted during testing. As discussed, it would have been possible to normalise comparative rates of change but the large degree of uncertainty associated with these results would have limited the value of any assessment. The number of runs to <10% mass loss are average values of all the repeat batches tested.

Catalyst Name	Mechanical Integrity	No. of Runs to <10% Mass loss	M_{Tot} HTP decomposed (g)
MnO_x-Al-1	✗		
MnO_x-γAl-1	✓	4.0	19.1
MnO_x-Zn-1	✗		
MnO_x-Ti-2	✓	2.0	9.1
MnO_x-Ce-2	✓	10.0	87.0
MnO_x-Ce/U-2	✓	6.5	38.8
MnO_x-Ce/U-3	✓	10.0	88.7
MnO_x-Ce/U-4	✓	10.0	90.0
MnO_x-Al-2	✗		
MnO_x-γAl-2	✓	6.0	26.9
MnO_x-Zn-2	✗		
MnO_x/Pt-Al-2	✓	2.0	2.7
0.5%Pt-Al	✓	7.0	24.4
0.5%Ru-Al	✓	2.0	6.0
1%Pt-Al	✓	6.0	19.4
2%Ru-Al	✗		
3%Ag-Al	✓	1.0	0.5
5%Pt-Al	✓	10.0	66.4
Ag-Foam	✗		
MnO_x-Ni-2	✓	10.0	90.0
MnO_x-Ni-2/R	✓	5.3	29.8
Ag-Gz-20	✓	10.0	74.3

Table 7-7: Assessment parameters for LTML testing

Due to its importance mechanical integrity has been given the highest weighting with any catalyst failing this parameter not being assessed further. It was not decided to weight either of the other two criteria as it was unclear which was the most important for thruster applications. The results of this ranking are shown in Table 7-8 where 1 is low and 16 is high (that is to say 16 shows the longest surviving or highest performing catalyst). The overall ranking was formed by the sum of each individual score with a normalised value relative to 1, where 1 is the highest achievable score as a result of this assessment.

Catalyst Name	M.I.	$N_{<10\%}$	M_{TOT}	Total	Normalised Total
MnO_x-Ce/U-4	✓	16	16	32	1.00
MnO_x-Ni-2	✓	16	16	32	1.00
MnO_x-Ce/U-3	✓	16	14	30	0.94
MnO_x-Ce-2	✓	16	13	29	0.91
Ag-Gz-20	✓	16	12	28	0.88
5%Pt-Al	✓	16	11	27	0.84
MnO_x-Ce/U-2	✓	9	10	19	0.59
0.5%Pt-Al	✓	10	7	17	0.53
MnO_x-γAl-2	✓	8	8	16	0.50
MnO_x-Ni-2/R	✓	6	9	15	0.47
1%Pt-Al	✓	8	6	14	0.44
MnO_x-γAl-1	✓	5	5	10	0.31
MnO_x-Ti-2	✓	4	4	8	0.25
0.5%Ru-Al	✓	4	3	7	0.22
MnO_x/Pt-Al-2	✓	4	2	6	0.19
3%Ag-Al	✓	1	1	2	0.06
MnO_x-Al-1	×				
MnO_x-Zn-1	×				
MnO_x-Al-2	×				
MnO_x-Zn-2	×				
2%Ru-Al	×				
Ag-Foam	×				

Table 7-8: Ranking of LTML assessment results

The results show that the manufactured catalysts have generally outperformed the procured catalysts with MnO_x-Ni-2 supported on metallic foam performing well. Silver gauze is also shown to compare well with the ceramic and metallic foam supported catalysts. This is consistent with the findings of other authors [59,63].

There are some differences between the results gathered and what had been expected. MnO_x-Ce/U-4 performed exceptionally well suggesting that Mn_2O_3 was very active with hydrogen peroxide, although initial performance was lower compared to MnOx-Ce/U-3. In both cases the base materials are identical so performance is not affected by changes in catalyst volume. Several authors have disagreed with these findings suggesting Mn_2O_3 has a lower performance

[57,69]. No definitive explanation can be given for this but due to the low sample size more repeat tests would have to be conducted to confirm this. During the characterisation MnO_x-Ce-2 was found to have the highest loading of all the ceria supported catalysts. It was expected that this would correlate to the highest lifetime but this is not the case. It is likely this is associated with the formation of residue and the removal of the active phase. It was suggested that due to the same internal structure the additional loading may have been in the form of surface deposits which were readily removed during early runs. This may also explain why initial performance was so high.

The comparison between MnO_x-Ni-2 and MnO_x-Ni-2/R has already been discussed however when ranked the differences between the two become even more apparent. Although the catalyst volume does vary significantly it is believed the change in performance is also related to the large difference in catalyst loading. 0.5%Pl-Al has outperformed 1%Pl-Al both overall and particularly in run 1 performance. This is contrary to the sealed reactor findings. 0.5%Pt-Al was tested within the preliminary instrumented catalyst bed and shown to be an effective catalyst. Silver foam was found to be an effective catalyst but was rejected on mechanical integrity grounds. This appears to indicate that silver foam has some promise as a catalyst but more work is required to improve the manufacturing process to produce a more robust structure.

7.2.3 Life-Time Mass Loss Summary

A simple piece of experimental apparatus has been developed to assess the performance of twenty-two candidate catalysts with extended exposure to hydrogen peroxide. Good consistency has been shown when assessing key parameters such as mechanical integrity and lifetime which has been verified through ‘ad-hoc’ testing. However there is considerable variation between individual runs in different batches. The source of these differences has been suggested with small sample size and the formation of active phase residue the main contributors. The lack of residue formation for procured catalysts resulted in an improved run-to-run consistency. Catalyst volume also varied between different catalysts and, to a less extent, between batches of the same catalyst. It was not possible to correct for these variations due to the limited number of runs which meant not all catalysts were taken to exhaustion.

The apparatus managed to successfully reject six catalysts on the basis of structural integrity; this was verified with additional ‘ad-hoc’ testing. Some catalysts which had been shown to perform well in the sealed reactor lost effectiveness when exposed to hydrogen peroxide for long durations. For example the performance of 0.5%Ru-Al reduced quickly with repeated exposure to hydrogen peroxide. This is consistent with previous work conducted by the University of Southampton in combination with DELTACAT Ltd. It was not possible to

compare catalysts on the change in performance between the first and last run due to the high level of uncertainty in the results. However a performance assessment based on the total mass decomposed was possible; this helped to separate out the best performing catalysts. With the completion of the laboratory based experiments the final down selection of candidate catalysts can take place.

7.3 Assessment of Highly Stabilised Hydrogen Peroxide

In chapter 3 reference was made to highly stabilised hydrogen peroxide. Many critics of HTP make reference to problems with long term storage as a reason for it not being more widely adopted by the space community [15,16]. One possible solution to this is the use of highly stabilised hydrogen peroxide or HSHP. This contains significantly higher concentrations of stabilisers in an effort to avoid self-decomposition.

If HSHP is to be used it must be shown that it does not adversely affect catalyst performance. It was thought the most appropriate assessment of the influence of stabilisers on catalyst performance was within the LTML. This allows the accumulative effect of poisoning to be quantified. Four catalysts were chosen for HSHP exposure; MnO_x-Ce/U-3, MnO_x-Ni-2/R, 5%Pt-Al and Ag-Gz-20.

As expected HSHP had a detrimental effect on catalyst performance with three of the catalysts being poisoned within two runs. An example of this can be seen when Figure 7-24 (Above) and Figure 7-29 (Below) are compared. The results are summarised in Table 7-9 which gives the total amount of hydrogen peroxide decomposed by each catalyst for both HSHP and standard PROPULSE™875 HTP.

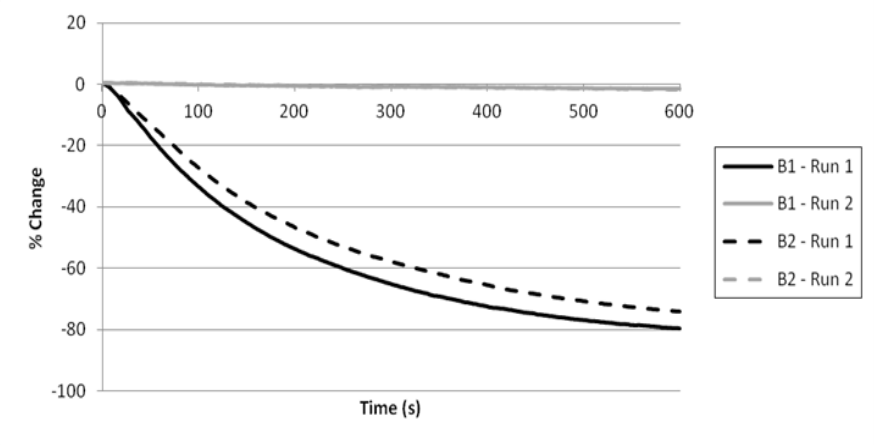

Figure 7-29: 5%Pt-Al Test and Repeat - % Gradient change - HSHP

Catalyst	Quantity of hydrogen peroxide decomposed (g)	
	Batch 1	Batch 2
MnO_x-Ce/U-3	0.10	0.05
MnO_x-Ni-2/R	0.45	3.74
5%Pt-Al	8.10	7.59
Ag-Gz-20	21.31	11.1

Table 7-9: Quantity of HSHP decomposed by catalysts

By comparison Ag-Gz-20 was relatively effective at decomposing HSHP with up to four runs being completed (Figure 7-30). It was noticed during these runs that a yellow discolouration of the HSHP occurred and afterwards a fine deposit was coating the flask. The yellow colouration is consistent with the formation of silver phosphate (Ag_3PO_4). The residue was found to be catalytic and it is therefore assumed that some of the silver had been dissolved and deposited on the walls of the flask.

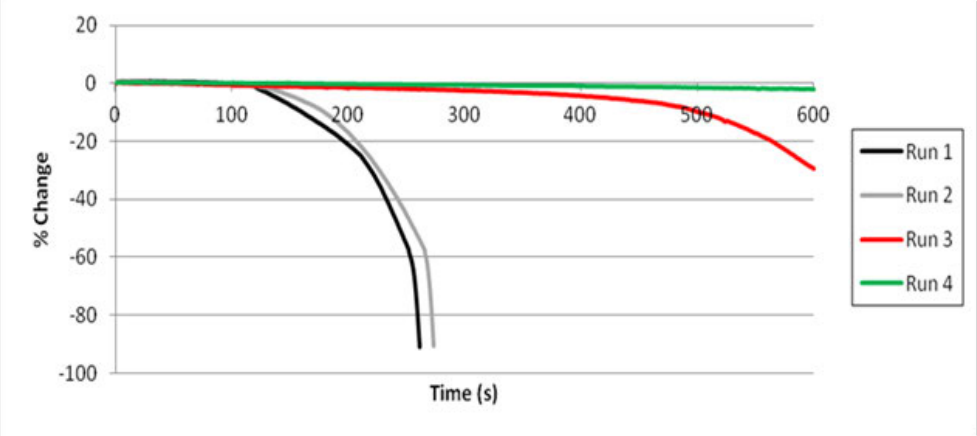

Figure 7-30: Ag-Gz-20 Batch 1 Test - % Gradient change - HSHP

The results are consistent with the findings of Pirault-Roy *et al* [70] who assessed the effect of phosphate ions and stannate ions on the performance of Ag and MnO_2 supported catalysts. The high phosphate content significantly lowered the performance of MnO_2 catalysts but had less of an effect on the Ag catalysts. The results of this assessment have shown that HSHP is not suitable for use with heterogeneous catalysts regardless of its improved storage capabilities.

7.4 Final Down-Selection

In the introduction to this chapter two questions were posed: how effective is the catalyst at decomposing hydrogen peroxide and how is this performance affected by extended peroxide exposure? The laboratory experiments performed in this study have attempted to provide answers to these questions. However the conditions seen by the catalysts during thruster operation differ to those of the sealed reactor and life-time mass loss apparatus. The most effective way of assessing these catalysts under realistic conditions is within a representative catalyst bed. The resources required to test catalysts under these conditions are considerably higher than have been employed so far so it is unrealistic to try to assess all the candidate catalysts using this method. Accordingly a down selection process is required to reduce the quantity of candidate catalysts to be tested.

Four forms of support materials have been assessed: manufactured ceramic-supported catalysts, procured ceramic-supported catalysts, metallic foam and metallic gauze catalysts. Each of these has different advantages and disadvantages related to available surface area, pressure drop, risk of mechanical failure and consistency. It has therefore been decided to take the most suitable, highest performing catalysts in each category forward for testing within a representative catalyst bed. In order to select the best catalysts the combined results of the laboratory experiments will be used. After successful testing within each of the apparatus the catalysts were ranked according to varying performance criteria. In both cases the results of this assessment were normalised to fall between zero and one. This allows the results to be directly compared irrespective of the number of criteria chosen and their resultant total.

Not all catalysts that started this process will form part of the final down-selection. Each of the experiments has identified a number of catalysts that have performed particularly badly or structurally failed so as to be ineffective for thruster applications. From the thirty-eight catalysts originally identified only fifteen have made it to the final down selection. Silver gauze will not be included in the down selection for two reasons. Firstly, the aim of this work is to find a catalyst that is able to decompose hydrogen peroxide concentrations above 95%. This is higher than the melting point of silver. Secondly, silver gauze underwent a different testing procedure in the sealed reactor and therefore no direct comparison is possible. This is not to say silver will not be tested within the catalyst beds being designed. Due to its extensive heritage it will act as a baseline comparator for the higher temperature catalysts being developed.

The completed selection process is shown in Table 7-10. The final down-selection is the sum of the normalised totals of the two sets of experimental results obtained from the sealed reactor and life time mass loss test rigs.

Unfortunately it is not as simple as taking the highest performing catalysts in each category. Other factors do affect this final selection. For example MnO_x-Ni-2 is not suitable for catalyst bed integration. Its large rectangular size will negatively impact the packing density, and the 90° corners risk being damaged or crushed within the catalyst bed. Accordingly MnO_x-Ni-2 will be rejected in favour of MnO_x-Ni-2/R. This smaller, circular support is much more suited to catalyst bed testing. This change is less significant than the table would indicate. Within the sealed reactor the performance of these two catalysts was almost identical. The LTML results do show a much greater difference, but as has been discussed the majority of this difference can be attributed to their differing volume.

Catalysts		LTML Ranking	SR Ranking	Down-Selection
Form	**Name**	**Normalised Total**	**Normalised Total**	**Total**
Metallic Foam	MnO_x-Ni-2	1.00	1.00	2.00
Ceramic (M)	MnO_x-Ce-2	0.91	0.88	1.79
Ceramic (M)	MnO_x-Ce/U-3	0.94	0.80	1.74
Ceramic (M)	MnO_x-Ce/U-4	1.00	0.59	1.59
Ceramic (P)	5%Pt-Al	0.84	0.63	1.48
Metallic Foam	MnO_x-Ni-2/R	0.47	0.96	1.43
Ceramic (M)	MnO_x-Ce/U-2	0.59	0.49	1.08
Ceramic (P)	0.5%Pt-Al	0.53	0.47	1.00
Ceramic (P)	1%Pt-Al	0.44	0.51	0.95
Ceramic (M)	MnO_x-Ti-2	0.25	0.55	0.80
Ceramic (P)	0.5%Ru-Al	0.22	0.54	0.76
Ceramic (M)	MnO_x-γAl-2	0.31	0.37	0.68
Ceramic (M)	MnO_x-γAl-1	0.38	0.22	0.60
Ceramic (P)	3%Ag-Al	0.06	0.47	0.53
Ceramic (M)	MnO_x/Pt-Al-2	0.19	0.29	0.48

Table 7-10: Down-Selection of Candidate Catalysts

The manufactured catalyst that lies second in the table is also unsuitable for catalyst bed applications. MnO_x-Ce-2 suffers from two main drawbacks. Its average length is more than 35% greater than the equivalent CeO2/U support with much less uniformity in its length. This increase in length may again reduce packing density while risking fracturing within the catalyst bed. LTML testing has confirmed that this catalyst in unlikely to fail due to hydrogen peroxide exposure but fracturing due to the mechanical loads placed upon it is more likely. Secondly there is a limitation in the quantity of base material available. Although it could be used within a

catalyst bed it is unlikely there would be enough for future thruster testing. Accordingly MnO_x-Ce-2 will be substituted for the next highest performing manufactured catalyst; MnO_x-Ce/U-3. This catalyst does not suffer from the same drawbacks.

Finally the highest performing procured ceramic catalyst is 5%Pt-Al; this can be procured in enough quantity and is of the right dimensions to be suitable for catalyst bed applications. The results of the down-selection have resulted in four catalysts being selected for continued investigation. They are;

Name	Form	Description
Ag-Gz-20	Gauze (20 mesh)	Procured 99.99% silver gauze with 0.356 wire diameter
5%Pt-Al	Ceramic pellets	Procured 5%wt. platinum loading on a 3.2mm diameter alumina pellet support
MnOx-Ce/U-3	Ceramic pellet	Manufactured 1.44mm diameter ceria pellets (CeO2/U) impregnated with MnxOy using manufacturing method 3
MnOx-Ni-2/R	Metallic foam	Manufactured 4mm nickel foam discs impregnated with MnxOy using manufacturing method 2

Table 7-11: Final down-selected catalysts

Although there are only the resources available to carry these four forward the results of the laboratory experiments have identified a selection of other catalysts which are of interest. Of particular interest is MnO_x-Ce/U-4 and Pt/Ir-Gz-150-HT, both have shown promise and are worthy of future investigation in the framework of future work.

8 Catalyst Bed Assessment of Down Selected Catalysts

The down-selected catalysts identified in chapter 7 have been shown to be effective under laboratory conditions but this does not necessarily correlate to good thruster performance. High performance under representative operating conditions can only be verified through instrumented catalyst bed testing. This chapter provides the results for both the pICB (preliminary instrumented catalyst bed) and hICB (highly instrumented catalyst bed); the design of these beds is detailed in chapter 5. Due to problems with both the instrumentation and test program the pICB was not subject to extensive testing and therefore the results will only be summarised here. The majority of this chapter will focus on the results from the hICB.

8.1 Preliminary Instrumented Catalyst Bed

The aim of the preliminary instrumented catalyst bed (pICB) was to provide design data for the engineering bread-board (EBB) thruster developed in chapter 9. The results from the pICB were used to determine the location of the decomposition plane as well as the effect of channelling. The manufacture and testing of the pICB occurred before the laboratory assessment in Chapter 7 had been completed. Therefore the two catalysts chosen to be tested were 0.5%Pt-Al (0.5% platinum on alumina pellets) and Ag-Gz-20 (metallic silver gauze). A full description of the apparatus and results can be found in the paper presented at the AIAA Joint Propulsion Conference in July 2011 [76], a copy of which can be found in Appendix C.

8.1.1 pICB results and assessment

At the beginning of each run the catalyst bed was pre-heated with short pulses of HTP. This was achieved by pulsing the flow control valve (FCV) with a duty cycle of 0.2 seconds open followed by 1.8 seconds closed. The pulsing sequence continued until the decomposition was judged to be nearly established at which time the solenoid valve was left fully open. The criterion used to decide this was an observed maximum temperature greater than 400°C.

A total of four runs were conducted with 0.5%Pt-Al. 401 pellets were placed within the catalyst bed with a single disc of nickel foam being positioned against the injector to help disperse the peroxide. In the case of silver gauze 157 discs were packed into the bed. The silver gauze was not compressed to avoid damaging the thermocouples. However it is understood that high compression helps to alleviate some of the problems of channelling flows [83]. As a result there was an increased risk of channelling within the bed in the present tests. Only two successful runs were conducted with Ag-Gz-20, there were however several other runs conducted which

showed undesirable characteristics. A low-frequency instability within the bed pressure, typically ±2.5bar at about 2-3 Hertz, was observed in these trial runs. Several other authors have detected similar pressure oscillations [63,77] in their work.

A full set of results for a typical run using both Ag-Gz-20 and 0.5%Pt-Al can be found in the conference paper provided in Appendix C. An example of the temperature profiles attained with 0.5%Pt-Al can also be found in Figure 8-1, here radial measurements are labelled with "(Rad)".

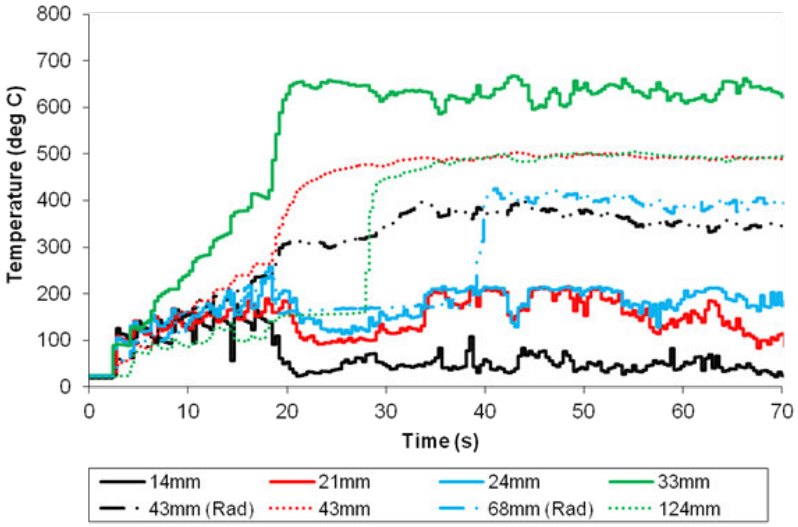

Figure 8-1: Temperature profiles for 0.5%Pt-Al

After an initial pulsing phase lasting approximately 18s the FCV is left open and the temperature at 33mm is seen to rise rapidly, reaching a steady state decomposition efficiency of 95.4%. This indicates that the change to a fully decomposed flow occurs close to this location; this was the same for all the pellets runs conducted. It can be seen that the radial temperature recorded at 43mm (Rad) is significantly below the axial measurement at the same location indicative of either a channelling flow or the cooling effect of the wall. After the peak temperature has been reached the temperature decreases due to heat losses caused by the high thermal capacity of the downstream flange in combination with the thermal capacity of the downstream pellets. It was found that the number of starting pulses that were needed reduced as the ambient bed temperature increased between runs. The temperature varied from 5°C for Run zero to 25°C for Run 3. This suggests that considerable benefit might be gained from even modest electrical heating of the bed before each run.

When the results for silver were compared with the pellet runs, the mass flow rate and pressure signals appeared to be significantly less noisy. This was likely due to the reduced susceptibility of the gauzes to move within the bed. The pellets can move within the bed and any mechanical failure or abrasion can lead to the formation of voids known for increasing thruster roughness [84]. The highest steady state temperature achieved with silver gauze showed a decomposition efficiency of only 74.5%. This is significantly lower than that achieved with ceramic pellets

even though the ambient and HTP temperature was higher. Many other authors have achieved higher decomposition efficiencies with silver; Jonker *et al* [77] achieved a decomposition efficiency of 92% while Palmer *et al* [66] reached a peak decomposition efficiency of 87%. In both runs with silver gauze consistently high temperatures were recorded by the thermocouple located close to the bed wall 68mm from the injector. In contrast the temperature in the core of the bed was limited to approximately 255°C; the boiling point of HTP at this pressure and concentration. This suggests that the majority of the flow is travelling down the centre of the catalyst bed limiting the core temperature but allowing the radial temperature to increase.

A comparison of the two catalysts has been made in Figure 8-2 which shows the temperature distribution along the length of the catalyst bed 49s into the run. The measurements indicated by a solid point on the graph refer to radial and not axial readings. The low radial measurements for 0.5%Pt-Al suggest some channelling is occurring. If the low temperature was associated with wall cooling the radial temperature should decrease with increasing distance from the maximum temperature this, however, is not the case.

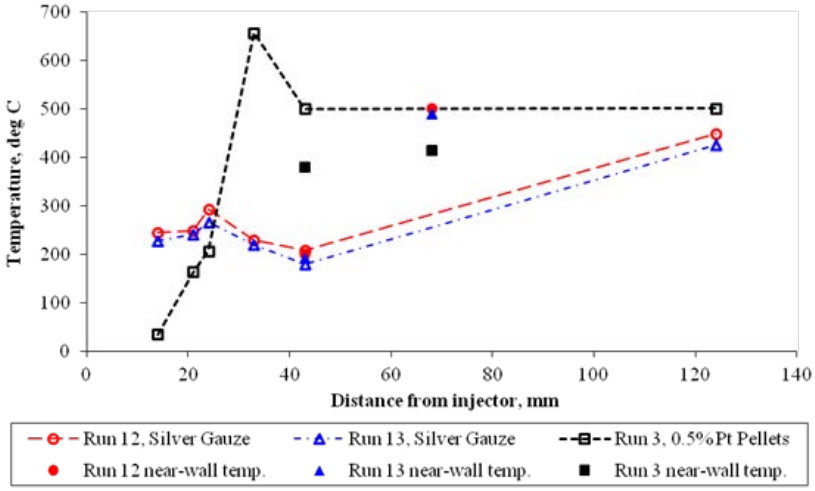

Figure 8-2:Temperature Distributions within Bed at t = 49 s

The graph suggests that the decomposition plane, which is associated with the peak activity, occurs at an L/D of approximately 2 for pellets but a much greater 4.5 for gauzes. This indicates that pellets are more reactive even though they have decomposed almost three times as much peroxide (Run 3) compared to silver gauze (Run 13).

Due to the notable differences in the starting conditions it is difficult to make an assessment on the start-up characteristics of the two catalysts and the limited repeat testing does not allow definitive conclusions to be drawn on the re-start capability of the catalyst. Both catalysts have showed improved characteristics at re-start which may indicate that their peak performance has yet to be reached. Some of the difference in performance between the two catalysts can be attributed to their surface area. Pellet based catalysts have surface areas orders of magnitude

greater than metallic gauze. This difference would be partially reduced if the compression used to pack the gauze was increased.

The pICB was able to provide an estimation of the decomposition plane as well as the optimal position of anti-channelling baffles. It therefore successfully achieved its primary aim of providing design data the EBB thruster. However, the inconsistent starting profiles and inability to conduct identical repeat tests made it unsuitable for catalyst lifetime assessment. It was in part due to these reasons that the hICB was developed.

8.2 Highly Instrumented Catalyst Bed

The hICB was developed in parallel with the EBB thruster to provide a more detailed investigation of the lifetime and re-start capability of the down-selected catalysts. In order to facilitate this, upgrades were made to the catalyst bed, data acquisition hardware and testing methodology. The aim was to assess catalyst performance during the most challenging phase of thruster operation when the catalyst was most likely to be quenched and under significant thermal stresses due to the rapidly changing conditions.

8.2.1 hICB Test Program

The test program for all the catalysts tested was identical. Once filled the catalyst bed was placed into position and connected, the bed was then electrically heated with a 610W heating element coiled around the outside of the catalyst bed. The target initial temperature for all runs was 50°C. For the experiment to begin, two axial temperature measurements had to show 50°C or greater. For all repeat runs the catalyst bed was allowed to fall below this initial temperature and then was electrically heated back up to 50°C. This ensured a more even distribution of heat rather than relying on residual heat from the previous run. When at temperature the software actuated the flow control valve (FCV) for 10s before the experiment was allowed to return to its initial conditions. For all catalysts a minimum of 18 runs were conducted.

A trade-off had to be made between a low starting temperature and a rapid turnaround between runs. At low temperatures weaknesses in the catalysts were more likely to be identified (in the form of low performance or quenching). But after the run had completed it took a significant amount of time to cool the catalyst bed to ambient conditions. Since all testing had to be completed in one day it was important to achieve as many runs as possible. Unfortunately there were too many instruments to douse the catalyst bed in water and rapidly lower the temperature. This trade-off also resulted in the bed not being clad in thermally insulating material. The high thermal mass of the bed led to significant thermal losses and resulted in uncertainty over radial temperature measurements. Consequently it is difficult to identify whether low radial

temperatures are associated with channelling or thermal losses through the wall. The completed hICB with instrumentation, electrical heater and FCV can be seen below;

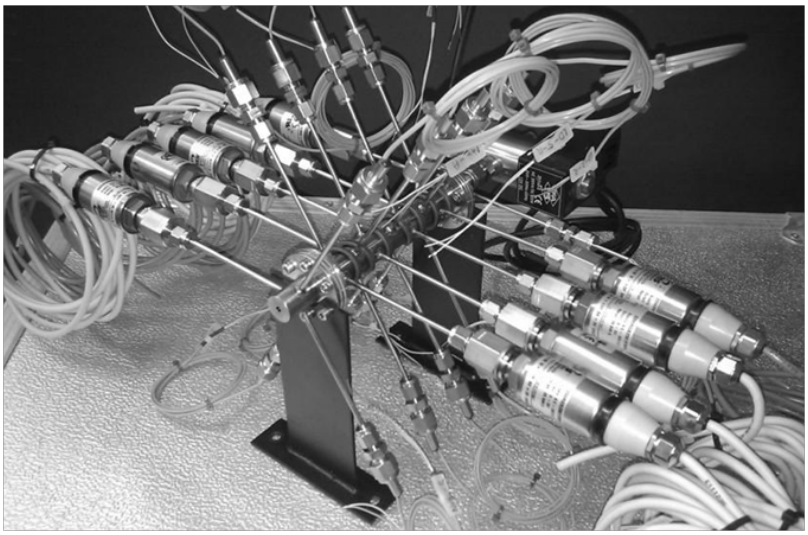

Figure 8-3: Assembled hICB

8.2.2 hICB Results

Due to the large quantity of data generated the results have been separated into two sections. The first section will review the complete data set as generated by a single run. This will be used to characterise the performance of each catalyst. The second section will compare all the catalysts against each other to give an indication of the most promising catalyst in terms of both performance and lifetime. A full set of experimental results has been archived and is available upon request. Unless otherwise stated -A and -R refer to axial (on the axis) and radial (1mm from the catalyst bed wall) temperature measurements respectively.

8.2.2.1 Single run performance

The first catalyst assessed was 5%Pt-Al, at 3.2mm in diameter these were largest pellet based catalyst tested. The axial and radial temperature distribution for Run 1 is shown in Figure 8-4. These stacked graphs show better the correlation between radial and axial temperature. Upon opening the FCV, with the exception of L/D0-A, there is a notable increase in temperature at all locations. This is expected as L/D0-A is located in front of the central injector hole so is constantly being quenched by the influx of cool peroxide. The radial measurement at L/D0 does show a higher temperature consistent with its position away from the main flow and several millimetres away from the nearest injector hole. Although temperatures at L/D1-A and L/D2-A initially rise rapidly they too are quickly quenched. It is conjectured that this occurred due to loose active phase, in the form of powder, being washed off the pellet surface. The very high surface area of the powder initiates decomposition but is soon washed downstream, so the local rate of decomposition drops.

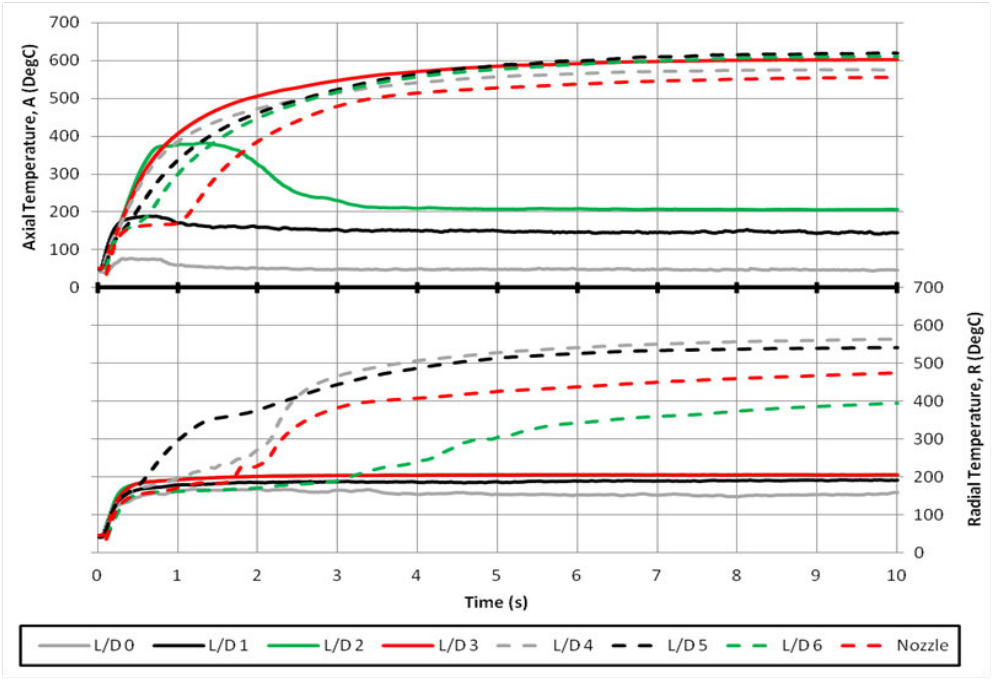

Figure 8-4: Axial and Radial Temperature Distributions (Run 1, 5%Pt-Al)

Axial and radial temperatures at L/D2 stabilise at ~200°C, just below the boiling point of peroxide at 242°C (with 87.5wt% at 13.3barA). This temperature indicates the flow is mainly in the liquid phase so the bulk of the decomposition is yet to occur. The axial temperature profile at L/D3 is seen to continuously rise during the run reaching a 'quasi' steady-state of 600°C. Although not the highest recorded temperature (this was 619°C measured at L/D5-A), it does reach 90% of this value in the shortest time at 3.37s. The measurements at L/D3 also provide the first indication of channelling. While the axial temperature rises steadily to 600°C the radial temperature does not exceed 207°C, this is consistent with an increased flow rate at the wall. The generation of gaseous decomposition products along the axis of the bed causes a locally higher pressure forcing flow out towards the wall. The increased flow rate reduces the achievable temperature by quenching the decomposition. This is consistent with the work conducted by Koopmans [49] who showed through numerical analysis that the void fraction (ratio of available space to space occupied by catalyst material) increased towards the wall with decreasing bed to pellet diameter ratio. This provides a less tortuous route for HTP to flow and increases the probability of channelling. The temperature at L/D4-A then begins to fall as the heat is absorbed from the decomposition products by the remaining pellets. Conversely the radial temperature at L/D4 is seen to rise to 563°C. Again this can be explained by the channelling effect initiated at L/D3. The liquid peroxide now starts to decompose generating a significant temperature increase. After this point the radial temperature reduces through L/D5-R and L/D6-R. It is likely that the radial nozzle temperature is higher than L/D6-R due to the large settling chamber which facilitates better mixing of the hotter axial and cooler circumferential flows. Here the hotter axial decomposition products can mix with the cooler radial gases to provide a more homogenous nozzle exit temperature. It is less clear why the axial temperatures

at L/D5 and L/D6 are higher than L/D4. It is hypothesised that the HTP decomposition occurring at L/D4-R generates a locally high pressure re-directing any un-decomposed peroxide into the core of the bed. Here it decomposes, re-energising the flow and leading to higher L/D5-A and L/D6-A temperatures. The flow is again channelling but being directed towards the core of the bed rather than towards the walls. The peak decomposition efficiency, η_{TH}, has been calculated using Eq. 2-12 with the adiabatic decomposition temperature being provided by the NASA CEA code [19]. The peak decomposition efficiency was found to be 89.6% located at L/D5, this is lower than that achieved with 0.5%Pt-Al in the pICB at 95.4%. The reasons for this may be related to the lower bed loading within the pICB. This resulted in a much shorter zone of decomposition as indicated by the 150°C temperature drop between measurements at 33mm (location of peak temperature rise) and 43mm. The higher bed loading in the hICB led to a much longer zone of decomposition with almost identical temperatures being recorded at L/D5 and L/D6 even so they were separated by 16mm. Neither bed was insulated in any way. The energy released by the decomposition was therefore spread over a larger volume resulting in lower peak values at any single location.

The pressure and mass flow rate results can be found in Figure 8-5. Initially there is a spike in the mass flow rate due to the lack of back pressure within the catalyst bed. As the catalyst bed pressure rises the mass flow rate reaches a steady state of 14.0g/s resulting in a bed loading of 69.5kg/s/m^2. For the most part the pressure profiles are as expected. There is a significant pressure drop of 3.5bar across the injector at an inlet pressure of 16.4bar; this is slightly higher than the design value of 3bar at a delivery pressure of 17bar. An unexpected phenomenon can be seen between 5 and 8s with the pressures measured at L/D1 and L/D2. Here the value of L/D2 is 0.59bar higher than that measured at L/D0. This difference cannot be explained by instrumentation inaccuracy which is a maximum of 0.063bar. It is not possible for this difference to be maintained for such a considerable amount of time without affecting the flow of HTP into the bed. A similar problem can be seen with the pressure data from L/D3 and L/D4. Although this error cannot be explained it is likely associated with thermal drift of the sensor as the bed temperature increases. General trends, however, can still be identified. The values for L/D0 - L/D2 are very similar which would tend to indicate a low pressure drop associated with liquid phase flow. After L/D2 the pressure drop increases significantly to 0.75bar, this is likely due to HTP phase transition from liquid to gas. This supports the argument that the decomposition plane is located between L/D2 and L/D3. The pressure drop over the entire catalyst bed (L/D0 – L/D6) as measured at 9s is 2.25bar. This is low compared to Musker [85] who recorded a pressure drop of 6bar for the same catalyst with an almost identical bed loading of 69kg/s/m^2 and bed length of 90mm. Although the catalyst bed pressure in monopropellant mode is not provided the combustion chamber pressure (in bipropellant mode) is given as approximately 8bar. This would suggest that the catalyst bed pressure was slightly lower than

the 10.4bar recorded in the current work. Wernimont [56] noted in his work that pressure drop tended to decrease with increasing chamber pressure. Koopmans also noted that pressure drop increased and void fraction decreased with increasing bed to pellet diameter ratio. In the current work this ratio is 5 whereas it was 12.5 in the work conducted by Musker. The pressure roughness, calculated using Eq. 2-13, was shown to be highest at L/D2 with a value of 3.38%. Since L/D2 showed some unusual readings it will be ignored resulting in L/D0 giving the highest value at 3.18%. The average value for all L/D positions was 2.69%.

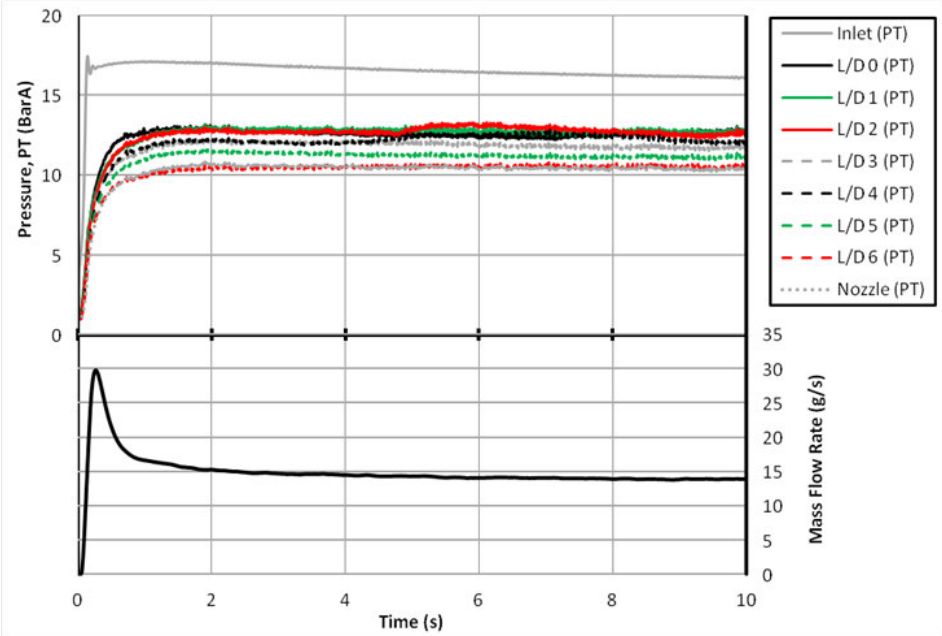

Figure 8-5: Pressure and mass flow rate (Run 1, 5%Pt-Al)

These results have allowed a detailed analysis of the first run with 5%Pt-Al. The effects of channelling can be seen and, with some confidence, the decomposition plane can be identified. However, pressure readings have shown some inconsistency. Unfortunately these grew throughout the experiment and by Run 18 the pressure transducer at L/D1 was showing highly anomalous readings. It was subsequently replaced before being re-tested in the laboratory. No errors were found during this re-testing with stable and accurate pressure measurements generated. This adds to the evidence that the source of error is thermal drift.

The second pellet based catalyst tested was MnO_x-Ce/U-3; this had shown promise during laboratory experiments with consistently high performance. Performance trends are based upon Run 2 not Run 1. Run 1 has not been shown due to unexpected pressure reading at L/D0. This means it is not possible to draw any conclusions concerning pressure drop, limiting the analysis. The temperature and pressure profiles for both runs are exceptionally similar so it is not felt that this is detrimental to the analysis. The axial and radial temperature profiles for run 2 are shown in Figure 8-6. Although the general trends are similar, MnO_x-Ce/U-3 can be seen to outperform 5%Pt-Al in this early run. For the reasons already discussed the temperatures at L/D0 remain low but the axial temperature measured at L/D1 is significantly higher than the equivalent run

for 5%Pt-Al. Measurements at L/D1-A can be seen to plateau at 203-232°C for approximately 0.65s, this is consistent with the boiling point of HTP. The temperature then continues to rise reaching a steady-state value of 615°C. Even as L/D1-A reaches a plateau, L/D2-A is seen to continually rise showing the fastest response time reaching 90% of the maximum bed temperature, t_{90} in 1.41s. L/D2-A also achieves the highest measured temperature of 664°C giving an excellent decomposition efficiency of 96.5%. It is the rising temperature downstream of L/D1-A which initiates thermal decomposition. This causes the decomposition plane to move upstream leading to the higher temperature measurements at L/D1-A later in the run. The axial results seem to indicate the decomposition plane lies slightly downstream of L/D1. The axial temperature is then seen to decrease after L/D2 as the heat generated is absorbed by the downstream pellets. At first the radial temperature profile at L/D1 seems to indicate channelling, however, it is also possible that this is partially the influence of thermal losses through the wall of the bed. Measurements at L/D1-A initially plateau before increasing, consistent with thermal decomposition causing the decomposition plane to move upstream. At the wall the heat maybe being transferred to the catalyst bed structure rather than the bulk fluid, as a result thermal decomposition is not initiated. As the axial temperature rises the channelling problem is exacerbated ensuring decomposition does not occur at the wall. This scenario is different to 5%Pt-Al where low radial temperatures were identified at L/D3, after the decomposition plane. This is consistent with a channelling flow. In the current case the decomposition plane is between L/D1 and L/D2 with L/D1-R showing low temperature, i.e. before the decomposition plane. L/D2-R shows a lower temperature and slower response compared to L/D2-A but the temperature is high enough to indicate phase transition and decomposition of the HTP. It is the opinion of the author that some channelling maybe

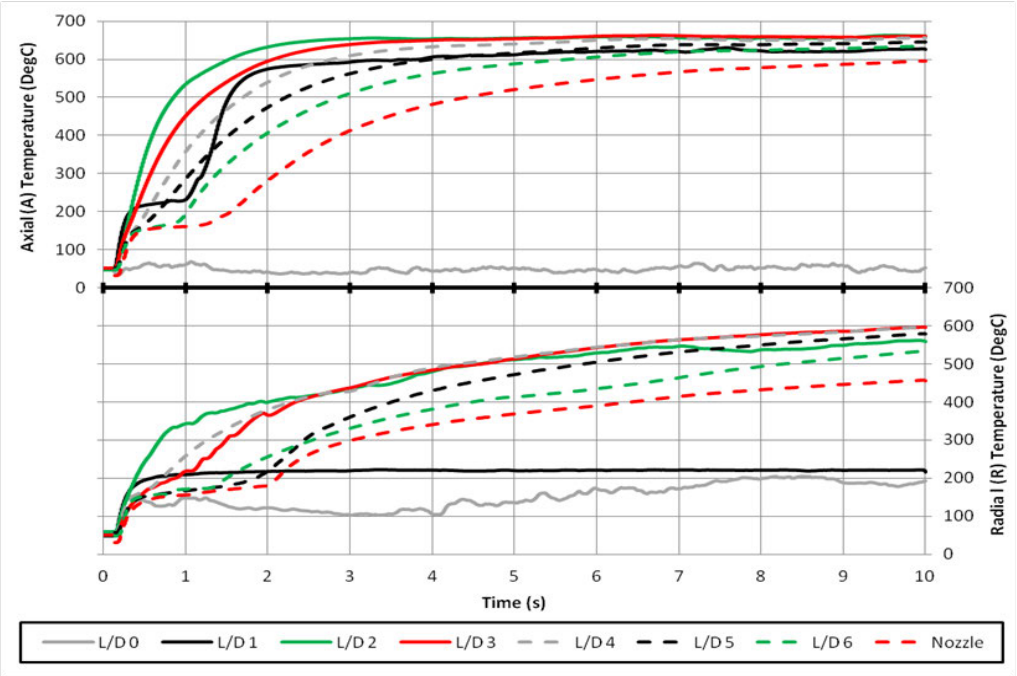

Figure 8-6: Axial and Radial Temperature Distributions (Run 2, MnO_x-Ce/U-3)

occurring but it is much reduced compared with 5%Pt-Al. This is in agreement with the work conducted by Koopmans [49].

The pressure and mass flow rate response can be found in Figure 8-7. What is immediately clear is that the reduced pellet size has resulted in a significant increase in pressure drop compared to 5%Pt-Al. This is due to a greater packing density and reduced void fraction. Accordingly the first run only had a steady-state flow rate of 11.81g/s, significantly lower than the design of 14g/s. This leads to a lower bed loading of 59kg/s/m^2 compared to 5%Pt-Al which may partially explain the improved performance. It can also be seen that the initial spike in mass flow rate is lower than with platinum pellets and this is due to the response time of the bed. With 5%Pt-Al the bed reached 10bar in 0.315s, with MnO_x-Ce/U-3 this was reduced to 0.125s. Initially there is very little pressure drop between L/D0 and L/D1, however, as the decomposition begins at L/D1 the temperature rises and the phase transition point moves upstream. This corresponds to an increasing pressure drop between L/D0 and L/D1 representative of gaseous flow. The pressure drop across the catalyst bed averaged over the last second of the run was found to be 8.02bar. Work conducted by Jo *et al* [86] assessed pressure drop as part of their investigation into chugging instability. Although their catalyst bed was much shorter at an L/D of 1.95 they calculated pressure drop in terms of bar/cm. They used a granular catalyst between 1.18 and 2.00mm in size. For this catalyst they achieved a pressure drop of 1.7bar/cm at a bed loading of 60kg/s/m^2. This is significantly higher than was achieved in the current work at only 0.83bar/cm. Although the nominal size is similar the granular form likely resulted in a better packing density which could be the source of this difference.

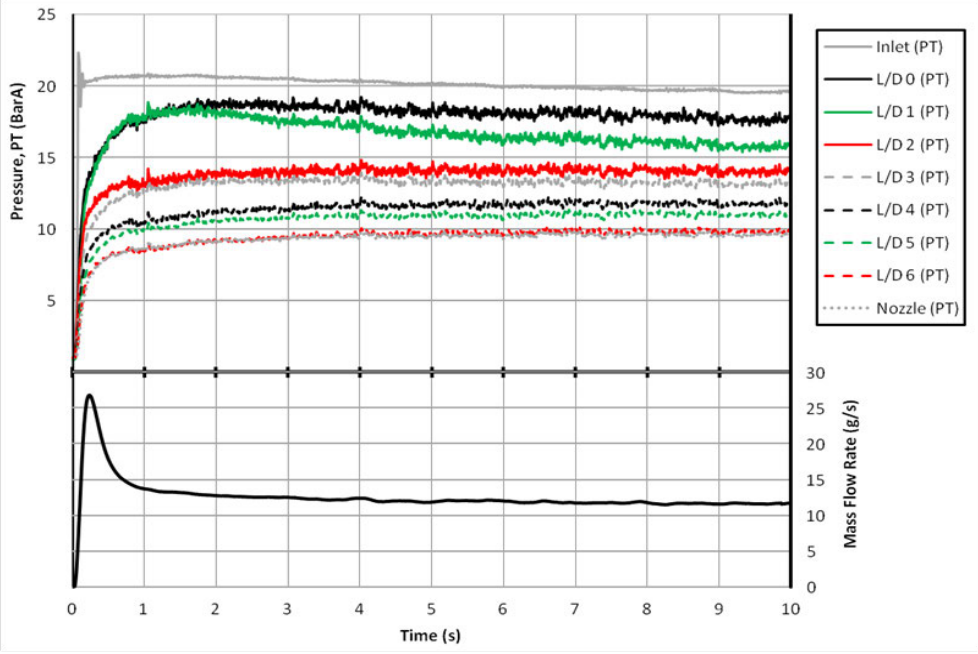

Figure 8-7: Pressure and mass flow rate (Run 2, MnO_x-Ce/U-3)

When assessing pressure roughness L/D1 shows the highest value of 6.3%. This is to be expected due to the moving decomposition plane. An average of all values shows a pressure roughness of 4.30%. This is 2% higher than 5%Pt-Al; the reason for this is not clear but maybe related to movement of the catalyst pellets within the bed or the formation of voids as identified in [84].

The third catalyst assessed was MnO_x-Ni-2/R. The first run with this catalyst showed a lower performance than with either of the other two catalysts as can be seen in Figure 8-8. Although liquid peroxide was never ejected from the nozzle the temperature in the first few seconds of operation failed to reach 200°C. After 3.5s the performance started to improve with L/D3 showing the quickest increase in temperature reaching t_{90} in 5.05s with the highest temperature of 507°C being recorded at L/D5. However, this only equates to a decomposition efficiency of 71.7%, far below that achieved by either of the other catalysts. At first it is unclear what caused decomposition to initiate at 3.5s but this can be explained when reviewing the pressure and mass flow rate data in Figure 8-9. The low temperatures within the bed result in a low bed pressure and high flow rate. Over the first few seconds of the run the chamber pressure starts to rise and conversely the flow rate begins to fall. As the flow rate decreases through 15g/s the temperatures begin to rise. This indicates that bed transitions from quenched to un-quenched at approximately this flow rate. The steady-state mass flow rate of 12.5g/s provided a bed loading of 62kg/s/m^2. The pressure data shows several inconsistencies with several of the locations showing a pressure higher than the bed inlet pressure. This is clearly impossible but is consistent with results obtained in the previous experiments, even though the pressure transducers were confirmed working before the start of this run. This again adds to the argument that the pressure readings are being corrupted by thermal effects. The pressure data shows a low pressure drop which has been estimated at only 1.23bar (ignoring L/D1 and L/D3 values). It can also be seen that there is significant roughness with L/D2, 4 and 6 showing over 17% roughness between 5 and 9 seconds. These local pressure oscillations can also be seen in the inlet pressure readings suggesting the injector plate was unable to dampen these quite significant oscillations. It is thought that the high pressure roughness is linked to the form of the catalyst. The nickel foam discs do not break apart easily but can be crushed and reshaped. As the bed pressure rises the discs are compressed, as a result voids form in the bed in which catalysts can move, leading to these high roughness values.

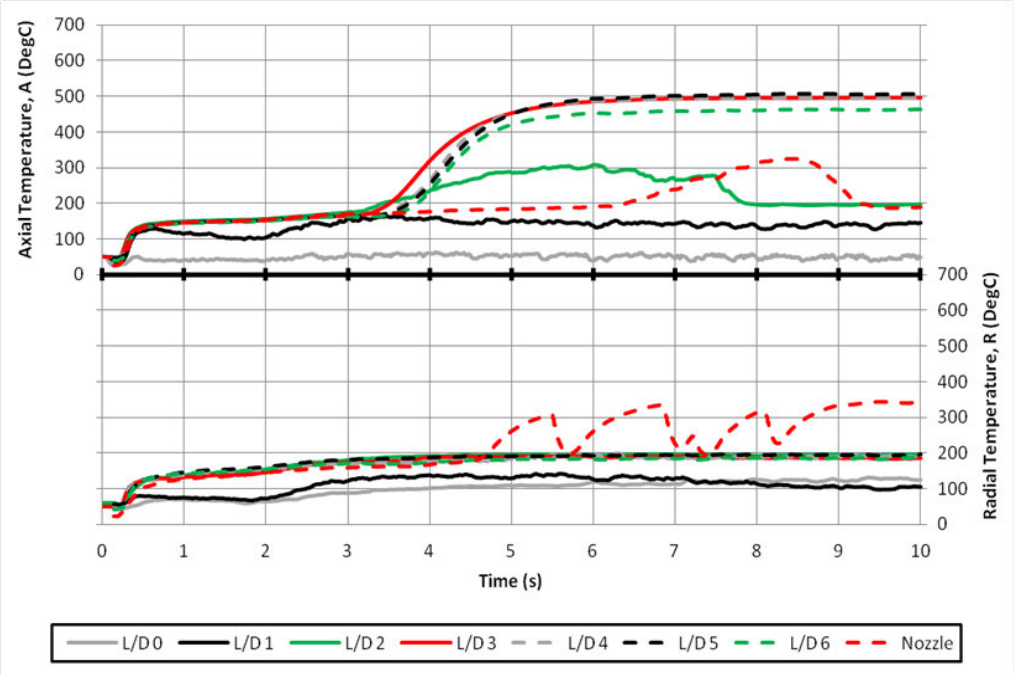

Figure 8-8: Axial and Radial Temperature Distributions (Run 1, MnO_x-Ni-2/R)

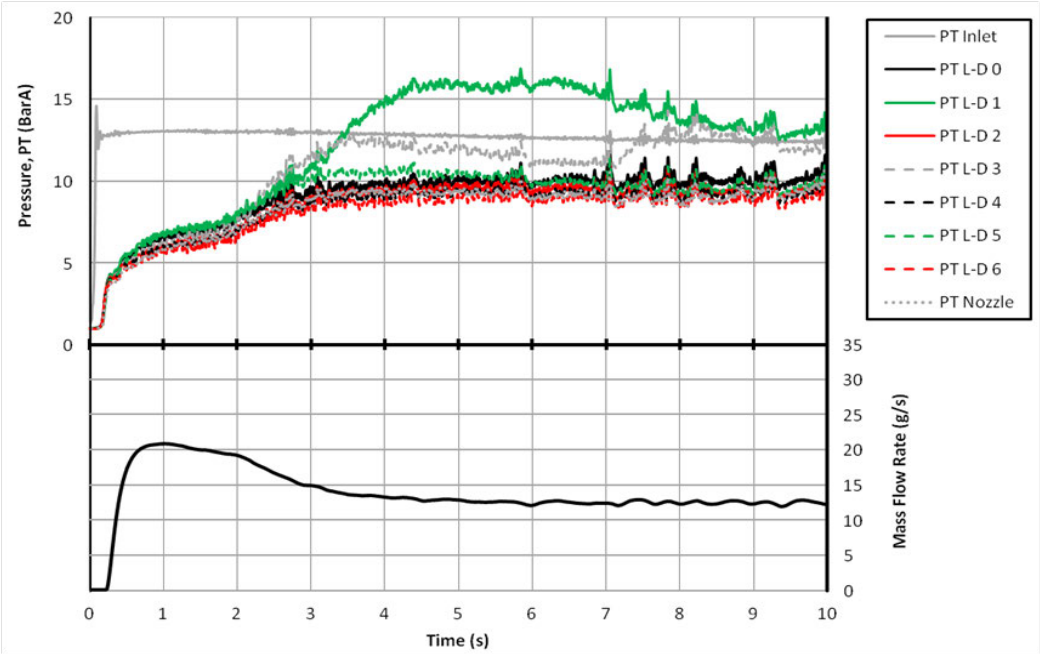

Figure 8-9: Pressure and mass flow rate (Run 1, MnO_x-Ni-2/R)

The final catalyst assessed was silver gauze. This catalyst will be used as a baseline comparator for the other catalysts. The first run was stopped after 5s due to liquid peroxide being ejected from the bed. The bed temperature and pressure failed to exceed 48°C and 1.37barA respectively, resulting in a mass flow rate of 22.4g/s and bed loading of 111kg/s/m^2. As a result this run has been excluded from any further analysis. In order to initiate decomposition the pre-heating temperature was increased to 100°C for the next run but was reduced back to 50°C for all subsequent runs. The initially poor performance is likely related to the 'activation' of silver

gauze. The silver was not pre-treated; so the surface was not pre-roughened. As discussed in chapter 3 exposure to HTP causes roughening of the surface by dissolving away some of the silver. This increase in surface area improves performance as has been identified by several authors [63,77,76]. The axial and radial temperature profiles for the first successful run, now designated Run 1, are shown below.

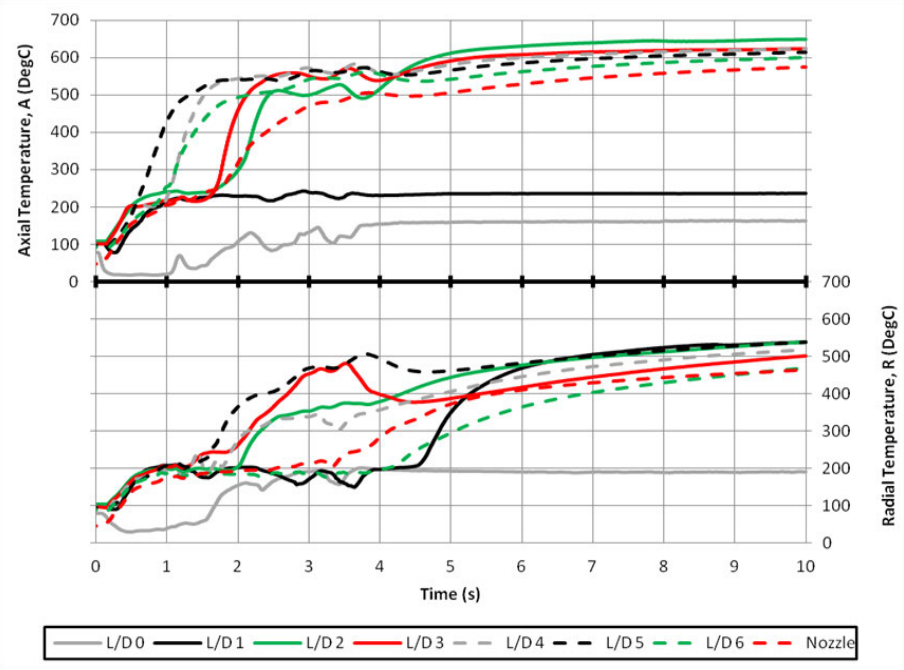

Figure 8-10: Axial and Radial Temperature Distributions (Run 1, Ag-Gz-20)

Again the general trends remain consistent. Decomposition initiates at L/D5-A but as the temperature rises the decomposition plane moves upstream with decomposition becoming stable at L/D2-A by the end of the run. Peak temperature is measured at L/D2-A with a maximum value of 649°C and resulting decomposition efficiency of 96.7%. L/D2-A also shows the quickest response to 90% of the maximum temperature in 4.53s. The radial temperature profile at L/D1 suggests that the flow maybe channelling along the axis of the bed. The low flow rate at L/D1-R allows decomposition to proceed unhindered. The injector design promotes flow down the axis of the bed using the impact of the flow on the catalyst to spread the propellant radially outward. This does not seem to have occurred with silver gauze. The gauze was placed into the bed without any compression in order to protect the thermocouples however compression pressures of 124 - 207bar are not uncommon [75]. It is understood from other authors that low compression promotes channelling [83]. The current work seems to be in agreement with these findings.

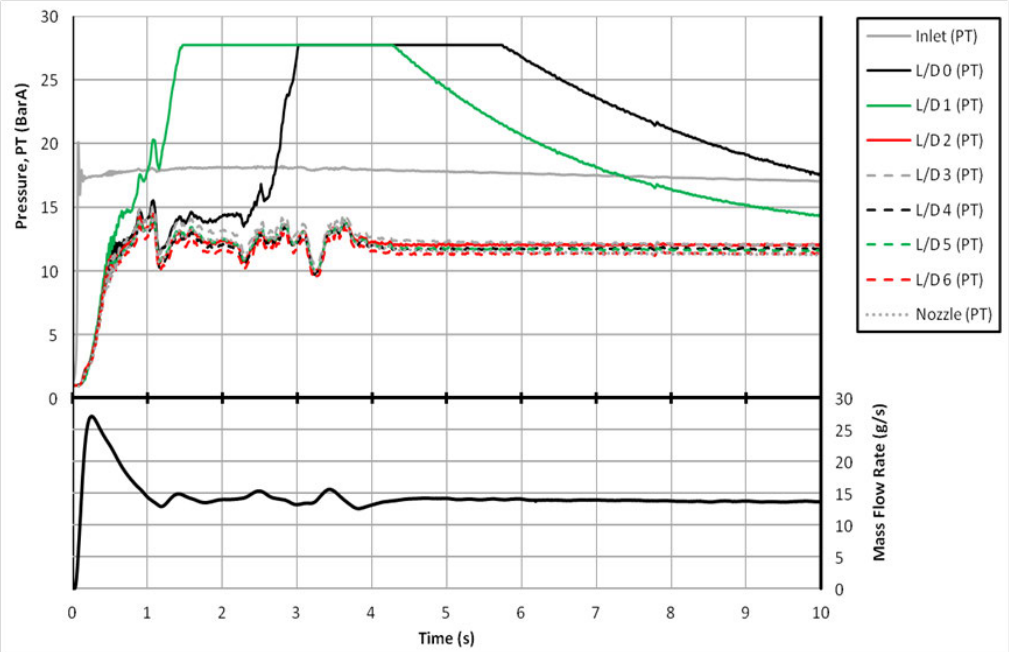

Figure 8-11: Pressure and mass flow rate (Run 1, Ag-Gz-20)

The lack of compression has resulted in a low pressure drop; it is not possible to provide precise readings due to the erroneous data recorded at L/D0 and L/D1 but it is estimated at 1.5bar across the bed. During the early stages of the run there is a considerable variation in the pressure which is replicated in the mass flow rate readings. However, during steady-state operation the readings became much more stable with approximately 2% pressure roughness and a stable flow rate of 13.7g/s. This leads to a bed loading of 68kg/s/m^2.

In summary, the results obtained from the hICB have shown consistent temperature trends across all catalysts but the erroneous pressure readings have resulted in limited usefulness of this data. Radial temperature profiles have enabled discussion on channelling flows with some catalysts being significantly more affected than others. In these early runs MnO_x-Ce/U-3 performed best, achieving high temperatures at L/D1 with the shortest delay. It also showed greater consistency between radial and axial temperatures. However, further investigation will be required to see if this trend continues.

8.2.2.2 Multi-run comparison

In total 18 runs were conducted in the hICB with all four of the catalysts tested, generating a significant body of data. However, for brevity it is not possible to review all the results attained to the level of detail discussed so far. As a result this section will investigate trends across multiple runs with the aim of identifying changes in catalyst bed performance with continued HTP exposure. The analysis will mainly focus on steady-state temperature, decomposition efficiency, initiation delay and location. Theses parameters will be based upon axial measurements but radial measurements will be used to identify channelling and how this

changed with continuing HTP exposure. During post-processing it was noted that although the signal sent from the control and acquisition hardware used to actuate the FCV lasted precisely 10 seconds there was an unknown delay in the valve opening. In some cases this delay was up to 0.5s. Accordingly the run length has been reduced to 9.5s rejecting the final 0.5s of data for all runs to maintain consistency. The start of the run is identified by an increase in inlet pressure. All steady-state values were taken between 5 and 9 seconds after run start.

The first catalyst to be investigated will be silver gauze, Ag-Gz-20, as this will form the comparator for all the remaining catalysts. Unfortunately during Run 5 the propellant tank supplying the peroxide ran dry leading to a run length of only 5s. Accordingly, it has been decided not analyse data from either Run 4 or Run 5. Although the flow rate was relatively constant for Run 4 reviewing the data found unexpected jumps in temperature and pressure. This is likely due to a mixture of nitrogen gas (the pressurant) and HTP flowing into the thruster. The steady-state performance remained relatively constant throughout all the runs; variations tended to be limited to the start-up performance. Accordingly Figure 8-12 shows the decomposition efficiency at various times during the first few seconds of operation. For comparison the steady-state decomposition efficiency (ηTH S-S) is also provided. Decomposition efficiencies were based on the peak temperature recorded at any location at the stated time instances. The graph shows a relatively inconsistent starting profile which may be associated with the lack of 'pre-activating' the gauze. The catalysts would have been roughened by the HTP at inconsistent rates resulting in the decomposition plane shifting within the bed. It can be seen that initial performance reduced during the first three runs. The reasons behind this are not clear but Run 2 and 3 show a slow temperature response; this led to a slow pressure response and significantly increased mass flow rate at the beginning of the run. As the bed pressure and temperature rose the mass flow rate decayed to a steady state of 14.57g/s. The high

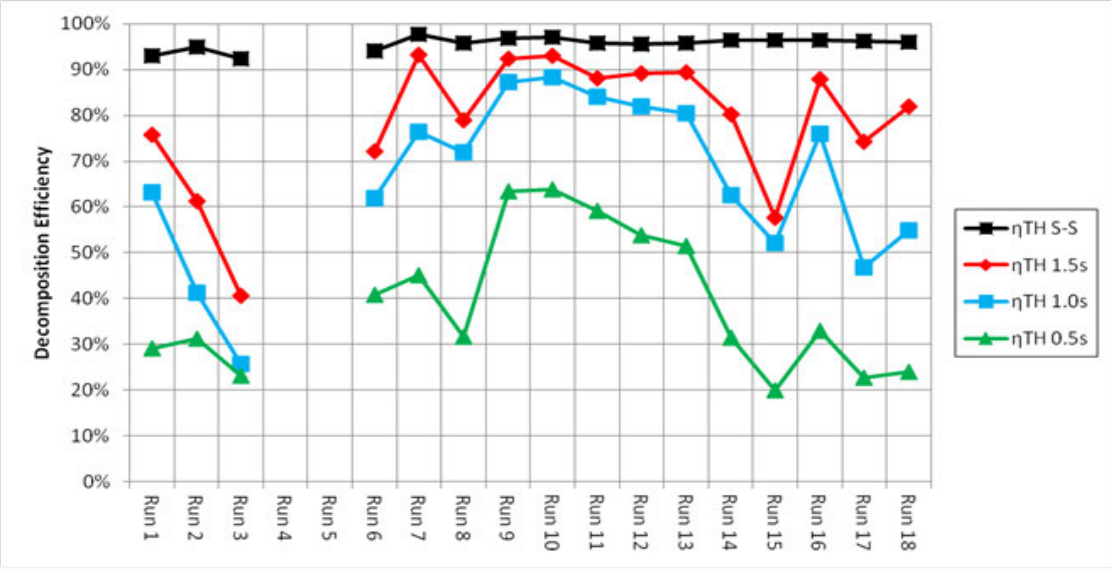

Figure 8-12: Decomposition Efficiency at various times, Ag-Gz-20

mass flow rate initially quenched the bed but as it fell the reactivity rate increased. The results show that, for the majority of runs after Run 5 (not shown), almost complete decomposition had been achieved within 1.5s of actuating the FCV. Runs 8, 15 and to a lesser extent 17 and 18 show a considerably drop in initial performance. Runs 15-18 are shown in greater detail in Figure 8-13 and Figure 8-14. It can be seen that after an initial spike in temperature the value falls before recovering. This is associated with a large spike in pressure which is high enough to stop peroxide flowing into the bed; as shown by the drop in mass flow rate. As the flow into the bed is momentarily halted the temperature drops before the catalyst bed recovers to a nominally steady-state. It would seem that the peroxide momentarily pooled in the bed before decomposing rapidly causing this pressure spike. The presence of pooling within the catalyst bed may suggest a reduction in initial performance. The downward trend in thermal efficiency

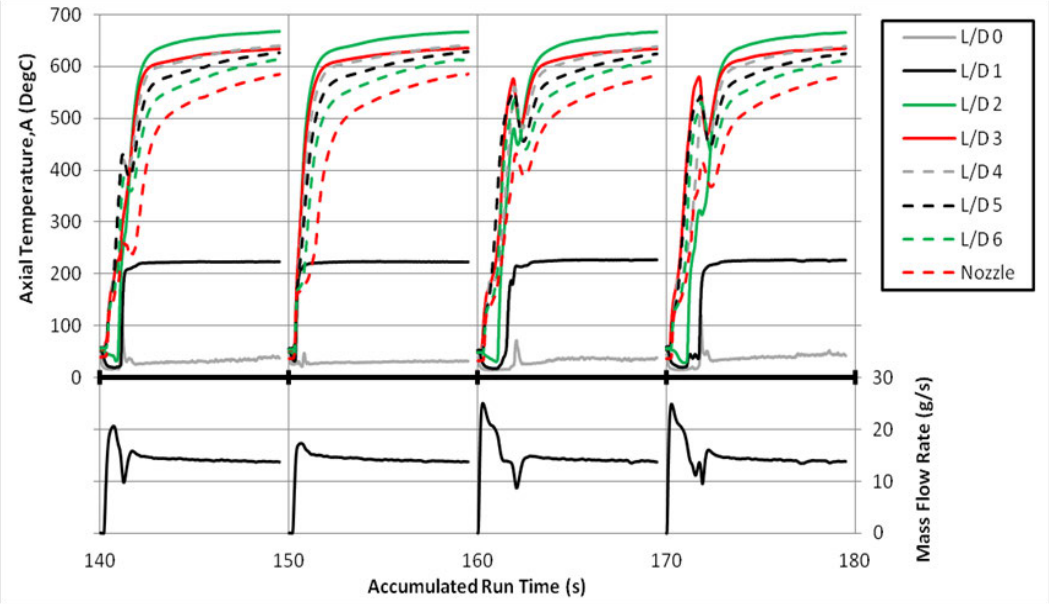

Figure 8-13: Axial temperature and mass flow rate, Runs 15-18, Ag-Gz-20

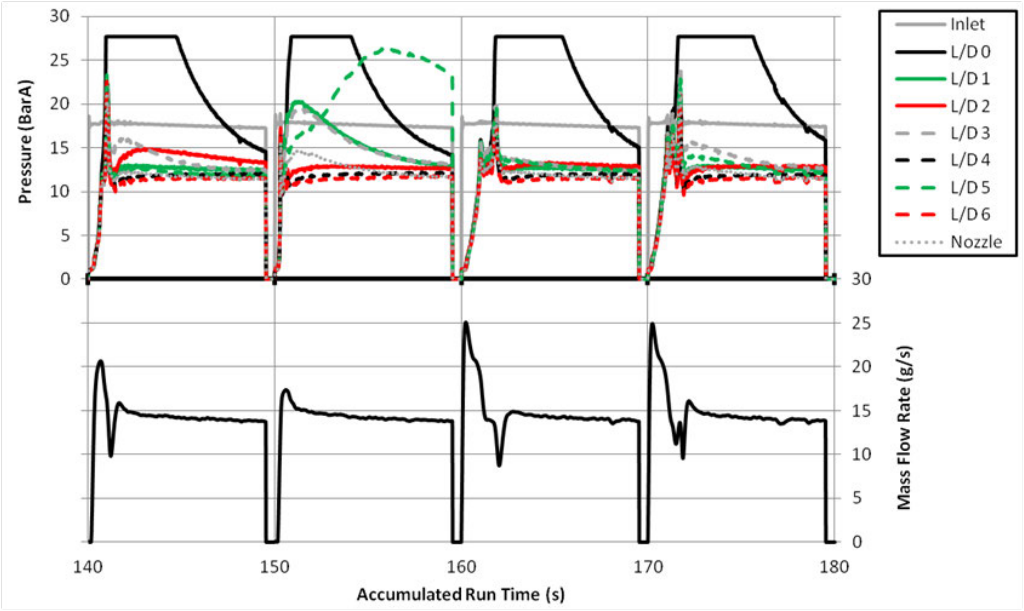

Figure 8-14: Pressure and mass flow rate, Runs 15-18, Ag-Gz-20

at both 0.5s and 1.0s suggests that initial performance has reduced slightly towards the end of the 18 runs.

The final graph shown in Figure 8-15 provides more details on both steady-state operation as well as initial performance in the form of time taken to reach 90% of the maximum bed temperature, t_{90} (as measured at any point within the bed). The value of t_{90} has been calculated at each L/D location, where t_{90} was not achieved no value is given.

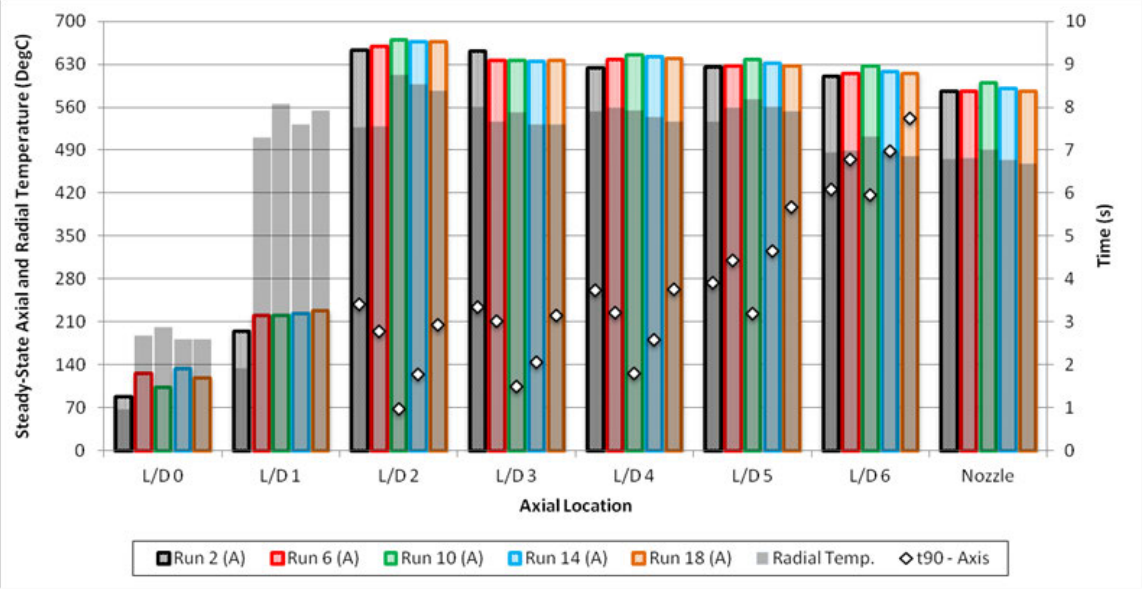

Figure 8-15: Steady state and initial performance, Runs 2,6,10,14,18, Ag-Gz-20

The data shows that radial temperatures are consistently higher than axial temperatures at L/D1; this is in accordance with the findings of the first run. It can also be seen that the majority of the decomposition has occurred by L/D2. This is reinforced with the low t_{90} values associated with L/D2. Although only a subset of the data is shown t_{90} can be seen to start to rise after Run 10, this is consistent with the findings of Figure 8-12 and adds to the evidence that performance is reducing towards the end of the test program.

With an understanding of silver gauze's performance it is possible to provide a comparison with the other catalyst materials tested. The first run performance of 5%Pt-Al had showed a significantly slower response profile compared to silver with a decomposition plane further downstream. Figure 8-16 again shows decomposition efficiencies at various times during the run. In addition the bar chart shows the difference between the values measured for 5%Pt-Al and those for Ag-Gz-20, $\Delta\eta_{TH}$.

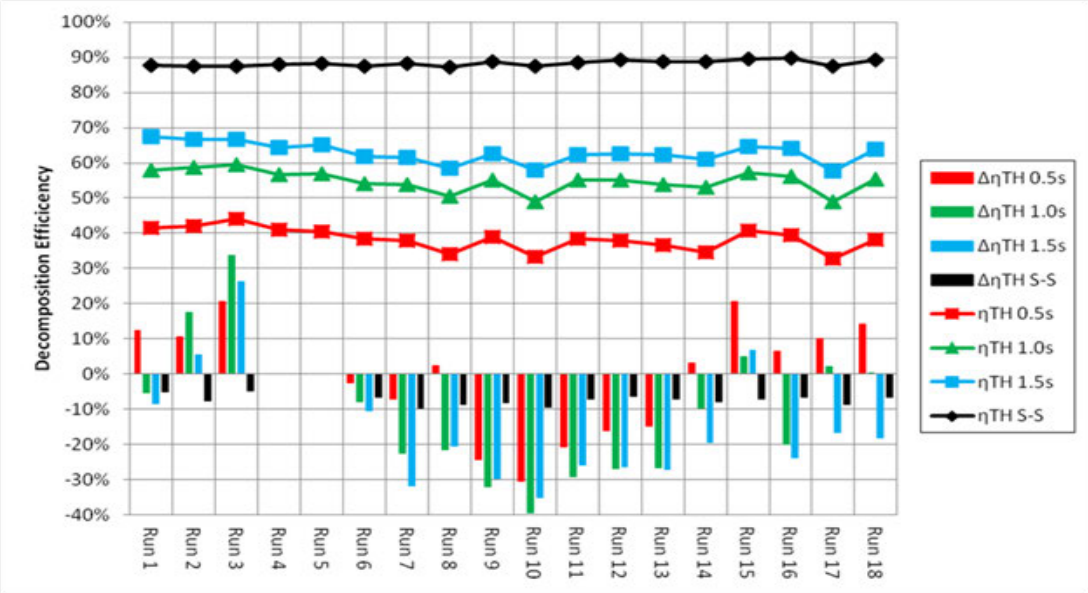

Figure 8-16: Decomposition Efficiency at various times, 5%Pt-Al

Unlike silver the results show a consistent performance throughout the 18 runs, however in steady-state the platinum never outperforms silver. The high level of consistency results in platinum achieving a higher $\eta_{TH\ 0.5s}$ in some cases but on average this value is lower than that of silver. The rate of change in temperature is also quicker with silver, with $\eta_{TH\ 1.5s}$ being much closer to the steady-state value compared to platinum. Although the general trend is for decreasing initial thermal efficiency over the 18 runs the values in the last three runs do not show the same level of decay that was found with silver. Due to the fluctuations with silver it is not possible to predict whether or not this trend would have continued. The second graph shown in Figure 8-17 provides the steady-state axial and radial temperatures along with t_{90} values. The channelling identified in Run 1 can be seen to continue for all subsequent runs with L/D3-R values being significantly lower than L/D3-A values. Consistently high values are identified at L/D3-A indicating that this is the location of the decomposition plane in the steady-state although this does regress in some runs to L/D2, likely due to thermal decomposition. The response time of the bed is much slower with platinum with the lowest t_{90} value of 3.38s compared to 0.98s with silver; this is in agreement with Figure 8-16. L/D5 shows low t_{90} values suggesting that decomposition initiates a long way down the bed before moving upstream resulting in high steady-state axial temperature values at L/D3. The highest steady-state temperatures are located at L/D5 implying that decomposition takes place over a much greater distance than with silver whose temperature drops after L/D2. This is related to channelling with axial decomposition occurring at L/D3 but radial decomposition occurring between L/D4 and L/D5; this re-energises the flow raising the temperature over the entire cross-section of the bed.

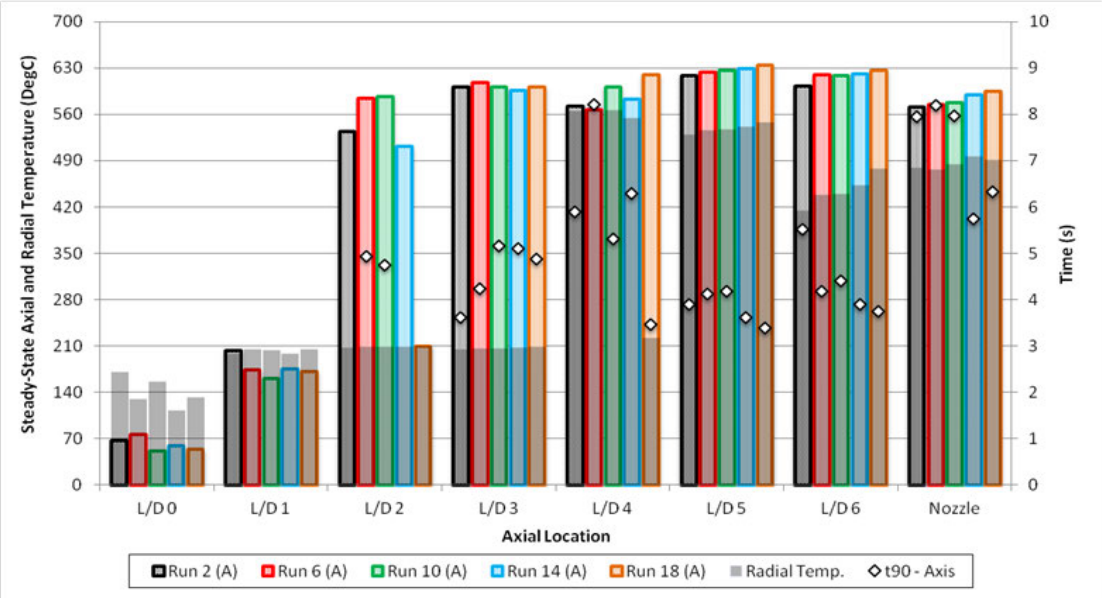

Figure 8-17: Steady state and initial performance, Runs 2,6,10,14,18, 5%Pt-Al

Performance is much more stable with 5%Pt-Al compared to Ag-Gz-20 however silver gauze performs better overall. It has higher steady-state temperatures which are reached quicker and occur further upstream in the catalyst bed. However it is worth noting that in the very first run with silver the bed flooded and the pre-heat temperature had to be raised, although it was reduced for subsequent runs.

The other pellet based catalyst assessed was MnO_x-Ce/U-3; this had performed better than Ag-Gz-20 in the first run (second run for MnO_x-Ce/U-3). As Figure 8-18 shows the performance of MnO_x-Ce/U-3 is improving over the 18 runs with the thermal efficiency at 0.5s, 1.0s and 1.5s all showing an increasing trend. The steady-state performance is equivalent to silver, averaging 0.38% higher overall. The decomposition efficiency at 0.5s is consistently higher than silver and grows steadily over the 18 runs with the final run shows a 48% improvement. The catalyst bed response is also equivalent to silver but much more stable reaching 91% in 1.5s during Run 18. The improved performance is also visible in Figure 8-19. Although the quickest response time for MnO_x-Ce/U-3 is slightly longer than silver (1.02s compared to 0.98s) this value is achieved in the final run. The response time is shown to consistently decrease throughout the 18 runs. In all runs L/D2 showed the highest temperatures both axially and radially, this implies that there was little or no channelling present within the bed. The reducing axial temperatures measured at L/D1 may indicate the decomposition plane is moving slowly downstream. The results show that decomposition is occurring across the entire cross section at the same time and is concentrated over a very small distance, unlike 5%Pt-Al and Ag-Gz-20.

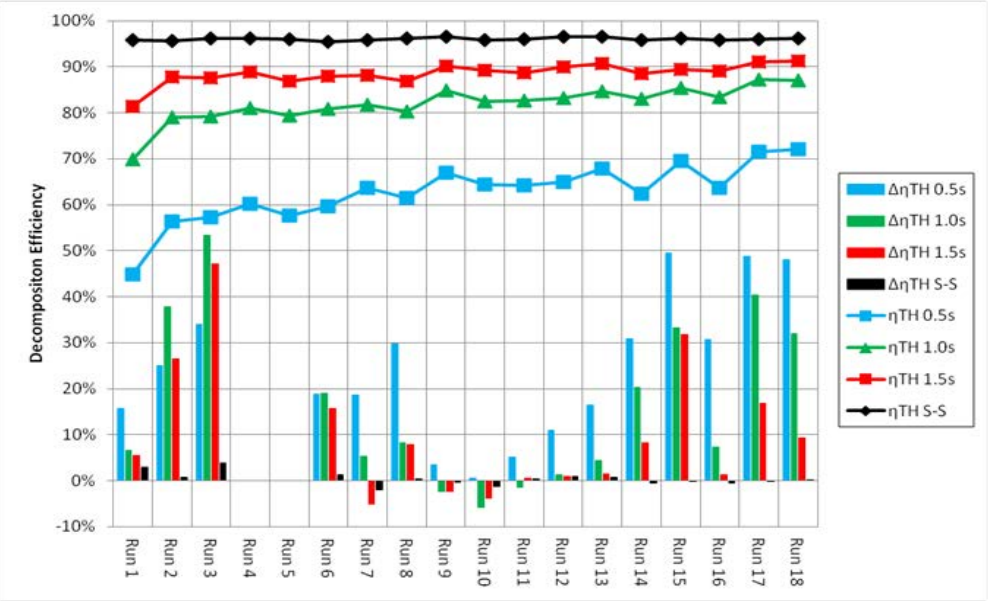

Figure 8-18: Decomposition Efficiency at various times, MnO_x-Ce/U-3

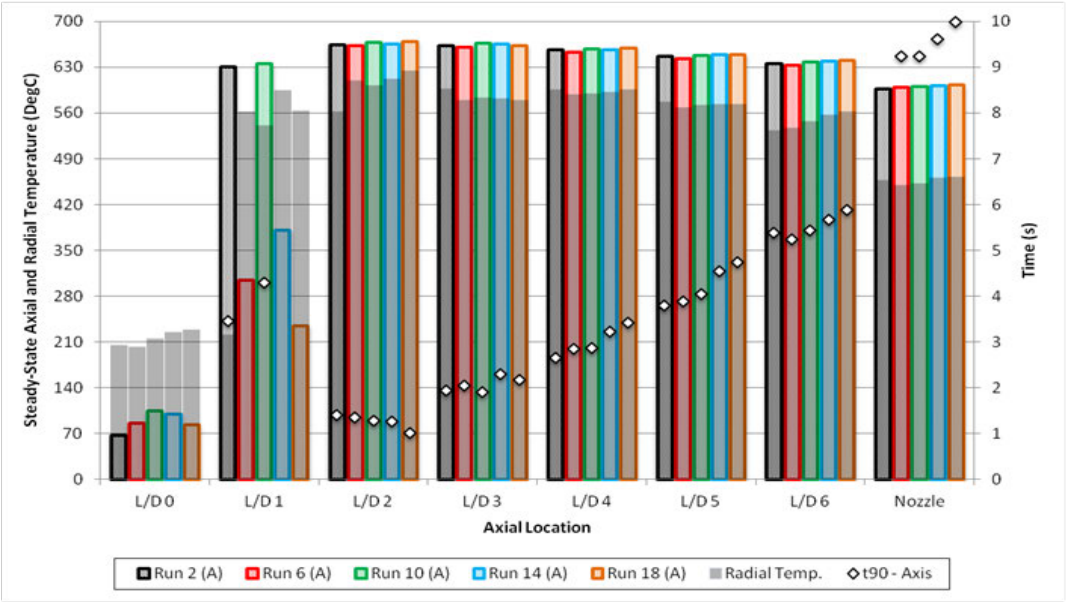

Figure 8-19: Steady state and initial performance, Runs 2,6,10,14,18, MnO_x-Ce/U-3

Overall MnO_x-Ce/U-3 has outperformed both 5%Pt-Al and Ag-Gz-20 in terms of initial response, steady state performance and lifetime. However it has a much higher associated pressure drop although the pressure roughness remains relatively constant throughout with a value in the nozzle averaging 3.81%.

The final catalyst assessed was MnO_x-Ni-2/R; the first run was poor only achieving a decomposition efficiency of 71.7% and taking over 5s to reach 90% of the maximum temperature. Over the 18 runs the steady-state decomposition efficiency improved significantly with a noticeable step increase after Run 1 and Run 6 as Figure 8-20 shows. The reasons for the poor Run 1 performance have already been discussed. Even after these increases in performance the decomposition efficiency averaged 8.4% below that of silver. The $\Delta\eta_{TH\ 0.5s}$ is seen to

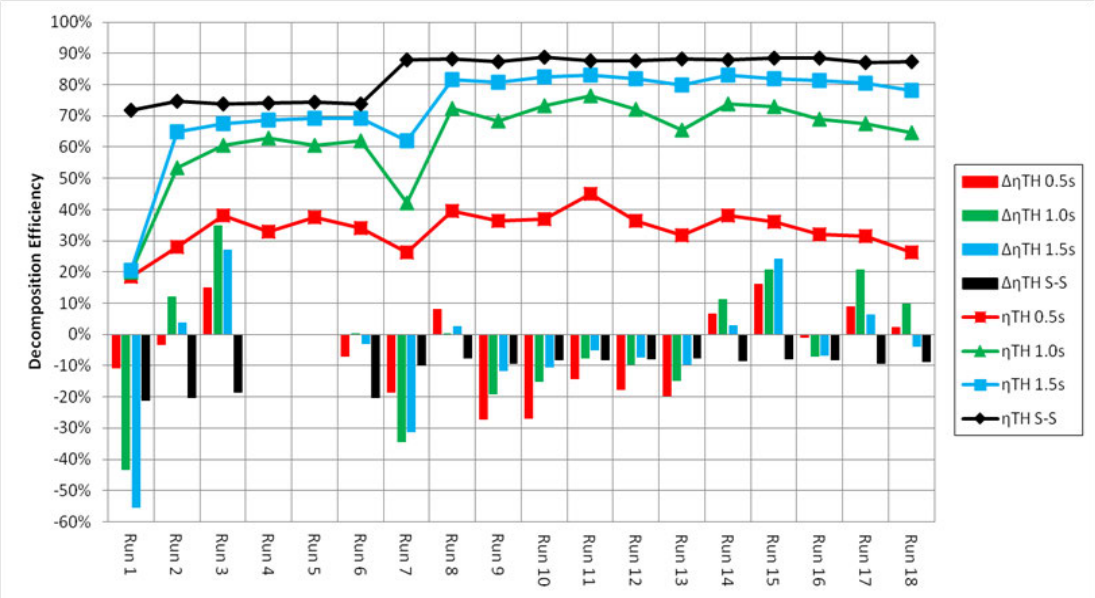

Figure 8-20: Decomposition Efficiency at various times, MnO_x-Ni-2/R

increase over the first 11 runs before starting to reduce; this trend is the same for measurements taken at 1.0s and 1.5s. Although the performance is below that of silver the response time is equivalent with the bed exceeding a decomposition efficiency of 80% after 1.5s. It is unclear why the bed performance increased so significantly after Run 6. The axial temperature and mass flow rate profiles for Runs 5-8 are shown in Figure 8-21. There is no significant change in mass flow rate over the four runs shown so the performance change is unlikely associated with effects such as quenching. The graph does show a temperature increase at L/D2 suggesting the decomposition plane is moving upstream consistent with an improving catalyst. The initially low rate of decomposition in combination with a nickel support material that is very effective at transferring heat may result in a heat being radiated away from the bed at the same rate as it is being generated. As the catalyst performance increases this equilibrium temperature rises. This may explain why a catalyst with the same active phase as MnO_x-Ce/U-3 failed to reach an equivalent temperature. The rapid heat transfer may also partially explain the low radial temperatures identified in Figure 8-22. It is unlikely that channelling alone would explain the consistently low radial temperatures over several L/D locations while the axial temperature was approaching 600°C. However the effect of channelling could be being exacerbated by a rapid transfer of heat to the wall which would act to further limit temperature rise. The low t_{90} values suggest that the catalyst has the potential to be very effective at decomposing HTP. These values are equivalent to Ag-Gz-20 and significantly lower than 5%Pt-Al. High axial temperatures can be seen at L/D2 with higher values still at L/D3. This suggest the decomposition plane is located slightly downstream of L/D2. Although this is further downstream than both silver gauze and MnO_x-Ce/U-3 it is upstream of the 5%Pt-Al decomposition plane.

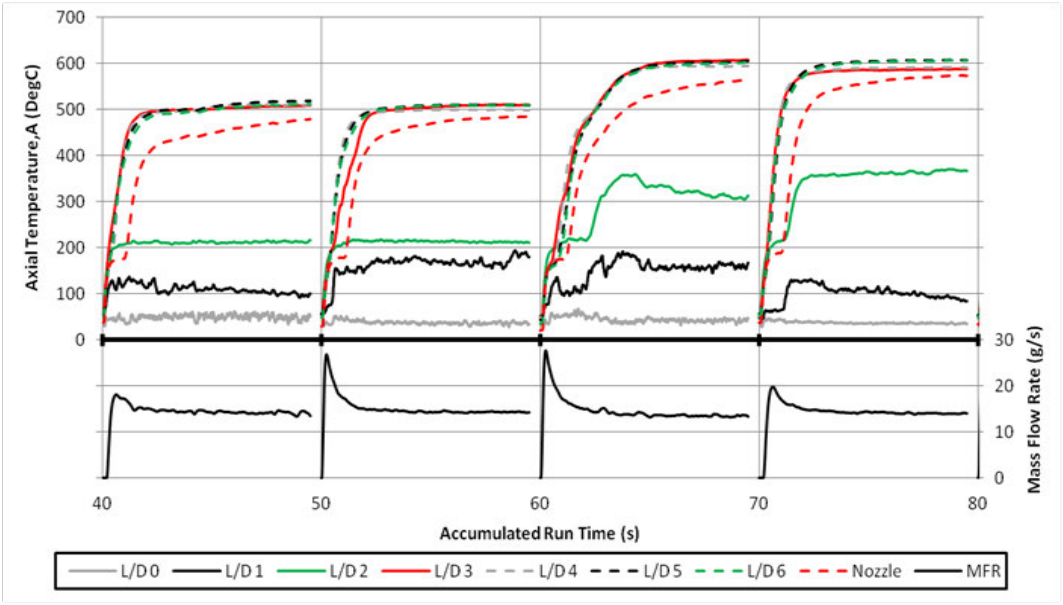

Figure 8-21: Temperature and mass flow rate, Runs 5-8, MnO_x-Ni-2/R

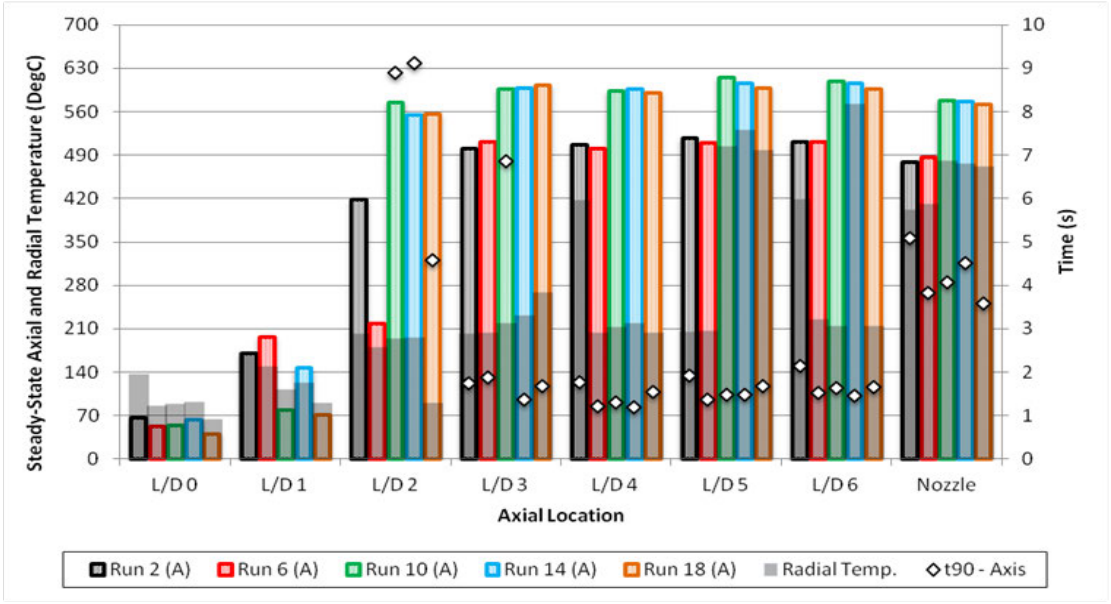

Figure 8-22: Decomposition Efficiency at various times, MnO_x-Ni-2/R

It is thought that MnO_x-Ni-2/R is a higher performing catalyst than steady-state temperatures would at first indicate. Insulating the catalyst bed may significantly improve the performance with this catalyst.

A summary of the key results can be found in the following table, where no values are given these data have been rejected due to inconsistencies. Values given for pressure drop and chamber pressure roughness should be used for comparison only due to the erratic pressure data acquired.

[151]

	Parameter	Run Number																	
		1	2	3	4	5	6	7	8	9	10	11	12	13	14	15	16	17	18
Ag-Gz-20	$\eta_{TH,S-S}$, (%)	92.9	95.0	92.3			94.0	97.7	95.8	96.8	97.1	95.8	95.5	95.8	96.4	96.5	96.5	96.1	96.0
	t_{90} (s)	4.52	3.35	4.07			2.78	1.29	2.04	1.03	0.98	1.27	1.26	1.29	1.78	2.26	1.48	3.02	2.93
	L/D_{t90}	2	3	4			2	4	3	2	2	3	2	2	2	2	2	2	2
	T_{max} (°C)	649	652	653			658	677	663	669	670	663	659	661	667	668	667	667	666
	L/D_{Tmax}	2	2	3			2	3	2	2	2	2	2	2	2	2	2	2	2
	$\dot{m}_{s-s}$ (g/s)	13.9	14.4	14.6			13.8	14.7	14.3	14.3	14.0	14.2	14.6	14.5	14.0	14.0	14.0	14.1	14.0
	CBL_{CSA} (kg/s/m^2)	69.1	71.6	72.6			68.6	73.1	71.1	71.1	69.6	70.6	72.6	72.1	69.6	69.6	69.6	70.1	69.6
	ΔP (bar)*																		
	$R_{PC,}$ Nozzle (%)*	2.0	6.6	28.0			2.0	5.0	2.5	1.7	2.6	2.1	1.2	1.1	1.8	2.4	4.3	2.8	3.6
	HTP_{TOT} (g)	144	295	459	618	670	815	964	1106	1247	1395	1542	1693	1836	1976	2116	2257	2403	2550
5%Pt-Al	$\eta_{TH,S-S}$, (%)	87.8	87.4	87.5	88.0	88.3	87.4	88.1	87.1	88.8	87.6	88.6	89.1	88.7	88.7	89.4	89.9	87.5	89.3
	t_{90} (s)	3.37	3.62	3.56	3.83	3.63	4.13	3.97	4.21	3.62	4.18	3.59	3.50	3.39	3.61	3.34	3.38	4.17	3.39
	L/D_{t90}	3	3	5	5	5	5	5	5	5	5	5	5	5	5	5	5	5	5
	T_{max} (°C)	619	518	616	624	624	623	626	623	628	627	629	631	628	629	632	635	630	634
	L/D_{Tmax}	5	5	5	5	5	5	5	5	5	5	5	5	5	5	5	5	5	5
	$\dot{m}_{s-s}$ (g/s)	14.0	13.8	14.4	14.0	13.9	13.9	14.1	14.0	13.9	13.9	14.7	14.5	14.7	14.6	14.2	14.3	14.3	14.7
	CBL_{CSA} (kg/s/m^2)	69.6	68.8	71.8	69.8	69.4	69.3	69.9	69.6	69.2	69.2	73.0	72.3	73.3	72.6	70.8	71.3	71.1	70.9
	ΔP (bar)*	1.9	2.6	1.9	2.0	1.7	1.8	1.9	1.8	1.8	2.1	1.9	1.7	1.8	1.8	1.8	1.7	1.7	1.7
	R_{PC} Nozzle (%)*	2.4	3.5	3.7	2.7	3.4	3.8	3.5	4.2	2.8	4.8	5.3	3.9	5.1	4.9	3.0	5.6	4.3	4.1
	HTP_{TOT} (g)	148	295	447	595	743	891	1039	1188	1336	1484	1632	1786	1941	2096	2240	2391	2536	2679

	Parameter	Run Number																	
		1	2	3	4	5	6	7	8	9	10	11	12	13	14	15	16	17	18
MnOx-Ni-2/R	$\eta_{TH,S-S}$, (%)	71.7	74.6	73.7	74.2	74.5	73.8	88.0	88.2	87.4	88.9	87.7	87.6	88.2	88.0	88.5	88.5	87.0	87.4
	t_{90} (s)	5.01	1.75	1.45	1.24	1.30	1.23	3.23	1.28	1.36	1.30	1.12	1.26	1.47	1.20	1.28	1.38	1.36	1.54
	L/D_{t90}	4	3	4	3	3	4	3	4	4	4	4	4	4	4	4	4	3	4
	T_{max} (°C)	507	517	516	513	519	511	608	607	603	614	605	602	607	606	611	609	600	603
	L/D_{Tmax}	5	5	5	5	5	3	3	5	3	5	3	5	3	5	3	3	5	3
	$\dot{m}_{s-s}$ (g/s)	12.5	13.8	14.2	14.2	14.1	14.3	13.5	14.0	14.5	14.2	14.2	14.6	14.3	14.2	14.4	14.8	14.7	15.0
	CBL_{CSA} (kg/s/m^2)	62.1	68.7	70.6	70.4	70.3	71.1	67.0	69.9	72.2	70.8	70.5	72.4	71.3	70.8	71.5	73.7	73.1	74.4
	ΔP (bar)*	1.2	1.7	1.9	2.9	1.9	2.7	2.1	1.6	1.5	1.6	1.6	2.0	0.9	1.2	1.7	1.8	1.1	1.1
	R_{PC} Nozzle (%)*	15.8	10.3	19.1	6.1	12.9	6.4	9.0	6.7	7.9	15.0	17.9	18.7	7.0	11.1	9.9	21.9	16.3	17.6
	HTP_{TOT} (g)	139	284	435	584	726	876	1021	1163	1316	1459	1608	1762	1912	2055	2206	2361	2516	2673
MnO_x-Ce/U-3	$\eta_{TH,S-S}$, (%)	95.8	95.7	96.1	96.1	96.0	95.4	95.8	96.1	96.5	95.7	96.1	96.5	96.5	95.9	96.3	95.8	96.1	96.2
	t_{90} (s)	1.95	1.41	1.43	1.31	1.55	1.35	1.38	1.52	1.15	1.29	1.30	1.24	1.15	1.26	1.13	1.29	0.99	1.02
	L/D_{t90}	2	2	2	2	2	2	2	2	2	2	2	2	2	2	2	2	2	2
	T_{max} (°C)	663	664	666	665	670	663	665	668	668	667	666	669	668	665	670	668	667	669
	L/D_{Tmax}	2	2	2	2	3	2	3	3	3	2	2	2	2	2	2	2	2	2
	$\dot{m}_{s-s}$ (g/s)	10.6	11.8	12.6	12.8	12.7	12.6	13.1	12.8	12.9	13.2	13.2	13.2	13.2	13.1	13.0	13.0	12.8	12.8
	CBL_{CSA} (kg/s/m^2)	52.8	58.8	62.7	63.4	63.2	62.9	65.1	63.5	64.2	65.8	65.6	65.6	65.6	65.3	64.6	64.7	63.9	63.8
	ΔP (bar)*		8.2	8.3	7.9	8.2	7.5	7.5	7.6	7.3	7.6	7.7	7.4	7.6	7.9	8.1	8.5	8.2	8.3
	R_{PC} Nozzle (%)*	3.5	3.3	5.0	3.9	3.7	6.1	4.0	4.4	4.6	4.1	3.7	2.8	3.2	3.2	3.4	3.5	3.4	2.6
	HTP_{TOT} (g)	107	233	365	490	621	752	886	1022	1154	1288	1413	1544	1675	1813	1950	2087	2222	2356

* These are approximate values and should only be used for comparison only.

Table 8-1: Summary performance data for hICB

Ag-Gz-20 shows stable steady-state temperatures with the peak temperature location initially moving downstream before regressing to L/D2 for the majority of the runs. Over the final 8 runs t_{90} can be seen to increase suggesting a slight reduction in performance consistent with earlier findings. The chamber pressure roughness in the nozzle can be seen to be relatively constant throughout with the exception of Run 3. This high reading is due to a varying mass flow rate which results in significant variation in the chamber pressure. The steady-state decomposition efficiency for 5%Pt-Al can be seen to increase slightly over the 18 runs with t_{90} remaining relatively constant. The data provides no evidence that the catalyst performance is reducing over these runs. Although performance is not reducing the decomposition plane is consistently further downstream than for any other catalyst tested. Chamber pressure roughness also remains relatively constant, another indication that performance is not decaying. The location of the peak temperature for MnOx-Ni-2/R is seen to oscillate between L/D3 and L/D5. Although a definitive reason cannot be given it is likely related to changes in the radial temperature distribution and losses through the wall. The performance is seen to be consistent with similar t_{90} and peak temperature values throughout the 18 runs. The chamber pressure roughness is high and growing slightly in the latter stages of the test. The reasons for a high chamber pressure roughness have already been given and will not be repeated here. The performance of MnOx-Ni-2/R is similar to 5%Pt-Al but still far below Ag-Gz-20. The final catalyst, MnO_x-Ce/U-3, shows the best overall performance. High peak temperatures and low response times are consistently seen at L/D2 with decomposition efficiencies equalling or exceeding Ag-Gz-20. This catalysts provides the strongest evidence that the performance is improving over the 18 runs with t_{90} response values reducing from 1.95s (Run 1) to 1.02s (Run 18). Due to the catalyst particle size the pressure drop is the highest of all the catalysts tested but nozzle pressure roughness is relatively constant. The average catalyst bed loading (and therefore flow rate) is the lowest of all the catalysts tested which may partially explain the improved performance.

The results of the hICB testing cannot provide definitive values for lifetime as no significant performance degradation is seen. It is the authors' opinion that silver shows some small signs of performance loss but additional runs would be required to verify this. 5%Pt-Al shows consistent readings with no signs of degradation. There is also no evidence of the decomposition moving downstream with MnOx-Ni-2/R however there is a small increase in nozzle pressure roughness. This does not necessarily imply catalyst degradation but is more likely due to the catalyst compacting within the bed. The final catalyst, MnO_x-Ce/U-3, shows an improving performance over the runs conducted. With the information available the catalysts can be ranked in the following order with regards to lifetime; MnO_x-Ce/U-3>>5%Pt-Al>MnOx-Ni-2/R>Ag-Gz-20. This order does not reflect the performance of the catalysts which would be ranked as follows; MnO_x-Ce/U-3>Ag-Gz-20>>5%Pt-Al>MnOx-Ni-2/R. This is not to say a catalyst bed filled with 5%Pt-Al would last longer than Ag-Gz-2 since the decomposition plane would start

much further upstream with Ag-Gz-20. In all cases MnO_x-Ce/U-3 is found to be the best catalyst.

8.3 Summary

Two instrumented catalyst beds have been tested; namely the preliminary Instrumented Catalyst Bed (pICB) and the highly Instrumented Catalyst Bed (hICB). Both have provided useful data with the pICB supplying key data used in the development of the Engineering Bread-Board (EBB) thruster described in the next section. The hICB has given a much more detailed review of the down-selected catalysts' performance over extended time periods.

The pICB achieved its primary aim; providing design data for the EBB but was unsuitable for assessing catalyst lifetime. This was due to insufficient instrumentation, inconsistent starting temperatures and inconsistent run length. It was due to these reasons that a second, more heavily instrumented, catalyst bed was developed; the hICB. There were some consistencies between the results obtained from these two beds. Both identified a preferential axial flow with silver which resulted in high radial temperatures. Radial channelling was identified with both 0.5%Pt-Al and 5%Pt-Al. Both theses catalysts had similar particle dimensions so it would be expected to see this trend in both beds. However this is where the similarities finished. The performance of Ag-Gz-20 within the hICB was much higher than the pICB, consistent with extensive previous use within the space industry and the findings of other authors [63,65,77].

Results from the hICB have shown that MnO_x-Ce/U-3 has excelled in all areas. This catalyst had the lowest initiation delay, highest performance and is predicted to have the longest lifetime. There was little evidence of catalyst degradation in any of the catalysts tested. The results have also allowed an assessment of the form and location of the decomposition plane. The decomposition plane is often referred to as a 2D finite thickness plane in which the decomposition occurs. This is clearly an over simplification but in the author's opinion this analogy can be extended so rather than a 2D plane the decomposition takes the form of a 2D surface of an oblate hemisphere. The shape of this hemisphere depends on the degree of channelling occurring along either the axis or radius. If no channelling occurs then the form of the decomposition plane reverts to 2D plane.

Unfortunately the hICB did suffer numerous instrumentation failures leading to erroneous pressure data. The precise reasons for this are still unclear as the instrumentation was shown to be operational before and after testing. It is believed that the problem is associated with localised heating at the surface of the pressure transducer which caused significant thermal drift. Even without this data the experiment is still considered a success.

9 Engineering Breadboard Monopropellant Thruster

The aim of this thesis is to assess the viability of hydrogen peroxide as a modern rocket propellant and develop the technology required to implement its use. All prior experiments have been conducted to assess the performance of catalysts under a range of conditions, but the performance of a thruster is dependent on more than just the catalyst employed. The instrumented catalyst beds were designed to test catalysts under conditions representative of a thruster and not the mechanical components themselves. Accordingly the next phase of this development process was to design a thruster more representative of a flight-like system. Up until now silver has been used as a comparator, however at this final stage it was decided not to test with silver. The catalyst and thruster designed in this work needed to be suitable for peroxide concentrations above those at which silver will survive.

The thruster described in this chapter referred to as an engineering breadboard or EBB thruster fulfilled this role. In this early stage of development not all design aspects were fully investigated, with only a low technology design representative of a TRL 3 or 4 thruster being manufactured. However, the information gathered provided valuable performance data on a range of components. In future work this data can then be used to refine the design leading to the production of a thruster with an equivalent TRL of 4 to 5. Details of TRLs can be found in chapter 1.

The EBB thruster instrumentation included a flow meter for identifying the HTP mass flow rate, load cell for thrust measurement and pressure and temperature sensors. This allowed performance characteristics such as C*, specific impulse and minimum impulse bit to be calculated, as well as continued catalyst assessment from pressure and temperature data.

9.1 Engineering Breadboard Design

9.1.1 Design Specifications

In order to successfully construct a monopropellant thruster, a mathematical model was generated to provide specific data relating to the key design features. The results of a market analysis conducted by the members of the GRASP consortium have been used as inputs to this model [17]. The review concluded that there was a market requirement for systems with thrust levels ≤20 N for spacecraft attitude control system (ACS) applications. In particular, the findings of this review indicated that there is significant demand for monopropellant systems with thrust levels of 1 N and 20 N, with only limited demand at intermediate thrust levels. A

small 1 N thruster provides significantly different challenges compared to a much larger 20 N thruster. These challenges mainly revolved around the machining of small components. It was felt that this places significant constraints on the instrumentation that could be used and that these machining and instrumentation limitations may limit the quantity of high quality data that could be captured. As a result it was decided that a 20 N (sea-level thrust) thruster offers more value to the research being undertaken.

A mathematical model was designed using MATLAB software by a research associate, Robert-Jan Koopmans. The inputs and outputs to this model can be found in Table 9-1. In order to validate these results a much simpler model was designed by the author, this is provided in Appendix D. There are several key differences between these two models; the first is the methodology used to calculate the maximum decomposition temperature. In the author's model these values are provided by the NASA CEA code [19], however the MATLAB model calculates these values directly from appropriate chemical data. Secondly, whereas the author's model uses fixed gas properties the working fluid properties in the MATLAB model are temperature dependant. Finally, the author's model defines the delivery pressure and calculates all downstream pressures; however the MATLAB model specifies the target chamber pressure and calculates all resultant pressures. As can be seen in Appendix D the outputs of the mathematical model differ from the MATLAB model. However, when the gas properties are fixed in the MATLAB model (as is the case with the simplified mathematical model) the values are almost identical. This gives confidence in the MATLAB code, the outputs of which were used to design the individual components of the EBB thruster.

Model Inputs	Thrust (target)	20 N
	Hydrogen peroxide concentration	87.5 %
	Plenum chamber pressure (target)	12 bar
	Injector pressure drop (target)	4 bar
	Catalyst bed pressure drop (estimated)	1 bar
	Decomposition efficiency (estimated)	95 %
	Injector discharge coefficient (estimated)	0.7
	Nozzle discharge coefficient (estimated)	0.9
Model Outputs	Tank pressure	17 bar
	Mass flow rate	17.7 g/s
	Specific impulse	115.1 s
	Chamber temperature	894.1 K
	Number of injector holes	4
	Injector throat diameter	0.5 mm
	Nozzle throat diameter	4.3 mm
	Nozzle exit diameter	6.5 mm

Table 9-1: Summary of input and output data provided by the MATLAB model

9.1.2 Catalyst Bed Design

In the case of the catalyst bed the main requirement was to minimise the mass and internal volume while still achieving complete decomposition of the hydrogen peroxide. A reduction in the internal volume not only helps to reduce the mass of the thruster but also improves performance by reducing the pressure drop and heat losses of the catalyst bed as well as the minimum impulse bit (MIB) of the thruster. However, for this project there are some other key requirements. The bed must be 'multi-use' i.e. be able to be filled and emptied on multiple occasions. The bed must also be able to take a variety of different catalyst types. Although initially two different beds were made, each must be able to take both ceramic pellet and metallic foam supported catalysts.

The key design parameter which affects the design of all other thruster components is the dimensions of the catalyst bed, or, more importantly the diameter of the catalyst bed. With the diameter fixed the dimensions of all connecting components could be determined. The minimum dimensions of the catalyst bed were mainly determined by specification of the maximum bed loading that can be tolerated. Typically two loading parameters, the mass flow rate per unit cross-sectional area (CSA) and the mass flow rate per unit wetted area of catalyst, are together able to provide some guidance concerning the required minimum catalyst bed diameter and length. Details of these parameters are provided chapter 2. The experimental data collected by the pICB was used in combination with values found in appropriate literature to provide the basis of the design.

Table 9-2 shows the results of this review as well as the results of the pICB tests given as reference [-]. Some sources have been covered in detail earlier in this thesis. In a number of cases the parameters have been calculated from the data provided within the literature; if this is unavailable the cell has been left blank. This data is more neatly summed up in Figure 9-1, which provides a histogram of the CSA catalyst bed loading. From this it is clear that in the majority of cases a CSA catalyst bed loading of 50 kg/s/m^2 or less has been chosen. Of particular note is the work conducted by Iarochenko *et al* [67] in Russia. The catalyst bed loading values stated come from many years of extended operation flight experience. A trade-off is required between a high catalyst loading and a low value of MIB. High catalyst loading may lead to incomplete decomposition, flooding of the catalyst material and short lived operation. However, low loading results in the bed diameter and therefore volume increasing which has a detrimental effect on the MIB. For the EBB thruster a target CSA catalyst bed loading of 50 kg/s/m^2 was chosen for all the catalyst beds tested. This gave a bed diameter of 21.2mm at the design flow rate. For simplicity of manufacture, the resulting bed diameter was rounded down to 21mm giving a true loading of 51.1 kg/s/ m^2 at the desired flow rate.

Ref	Catalyst type	Flow rate (kg/s)	Bed Diameter (mm)	Bed Length (mm)	CSA Bed Loading (kg/s/sq-m)	L/D
[-]	Pellet	3.53E-03	16.0	33.0	17.6	2.06
	Gauze	3.53E-03	16.0	68.0	17.6	4.25
[59]	Gauze	2.50E-3 - 6.00E-3	12.5	20.0	20 – 48.9	1.60
	Gauze	3.00E-3 - 5.00E-3	12.5	50.0	24.4 - 40.7	4.00
[60]	Pellet	1.45E-02	26.0	26.0	27.3	1.00
[64]	Gauze			38.1	234.1	
	Gauze	9.24E-02	31.9	57.9	116.7	1.82
[65]	Gauze	9.08E-02	25.4	35.1	179.3	1.38
	Gauze	1.16E-01	38.1	31.0	101.9	0.81
	Gauze	7.81E-02	25.3	38.1	154.7	1.51
[67]	Gauze / pellets	5.30E-03	12.0	42.0	46.9	3.50
	Gauze / pellets	8.40E-03	14.0	42.0	54.6	3.00
	Gauze / pellets	5.10E-02	35.0	48.0	53.0	1.37
	Gauze / pellets	6.90E-02		48.0		
	Gauze / pellets	1.01E-01	60.0	48.0	35.7	0.80
[87]	Pellet			76 - 102	93.3	
	Gauze			13 - 152	116.7 - 235	
[88]	Monolithic	5.00E-04	10.2 x 10.3	13.6	4.8	1.33
	Monolithic	5.00E-04	9.1 x 9.5	15.5	5.8	1.60
[89]	Gauze	9.07E-01	64.3		281.2	
[90]	Gauze	1.14E+00	74.0		270.0	
	Gauze	1.14E+00	51.0		560.0	
[91]	Monolithic	3.30E-01	31.9	14.3	421.0	0.45
	Monolithic	3.30E-01	31.9	13.1	421.0	0.41
[92]	Gauze	1.60E-02	14.3	43.2	100.0	3.02
[93]	Gauze			51.0	112.5	

Table 9-2: Literature review of catalyst bed loading parameters

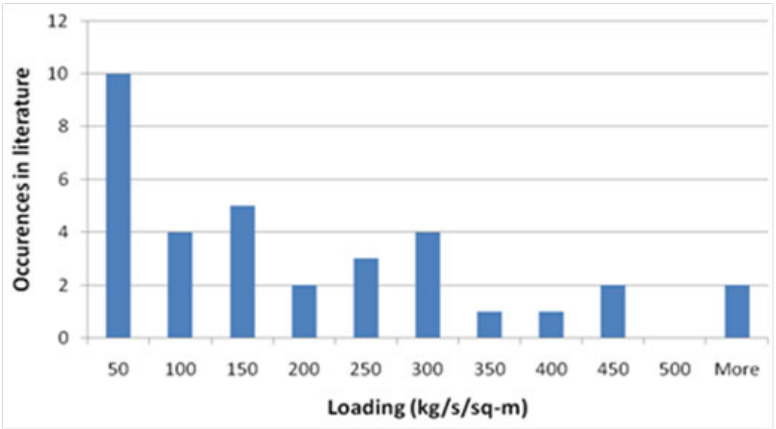

Figure 9-1: Histogram of CSA catalyst bed loading as identified in literature

The literature did not provide enough detail to allow the mass flow rate per unit wetted area of catalyst to be assessed. As a result it was instead decided to estimate an appropriate catalyst bed L/D ratio using the data collected from the literature. The research had showed that there is no direct correlation between the loading and the associated L/D ratio. The ratios tend to vary between 0.5 and 4.0 depending on the application. Smaller L/D values improve performance by reducing the mass and physical size of the thruster but also reduce the lifetime of the bed as the catalyst is quickly exhausted, with the opposite being true for larger L/D ratios. The EBB thruster is an experimental thruster which was required to operate for long periods of time so extended steady state performance could be assessed. As a result it was decided to be cautious and to choose larger L/D values rather than smaller ones. Initially two catalyst beds were designed. From the pICB results gathered using 0.5%Pt-Al a suitable L/D value of 2.25 was identified, this will be referred to as catalyst bed '1'. The second, and longer, of the two beds subsequently referred to as catalyst bed '2' used an L/D value of 3.25. This is to account for the unknown performance associated with the higher bed loading of 50kg/s/m^2 of the EBB compared to 17.6kg/s/m^2 for the pICB. These values lie within the range, not only identified in the general literature review, but also in the specific work of Iarochenko *et al* [67]. If both beds were filled with 5%Pt-Al the mass flow rate per unit wetted area of catalyst in the short bed is 1.3 kg/s/m^2 and for the long bed is 0.9 kg/s/m^2. The values presented are based on the Euclidean geometry only.

Evidence of flow channelling has been identified in the preliminary (and heavily) instrumented catalyst bed so steps were needed to minimise this problem within the EBB thruster. Anti-channel baffles are widely used within hydrogen peroxide thrusters; Lee *et al* [63] used a drilled plate with a 50% open area half way along his 47mm catalyst bed to avoid channelling. Performance data for the resultant thruster can be found in chapter 3. Jonker *et al* [77] reviewed in chapter 4 used 5 anti-channelling baffles of unknown shape located at 2, 10.8, 16.1, 21.4 and 26.7mm along the 34mm catalyst bed (as measured from the injector plate). Early work by Runckel *et al* [65] utilised 2 ring-like baffles fitted tightly against the bed wall; however, no details are provided on how far these rings protruded into the bed. Within the 35mm bed the first was located immediately downstream of the injector with the second approximately 5mm further downstream. It can be seen that there is little consensus on the ideal location of these baffles with each author choosing different numbers and locations with no clear reasoning given. Douglas *et al* [87] provided some clarity on the subject suggesting that for beds less than 102mm (4 inches) in diameter flow channelling was a significant issue. He indicated that baffles should be placed every 2.5-5cm along the bed (1-2 inches) with a minimum protrusion into the bed of 3.2mm.

Many authors have used multiple anti-channelling baffles which can be removed from the bed. However in the case of the EBB it was decided to machine the baffle directly into the bed wall. To successfully use removable metallic rings it was felt that a significant clearance between the ring and the wall would be required. This would be necessary to ensure the baffle did not become stuck against the bed wall after several heat cycles or during insertion and extraction. This would result in some of the flow being able to pass between the baffle and the wall making the anti-channelling baffle less effective. However, in order to facilitate loading of multiple types of catalyst into the EBB thruster only one baffle was used. The single baffle allows successful packing (or removal) of the catalytic material from both ends of the bed.

Due to the lack of consensus within the literature the results from the instrumented catalyst bed have been used to provide the location of this baffle. The aim of the baffle is to re-direct the liquid peroxide into the bed and should therefore be placed before the location of peak temperature where the majority of the peroxide flow is still un-reacted. If placed too close to the injector the peroxide may pass around the baffle and back out to the outside wall without reacting due to the quenching effect of the cool peroxide upstream. If the baffle is located too far downstream the peroxide may have already decomposed thus making the baffle unnecessary. During pICB testing with 0.5%Pt-Al the peak temperature had occurred in all cases at SP5 which was located at an X/D of approximately 2, where X is the distance from the entrance of the bed. Low temperatures were detected at SP2 and SP4 which lay between an X/D of 0.875 and 1.5. It was therefore decided to place the centre of the anti-channel baffle in the middle of the short bed (bed 1) resulting in an X/D of 1.125. This falls approximately half way between the two standpipes in the pICB that detected the low temperatures. It was unclear where to locate the baffle for the longer bed (bed 2) as at the EBB design stage testing with 5%Pt-Al had not been conducted. Therefore the design for the shorter bed has been scaled for the longer bed. This has resulted in the baffle being located at an X/D location of 1.625, half way along the catalyst bed.

Some modifications to the EBB thruster design were made after the first few runs had been conducted. Preliminary analysis of EBB runs conducted with 5%Pt-Al catalyst indicated that the peroxide failed to fully decompose within the catalyst bed. Initial testing had been conducted with the shorter of these two beds (Bed 1). It was hypothesised that using the longer of these two beds would ensure full decomposition but at the cost of reduced thrust-to-weight ratio and MIB performance; accordingly an alternative solution was sought. The results had shown a significant discrepancy between C* as calculated using the measured nozzle plenum temperature and C* calculated using the measured nozzle plenum pressure and the mass flow rate data. This discrepancy, in combination with photographic evidence of the retainer plate, suggested a significant channelling problem. This evidently resulted in a high temperature on

the axis (where the nozzle plenum thermocouple is located) but a much lower temperature at the catalyst bed wall. In an attempt to reduce the channelling a third catalyst bed, again with L/D = 2.25, was designed. This had a much taller anti-channelling baffle, which extended 6mm into the bed instead of 3.5mm for the first two designs.

The catalyst beds were bolted to the rest of the thruster via flanges at either end. At the upstream end of the bed a Viton o-ring was used to seal between the injector plate and catalyst bed. Viton o-rings could not be used at the downstream end since the o-ring will not survive the high bed temperatures achieved. In order to minimise the flange thickness it was decided not to use any o-rings, instead a Klingersil gasket was placed between the catalyst bed and nozzle. This would gradually succumb to the high temperature conditions so required regular replacement. An image of catalyst beds 1 and 2 can be found in Figure 9-2 and a summary of all the design values in Table 9-3. All the components of the EBB thruster are manufactured from stainless steel 316 to ensure compatibility with HTP.

	Catalyst bed 1	Catalyst bed 2	Catalyst Bed 3
Diameter, mm	21	21	21
Length, mm	47.25	68.25	47.25
L/D	2.25	3.25	2.25
Number of baffles	1	1	1
Location of baffle (in terms of X/D)	1.125	1.625	1.125
Baffle height, mm	3.5	3.5	6
CSA catalyst bed loading, kg/s/m2	51.1	51.1	51.1
Gauze wetted SA bed loading, kg/s/m2	0.4	0.28	0.4
Pellet wetted SA bed loading, kg/s/m2	1.3	0.9	1.3

Table 9-3: Dimensions and analysis of the EBB catalyst beds

Figure 9-2: Catalyst beds 1 (Left) and 2 (Right), central temperature measurement standpipe not shown

9.1.3 Injector design

The primary aim of the injector is to deliver a uniform dispersion of hydrogen peroxide onto the catalyst material. In the case of the EBB however, there were several other criteria which must be met. A sufficient pressure drop was required across the injector plate to decouple any pressure oscillations in the bed from the hydrogen peroxide supply upstream. More information on this requirement can be found in chapter 5. In order to help minimise the MIB the 'dead space' between the flow control valve (FCV, which controls the entry of peroxide into the thruster) and the start of the catalyst bed must be made as small as possible. 'Dead spaces' are volumes that must be filled with HTP, such as supply lines, but do not help in the decomposition process or generation of thrust. Finally, it was necessary to provide access for instrumentation. As well as measuring pressure and temperature of the incoming flow consideration must be placed on connecting a thrust measurement device to the back of the thruster, preferably along the thrust axis.

Injector design has been identified as having a significant influence on the performance of the catalyst bed. A poorly designed injector can cause severe quenching of the upstream part of the catalyst bed or even damage the catalyst material itself [87]. Goto *et al* identified catalyst degradation in a 1N hydrazine thruster due to the injector design [84]. In his original design a single tube was used to deliver the propellant similar to that utilized in the pICB. However, this design resulted in significant catalyst (Shell 405) degradation. The modified injectors used either a showerhead design (the number of orifices is not given) or a mesh diffused injector. The mesh injector consisted of a metallic mesh (of unknown dimensions) being placed between the delivery pipe and catalyst. Both these methods increased the catalyst bed exposure region and were found to alleviate the catalyst degradation problem. The mesh type injector was also found to provide the most stable decomposition and was identified as being the most suitable injector of all the injectors tested in his work.

Work carried out by the Rocket Research Corporation assessed a range of showerhead and Rigimesh injectors on 0.5, 5 and 50lbf thrusters [94]. Rigimesh is a porous metal injector made from a sintered woven wire sheet. The results of a range of tests indicated that the Rigimesh injectors did not perform well, leading to higher pressure oscillations and pressure decay times. This was attributed to their variable porosity, a result of the manufacturing process. Showerhead injectors with approximately 6 holes per square inch (~1 hole per square centimetre), placed in contact with the catalyst, were found to give the highest performance. It was possible to lower the injector hole density by up to a factor of two without serious degradation in catalyst bed performance. Low pressure drop (10-15% of steady state chamber pressure) showerhead injectors gave reduced cold bed response times. The catalyst material was able to decompose

more HTP than was being supplied so the higher initial mass flow rate flux due to the low pressure drop gave a lower response time without flooding the bed.

Douglas *et al* provides a contradictory assessment of injectors used in monopropellant gas generator designs [87]. He argued that swirl-cup or full cone nozzles offset from the catalyst bed provided greater performance than equivalent showerhead designs (direct liquid jet injectors). He identified direct injectors as one of the main causes of channelling flow, which could be alleviated slightly by offsetting the injector from the catalyst material but was only cured completely by atomizing the flow. He proposed two possible methods: either directing the showerhead injectors into distribution plates with the resulting splash atomising the flow or using full cone/ swirl-cup nozzles. Both resulted in a more even distribution of flow which did not penetrate or quench the bed.

The final argument is provided by An *et al* [95]. In this more recent work a 19 orifice (300µm diameter) showerhead injector was compared to a full cone spray nozzle. It was found that the spray nozzle had to be set back from the catalyst material in order to allow the flow to develop; this was not the case with the showerhead injector. As a result the catalyst bed with the showerhead injector had a much smaller 'dead space' volume; this meant impingement on the catalyst bed by the HTP occurred faster, reducing the initiation delay and increasing the rate of pressure rise.

All the sources agree that increasing the initial area of the catalyst bed exposed to the HTP improves catalyst bed performance and can increase catalyst bed life. There are three main methods identified as achieving this: showerhead injectors, showerhead injectors with metallic mesh screens or full cone/swirl-cup nozzles. The majority of sources agree placing the injector plate in contact with the catalyst material improves performance, although the reasons given for this improvement vary. This leads to the rejection of the nozzle-type injectors due to the dead-space required to develop the flow.

Based on the literature review and the initial requirements the injector was constructed of two sections. The first is an injector plate with a shower head injector design. To produce a uniform flow a large number of holes are required. However, as the number of holes increases the diameter of the holes must decrease to maintain the same pressure drop. The manufacturing techniques initially available to the author limited the minimum hole diameter to 0.5mm. Consequently the injector plate consisted of 4x 0.5mm holes distributed evenly over the plate referred to as injector 'A'. This resulted in a pressure drop of 4 bar across the injector plate; this represents 33% of the target chamber pressure, slightly above the 20-30% recommended by [96]. Figure 9-3 shows a raised protrusion surrounding the injector holes allowing a metallic

foam diffuser to be inserted. Preliminary testing showed using this injector plate delivered a lower than expected performance. This was attributed in part to the injector plate geometry which, it was conjectured, may have resulted in a quenching of the catalyst material directly downstream of the injector. Accordingly a second injector plate was manufactured. This was again a shower-head design but with 16 x 0.22mm diameter holes. The 4 and 16-hole injectors can be seen in Figure 9-3. Two variances of the 16-hole injector were used; the first, referred to as injector 'B' incorporated a diffuser, consisting of two nickel foam discs, placed over the injector plate. Meanwhile, injector 'C' was the same injector disc but without the nickel foam diffuser. The details of these three injectors are summarised in Table 9-4.

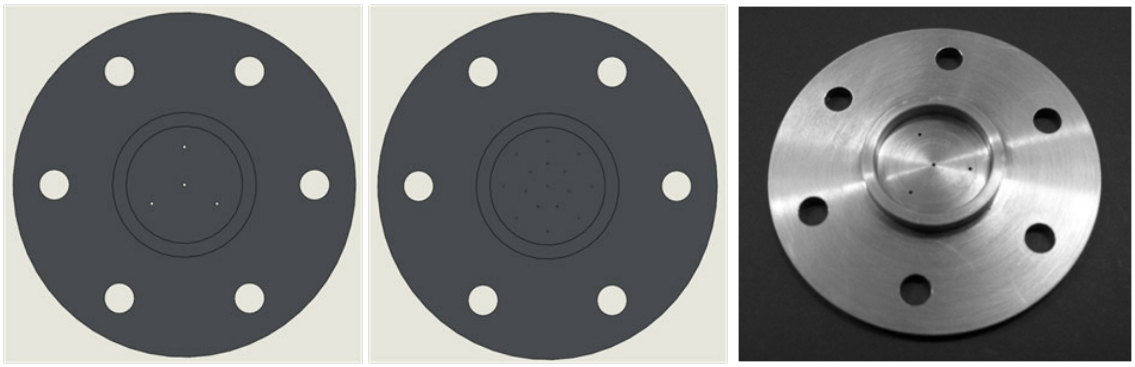

Figure 9-3: CAD model of Injector 'A' (Left), Injector 'C' (Centre) and machined injector 'A' (Right)

Injector Plate Type	No. Of holes	Hole Ø (mm)	Diffuser
A	4	0.50	×
B	16	0.22	✓
C	16	0.22	×

Table 9-4: Injector geometries tested

The second part of the injector is the injector manifold. This component must not only minimise the dead space between FCV and catalyst bed but also provides access for a thermocouple and pressure transducer, to enable the peroxide delivery pressure and temperature to be monitored and recorded, while providing clearance to connect the thrust measurement load cell to the back of the thruster. A 30mm, thick walled (1.5mm) delivery pipe connects the solenoid to the manifold, and served two purposes. It is thick walled with a small internal diameter (3mm) to minimise the dead space and support the heavy solenoid valve, but also helps to reduce the soak back of heat through the thruster which may damage the valve. The delivery pipe connects to the central channel as shown in Figure 9-4; also connected are two standpipes, one to measure temperature and the other pressure. A small plenum chamber is located at the front of the manifold where it connects to the injector plate. This provides the flow with access to all the

injector holes. In order for the load cell to be connected along the thrust axis a nut has been tack welded in the centre of the manifold. This connects via threaded studding to the load cell. The injector manifold is bolted to the injector plate and the catalyst bed via the flange. This led to a significant mass at the 'cold' end of the thruster. The large mass acts as a heat sink to protect the solenoid valve; since it is at the 'cold' end of the thruster it has a minimal impact on thruster performance.

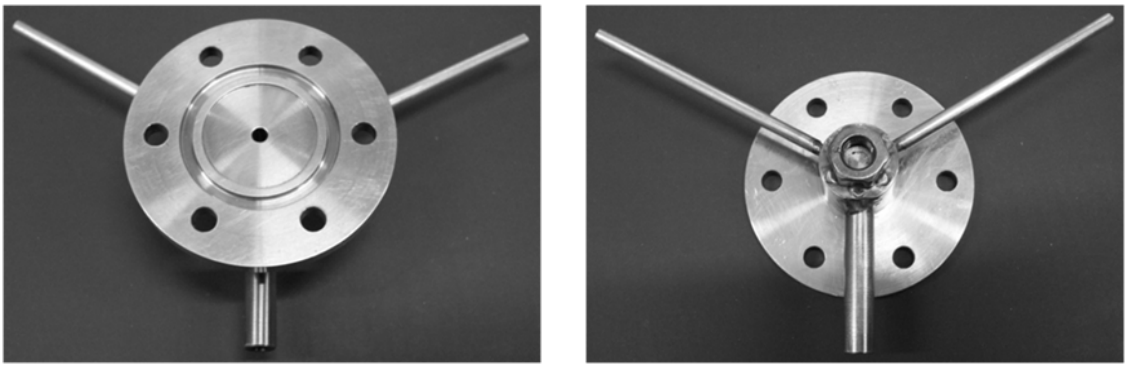

Figure 9-4: Injector manifold, from the Front (Left) and Back (Right)

9.1.4 Retainer Plate

The purpose of the retainer plate is to stop the catalyst material from being lost from the catalyst bed and ejected out of the nozzle. It must be removable to allow access to the bed so the catalyst can be loaded and unloaded. The main requirement however was to maximise the open area and minimise the mass. By doing so, both the pressure drop and heat losses are minimised.

Historically the majority of retainer plates have circular holes [65,77,74,93] but due to the small diameter of the bed this would lead to a relatively small open area in the EBB thruster. The larger the hole compared to the surrounding material and the greater the number of holes, the bigger the percentage open area. However, the diameter of the retainer plate holes is limited by two factors; the first is the size of the catalyst being placed within the bed. The greatest concern is MnOx-Ce/U-3 which has, as its smallest dimension, a diameter of 1.44mm. The second limit is that of the nozzle throat diameter. If any particle was to pass through the retainer plate into the nozzle it must also be able to pass through the throat and out of the thruster. If it were to get caught in the nozzle it could block the throat and this would quickly lead to a dangerous over-pressurisation. As a result it was decided that no hole should be larger than 2.2mm in diameter, with a nickel foam disc used to stop the smallest catalyst being ejected. To maintain strength within the retainer plate a minimum of 1mm separation is maintained between all the holes. A number of circular hole orientations were examined to maximise the percentage open area. Numerous research studies have been conducted into the maximum packing density of circles within a circle with 37 congruent circles being identified as the most efficient use of space [97].

This information was used to design a CAD drawing of the retainer plate shown in Figure 9-5 which provided an open area of 41%. It can be seen that with a hole diameter of 2.2mm and a 1mm minimum separation distance 37 holes is the maximum that can be included. The figure shows the circular holes touching the outside diameter; this is the part of the retainer plate seen by the flow not the overall diameter of the plate which is larger, providing additional material and structural integrity.

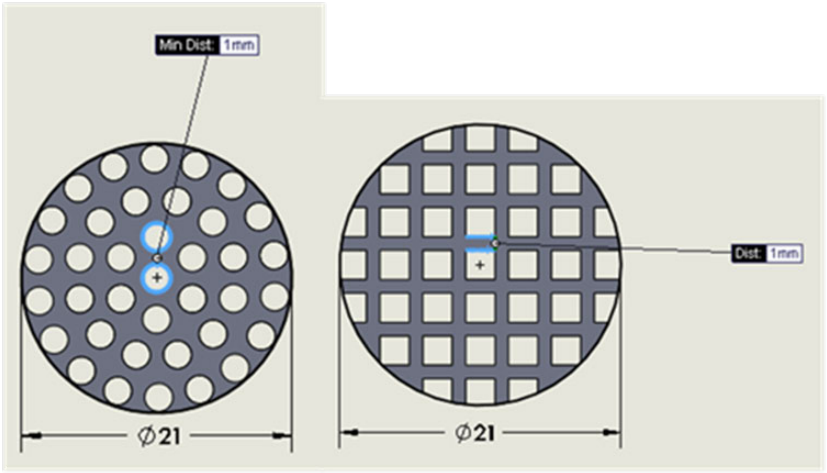

Figure 9-5: Circular and square designs for the EBB retainer plate

Instead of circular holes, square holes were identified as providing a larger open area. Square holes have several advantages. The separation distance is consistently 1mm; with circular holes this value is a minimum distance and at most points the separation is considerably larger than this. The wire cutting machine used to make the retainer plate allows partial square holes to be cut, whereas drilling the retainer plate results in only full, circular holes. Thus the use of square holes increases the open area that is possible. The final design consisted of 37 square holes (2.2x2.2mm) with a separation distance of 1mm. This gave an open area of approximately 47%.

The final requirement was to minimise the mass. The thickness of the retainer plate was set at 2mm. With such a large open structure and without the benefit of thermo-mechanical stress modelling it was decided not to reduce this thickness since the safety factor was unknown. The retainer plate sits within a recess in the nozzle flange, avoiding the need for its own separate flange and sealing gasket. The final manufactured retainer plate can be seen in Figure 9-5.

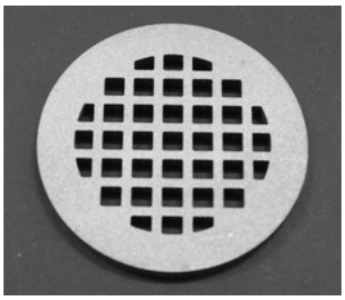

Figure 9-6: EBB retainer plate

9.1.5 Nozzle

The nozzle throat and exit diameters were specified in the early design stage as 4.3mm and 6.5mm respectively. A discharge coefficient of 0.9 was applied to the throat area. Subsequent testing has shown that this was far too low and that a discharge coefficient, if used at all, should have been much closer to 1. This has resulted in poorer than expected thruster performance. The main design challenge was to successfully integrate pressure and temperature instrumentation into the nozzle component as well as identifying a suitable nozzle divergence angle for the EBB thruster. As with all 'hot' end components it is important to minimise mass so as to maximise performance.

The decision was taken to use a simple conical nozzle even though this results in some loss of performance due to flow divergence. A trade-off is required between large and small nozzle divergence angles. Large angles give a much shorter and lighter nozzle but cause a reduction in performance due to the large divergence losses. Meanwhile small angles reduce divergence losses but at the expense of increased heat and frictional losses as well as an increase in the nozzle mass. However, the loss due to flow divergence is predictable and a correction can be retrospectively applied according to the equation below:

$$\lambda = \frac{1}{2}(1 + \cos\theta) \qquad \text{(Eq. 9-1)}$$

Here, λ is the correction factor which can be applied to the ideal nozzle exit momentum to predict the true performance. In this equation the nozzle divergence angle is represented by 2θ, where θ is the half angle. Literature suggests that the value of θ should lie between 12 and 18 degrees [96,98] depending on the application. Also investigated was the new ECAPS 1N monopropellant thruster which uses a green ADN oxidiser. Using Figure 9-7 the nozzle divergence angle was estimated at 30° giving a half angle of approximately 15°. In light of this investigation it was decided to set the nozzle divergence angle at 30° which gives a correction factor of 0.983.

Figure 9-7: ECAPS HGHP 1N thruster [99]

To assess fully the performance of the thruster the stagnation temperature and pressure must be measured. To measure temperature a standpipe has been welded to the convergent section of the nozzle. This allows a thermocouple to be positioned on the thrust axis. The location of the

pressure tapping is more complicated. If this tapping is placed at a similar location to the thermocouple the pressure measured would not be the true stagnation value. Instead it was decided to place the tapping just downstream of the retainer plate where, it is expected, the velocity would be close to zero. A channel has been cut in the recess in which the retainer plate is positioned. This channel links the bed to the pressure standpipe welded to the nozzle flange. With some consideration to the orientation of the retainer plate the pressure measured will be of the stagnated flow just downstream of the retainer plate. The completed nozzle is shown in Figure 9-8.

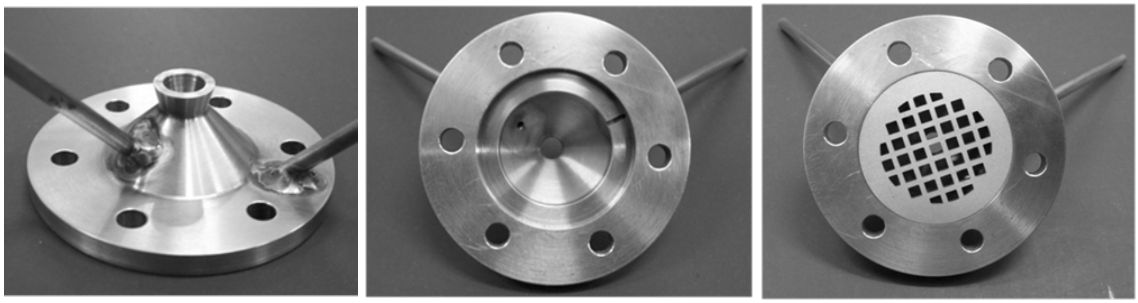

Figure 9-8: EBB nozzle showing standpipe locations (Left), pressure tap channel (Centre) and with retainer plate inserted (Right)

9.1.6 EBB Design Summary

Based on the GRASP market analysis [17] the author has decided to construct a 20 N-class (sea-level thrust) Engineering Breadboard (EBB) monopropellant thruster. Key design features were provided by a combination of a literature review, numerical modelling and experimental results (from the pICB). The design reasoning behind all the EBB components has been given. The bolt-up design facilitates both rapid catalyst and component changes allowing various configurations to be tested. A list of these configurations can be found in the next section. A schematic of the assembled EBB thruster can be found in Section 9.3.

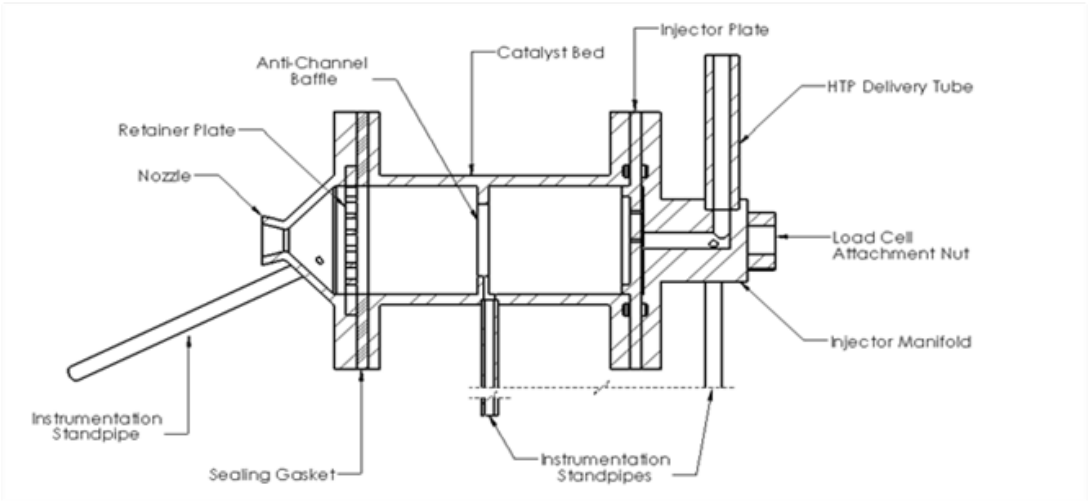

Figure 9-9: Schematic of EBB thruster

9.2 EBB Instrumentation and Uncertainty

The EBB instrumentation was similar to that used for the hICB so will not be covered in detail here. A summary of the instrumentation and its location can be found below. When this testing was conducted the NI9213 high acquisition rate temperature module was not available so temperature measurements are limited to a maximum acquisition rate of 5Hz. The rest of the instruments were acquired at 200Hz with some runs acquired at 500Hz for reasons described in the next section.

Location	Measurement Type
Propellant delivery rig	Pressure
	Mass flow rate
Test stand	Thrust
Injector manifold	Pressure
	Temperature
Catalyst Bed (mid-point)	Temperature – Axial
Nozzle	Temperature – Axial
	Pressure

Table 9-5: EBB Instrumentation - all configurations

It was not possible with the time and resources available to conduct repeats of every run under the same conditions; this makes a definitive statement on measurement and run-to-run uncertainty difficult. However, each run recorded two seconds of data before the delivery valve opened and after the valve had closed. This allowed any measurement drift to be identified as well as providing datum values. The accuracy of the instrumentation has been discussed in chapter 5 but is also summarised below for completeness. The error listed is the total error including the National Instruments and any signal conditioning hardware.

- K-type thermocouples; ±0.8% at 600°C
- Pressure transducers; ±1.81% assuming the PT is operating between -20°C and +80°C, although it is possible that the pressure transducers were exposed to higher temperatures than this.
- Volumetric flow meter; ±1.65% including frequency to voltage converter. The converter was shown experimentally to have a time delay of <100ms between the frequency input and voltage output. As with the instrumented catalyst beds the location of flow meter caused a time lag between the point of measuring the flow and it entering the thruster, further details of this are provided in chapter 5.
- A tension and compression 0-45N load cell with an accuracy of ±0.52% including an Omega Wheatstone bridge amplifier. The amplifier was shown experimentally to have a time delay of <50ms but no minimum input duration so although the signal lagged it

precisely followed variations in thrust. To minimise the error the load cell was calibrated with test weights once the thruster had been integrated into the test stand and connected to the load cell.

In order to calculate the characteristic velocity, C*, the throat area needed to be calculated. The nozzle throat diameter was assessed using a macroscope and graticule and found to be 4.28mm, -0.5% below the 4.3mm design value.

Knowing these values allowed the total error for a range of performance parameters to be calculated, these performance indicators will be used throughout this chapter to quantify thruster performance. Further description of these terms will be provided in the following sections.

- Characteristic velocity based on pressure, C^*_{PRESS}; -4.49%, +2.46%
- Characteristic velocity based on temperature, C^*_{TEMP}; ±0.33%, however this includes values generated by the NASA CEA code which has an unknown accuracy.
- Specific impulse, I_{SP}; ±2.17%

To take accurate thrust measurements a suitable test-stand was required. The stand had to be mobile, able to secure the thruster safely in various configurations and provide accurate thrust measurements. A test stand utilising a pendulum thrust measurement technique was employed. To minimise the influence on the thrust measurement the propellant inlet was orientated at 90° to the thrust axis, with all feed lines and instrumentation cables guided down the pendulum arm. The thruster was attached via the flanges on the catalyst bed. It was possible to adjust the load cell and thruster assembly in all 3 axes to ensure correct alignment. Once aligned the thruster was attached to the load cell via a threaded bar and calibrated using test weights between 40 and 1040grams. The test stand with integrated thruster can be seen in Figure 9-10.

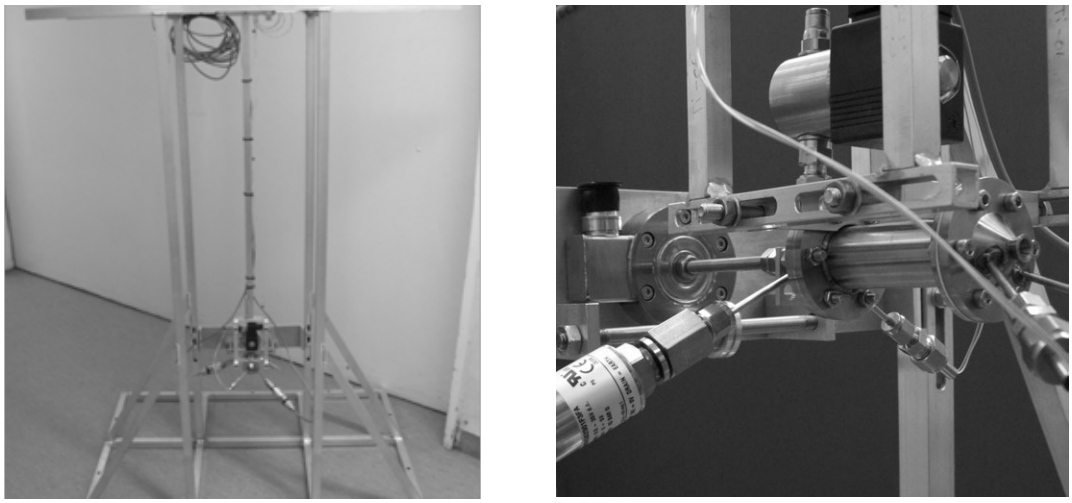

Figure 9-10: Test stand and integrated thruster

9.3 EBB Test Program

A total of 38 runs have been conducted using a combination of either an electrical heating coil or short pulses of HTP to pre-heat the bed. Electrical heating was initially limited to 200°C due to material limitations; however, during testing it was found this temperature could be increased to 250°C without damaging the seals used within the injector manifold. There was no temperature limitation with pulsed pre-heating since the cool liquid peroxide kept the injector assembly below 200°C. Not all runs will be described as some were for instrument calibration and verification and some were multiple repeats to ensure consistency.

Various configurations have been assessed; with differing combinations of injector, catalyst bed, catalyst material and pre-heating methodology being tested. These are summarised within Table 9-6. The run designation, described below, gives a full overview of the thruster configuration.

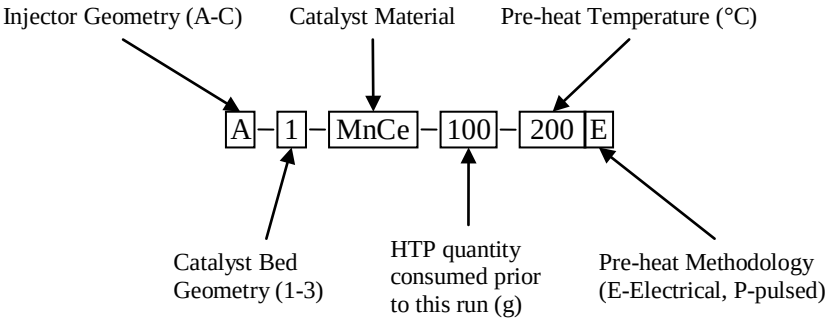

In addition to the pre-heating methodology various pulsed heating profiles have been employed; these are indicated in the footnotes attached to Table 9-6. In some cases the target temperature, used to identify the end of the pulsed pre-heating phase, was never met. As a result these runs only had a pulsing phase and no steady-state regime.

Unfortunately towards the end of the test program the mass flow meter frequency to voltage converter stopped working. It was therefore necessary to deduce the flow rate directly from the pulses generated by the flow meter. To do this it was necessary to increase the acquisition rate from 200Hz to 500Hz to fulfil the Nyquist criterion. All the run details have been summarised in Table 9-6. ‘HTP Consumed’ is the HTP throughput in a single run with ‘Total HTP’ the total amount of HTP to which the catalyst had been exposed before this run. It can be seen that 5%Pt-Al (Charge1) had accumulated a total exposure of 8.195kg of HTP; this may explain its reduction in performance by the end of the test campaign.

Run Designation	Total HTP (g)	HTP Consumed (g)	HTP Temp. (°C)	Pre-heat Temp. (°C)	Approx. Run Duration (s)
A-1-PT(I)-0-200E	0	33	5	200	5
A-1-PT(I)-33-200E	33	365	5	200	20
A-1-PT(I)-398-200E	398	260	6	200	15
A-1-PT(I)-658-450P	658	548	6	450 [1]	51
B-1-PT(I)-1206-200E	1206	69	16	200	7
* B-1-PT(I)-1275-500P	1275	144	17	500 [1]	50
* B-1-PT(I)-1419-500P	1419	254	18	500 [2]	110
* B-1-PT(I)-1673-500P	1673	93	23	500 [3]	90
B-1-PT(I)-1767-400P	1767	208	21	400 [2]	170
C-3-PT(I)-1974-350P	1974	188	17	350 [1]	30
C-3-PT(I)-2163-250P	2163	744	17	250 [1]	69
C-1-PT(I)-2906-250P	2906	464	17	250 [1]	38
C-1-PT(I)-3371-200E	3371	491	18	200	30
C-1-PT(I)-3862-250P	3862	285	19	250 [1]	30
C-1-PT(I)-4147-250P	4147	370	19	250 [1]	48
C-1-PT(I)-4517-250P	4517	723	20	250 [1]	101
C-1-PT(I)-5240-200E	5240	331	13	200	24
C-1-PT(I)-5571-200P	5571	375	12	200 [1]	29
C-1-PT(I)-5946-200E	5946	460	12	200	47
# C-1-PT(I)-6406-250E	6406	118	26	250	9
# C-1-PT(I)-6524-200E	6524	251	24	200	14
# C-1-PT(I)-6774-150E	6774	260	23	150	15
# C-1-PT(I)-7034-100E	7034	252	21	100	13
# C-1-PT(I)-7286-50E	7286	228	22	50	14
# C-1-PT(I)-7514-NONE	7514	221	20	NONE	12
# C-3-PT(I)-7734-200P	7734	100	20	200 [1]	9
# C-3-PT(I)-7835-200P	7835	360	19	200 [1]	16
C-2-PT(II)-0-250P	0	170	16	250 [1]	20
C-2-PT(II)-170-250P	170	814	15	250 [1]	69
C-1-MnNi-0-200P	0	157	13	200 [1]	12
C-1-MnNi-157-200P	157	161	16	200 [1]	14
C-1-MnNi-317-200P	317	207	14	200 [1]	15
C-1-MnNi-524-NONE	524	213	14	NONE	15
C-1-MnCe-0-200P	0	190	10	200 [1]	15
C-1-MnCe-190-200P	190	350	10	200 [1]	24
C-1-MnCe-540-200P	540	328	10	200 [1]	21
C-1-MnCe-867-NONE	867	328	10	NONE	22

Table 9-6: Summary of runs conducted

* No steady state was achieved

Flow meter converter failed

[1] Pulse heating profile On: 0.20s; Off: 1.80s
[2] Pulse heating profile On: 0.05s; Off: 1.95s
[3] Pulse heating profile On: 0.03s; Off: 4.97s

PT(I): 5%Pt-Al (1st Charge)
PT(II): 5%Pt-Al (2nd Charge)
MnNi: MnOx-Ni-2/R
MnCe: MnOx-Ce/U-3

9.4 EBB Results

Not all runs will be detailed here: only those runs that provide insight into the performance will be described. A full set of test results have been archived and are available on request. The results of this test program have allowed comparisons of the following features: injector geometry, pre-heat methodology, pre-heat temperature, catalyst bed geometry, catalyst type and finally, influence of catalyst bed geometry on minimum impulse bit (MIB). Each of these parameters will be looked at in isolation. Since the same catalyst material was used in various configurations the total throughput of peroxide the catalyst material was exposed to varied greatly between runs. This undoubtedly had an influence on thruster performance and must be taken into consideration when comparing data. Unless otherwise stated all values given are for steady state and the C* values are based on measured nozzle plenum pressure and mass flow rate, not nozzle plenum temperature (see chapter 2). This is because temperature is a point measurement compared to pressure which is representative of the entire thruster cross section at that location. The C* efficiency is obtained by taking the measured value of C* and dividing by the theoretical value provided by the NASA CEA code [19].

9.4.1 Effect of Injector Geometry

Three injectors have been tested, identified as injector A, B and C (see section 9.1.3). Three runs have been chosen to represent these changes; these are listed in Table 9-7. All tests were conducted with 5%Pt-Al (Charge 1). Note that, because steady-state conditions were not achieved in B-1-PT(I)-1275-500P, there is no value of mass flow rate and catalyst bed loading quoted for this run.

Run Designation	$\dot{m}_{S-S}$ (g/s)	CBL_{CSA} ($kg/s/m^2$)	Run Duration (s)
A-1-PT(I)-658-450P	20.50	59.2	51
B-1-PT(I)-1275-500P	-	-	50
C-1-PT(I)-3862-250P	18.13	52.3	30

Table 9-7: Runs used to assess injector geometry

Due to the variable starting conditions it is not possible to base this assessment on initial starting conditions although it is understood that injector geometry can have a significant effect on initial performance [95]. Ideally the runs selected would have had the same starting temperature and consistent pre-heating profile. Pulsed pre-heating was chosen over electrical pre-heating due to an unexpected nozzle plenum pressure profile at the beginning of the run. This was identified in varying degrees for all injector geometries utilising electrical heating and will be covered in more detail in the next section. Subsequently initial performance could not be compared and instead comparisons will focus on steady-state properties for the runs selected.

A typical run profile for a pulsed pre-heat run can be seen in Figure 9-11. Although not shown the steady state catalyst bed temperature, measured at the centre point of the bed (L/D = 1.125), failed to exceed 200°C, this indicates that decomposition is occurring in the downstream section of the bed. After an initial pulsing phase which was used to increase the bed temperature to a threshold of 450°C a steady state mass flow rate of 20.5g/s was achieved. Some of the pulses are not detected by the flow meter; this is due to the voltage to frequency converter requiring a minimum number of samples before generating an output. It can also be seen that there is a drop in the recorded mass flow rate before the other parameters at the end of the run; this is associated with peroxide depletion and the length of the line between the flow meter and EBB thruster.

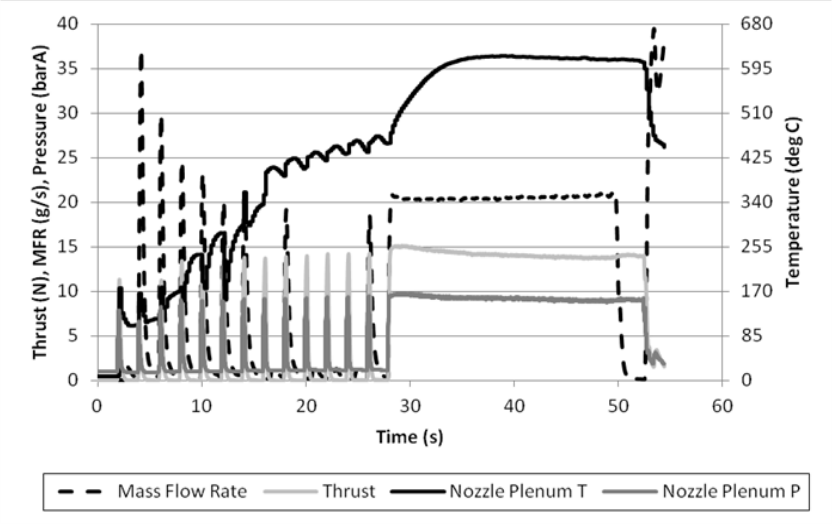

Figure 9-11: A-1-PT(I)-658-450P steady-state parameters

In steady state a thrust of 14.0N is generated with a nozzle plenum pressure and temperature of 9.1barA and 616.6°C respectively. This is below the design values of 20N at 12barA. This is mainly due to overly large throat area as a result of the discharge coefficient applied. The thruster performance, when assessed using the nozzle plenum temperature, appears to be good. Using equation 2-12 the decomposition efficiency is found to be 92.5%. Equations 2-9 and 2-11 showed C* could be calculated in two ways; one based on chamber temperature, C^*_{TEMP} and the other on chamber pressure C^*_{PRESS}. When C^*_{TEMP} is calculated it is found to be 892m/s, providing an excellent C* efficiency (Eq. 2-10) of 98.5%. However, C^*_{PRESS} is only 647m/s resulting in an efficiency of 72.0%. This is a difference, ΔC^*, of 27%. Since temperature measurements are point measurements the most likely reason for this discrepancy is a significant temperature gradient between the catalyst bed axis (where the temperature is measured) and the wall. A similar discrepancy was found with all runs utilising injector A. This is further supported by Figure 9-12 which shows a visible plume and evidence of liquid formation around the nozzle would not be expected if the mean exit temperature was exceeding 600°C.

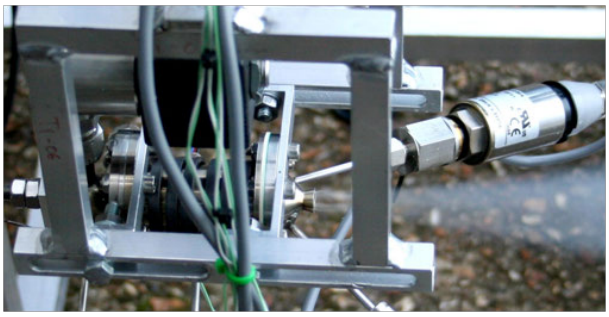

Figure 9-12: Steady-state firing EBB run A-1-PT(I)-658-450P

With the presence of an anti-channelling baffle within the thruster the significant variation between C^*_{TEMP} and C^*_{PRESS} was unexpected. It was theorised that this discrepancy maybe due in part to injector geometry. The limited number of holes in injector A promoted channelling by quenching the upstream section of the catalyst bed. As a result decomposition did not occur until downstream of the anti-channelling baffle. The decomposition initiated flow channelling and with no anti-channelling baffle further downstream the flow at the wall never fully decomposed. As a result of this preliminary assessment injector designs B was developed with the aim of producing a more evenly distributed flow at the injector in an attempt to reduce quenching.

Four runs were conducted using catalyst bed 1 and injector B. It was hoped the presence of the diffusing nickel foam discs would further distribute the flow; unfortunately this did not occur. Run B-1-PT(I)-1206-200E, which utilised an electrical heater to pre-heating the catalyst bed to 200°C, failed to achieve a nozzle plenum temperature above 210°C. Subsequently pulsed pre-heating was used to further raise the catalyst bed temperature before fully opening the FCV. Figure 9-13 shows the temperature profiles from B-1-PT(I)-1275-500P and provides a typical example of the temperature distributions achieved.

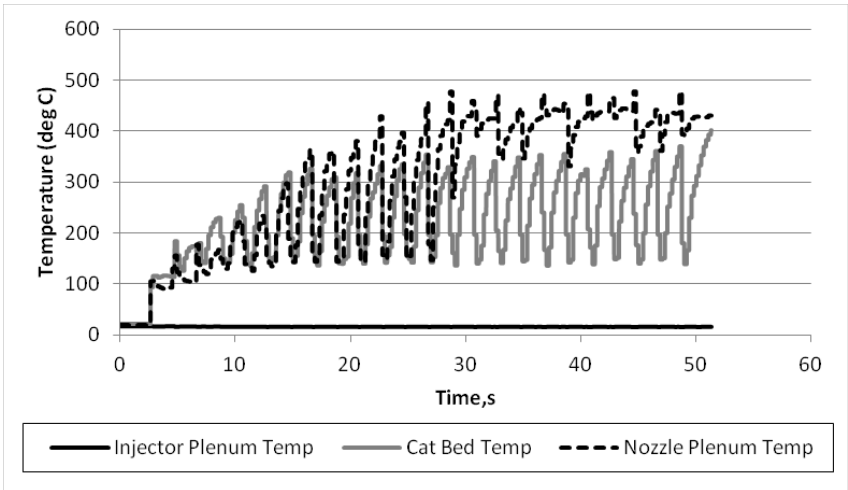

Figure 9-13: B-1-PT(I)-1275-500P temperature profiles

The target temperature for fully opening the FCV was 500°C; since this was never achieved the valve was never left open and so a steady-state condition was not achieved. By the final run with this injector (B-1-PT(I)-1767-400P) the target temperature had been reduced to 400°C and

this was achieved, however when left open the steady state nozzle plenum temperature again dropped to below 200°C. Rather than improving the uniformity of propellant injection, it appears the nickel foam diffuser had acted as a blockage to the flow. It is probable that the HTP had flowed around the edges of the nickel foam discs promoting flow along the wall of the bed. As a result the nickel foam discs were removed for future testing, resulting in injector C.

When the results for injector C are reviewed they initially indicate a poorer performance than that of injector A. The results of C-1-PT(I)-3862-250P can be seen in Figure 9-14. Although not shown the catalyst bed temperature fails to exceed 200°C suggesting once again that decomposition is mainly occurring in the downstream section of the bed.

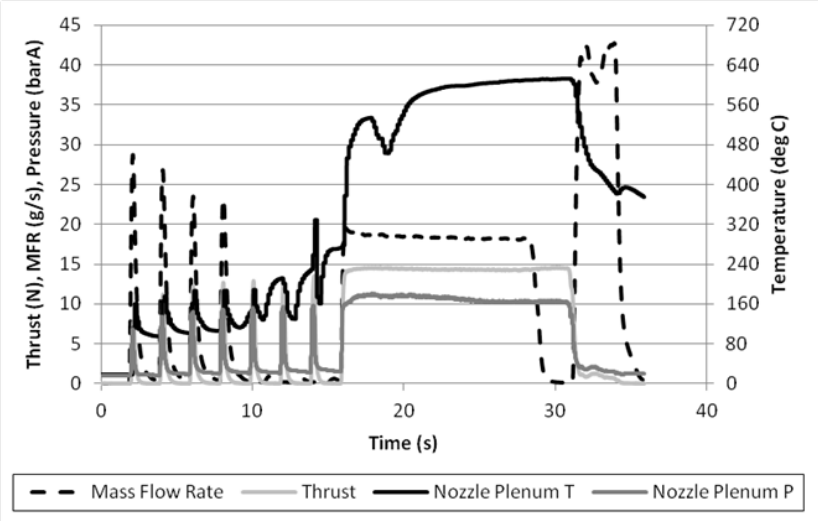

Figure 9-14: C-1-PT(I)-3862-250P steady-state parameters

The nozzle plenum temperature shows a momentarily reduction approximately 19s into the run. It is thought that this associated with better mixing of the hotter axial flow compared with the cooler circumferential flow in the nozzle plenum. So although channelling still occurs the channelled circumferential flow is decomposing further upstream providing greater distance for the gasses to mix. This may be related to a reduction in quenching at the injector associated with the better flow distribution. The result is a poorer temperature response overall but when comparing C* values it would seem much more representative of the entire cross-section. C-1-PT(I)-3862-250P has a lower mass flow rate but generates higher nozzle plenum pressure (10.3barA) and thrust (14.3N); this results in a higher I_{SP} of 80.3s compared to 69.5s in A-1-PT(I)-658-450P. Although I_{SP} has increased it is still significantly lower than the design value of 115.1s. C^*_{PRESS} is also improved, increasing from 647s to 824s, giving a C* efficiency of 90.7%. The decomposition efficiency has reduced to 88.1% corresponding with a lower C^*_{TEMP} of 881m/s. However the difference between these C* values has decreased from 27% in A-1-PT(I)-658-450P to 6.5% in C-1-PT(I)-3862-250P. These values are typical for tests conducted in this configuration. It would seem that changing the injector geometry has improved the temperature distribution in the nozzle plenum and the overall thruster performance. The results

are summarised in Table 9-8. Due to the performance improvement and greater consistency in results all further testing was conducted using injector C.

Run Designation	η_{TH} (%)	F (N)	I_{SP} (s)	C^*_{PRESS} (m/s)	C^*_{TEMP} (m/s)	ΔC^* (%)	η_{C^*} (%)
A-1-PT(I)-658-450P	92.5	14.0	69.5	646.7	885.6	27.0	72.0
B-1-PT(I)-1275-500P	-	-	-	-	-	-	-
C-1-PT(I)-3862-250P	88.1	14.3	80.3	823.7	881.1	6.5	90.7

Table 9-8: Summary results for comparison of injector geometry

9.4.2 Effect of Pre-heating Methodology

As has already been discussed two methods of pre-heating were utilised within the EBB test program; namely pulsing with HTP and electrical heating via an external heater coiled around the catalyst bed. The two runs; C-1-PT(I)-5240-200E and C-1-PT(I)-5571-200P which will be used for comparing these different pre-heating methods are detailed in Table 9-9; supplementary data will be provided by A-1-PT(I)-398-200E. In both cases the same catalyst, thruster configuration and pre-heat temperature was used. When these tests were conducted the catalyst material had already been exposed to at least 5.57kg of propellant and there were signs that the performance had begun to degrade. However since the catalyst in both tests had similar propellant exposure direct comparisons are still possible.

Run Designation	$\dot{m}_{S-S}$ (g/s)	Run Duration (s)
C-1-PT(I)-5240-200E	16.1	24
C-1-PT(I)-5571-200P	18.6	29
A-1-PT(I)-398-200E	*20.0*	*15*

Table 9-9: Runs used to assess pre-heat methodology

A five second subset of the data from C-1-PT(I)-5571-200P is shown in Figure 9-15. This graph captures the final pulse and the start of the steady state period. When the final pulse is completed the nozzle plenum temperature, which was consistently higher than the bed temperature, is at 190°C. After the valve closes the temperature continues to rise and as a result when the FCV is left open the nozzle plenum temperature is 259°C and the bed temperature is 164°C. As with previous runs there is a lag in the flow meter response when the valve is left open. A small time lag in comparison to nozzle plenum pressure can also be seen with the thrust measurement. A response lag in the order of a few milliseconds between the pressure and thrust would be expected but this is approximately 50 milliseconds. This is likely due to the response time of the load cell amplifier which can be up to 200ms, although this data shows it is significantly less than this.

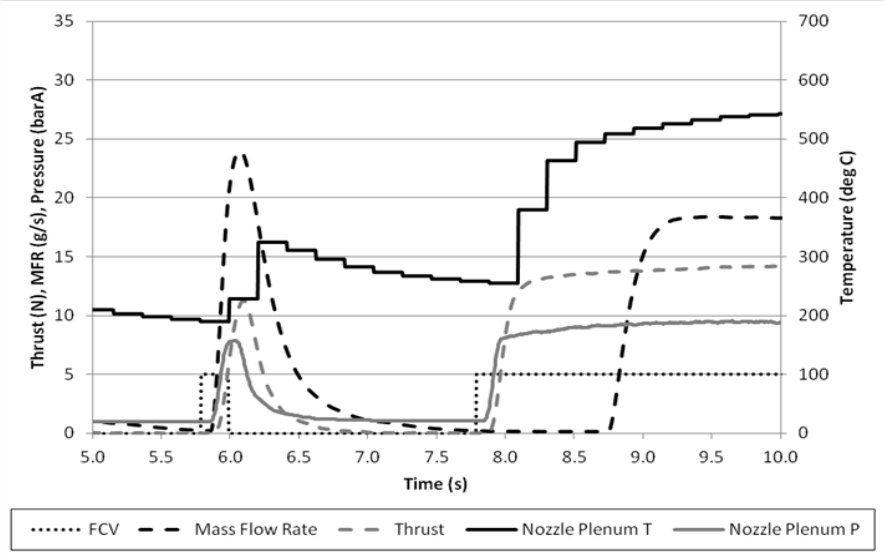

Figure 9-15: C-1-PT(I)-5571-200P initial performance

Initial performance has been quantified in terms of time taken to reach 90% of steady state temperature, t_{90} and time taken to reach 90% of steady state pressure, t_{90P}. For C-1-PT(I)-5571-200P these values are 1.36s and 0.16s respectively. The temperature and pressure profiles are consistent with an immediate catalyst response with no indications of quenching. The nozzle plenum temperature remains high for the remainder of the run reaching a steady state value of 579°C, corresponding to a decomposition efficiency of 85.5%. This is lower than achieved in earlier runs and consistent with signs of catalyst exhaustion.

An equivalent five second profile is provided for C-1-PT(I)-5240-200E in Figure 9-16. Thrust and mass flow rate response lags are again seen. The nozzle plenum temperature when this run is initiated is only 93°C but the bed temperature is 201°C.

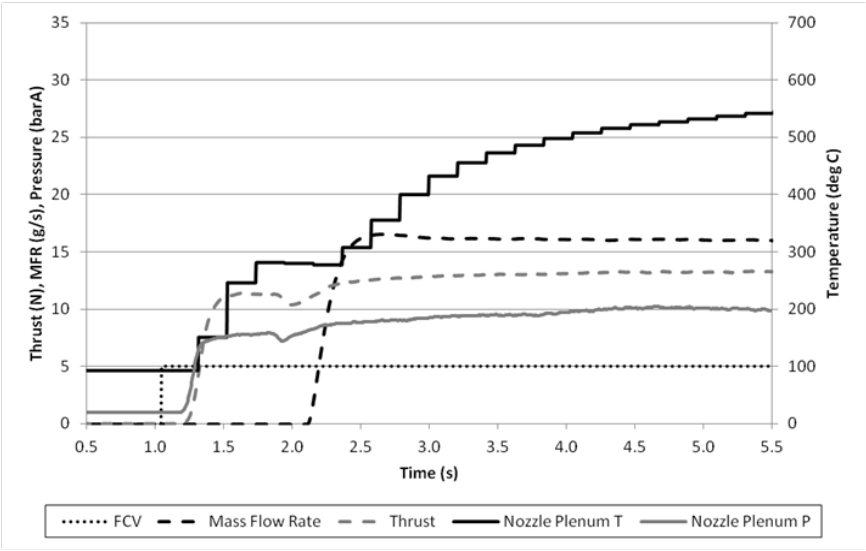

Figure 9-16: C-1-PT(I)-5240-200E initial performance

This is expected as it is the catalyst bed section which is heated not the nozzle. A brief drop in pressure and thrust can be indentified 0.83s after the valve is opened. This is likely a real effect

since it is detected by two different instruments; it also coincides with a momentary plateau in nozzle temperature at 280°C. Although this is higher than the boiling point of HTP (215°C at 7.5barA) it is still likely associated with the phase transition. This may indicate momentary quenching of the catalyst. It is known from the hICB data that initially there is a spike in the mass flow rate until the bed pressure rises and it is this that may quench the catalyst. The result of this possible quenching is a delay in reaching t_{90} and t_{90P} which for this run are 3.63s and 0.43s respectively. In earlier runs which also utilise electrical heating the drop in pressure is much more significant. A-1-PT(I)-398-200E shown below shows a drop in pressure of over 5.5bar. In this run the initial mass flow rate is successfully captured and shows a peak value of 40g/s. There is however no evidence of a temperature plateau in either the bed or nozzle plenum. It is thought that the combination of a more reactive catalyst and slow rate of temperature acquisition may have resulted in this plateau being missed. It is the opinion of the author that the drop in pressure is the result of catalyst bed quenching.

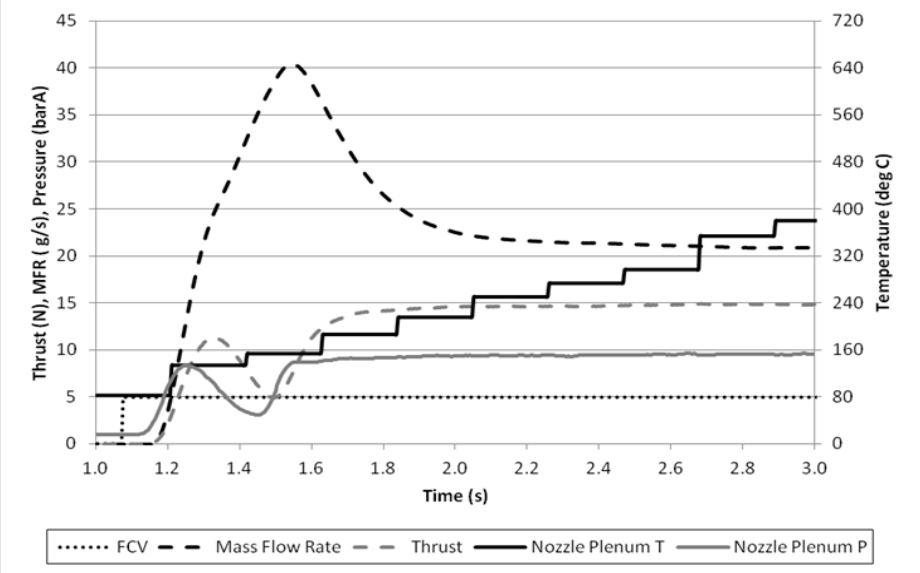

Figure 9-17: A-1-PT(I)-398-200E initial performance

The investigation shows that pulsing results in an improved initial performance for the same target temperature. The data is summarised in Table 9-10 and shows initial temperatures (i.e. when the FCV is first opened) and initiation delay times. It is theorised that pulsing results in an uneven temperature distribution within the bed with the highest temperature rise associated with where HTP decomposition is most likely to occur, since it is HTP decomposition in the pulsing phase which generates the temperature rise. This locally high temperature improves catalytic reactivity at this location and results in the improved performance. Electrical heating evenly distributes heat over the entire catalyst bed; however when the FCV is opened the upstream section of the catalyst bed is immediately quenched so the thermal energy applied to this section is essentially wasted. However the lack of instrumentation within this thruster means there is insufficient data to fully validate this hypothesis.

Run No.	Initial T_{bed} (°C)	Initial T_{noz} (°C)	t_{90} (s)	t_{90P} (s)	S-S η_{TH} (%)
C-1-PT(I)-5240-200E	201	93	3.63	0.430	85.6
C-1-PT(I)-5571-200P	164	259	1.36	0.160	85.5
A-1-PT(I)-398-200E	*203*	*83*	*5.60*	*0.150*	*90.7*

Table 9-10: Summary results for comparison of pre-heat methodology

There are several significant drawbacks with pulsing in terms of real life applications. Firstly, pulsing consumes propellant. It has already been noted that the most suitable application of HTP thrusters is on small, low cost satellites. These tend to be volume limited so increasing propellant tank size to account for pre-heat pulsing is not a preferred option. Secondly the thrust generated during the pulsing phase cannot be accurately predicted. For small thrusters like those associated with station keeping accurate predictions of thrust profiles are important in order to determine thruster on times and duration. It is for these reasons that commercial thrusters utilise electrical pre-heating.

9.4.3 Effect of Pre-heat Temperature

A range of pre-heating temperatures have been applied to the EBB thruster both in pulsed and electrically pre-heating modes. It has been shown that even when a target pulsing temperature is set it is unlikely to be met accurately. Therefore assessment of pre-heating temperatures will focus on electrically pre-heated beds. Five runs have been identified for this assessment; details of these runs can be found below. In all cases the same catalyst, 5%Pt-Al (Charge 1) and thruster configuration was used. The results indicate that catalytic performance had degraded due to the high throughput of propellant. Contrary to being detrimental to the assessment the partially exhausted catalyst bed has been shown to be increasingly sensitive to start temperature.

Run Designation	Cat. Bed Start Temp (°C)	$\dot{m}_{S-S}$ (g/s)	CBL_{CSA} (kg/s/m^2)	Run Duration (s)
C-1-PT(I)-6406-250E	250	19.3	55.7	9
C-1-PT(I)-6524-200E	200	20.2	58.3	14
C-1-PT(I)-6774-150E	150	20.0	57.6	15
C-1-PT(I)-7034-100E	100	21.0	60.6	13
C-1-PT(I)-7286-50E	50	20.3	58.5	14
C-1-PT(I)-7514-NONE	AMBIENT	22.0	63.5	12

Table 9-11: Runs used to assess pre-heat temperature

Temperature profiles for C-1-PT(I)-6406-250E and C-1-PT(I)-6774-150E are shown in Figure 9-18 and Figure 9-19. It can be seen that a reduction in start temperature results in a decrease in peak temperature within the catalyst bed, with the decomposition plane moving downstream. Unexpectedly the response time, t_{90}, of the bed remains relatively constant for pre-heat

temperatures between 150 and 250°C. However, due to the low temperature signal acquisition rate no definitive statement on the response times can be made. As pre-heat temperature decreases thruster performance is also seen to reduce as shown by Table 9-12. Below a pre-heat temperature of 150°C the performance of the thruster falls significantly with steady state nozzle plenum temperatures failing to exceed 200°C and visual evidence of liquid being ejected from the nozzle.

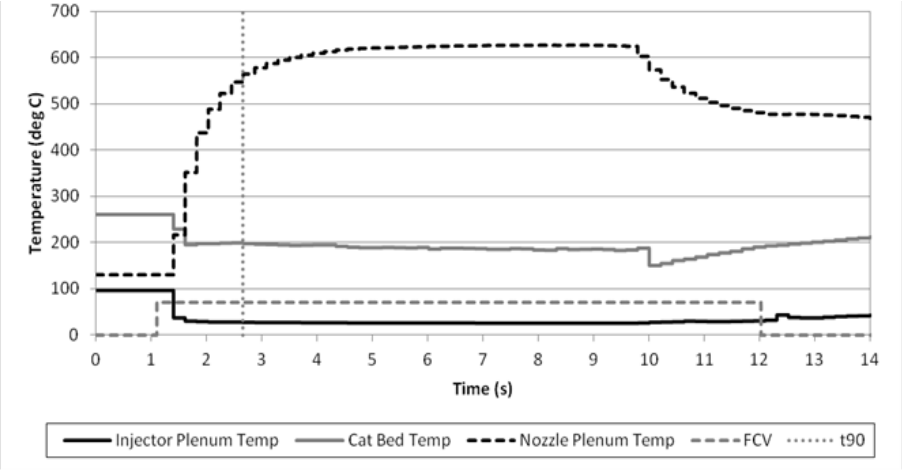

Figure 9-18: C-1-PT(I)-6406-250E temperature profiles

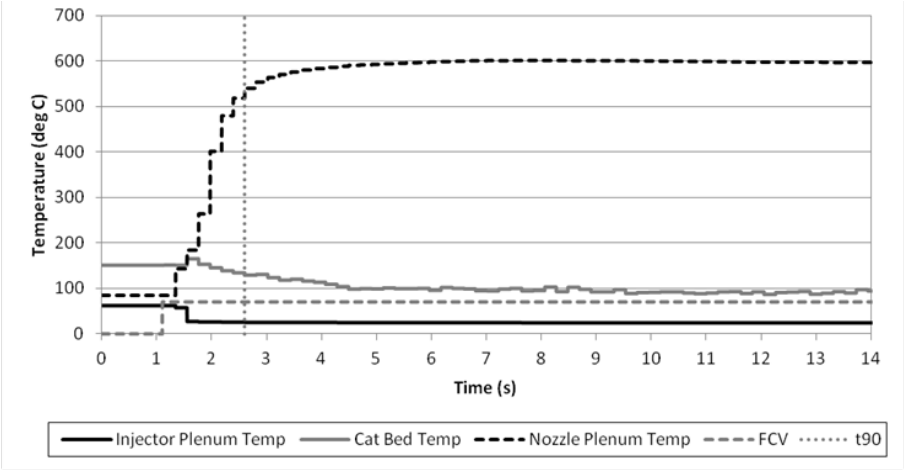

Figure 9-19: C-1-PT(I)-6774-150E temperature profiles

Run Designation	T_{bed} (°C)	T_{noz} (°C)	η_{TH} (%)	P_{noz} (barA)	F (N)	η_{C^*} (%)
C-1-PT(I)-6406-250E	188	621	88.8	9.4	15.3	77.7
C-1-PT(I)-6524-200E	142	601	86.1	9.1	14.7	71.9
C-1-PT(I)-6774-150E	90	597	85.9	8.9	14.0	70.7
C-1-PT(I)-7034-100E	155	184	24.3	7.2	10.7	54.4
C-1-PT(I)-7286-50E	148	180	23.6	5.9	8.6	46.9
C-1-PT(I)-7514-NONE	120	177	23.5	5.6	7.9	40.5

Table 9-12: Summary results for comparison of pre-heat temperature

Figure 9-20 shows the temperature profiles at a starting temperature of 100°C; it can be seen that initially the nozzle plenum temperature slightly exceeds 200°C but then decays. This suggests that pre-heat temperature is below that required to achieve full decomposition within the catalyst bed.

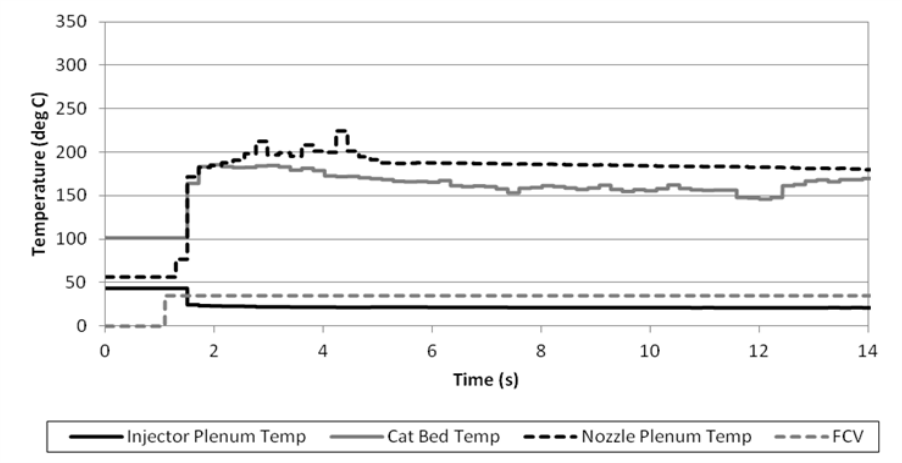

Figure 9-20: C-1-PT(I)-7034-100E temperature profiles

The results have shown that, especially towards the end of life, catalyst performance is highly dependent on initial temperature. In order to maintain performance temperatures above 150°C are required and preferably above 200°C. It is known from the hICB results that at the beginning of life 5%Pt-Al can generate high decomposition temperatures at an L/D of 2 with an initial bed temperature of 50°C. However the current data shows the performance falls significantly with prolonged HTP exposure.

9.4.4 Effect of Catalyst Bed Geometry

The final mechanical component to be reviewed is the catalyst bed. Three catalyst beds have been tested, with varying L/D values and anti-channelling baffle heights. The three runs chosen to investigate these parameters are given in Table 9-13. All utilised 5%Pt-Al as the catalyst and a pulsed pre-heating profile of 0.2s on followed by 1.8s off.

Run Designation	$\dot{m}_{s-s}$ (g/s)	CBL_{CSA} (kg/s/m^2)	Run Duration (s)
C-1-PT(I)-2906-250P	18.13	52.3	38
C-2-PT(II)-0-250P	17.67	51.0	20
C-3-PT(I)-1974-350P	17.38	50.2	30

Table 9-13: Runs used to assess catalyst bed geometry

The temperature profiles for these three runs reveal a lot about their respective performances. The temperature profile for C-1-PT(I)-2906-250P is shown in Figure 9-21. Like previous runs in this configuration (Figure 9-14) there is a drop in nozzle plenum temperature, however,

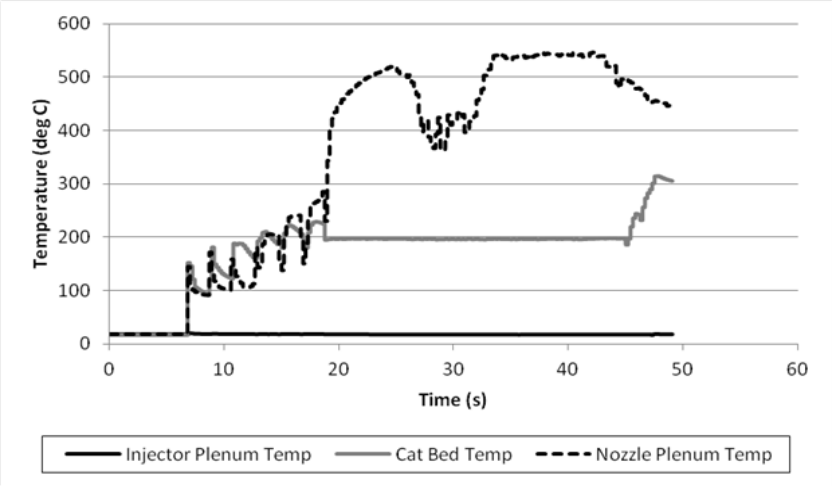

Figure 9-21: C-1-PT(I)-2906-250P temperature profiles

in this run it is for a significantly longer period of time, resulting in a poorer decomposition efficiency of only 78.6%. Again this is likely due to mixing of the cooler radial gas with the hotter axial gas in the nozzle. This indicates the presence of flow channelling which is not seen with catalyst bed 3. The temperature profiles for C-3-PT(I)-1974-350P are shown in Figure 9-22. Nozzle plenum temperature is still seen to be rising at the end of this short run suggesting a steady-state temperature is never reached. There is no evidence of channelling while ΔC* is still small at 7.3% indicating a homogenous nozzle plenum temperature. The increase in baffle height has resulted in an increase in pressure drop from 6.8bar to 7.9bar. This is to be expected and is one of the drawbacks with increasing the baffle height. It could be argued that the decrease in channelling was partially due to an increase in initial start temperature and reduced exposure to propellant. However, catalyst performance was high even with greater propellant exposure (C-1-PT(I)-3862-250P), and significant channelling was identified in other runs at higher initial temperatures (A-1-PT(I)-658-450P). This suggests that higher initial temperature does not necessarily reduce channelling. It is therefore the opinion of the author that increasing anti-channelling baffle height has led to a reduction in channelling and improved performance.

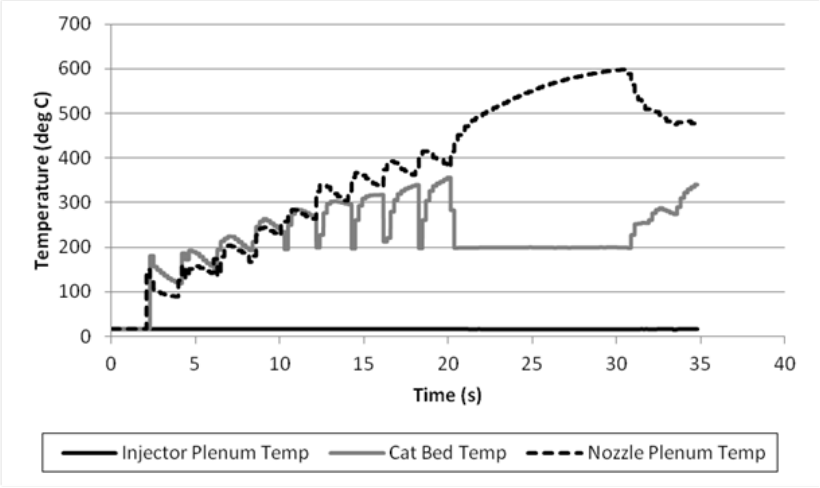

Figure 9-22: C-3-PT(I)-1974-350P temperature profiles

The temperature profiles for C-2-PT(II)-0-250P are shown in Figure 9-23. It can be seen that the bed temperature is significantly higher than with the shorter beds. This is consistent with the measurement point being further downstream in this configuration (at an L/D value of 1.625 compared with 1.125). Since significant decomposition is already occurring the anti-channelling baffle is more effective at directing the radial flow into a much hotter core flow. This has resulted in a more homogenous nozzle plenum exit temperature with a difference in C* measurements of only 5.9%. The longer bed has also resulted in a C* efficiency of 91.5%; the highest of any configuration with this catalyst. Figure 9-24 supports the argument that there is little to no channelling occurring within this bed. The left hand image shows the retainer plate after testing with catalyst bed 1 and catalyst PT(I); significant discolouration due to temperature is limited to the centre nine squares. Meanwhile the image on the right taken after run C-2-PT(II)-0-250P (with catalyst bed 2) shows significant discolouration over the majority of the retainer plate indicating a much more even temperature distribution.

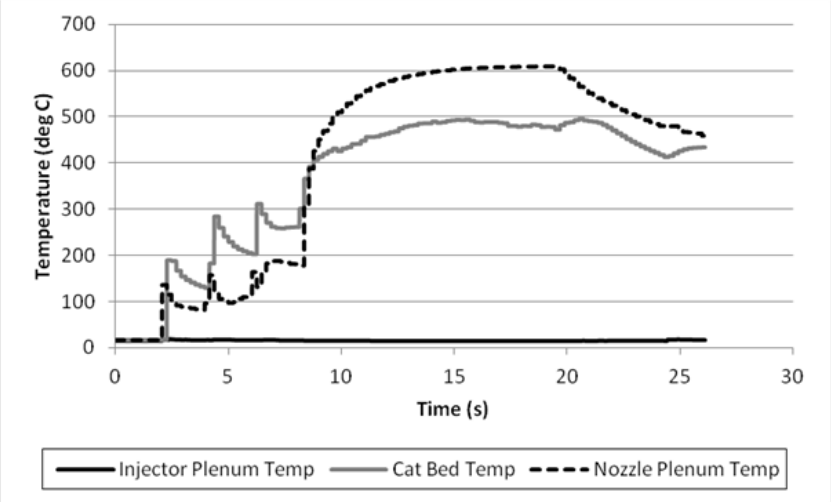

Figure 9-23: C-2-PT(II)-0-250P temperature profiles

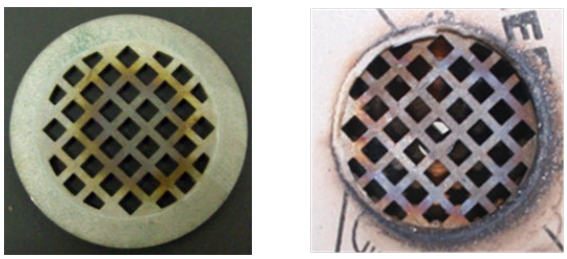

Figure 9-24: Retainer plate images, before (left) and after (right) testing with catalyst bed 2

Unexpectedly the pressure drop with bed 2 is surprisingly low at only 6.4bar. The reasons for this are unclear as it would be expected to be significantly higher due that the increased length of gaseous flow. The increased length has resulted in an increased time to 90% of the steady state pressure. With catalyst bed 1 and 3 these values were similar at 0.100s and 0.096s respectively; however catalyst bed 2 has an associated $t_{90\%P}$ of 0.156s, an increase of 56%. This would be expected as the internal volume of catalyst bed 2 is 44% greater than catalyst bed 1.

This catalyst bed has clearly outperformed either of the other two, as the results in Table 9-14 show. However for ACS thrusters minimum impulse bit (MIB) is an important parameter which is significantly affected by pressure build up time. MIB will be the subject of further investigation later in this chapter.

Run Designation	η_{TH} (%)	t_{90P} (%)	ΔP (bar)	I_{SP} (s)	C^*_{PRESS} (m/s)	ΔC* (%)	η_{C^*} (%)
C-1-PT(I)-2906-250P	78.6	0.100	6.8	86.6	763	9.9	84.2
C-2-PT(II)-0-250P	88.7	0.156	6.4	94.0	829	5.9	91.5
C-3-PT(I)-1974-350P	82.6	0.096	7.9	90.1	799	7.3	88.1

Table 9-14: Summary results for comparison of catalyst bed geometry

9.4.5 Comparison of catalyst performance

Although the majority of the testing program has been conducted with 5%Pt-Al, two additional catalysts have been assessed within the EBB thruster, namely MnOx-Ni-2/R and MnOx-Ce/U-3. Five runs have been used to assess performance with their details listed in Table 9-15. In all cases the configuration was catalyst bed 1 and injector C. Where pre-heating was applied this was achieved with pulsing.

Run Designation	$\dot{m}_{S-S}$ (g/s)	CBL_{CSA} (kg/s/m^2)	Run Time (s)
C-1-PT(I)-3862-250P	18.13	52.3	30
C-1-MnNi-317-200P	18.48	53.4	15
C-1-MnNi-524-NONE	18.60	53.7	15
C-1-MnCe-540-200P	17.87	51.6	21
C-1-MnCe-867-NONE	16.18	46.7	20

Table 9-15: Runs used to assess catalyst performance

The steady state parameters for C-1-PT(I)-3862-250P can be found in Figure 9-14 and will not be repeated here. The figure showed that the temperature rose steadily reaching a stead state nozzle plenum temperature of 606°C and a corresponding thermal efficiency of 88.1% after an initial pulsing phase of seven pulses. The nozzle plenum temperature profile also showed a momentary decrease as a result of the better mixing between the cool radial and hot axial flows that occurred due to flow channelling. The presence of channelling was not found with either of the other two catalysts tested.

The performance of the MnOx-Ni-2/R was significantly better than 5%pt-Al. It can be seen from Figure 9-25 that only a single pulse was needed to reach the required temperature with the catalyst bed responding immediately. When the FCV was left open the nozzle plenum

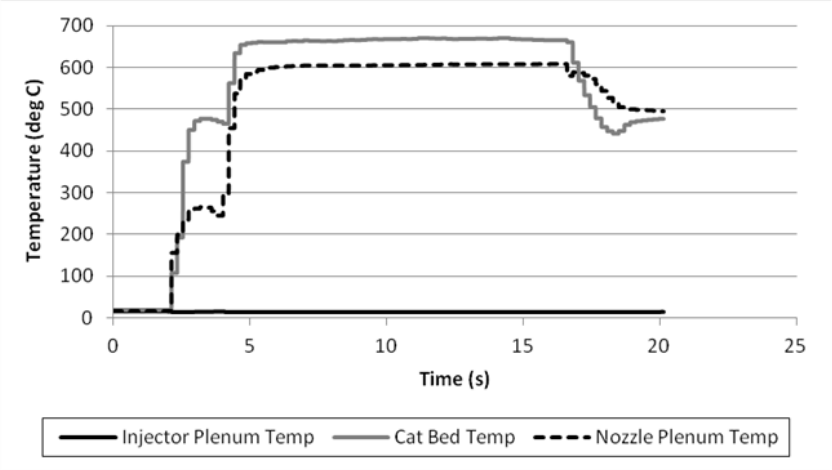

Figure 9-25: C-1-MnNi-317-200P temperature profiles

temperature responded quickly with a t_{90} of 1.18s before reaching a steady state of 606°C (equating to a thermal efficiency of 89.3%). However this was not the highest measured temperature. The catalyst bed temperature responded faster, reaching t_{90} in only 0.97s and achieved a higher steady state value and thermal efficiency of 658°C and 97.0% respectively. This catalyst generated consistently higher temperatures in all the tests conducted. The loss in temperature between the catalyst bed and nozzle is likely due to the high conductivity of the metallic catalyst support which conducted heat to the catalyst bed walls more effectively. The performance data shown in Figure 9-26 shows a rapid response in both pressure and thrust, with a η_{C^*} and I_{SP} of 93.1% and 99.1s respectively. However, this is lower than would have been achieved if it were not for significant thermal losses. The data also shows no channelling with a ΔC* of only 4.3%. It was noted that the pressure profile was rougher than had been found with 5%Pt-Al. When calculated the pressure roughness (defined in Eq. 2-13) was 10.5%, twice that of C-1-PT(I)-3862-250P at only 5.1%. This is consistent with the findings of the hICB.

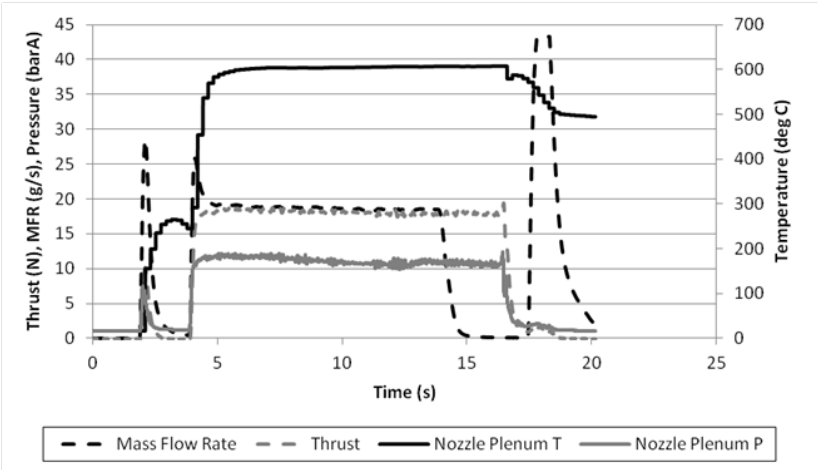

Figure 9-26: C-1-MnNi-317-200P steady-state parameters

The high performance gave confidence in conducting a test with no pre-heating. As can be seen from Figure 9-27 the catalyst again responded rapidly. Catalyst bed temperatures reached a steady state value of 658°C and nozzle plenum temperature of 607°C. Pressure and temperature response times (to 90% of steady state) increased from 0.62s and 0.16s with pre-heating to 0.97s

and 0.47s without. As had been seen with electrically pre-heated beds in earlier runs there was a drop in pressure after an initial spike, however due to the improved reactivity this transient only lasts 0.11s. This is responsible for the increase in time taken to reach 90% of the steady state pressure. Steady state performance values are almost identical to the pre-heated run with a C* efficiency of 93.9% and an I_{SP} of 98.3s. As with the pre-heated run the steady state pressure roughness is higher than 5%pt-Al at 8.64%. Post testing inspection showed no damage to the catalyst so, as with the hICB, this roughness is likely associated with compression of the catalyst within the bed.

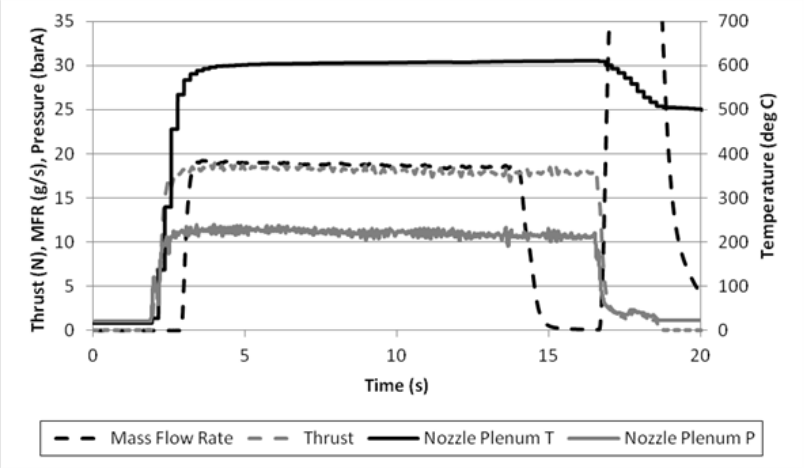

Figure 9-27: C-1-MnNi-317-NONE steady-state parameters

The temperature profiles of MnOx-Ce/U-3, shown in Figure 9-28, were similar to MnOx-Ni-2/R although the response time was slower. The catalyst bed temperature reached t_{90} in 1.26s with a steady state value of 653°C. However, unlike MnOx-Ni-2/R the high temperature is maintained resulting in a nozzle plenum temperature of 659°C and associated response time of 1.89s. Again only a single pulse is required to pre-heat the thruster.

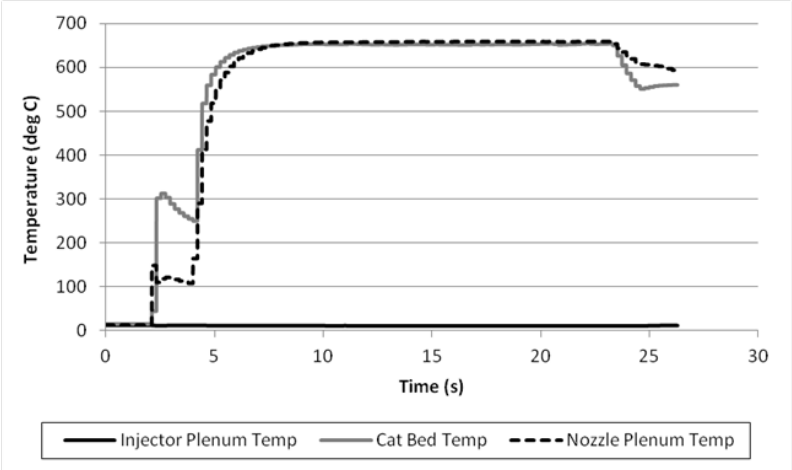

Figure 9-28: C-1-MnCe-540-200P temperature profiles

As a result of the higher nozzle plenum temperature the overall performance of the thruster is improved. The thrust is seen to peak at 19.9N, the highest of any run, before reducing slightly to a steady state of 19.0N; when combined with a measured mass flow rate of 17.9g/s the resultant

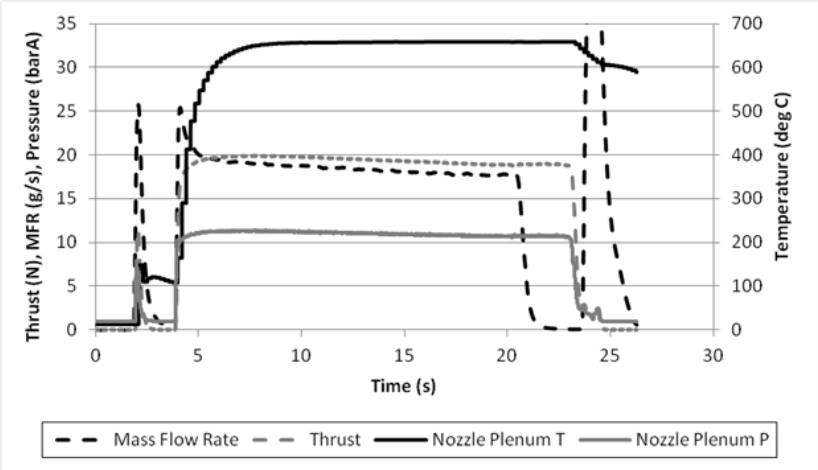

Figure 9-29: C-1-MnCe-540-200P steady state parameters

I_{SP} is 108.6s. The characteristic velocity, based on steady state pressure, is 877m/s with a C* efficiency of 97.3%. The pressure roughness is also low at only 4.4%; however, the pressure drop is significantly larger at 7.5bar compared to 5.9bar with MnOx-Ni-2/R. C-1-MnCe-867-NONE was conducted with no pre-heating and as Figure 9-30 shows the performance was even better. The catalyst bed temperature takes slightly longer to respond with a t_{90} value of 1.76s however the pressure responds faster at 0.15s compared to 0.20s when pre-heating was applied. Pressure drop has increased slightly with a steady state value of 8.3bar. When C* and I_{SP} values were calculated they were found to be 112.9s and 928m/s. These were the highest values achieved during any run with a C* efficiency of 102.8%. Although C* efficiencies greater than 100% are clearly unrealistic, this value can be explained by measurement uncertainty described earlier. The result of this uncertainty assessment shows C* values, when based on pressure, have a maximum uncertainty of -4.49% depending on the temperature drift associated with the pressure transducers. This means η_{C^*} could be as low as 98.31% but this is still very high and an indication of excellent catalyst performance.

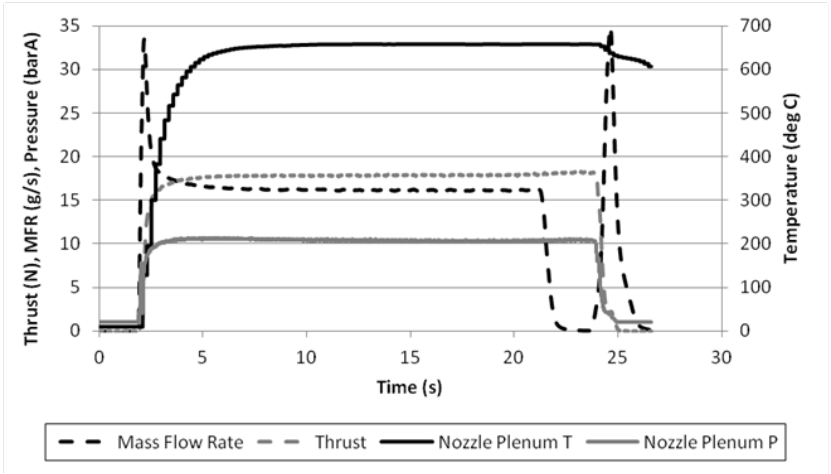

Figure 9-30: C-1-MnCe-867-NONE steady state parameters

Unfortunately MnOx-Ce/U-3 was the only catalyst to show signs of mechanical degradation when removed from the thruster, as shown in Figure 9-31. This is consistent with the increasing

pressure drop over the four runs conducted. As will be discussed in the final chapter it is felt that re-designing the thruster could reduce catalyst degradation.

To summarise, the results from the tests with different catalysts have been separated into two tables: Table 9-16 shows pressure and temperature results, including initial response, and Table 9-17 shows the overall thruster performance in steady state. Both show that MnOx-Ce/U-3 and MnOx-Ni-2/R have significantly outperformed 5%Pt-Al in nearly all areas, with the only exception being the pressure response time, t_{90P}. The reasons for this are unclear as the improved temperature response should have been associated with an improved pressure response.

Figure 9-31: MnOx-Ce/U-3 after runs 23-26

Run Designation	T_{bed} (°C)	T_{noz} (°C)	η_{TH} (%)*	t_{90} (s)*	P_{noz} (barA)	t_{90P} (%)	ΔP (bar)
C-1-PT(I)-3862-250P	196	606	88.1	4.230	10.3	0.110	6.1
C-1-MnNi-317-200P	669	606	98.6	0.615	10.7	0.155	5.9
C-1-MnNi-524-NONE	658	607	97.0	0.970	10.9	0.470	5.7
C-1-MnCe-540-200P	653	659	98.0	1.255	10.8	0.200	7.5
C-1-MnCe-867-NONE	655	657	97.7	1.760	10.3	0.150	8.3

* As measured at either catalyst bed or nozzle plenum location

Table 9-16: Catalyst comparison: temperature and pressure performance

Run Designation	F (N)	I_{SP} (s)	C* (m/s)	η_{C^*} (%)
C-1-PT(I)-3862-250P	14.3	80.3	823	90.7
C-1-MnNi-317-200P	18.0	99.1	842	93.1
C-1-MnNi-524-NONE	17.9	98.3	850	93.9
C-1-MnCe-540-200P	19.0	108.6	877	97.3
C-1-MnCe-867-NONE	17.9	112.8	928	102.8

Table 9-17: Catalyst comparison: Thruster performance

9.4.6 Analysis of minimum impulse bit (MIB)

The final part of this chapter will assess the thrusters' transient performance with each of the three catalyst bed geometries. Part of the operational requirements for a thruster in this thrust range is to perform short, controlled, repeatable pulses. Airbus Defence and Space quote an MIB variability (at a minimum delivery pressure of 5.5barA and pulse duration of 0.05s) of ±12% for their 1N hydrazine thruster [33]. In order to assess the transient performance of the thruster, impulse bit tests were conducted using a series of short pulses varying from 200ms to 30ms in runs 11, 13 and 18. These runs are summarised in Table 9-18 with all using injector C, 5%Pt-Al catalyst and a pulsed pre-heating profile.

Run No.	Cat. Bed Internal volume (cm^3)	$\dot{m}_{S-S}$ (g/s)	CBL_{CSA} ($kg/s/m^2$)
C-1-PT(I)-4517-250P	16.756	17.0	49.1
C-2-PT(II)-170-250P	24.029	17.8	51.4
C-3-PT(I)-2163-250P	16.740	16.5	47.6

Table 9-18: Runs used to assess MIB

The pulses occurred in sets of four with the pulse duration being controlled through LabVIEW; after each of the pulses there was a 1s delay before the next pulse was fired. Between sets of pulses the FCV was left fully open so that the thruster could regain a "steady-state" condition before the next pulse set commenced. The first set of pulses were 200ms in duration, then 100ms, 50ms and finally 30ms. At the lower timescales the FCV is no longer operating within specifications and would not be opened fully. There was no way of avoiding this problem with the resources available. A typical run profile is provided in Figure 9-32.

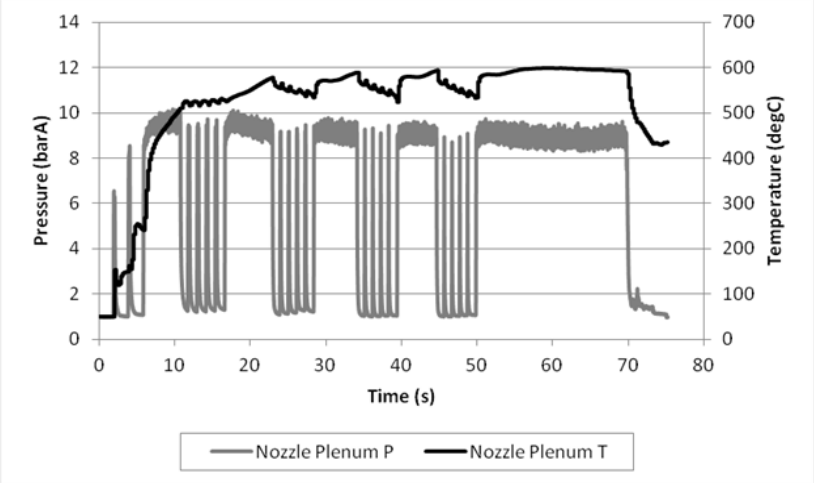

Figure 9-32: C-3-PT(I)-2163-250P nozzle plenum temperature and pressure

The pressure profile shows a slight decrease for reducing pulse width; this is to be expected as the quantity of propellant in the bed decreases with the reduced valve opening time. This also leads to a reduction in thrust generated as shown in Figure 9-33. For pulse widths of 200ms,

100ms and 50ms the thrust generated is consistent over all four pulses. However the 30ms pulses show much greater variation. This is likely associated with the operation of the FCV, which is out of specification for pulses of such short duration.

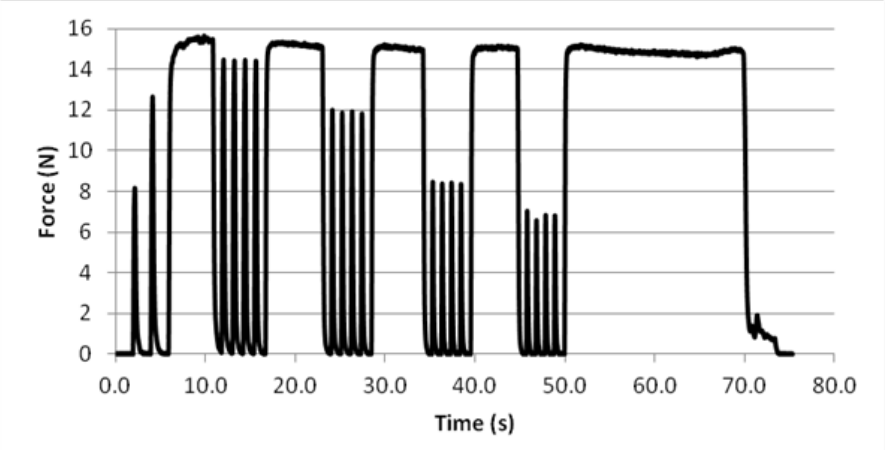

Figure 9-33: C-3-PT(I)-2163-250P thrust profile

A detailed view of the 100ms pulse train in C-3-PT(I)-2163-250P is provided in Figure 9-34 and shows both thrust and nozzle plenum pressure. The delay between the rise in pressure and rise in thrust is similar for all three runs. In this case the delay during thrust rise is 0.06s and during thrust decay is 0.12s. It is unclear how much of this delay is associated with the response time of the load cell and amplifier. It can be seen that there is a high level of consistency between each of the pulses, with a peak thrust of 11.9N ±0.1N. For each pulse the total impulse was calculated. For the four pulses shown in Figure 9-34 the values are as follows; 2.27Ns, 2.19Ns, 2.18Ns and 2.13Ns. The results show good consistency with a difference of only ±3.2%.

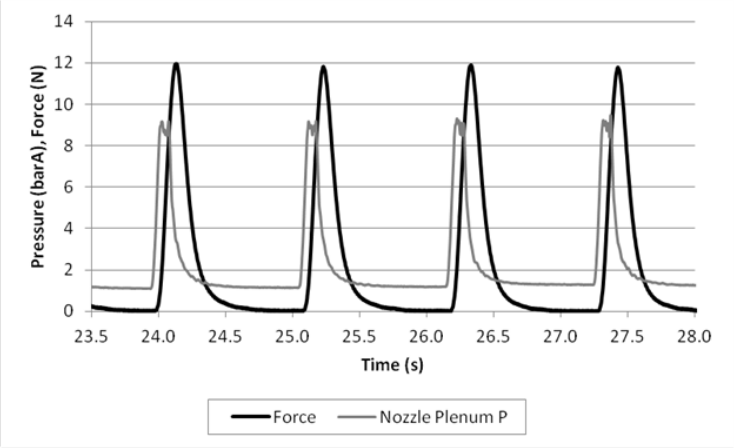

Figure 9-34: C-3-PT(I)-2163-250P thrust and nozzle plenum pressure for 100ms pulses

The three runs chosen to illustrate MIB performance use two different length catalyst beds, giving rise to different internal volumes which may affect both the rise and decay times of the pressure and thrust. Differences in t_{90P} were seen during previous investigations. In order to compare the different beds a single 100ms pulse will be looked at in detail. Figure 9-35 shows the thrust response for the three runs. In all cases the response time is almost identical with thrust starting to increase 70ms after the valve is opened. This is slightly unexpected as it would

be expected that the longer bed (C-2-PT(II)-170-250P) would take longer to fill as had been shown earlier. However the nozzle plenum pressure response is in agreement with the thrust data. Although the pressure in C-2-PT(II)-170-250P does not return to ambient the rise and fall times match the other runs almost exactly. It is unclear why the pressure fails to fully decay while the thrust does, this maybe an indication of instrumentation error or a blocked standpipe but when examined no evidence of this was found.

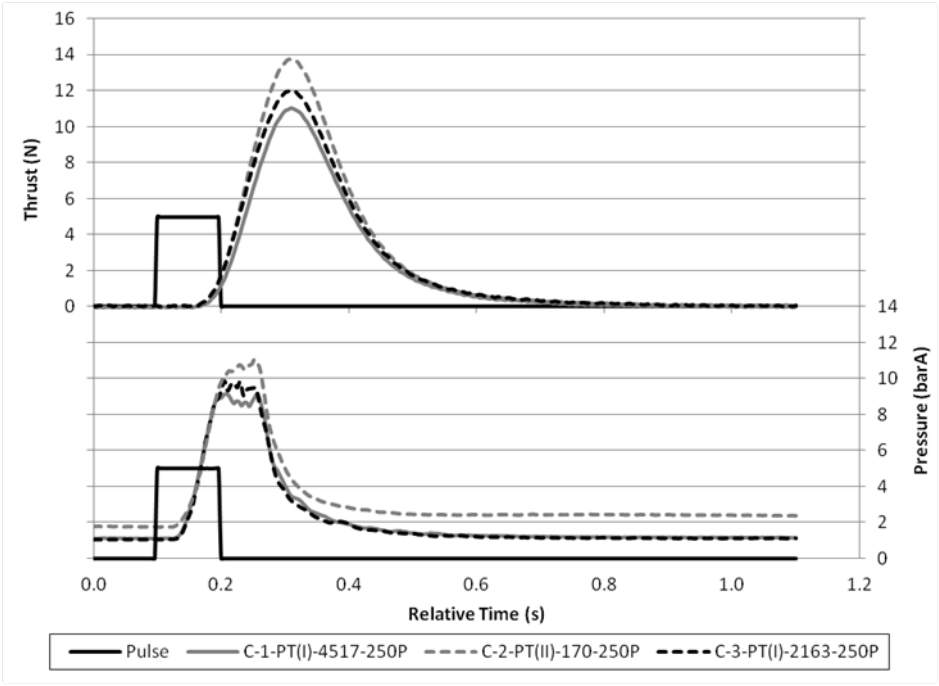

Figure 9-35: Thrust and pressure response for 100ms pulse

The results of this assessment can be found in Table 9-19 which shows MIB, the percentage variability, Δ_{MIB}, and the time to peak thrust, t_{Fmax}, for each pulse width. These data shows that the thruster performed consistently across all pulse widths tested. The greatest variability came with the shortest pulse of 30ms; however, it is unclear how much of this difference is associated with the FCV which was being operated below its minimum opening time. Unexpectedly the response of all beds was nearly identical both in terms of pressure and thrust build-up. Few reasons can be provided for this, with the most likely possibility being an insufficiently high data acquisition rate. It is theorised that although the response times were similar the small differences, in terms of milliseconds, were undetectable at acquisition rates of only 250Hz. C-2-PT(II)-170-250P produced the highest impulse; this is consistent with earlier findings identifying this catalyst bed as producing the highest performance. However, complete decomposition should have occurred in all beds due to the low mass of propellant entering the bed. It is thought the higher impulse values are a direct result of reduced catalyst exposure to propellant. Although catalyst bed 2 had an internal volume 43.5% larger than catalyst bed 1 the catalyst had only been exposed to approximately one-fifth of the propellant at 984g compared to 5240g. As a result there was less catalyst degradation in catalyst bed 2 and so it responded faster generating a higher nozzle plenum pressure and thrust.

Pulse width (ms)	Parameters	C-1-PT(I)-4517-250P	C-2-PT(II)-170-250P	C-3-PT(I)-2163-250P
200	MIB (Ns)	2.76	3.70	3.38
	ΔMIB (%)	±1.64	±5.52	±2.33
	t_{Fman} (s)	0.290	0.288	0.288
100	MIB (Ns)	1.56	2.45	2.20
	ΔMIB (%)	±2.51	±2.07	±3.18
	t_{Fman} (s)	0.210	0.208	0.208
50	MIB (Ns)	0.96	1.52	1.33
	ΔMIB (%)	±7.81	±3.16	±2.86
	t_{Fman} (s)	0.180	0.176	0.180
30	MIB (Ns)	0.74	1.08	1.04
	ΔMIB (%)	±19.24	±8.04	±4.43
	t_{Fman} (s)	0.180	0.172	0.168

Table 9-19: Summary results for comparison of MIB

9.5 Summary

This chapter has covered the development and testing of a 20N sea level thruster in various configurations. The design has been influenced by both proceeding work on the pICB and design values found in appropriate literature. As a result a nominal catalyst bed loading of 50kg/s/m^2 was chosen with particular attention paid to injector geometry and anti-channel baffle location and size. To allow accurate measurements to be taken a test stand was also developed.

The test program attempted to quantify the performance of each of these features as well as assessing the performance of three catalysts; 5%Pt-Al, MnOx-Ce/U-3 and MnOx-Ni-2/R. The majority of work focused on 5%Pt-Al. Although this was not the highest performing catalyst it was more sensitive to thruster design changes. Unfortunately the results were influenced by catalyst degradation due to HTP exposure. The catalyst was exposed to a total of 8.195kg of propellant; more than three times that of the hICB and therefore consistent catalyst performance could not be guaranteed.

The results have shown that improving propellant distribution at the injector improves performance and leads to a more homogenous nozzle plenum temperature. The same can be said of increasing the anti-channel baffle height within the bed, although this did increase the pressure drop measured across the catalyst bed. Increasing the overall catalyst bed length improved performance and although it was thought this would affect minimum impulse bit there is little data to support this. Pre-heating was identified as important especially with a partially exhausted catalyst. Pulsed pre-heating was shown to be most effective but for commercial

applications it is unlikely to be suitable due to the additional propellant consumption and inconsistent thrust profile. Finally it was found that thruster performance was significantly improved using either MnOx-Ce/U-3 or MnOx-Ni-2/R compared with 5%Pt-Al, although thermal losses disproportionally affected MnOx-Ni-2/R.

10 Post Testing Characterisation

After successful testing within the hICB and EBB thrusters the catalysts were subject to further characterisation. Three catalysts MnO_x-Ce/U-3, MnO_x-Ni-2/R and 5%Pt-Al were sampled after testing within the EBB thruster with the fourth, Ag-Gz-20 sampled after hICB testing. Ag-Gz-20 has been included in the characterisation for comparison.

10.1 Silver Gauze (Ag-Gz-20)

Silver gauze was assessed within the hICB to act as a baseline comparison for the other catalysts tested. The goal of this work is to identify catalysts with similar or improved catalytic properties compared to silver but which can be used with hydrogen peroxide concentrations exceeding 95wt%. In total Ag-Gz-20 was exposed to 2744 grams of HTP with analysis being conducted on gauzes taken from the first 10% of the catalyst bed. The silver catalyst has not been subject to pre-treatment which has been identified as improving performance [63,65,66]. Previous work [7,73,100] has shown that silver can be poisoned or dissolved by HTP. This has been associated with the use of stabilisers required to minimise accidental decomposition by contaminants.

EDX analysis was conducted to identify the presence of stabilisers on the surface of the silver. Figure 10-1 and

Table 10-1 show that no evidence of these contaminants can be found but there was evidence that the silver had been oxidised. The EDX results show the presence of oxygen, and macroscope images show a darkening of the silver consistent with the formation of silver oxide as can be seen in Figure 10-2.

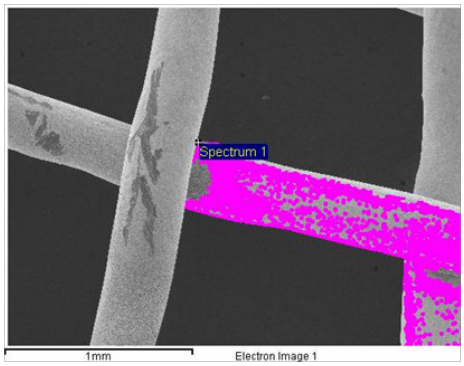

Figure 10-1: EDX image for post-test Ag-Gz-20 (x50)

Spectrum	O	Ag	C
1	13.43	78.96	7.60

Table 10-1: EDX results showing elements by %weight

Macroscope images also show evidence of silver degradation. The circled sections of the image shown in Figure 10-2 indicate a thinning of the silver wire used to make up the gauze, consistent with the silver being dissolved. These effects have been noted by other authors [7] assessing catalyst bed performance. The image also shows areas of damage where the gauze has broken; qualitative assessment indicated a reduction of structural integrity compared to the unexposed silver gauze shown in Figure 10-3.

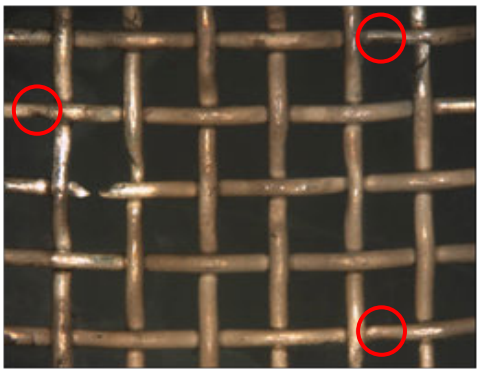

Figure 10-2: Post-test Ag-Gz-20 (x10)

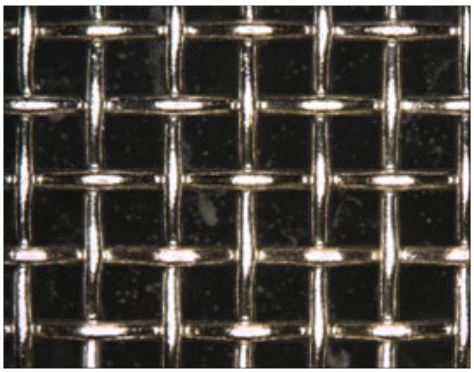

Figure 10-3: Untested Ag-Gz-20 (x10)

It was noted during testing that the silver improved in performance over time. This has been referred to as “activation” by several authors [63,76,77]. SEM images of the gauze show that this may be due to an increase in surface area caused by contact with the HTP. Figure 10-4 shows a high magnification image of the gauze before and after testing. It can be seen that the surface roughness, and therefore contact area has been significantly increased by prolonged contact with the peroxide. This can be replicated by various surface treatments which roughen the surface before exposure to HTP thus negating the need to ‘activate’ the catalyst.

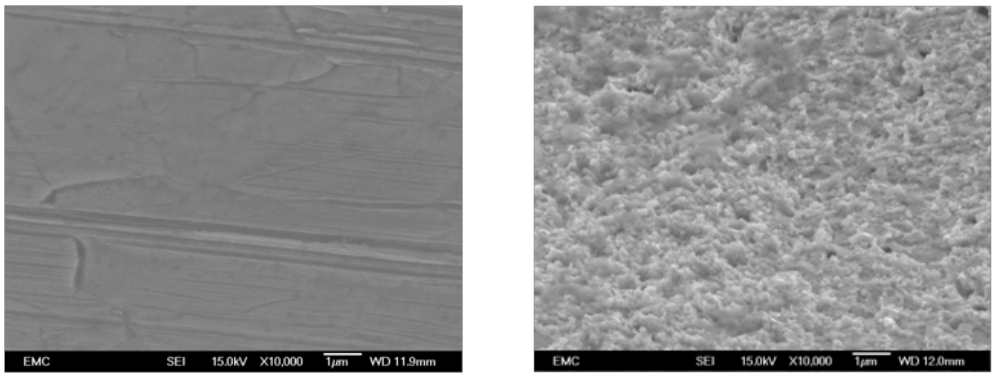

Figure 10-4: SEM images (x10,000) untested Ag-Gz-20 (Left) and post-test Ag-Gz-20 (Right)

The results of this analysis have shown that silver gauze is affected by contact with HTP even at decomposition temperatures below its melting point. Although no contamination was identified changes to both structural integrity and surface topology were seen. However, it is likely this contact has improved the performance of silver gauze by increasing its surface area but at the expense of its lifetime.

10.2 Mn_xO_y on ceria (MnO_x-Ce/U-3)

This catalyst was assessed experimentally within the EBB thruster, being exposed to a total of 1049 grams of HTP. Upon removal from the bed it was evident that some catalyst failure had occurred. Figure 10-5 shows the extracted catalyst; particles of broken catalyst are clearly identifiable. At the end of the catalyst bed, upstream of the retainer plate, there is a retaining disc of nickel foam, shown in Figure 10-6. This has been partially blocked by particles of damaged catalyst transported downstream. The material build-up has occurred where the flow is blocked by the downstream retainer plate. Although some catalyst failure has occurred no significant decrease in performance was seen. An increase in pressure roughness from 4.13% to 5.36% was noted. However, there was some run-to-run variation with this value so this cannot be solely attributed to catalyst failure and increasing void fraction.

Figure 10-5: Extracted MnOx-Ce/U-3

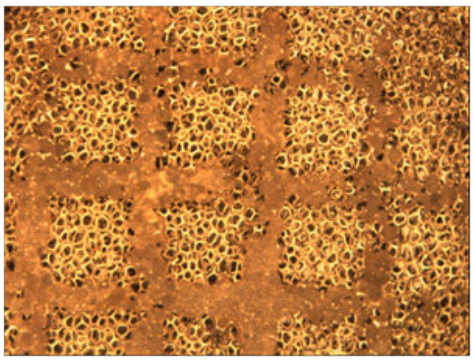

Figure 10-6: Retaining metal mesh (x6.3)

When assessed, EDX analysis showed no presence of contaminants but it was not possible to determine whether the percentage loading had changed. BET surface area measurements revealed a decrease in surface area from 37 to 31m^2/g suggesting some of the pores had been damaged. Surface abrasion is visible in Figure 10-7 and is consistent with the catalyst moving around and impacting itself within the bed. The abrasion has removed the outer layer of active phase revealing the lighter coloured support beneath.

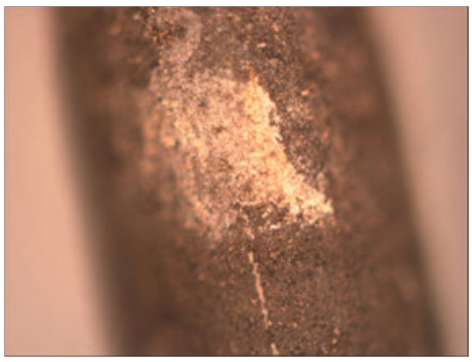

Figure 10-7: Post-test damage of MnOx-Ce/U-3

SEM images also show evidence of surface abrasion with a visible reduction in surface roughness. Internally there is no visual change in the structure of the catalyst. These findings are consistent with the reduction in BET surface area.

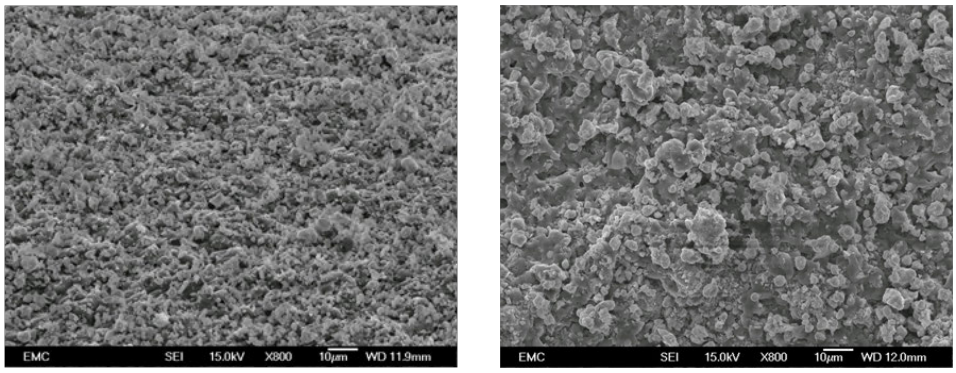

Figure 10-8: SEM images of MnOx-Ce/U-3 before (Left) and after (Right) exposure to HTP (x800)

The results of this assessment have shown catalyst damage has resulted from use within the EBB thruster. Although no definitive statement can be made of the source of this damage it is likely that some pellets failed due to thermal shock or damage caused before installation. This probably resulted in an increase in catalyst bed void fraction meaning the pellets were no longer mechanically locked in position and able to move. As Figure 10-7 and Figure 10-8 show, this led to additional mechanical damage being caused, further increasing the quantity of damaged pellets and exacerbating the problem. Similar damage to pellets has been noted in previous monopropellant thruster work [74,84].

10.3 MnxOy on Nickel Foam (MnOx-Ni-2/R)

This catalyst was exposed to a total of 737 grams of HTP within the EBB thruster. Post test samples have been taken from the upstream and downstream sections of the catalyst bed. The upstream catalyst was taken from directly in front of the injector plate. No visual damage was identified when the catalyst was removed from the thruster. Macroscope images of the catalyst at these two locations can be seen in Figure 10-9. The upstream catalyst has had significant quantities of the active phase removed. This is likely due to the jet of the HTP from the injector removing the active phase from the support. This possibility was identified during initial characterisation where it was noted that the active phase seemed mechanically, rather than chemically, bonded to the support.

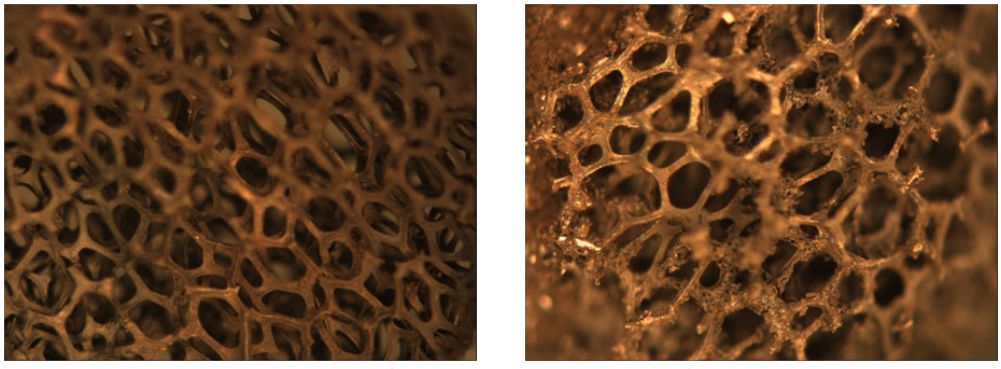

Figure 10-9: Macroscope image of MnO_x-Ni-2/R upstream (Left) and downstream (Right)

This is supported by EDX analysis which showed a reduction in the manganese content on the surface of the catalyst shown in Figure 10-10 and Table 10-2. However considerable quantities of manganese remain.

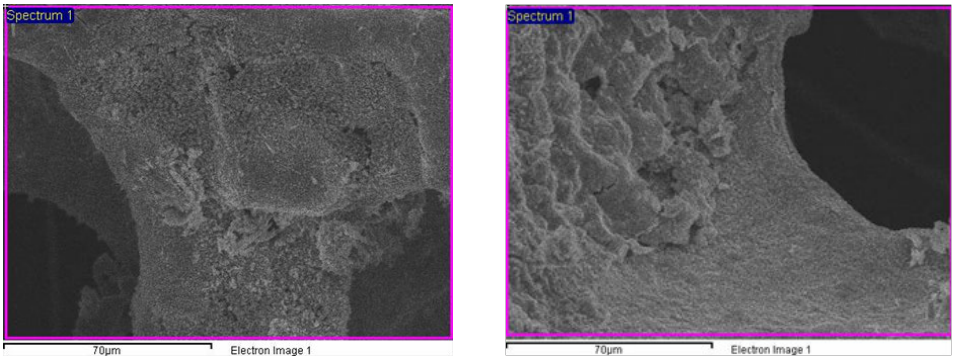

Figure 10-10: EDX image of MnO_x-Ni-2/R before (Left) and after (Right) exposure

MnO_x-Ni-2/R	**Elements (wt%)**			
	O	**Na**	**Mn**	**Ni**
Before Exposure	25.76	15.39	42.76	16.09
After Exposure	31.03	19.76	30.19	19.02

Table 10-2: EDX analysis of MnO_x-Ni-2/R before and after exposure

SEM Images of the catalyst identified the formation of unknown crystalline structures after exposure. Under the microscope these looked silver/white in colour, both images can be found in Figure 10-11. Point analysis by EDX (Figure 10-12) suggests these are formations of sodium oxide due to the presence of only sodium and oxygen. It is not understood why these formed however they only formed on the upstream sample; the downstream sample remain unchanged. Sodium is present in the precursor solution, sodium permanganate, and in the peroxide itself, in the form of sodium nitrate (12.0 – 20.0mg/l).

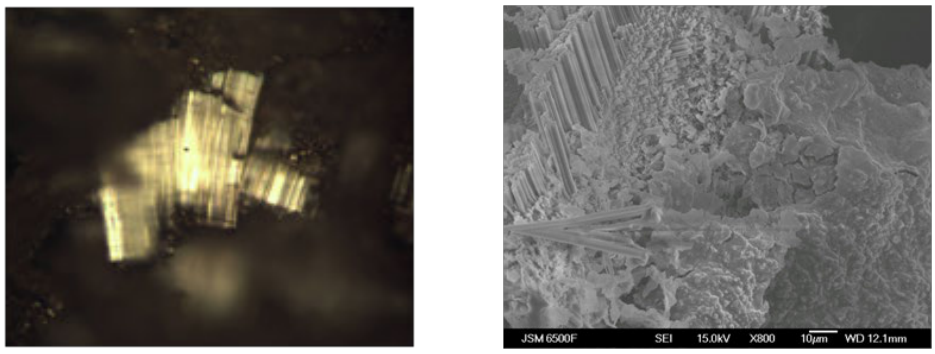

Figure 10-11: Microscope (Left) and SEM (Right) images of MnO_x-Ni-2/R crystalline formations

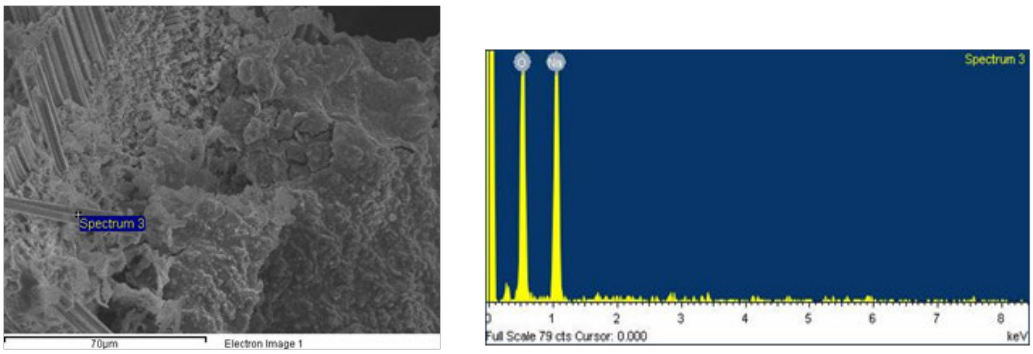

Figure 10-12: EDX Spectrum of crystalline formations on MnO_x-Ni-2/R

The analysis has shown some catalyst degradation as a result of exposure. Although no structural failure occurred some of the active phase on the upstream catalyst was removed. This was predicted by earlier characterisation which had suggested a poor attachment between the active phase and the support.

10.4 5% Platinum on Alumina (5%Pt-Al)

The final catalyst had been procured so was not subject to characterisation before being tested. At the time the catalyst was characterised it had been exposed to a total of 6238 grams of HTP. There was some indication of structural failure with a small percentage of the pellets having split. Unlike MnO_x-Ce/U-3, no disintegration of the support was identified when the material was removed from the catalyst bed. Figure 10-13 shows macroscopic images of the catalyst before and after testing; the post-test sample was removed from the upstream portion of the bed but the precise location is unknown. EDX analysis did not reveal the presence of any contaminants.

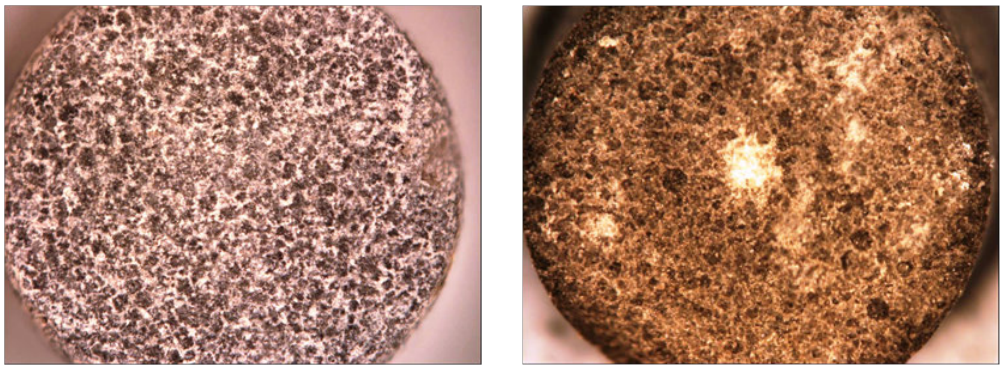

Figure 10-13: Microscope image of 5%Pt-Al before (Left) and after (Right) exposure

The surface area was measured and found to have reduced slightly from 92 to 88m^2/g indicating some damage may have occurred. This reduction in surface area is supported by SEM images of the catalyst. As can be seen from Figure 10-14 there seems to have significant surface abrasion similar to that of MnO_x-Ce/U-3. No other damage was observed.

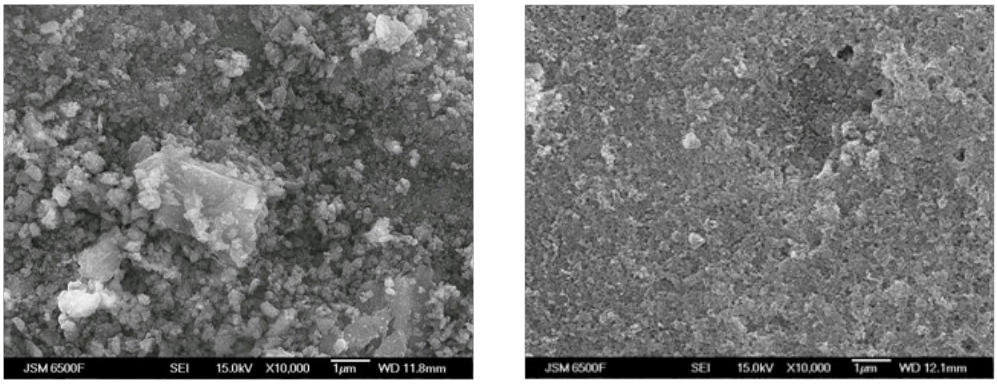

Figure 10-14: SEM image of 5%Pt-Al before (Left) and after (Right) exposure

The results indicate that 5%Pt-Al performed well structurally with little change in the surface area. Visually there was also no significant reduction in the active phase.

10.5 Post-Testing Characterisation Summary

The analysis shows that all the catalysts tested suffered varying degrees of damage with 5%Pt-Al suffering least. However, when characterisation was conducted 5%Pt-Al had only been used within pre-heated catalyst beds either using an external heater or pulses of HTP. Both MnO_x-Ni-2/R and MnO_x-Ce/U-3 had been subjected to cold-starts (i.e. no pre-heating). This means 5%Pt-Al received less thermal shock and may explain the decrease in damage seen, even so it had the greatest throughput of HTP.

Silver gauze, used as a baseline comparator, showed signs of degradation. The results gathered help explain how this degradation may have actually improved performance and provides a better understanding of the need to 'activate' the catalyst. Only MnO_x-Ce/U-3 showed appreciable signs of structural failure; however this did not significantly affect performance and it is believed that, with appropriate thruster design modifications discussed in Chapter 11, the damage to the catalyst can be partially mitigated.

The performance of all the catalysts was excellent with no significant degradation over time. The space industry accepts that some catalyst degradation is to be expected as long as it does not considerably affect end of life performance. Catalyst loss in hydrazine thrusters can be appreciable approaching 40% at the end of an extended qualification program [31,84]. However void fractions in production hydrazine thrusters tend to vary between 2.5% and 6.3% [32,101] at end of qualified life. It is for these reasons that none of the catalysts tested should be excluded from future assessment.

11 Conclusions and Recommendations

This final chapter summarises the results of the project and provides recommendations for the direction of future research. This chapter also provides information on the contribution of this work to the application of hydrogen peroxide within the space community.

11.1 Project Summary

This work started by providing a brief history of hydrogen peroxide and its application within space propulsion. It was seen that after extensive early use it was gradually replaced by other propellants which could achieve higher performance, with its main competitor being hydrazine and its derivatives. However with the ever increasing restrictions on handling and storage, the costs associated with these propellants have increased significantly. This can disproportionately affect small, low cost satellite providers. This in combination with the recent REACH guidelines which listed hydrazine of a substance of very high concern has led to a renewed interest in 'green' or low toxicity propellants. Hydrogen peroxide (HTP) is one such propellant. The space industry is negatively biased towards HTP due to incidents and challenges in its storage faced during the early years of space propulsion. However, with improved production standards and safe handling these concerns may well be misplaced. An initial storability assessment conducted as part of this work has shown that HTP can be safely stored for extended periods of time without self-decomposition. The GRASP project was set-up to further investigate green propellants and provide a groundwork for future development. The current project has been supported by, and provided support for, this program.

Chapters 3 and 4 undertook a detailed literature review of currently used catalysts and test processes. The focus was limited to metallic gauze, ceramic supported and metallic foam type catalysts. From this research a range of active phases were identified for further investigation which led to the development of catalysts based on various support type and active phase combinations. The literature also showed the wide range of methods used to assess catalysts, these tended to follow either a 'chemical' or 'engineering' approach. The various merits of both these approaches have been discussed, with authors often using a combination of these techniques. As a result it was decided to conduct preliminary testing using laboratory hardware with the highest performing catalysts being subject to resource intensive catalyst bed testing. An overview of the research methodology is provided in chapter 1.

Chapter 5 provided details on the design of four pieces of apparatus; two pieces of laboratory apparatus and two instrumented catalyst beds. The first piece of laboratory apparatus, the sealed

reactor (SR) was used to assess initial performance by impulsively introducing $3cm^3$ of HTP into a sealed vessel containing the catalyst sample. Performance was determined by measuring rate of change of both temperature and pressure. The second piece of laboratory apparatus, the life-time mass loss (LTML) experiment, assessed extended exposure of the catalyst to hydrogen peroxide. A single particle of the catalyst was exposed to 10g of HTP for up to 10 minutes and as the gaseous decomposition products escaped the change in mass was recorded. This was repeated up to a maximum of ten times with the catalyst required to decompose at least 1g during the experiment to progress to the next run. The chapter went on to provide details of two catalyst beds; the preliminary instrumented catalyst bed, pICB, and the highly instrumented catalyst bed, hICB. The pICB has not been discussed in detail since this catalyst bed was only developed to provide design data for the EBB thruster and not assess catalysts. Reviewing the pICB design various improvements were identified, these were incorporated into the hICB. This bed tested the catalyst at bed loadings representative of the EBB thruster but with a significantly increased bed length. At each L/D location axial temperature, radial temperature and pressure were recorded. Unfortunately pressure measurements consistently showed erroneous readings so were rejected from the majority of the analysis. The chapter finished by providing the instrumentation used in each piece of apparatus.

Chapter 6 provided details of the procurement and manufacture of catalysts based on metallic gauze, metallic foam or ceramic pellet support materials. Catalyst characterisation was then used to refine the manufacturing process by modifying impregnation duration, frequency and calcination temperature. This resulted in the production of 38 catalyst combinations. Analysis showed, as expected, that increasing active phase content reduced surface area; however this did not necessarily correlate to improved performance. It was theorised that the surface distribution of catalyst was more important than overall catalyst loading. The results of the catalyst assessment conducted in chapters 7 and 8 supported the findings of the catalyst characterisation.

Chapter 7 presented the results for the laboratory assessment which was used to down-select the catalysts before testing within the hICB and EBB thruster. The sealed reactor was used to reject catalysts which showed either poor initial performance or structural weaknesses. The apparatus was shown to produce consistent and repeatable results. Low performing catalysts were easily identified and rejected; however the performance of the best catalysts were similar. Catalysts which showed good performance were then tested within the LTML apparatus. As well as assessing catalyst performance, structural integrity was also investigated. Unfortunately due to the small sample of catalyst used there was significant variability in the results although conclusions regarding comparative performance could still be drawn. A combination of SR and LTML results were used to down-select the 38 catalysts to a final selection of four; Ag-Gz-20, 5%Pt-Al, MnOx-Ce/U-3 and MnOx-Ni-2/R.

Chapter 8 provided the results from both the pICB and hICB, but with the majority of the chapter dedicated to the hICB. Two catalysts were tested within the pICB; 0.5%Pt-Al and Ag-Gz-20. The results gave likely locations of the decomposition plane and were used to define bed length and anti-channel baffle location within the EBB thruster. All four catalysts were tested within the hICB with the total throughput for each catalyst varying between 2.36kg and 2.68kg. No significant degradation in performance was noted with any of the catalysts although both 5%Pt-Al and MnOx-Ni-2/R suffered heavily from channelling along the walls of the bed. Inversely the temperature profiles of silver indicated that flow was preferentially flowing along the axis, suppressing the axial temperature but allowing the radial temperature to increase. The final catalyst, MnOx-Ce/U-3, showed consistently high radial and axial temperatures indicative of little or no channelling and was also the only catalyst to show continuing improvement over the 18 runs conducted. This chapter concluded that all the down-selected catalysts would provide good performance within the EBB thruster.

The culmination of this work was the development and testing of a 20N (sea-level) engineering bread-board (EBB) thruster. Chapter 9 provided an in-depth review of the design process with the aim of assessing different mechanical components such as injector geometry, bed geometry and anti-channel baffle geometry. In addition the effect of pre-heating methodology and temperature were also assessed. The results showed that performance was improved by either improving HTP distribution at the injector, increasing baffle height or increasing bed length. As had been shown with the hICB, performance improved significantly when 5%Pt-Al was replaced with either MnOx-Ni-2/R or MnOx-Ce/U-3. It was also found the thruster could be successfully started with no form of pre-heating with the latter two catalysts. When pre-heating was used, pulsing with HTP was found to be more effective than electrical heating. 5%Pt-Al was exposed to almost than 8.2kg of propellant, far exceeding that of the hICB. It was noted that performance dropped significantly towards the end of the test program. The consequence of this was a much greater sensitivity to start temperature with the thruster failing to respond properly at pre-heat temperatures below 150°C. The final part of the assessment was a review of transient performance in the form of minimum impulse bit (MIB) testing. All three catalyst beds were tested but even though their volumes varied greatly the transient performance was almost identical. This was attributed to two factors: firstly the data acquisition rate of 250Hz was probably not high enough to record the small differences in response times. Secondly, in each case the catalyst material had been exposed to significantly different quantities of propellant and it is thought that this affected the catalyst response times regardless of thruster configuration.

After successful testing within the EBB thruster the down-selected catalysts were subject to further characterisation in chapter 10. In all cases some catalyst degradation was identified with 5%Pt-Al showing the least damage. MnOx-Ce/U-3 showed evidence of structural failure while

removal of the active phase was identified with MnOx-Ni-2/R. The characterisation of silver gauze showed that changes in surface topology as a result of HTP exposure can actually improve performance. However, in all cases it was felt that level of degradation was not high enough to reject any of these catalysts from further investigation in the context of future work.

11.2 Contributions to the field

This thesis has developed a range of novel catalysts and assessment techniques which will be summarised below in arbitrary order.

- Three novel catalysts have been identified for use with hydrogen peroxide. Although in some cases variants of these catalysts already exist the combination of substrate, active phase and manufacturing method is unique. The first of these, 5% Pt-Al, was identified by DELTACAT Ltd as being of scientific and commercial interest. Its performance was then investigated extensively by DELTACAT Ltd, using both monopropellant and bipropellant thrusters. The related LTML and hICB work described in this thesis complements this earlier body of knowledge. Hydrogen peroxide thrusters are now being developed by Airbus Defence and Space utilising this catalyst [102]. The second of these is MnOx-Ni-2/R. This catalyst has showed consistently high performance although its high thermal conductivity will require new approaches to thruster design to minimise heat losses. Finally, MnOx-Ce/U-3 has been shown to be a very effective catalyst and its dimensions lend itself to use within small thrusters. This catalyst is currently the subject of further investigation in combination with Surrey Satellite Technology Ltd [103]. Both the MnOx-Ni-2/R and MnOx-Ce/U-3 catalysts demonstrated a good cold-start capability.

- The LTML apparatus is the first piece of equipment, to the author's knowledge, to assess catalyst longevity based on a mass loss technique. The majority of laboratory experimentation assesses performance based on pressure and temperature measurements. Although ripe for improvement this apparatus provides a good indication of longevity by assessing the most challenging regime: initially quenching the catalyst at ambient conditions.

- The hICB is the first time this combination of instrumentation and test program has been used. The original design was based on the work conducted by Blank *et al* [75]; however the addition of both radial and axial temperature measurements has provided a unique insight into channelling and flow processes. This, in combination with a test program based on the work of Tian *et al* [60], has provided great insight into catalyst performance and longevity.

11.3 Improvements and the future…

In this final section improvements to the apparatus and test programs will be suggested. The author will also suggest the direction future research should take to achieve the ultimate goal of replacing, or at least providing a serious competitor to, hydrazine. The improvements described here will focus on catalyst development and experimental apparatus; with the author's limited knowledge in chemical processes it would inappropriate to describe specific improvements within this field which is best left to chemists who have a detailed knowledge of the subject matter.

This thesis has tested a wide range of catalysts with varying active phase, geometries and support structures. Future work should focus on developing catalysts that have shown to perform well in this work. Considerable focus should be placed on the manufacturing method used to produce catalysts based upon manganese oxides. Although some variation in methodology was assessed it is felt that this could be significantly expanded. Much greater variation in the number of impregnations and the concentration of the impregnation solution should be investigated. It is thought that that reducing the viscosity of the solution and increasing impregnation frequency and time may lead to a higher catalyst loading. Alterations in the precursor materials and calcination temperatures may also prove interesting.

The sealed reactor has been used to good effect in down-selecting possible catalysts; however some of its shortcomings are clear. The main area of improvement is decreasing the thermal mass associated with the equipment. Preliminary calculations indicated there would be significant pressure increases within the vessel; these were clearly overestimated. Ideally the volume of this reactor should be reduced and the reaction chamber held within the vessel itself not linked via standpipes. This would result in more sensitive pressure measurements which would respond quicker. The peroxide injection method should be improved such that no gas from the injection system enters the vessel; although this can be calibrated out, its influence on the system is unknown. Finally, every effort should be used to ensure intimate reaction between the peroxide and catalyst is maintained throughout the experiment. From the perspective of conducting the experiment the sealed reactor should be redesigned to facilitate quicker turnaround times increasing the number of experiments that can be conducted.

The LTML apparatus suffered from a lack of repeatability for several reasons. Firstly, a single particle of catalyst was insufficient to negate particle to particle variations. Increasing the quantity of catalyst tested would improve this. The experiment should be based on a fixed volume of catalyst as it has already been identified that this is a more important criterion within thruster design than the Euclidian surface area of the catalyst. The result of this would mean increasing the quantity, or reducing the concentration, of hydrogen peroxide used. This would

be necessary to ensure the experiment does not reach completion too quickly. It may also be prudent to increase the number of runs conducted to maximise the lifetime assessment. Another concern was how the catalyst particles moved within the fluid. It was noted that the highly reactive catalysts tended to move on the surface of the HTP, limiting the contact area between the two. Future developments should include a way of weighing down the catalyst sample to ensure consistent contact between catalyst and HTP for the majority of the experiment. Finally an improvement in instrumentation is required. In addition to increasing the temperature acquisition rate a second thermocouple should be included to measure the gas temperature above the decomposing fluid. This would be useful in separating out very reactive catalysts, where the liquid temperature rapidly reached the boiling point of HTP but could go no higher. Due to the increased catalyst volume and therefore reactivity it would also be necessary to improve the response time of the scales or replace these with a load cell.

Although two catalyst beds were developed the hICB was already a redesign and improvement of the pICB, therefore only the hICB will be considered. With the current apparatus few improvements can be made. The most significant change would be to identify and correct the source of the pressure anomalies. If this is related to localised decomposition within the standpipe a mesh may be required at the entrance to the standpipe to ensure no particles of catalyst were able to enter. One major redevelopment would be to convert the hICB into a modular catalyst bed. Each module would have a fixed L/D ratio and three measurement standpipes consistent with the hICB. This would allow not only the bed length to be varied but the introduction of modular sections with anti-channelling baffles. This would allow the location, quantity and geometry of the baffles to be modified quickly and easily. This could also facilitate an increase in instrumentation density. Currently this is limited due to the access required to weld the standpipes. If each module was machined separately this limitation could be removed. Considerable thought would be required on how to seal between the modules; it is envisioned that this may be achievable with soft metallic seals. Instead of each module being flanged the modules could be held together with tie rods connecting the injector to the nozzle. The test program employed seemed appropriate; however it is clear that the number of runs conducted should be increased. Catalyst degradation was identified with 5%Pt-Al after 8kg of propellant had been consumed within the EBB thruster, almost four times that used within the hICB. The test program successfully negated the effect of distance between the flow meter and FCV. However little could be done about the time lag induced by the frequency to voltage converter. It is suggested that the volumetric flow meter be replaced by a Coriolis flow meter which would give direct measurements of mass flow rates. For the hICB a better solution would be to implement a mass flow controller. Maintaining a consistent mass flow rate by tuning the delivery pressure is a challenging and time consuming process. For catalyst comparisons a

consistent bed loading is required and this is best achieved by controlling the flow rate into the bed.

The final piece of apparatus to be reviewed is the EBB thruster. The thruster itself allowed a wide range of comparisons to be undertaken; however some improvements can be identified, mainly with the test program. The first design change noted for the thruster is an adjustment to the nozzle pressure tap. There was a concern that the tortuous route to the pressure transducer may influence the apparent pressure response time of the thruster however it is unclear from the results whether this was the case. If the nozzle included a small settling chamber the tap could be inserted perpendicular to the flow, this may also improve the temperature distribution in the nozzle plenum. One of the areas which should be assessed is variation in bed diameter while maintaining constant volume. This can improve packing density and influence factors such as chugging [49,104]. The main improvement would be to construct a thruster with a completely welded downstream end, thus minimising thermal losses. However care would have to be taken that catalyst could still be inserted and removed easily. The test program needs to be modified considerably. Electrical pre-heating should be used throughout to provide a consistent heating profile. The run length should be fixed and then run stopped with propellant remaining in the delivery tank to avoid problems with mass flow rate measurements reducing before the end of the run. If variations in design are to be assessed in future the catalyst charge should be changed regularly to ensure consistent catalyst performance. In the longer term, when the design has been finalised and tested at sea level conditions, vacuum testing should be conducted.

The current work is just the first step in developing a viable satellite propulsion system. A significant quantity of research around the world has been conducted on catalyst and thruster development. However a thruster is merely one component of a propulsion system. Very little focus has been placed on developing viable tanks or valves for use with HTP. One of the greatest concerns is the lack of a definitive study on HTP storability. Although there is much here-say and conjecture both for and against HTP as a storable propellant no-one has taken the lead on fully investigating this. The current work has provided some details on storability and has given the author confidence that HTP is a storable propellant. However, until the space community can be shown the HTP is storable over extended periods of time they will never be prepared to use it. Without this study in the author's opinion all other HTP research is redundant and this must be, without doubt, the next step in hydrogen peroxide development. After it has been shown to be storable, by an independent party in accordance with a program backed by the industry, then tanks and values must be developed and qualified. Catalyst and thruster technology is already at TRL 3-4 and with minimal effort this can be increased to 6-7. However the peripheral equipment required is much further away from a flight ready status.

Appendix A Gauze Calculations

This section will calculate gauze density, approximate free volume and approximate surface area. The first step is to select a small area from this point forward referred to as (δs) from the overall gauze as shown in diagrams below:

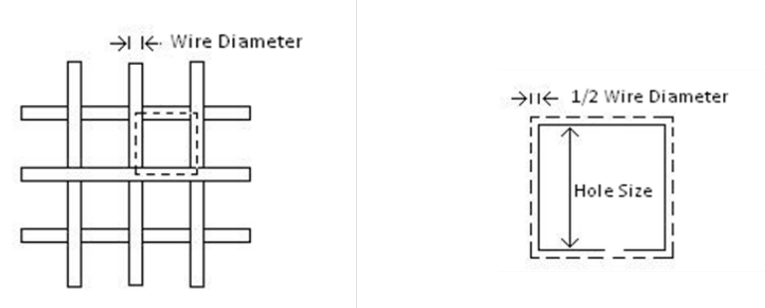

Figure A-1: Gauze Schematic

$$l_s = w_s = (Hs + D_w)$$

Where Hs is the hole size (the hole is also square) and D_w is the wire diameter.
The wire weaves above and below the other wires as shown in the diagram below. The depth (d_s) of the section is given by:

$$d_s = (2 \cdot D_w) \qquad \text{(Eq. A-1)}$$

Figure A-2: Gauze Cross Section

The cross section of the wire needs to be calculated, the cross section looks similar to that shown below. Several assumptions have been made, the major one being that the curvature of the wire due to the weave has not been accounted for. However, the wire is accounted for twice at each corner this is because the wire does weave over itself at the corners.

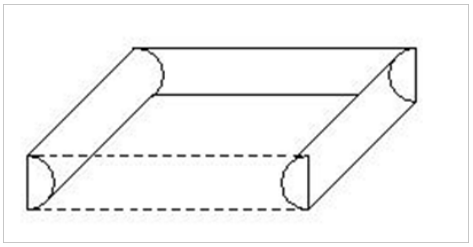

Figure A-3: Gauze wire cross-section

Gauze density calculations:

First, the cross sectional area (CS_w) of the wire is calculated using:

$$CS_w = \frac{\pi \cdot {D_w}^2}{4} \qquad \text{(Eq. A-2)}$$

However, the wire on each side of the section represents only half the total wire cross section (each wire is cut in half; $1/2 \cdot CS_w$).

The wire volume ,δV_w, for the section can then be calculated by multiplying the wire cross section by the length of the four sides. This accounts for the fact that the wire is double thickness in the corners due to the weave:

$$\delta V_w = \frac{CS_w}{2} \cdot \left((Hs + D_w) \cdot 4\right) \qquad \text{(Eq. A-3)}$$

The total volume of the section, δV_s, also needs to be calculated according to the following equation.

$$\delta V_s = l_s \cdot w_s \cdot d_s = (Hs + D_w)^2 \cdot (D_w \cdot 2) \qquad \text{(Eq. A-4)}$$

From this the volume of wire per cm^3 of packed gauze, v_w, can be calculated:

$$v_w = \left({}^{1}/_{\delta V_s}\right) \cdot \delta V_w \qquad \text{(Eq. A-5)}$$

The density of the metal, ρ_m is then multiplied by the volume of wire per unit volume of gauze to give the gauze density, ρ_g:

$$\rho_g = v_w \cdot \rho_m \qquad \text{(Eq. A-6)}$$

Wire Surface Area Calculation:

This time the circumference of the wire, C_w needs to be calculated using:

$$C_w = \pi \cdot D_w \qquad \text{(Eq. A-7)}$$

However, the wire on each side of the section represents only half the total wire circumference (each wire is cut in half; $1/2 \cdot C_w$).

This then allows the surface area of the wire for the section, δA_w to be calculated using the equation A-8. Again the corners have been counted twice; for an incompressible material this is accurate since the contact between the two wires is infinitesimally small.

$$\delta A_w = \left({}^{1}/_{2} \cdot C_w\right) \cdot \left((Hs + D_w) \cdot 4\right) \quad \text{(Eq. A-8)}$$

The total surface area is now known for the volume of the section. This can then be used to calculate the wire surface area per cm^3 of packed gauze using the following equation:

$$a_w = \left({}^{1}/_{\delta V_s}\right) \cdot \delta A_w \quad \text{(Eq. A-9)}$$

Finally this can be used to give the surface area per gram of gauze, the specific surface area, a_g. This is done by dividing the value calculated in equation A-9 by the gauze density according to:

$$a_g = \frac{a_w}{\rho_g} \quad \text{(Eq. A-10)}$$

Free Volume Calculation:

The free (open area) volume per section, δV_f is the volume of the total section minus the volume of wire:

$$\delta V_f = \delta V_s - \delta V_w \quad \text{(Eq. A-11)}$$

From this the free volume per cm^3 of packed gauze, v_f, can be calculated:

$$v_f = \left({}^{1}/_{\delta V_s}\right) \cdot \delta V_f \quad \text{(Eq. A-12)}$$

This can be used to give the open volume per gram of gauze, the specific open volume, v_o:

$$v_o = \frac{v_f}{\rho_g} \quad \text{(Eq. A-13)}$$

Finally the ratio of free volume to wire volume per cm^3 of packed gauze is given as, $v_f : v_w$

The Mathematical model spreadsheet:

Mesh Parameters

Mesh Size	20	
Resultant Hole size, *Hs* (mm)	0.84	8.4E-2 cm
Wire diameter, D_w (mm)	0.356	3.56E-2 cm
Overall disc diameter, D_d	16. mm	1.6 cm
Overall disc area, a_d	201.06 mm^2	02.011 cm^2
Overall disc volume, V_d	143.156 mm^3	1.43E-1 cm^3

Density Calculation

1/2 · Wire cross section area, CS_w	0.05 mm^2	4.98E-4 cm^2
Wire volume per section, δV_w	0.238 mm^3	2.38E-4 cm^3
Total volume of section, δV_s	1.018 mm^3	1.02E-3 cm^3
Volume of wire per cm^3, v_w	0.234	
Overall volume of wire in disc, V_s	0.033 cm^3	
Wire Material	Silver	
Density (g/cm^3), ρ_m	10.490	
Gauze Density (g/cm^3), ρ_g	2.452	

Surface Area Calculation

1/2 · Wire Circumference, C_w	0.559 mm	0.056 cm
SA of wire (per section), δA_w	2.675 mm^2	2.68E-2 cm^2
SA of wire per cm^3, a_w	26.267 cm^{-1}	
SA of wire per gram, a_g	10.711 cm^2 / g	
Overall SA of disc, A_d	52.814 cm^2	

Free Volume

Free volume per section, δV_f	0.78 mm^3	7.8E-4 cm^3
Free volume per cm^3, v_f	0.766	
Free volume per gram, v_o	0.312 cm^3 / g	
Ratio of free volume : wire volume, per cm^3	3.28 : 1	
Overall free volume per disc, V_o	01.541 cm^3	

Appendix B Market Research

This is a review of the catalytic gauzes that can be purchased from the three largest suppliers of chemicals and chemical apparatus. There are, of course, many more suppliers but these suppliers could be relied on to provide a prompt service and high quality products. The three suppliers mentioned are: Alfa Aesar (a Johnson Matthey Company), Sigma-Aldrich Co. and Fisher Scientific UK Ltd.

The main product lines being investigated are gauzes; however sponges are covered as well. From the report it can be seen that these are probably unsuitable for use in a rocket thruster. The following metals have been investigated: Silver, Palladium, Platinum, Ruthenium and Nickel. These costs were accurate at the time of procurement in November 2009.

Supplier	Metals	Ratio / Purity	Wire Diameter (mm)	Mesh No.	Hole Size, estimated (mm)	Available Sizes (mm)	Cost per sheet (£)
Alfa Aesar	Silver Gauze	99.90%	0.115	80	0.177	25 x 25	34.35
						75 x 75	106.90
						150 x 150	409.85
						300 x 300	1110.70
Alfa Aesar	Silver Gauze	-	0.356	20	0.841	75 x 75	43.90
						150 x 150	112.35
						300 x 300	349.90
Alfa Aesar	Silver Gauze	-	0.0764	50	0.297	75 x 75	128.45
						150 x 150	341.35
						300 x 300	1021.85
Sigma Aldrich	Silver metal filter membrane	99.97%	-	-	0.0002	13	356.50 (100 pack)
Sigma Aldrich	Silver metal filter membrane	99.97%	-	-	0.00045	13	292.00 (100 pack)
Sigma Aldrich	Silver metal filter membrane	99.97%	-	-	0.0008	13	292.00 (100 pack)
Sigma Aldrich	Silver metal filter membrane	99.97%	-	-	0.0012	13	292.00 (100 pack)
Sigma Aldrich	Silver metal filter membrane	99.97%	-	-	0.0030	13	292.00 (100 pack)
Sigma Aldrich	Silver metal filter membrane	99.97%	-	-	0.0050	13	292.00 (100 pack)
Note: Sigma and Fisher also do a range of foils (up to 1mm thick), evaporation slugs, wires and silver on ceramic substrate							

Table B-1: Silver metallic catalyst suppliers

Supplier	Metals	Ratio / Purity	Wire Diameter (mm)	Mesh No.	Hole Size, estimated (mm)	Available Sizes	Cost per sheet (£)
Alfa Aesar	Palladium metal sponge	99.95%		-100 +325	0.149 – 0.044	1 gram	85.65
						5 grams	386.30
						25 grams	1794.40
Fisher Scientific	Palladium Metal Sponge	99.90%				1 gram	46.50
Sigma Aldrich	Palladium metal sponge	99.90%				1 gram	43.00
						5 grams	178.50
Alfa Aesar	Palladium : Nickel gauze	95:5wt%	0.1578mm	50	0.297	75 x 75 mm	266.45
						150 x 150 mm	879.55
Note: Sigma and Fisher also do a range of foils (up to 1mm thick), evaporation slugs, wires and palladium on ceramic substrate							

Table B-2: Palladium metallic catalyst suppliers

[217]

Supplier	Metals	Ratio / Purity	Wire Diameter (mm)	Mesh No.	Hole Size, estimated (mm)	Available Sizes	Cost per sheet (£)
Alfa Aesar	Ruthenium Sponge	99.95%		-20	< 0.841	0.2 grams	16.85
						2 grams	51.15
						10 grams	187.25
						50 grams	698.75
Sigma Aldich	Ruthenium Sponge	99.90%		-100	< 0.149	1 grams	64.60
						5 grams	234.50
Note: Sigma and Fisher also do a range of foils (up to 1mm thick), evaporation slugs, wires and ruthenium on ceramic substrate							

Table B-3: Ruthenium metallic catalyst suppliers

Supplier	Metals	Ratio / Purity	Wire Diameter (mm)	Mesh No.	Hole Size, estimated (mm)	Available Sizes	Cost per sheet (£)
Alfa Aesar	Platinum Gauze	99.90%	0.0762	100	0.149	25 x 25	188.35
						50 x 50	538.25
Alfa Aesar	Platinum Gauze	99.90%	0.198	45	0.354	25 x 25	195.85
						50 x 50	587.45
Alfa Aesar	Platinum Gauze	99.90%	0.100	52	0.280 – 0.297	25 x 25	100.60
						50 x 50	307.10
						75 x 75	416.25
						100 x 100	772.55
Alfa Aesar	Platinum Sponge	99.98%		-60	< 0.250	1 gram	103.40
						5 grams	405.55
Alfa Aesar	Platinum Sponge	99.90%			< 2	1 gram	101.45
						5 grams	391.65
Sigma Aldrich	Platinum Gauze	99.90%		52	0.280 – 0.297	25 x 25	104.50
						50 x 50	318.00
Sigma Aldrich	Platinum Gauze	99.90%		100	0.149	25 x 25	195.00
						50 x 50	558.00
Sigma Aldrich	Platinum Sponge	99.90%				1 gram	105.00
						5 grams	406.00
Note: All three suppliers do a range of foils (up to 1mm thick), evaporation slugs, wires and Fisher focus on platinum on ceramic substrate							

Table B-4**: Platinum metallic catalyst suppliers**

[218]

Supplier	Metals	Ratio / Purity	Wire Diameter (mm)	Mesh No.	Hole Size, estimated (mm)	Available Sizes	Cost per sheet (£)
Alfa Aesar	Nickel Gauze		0.100	100	0.149	75 x 75	40.90
						150 x 150	87.15
						300 x 300	233.30
Alfa Aesar	Nickel Gauze		0.180	20	0.841	850 x 425	112.35
						850 x 850	190.50
Alfa Aesar	Nickel Gauze		0.130	40	0.420	300 x 600	52.25
						600 x 1200	174.45
Alfa Aesar	Nickel Gauze		0.050	50	0.297	75 x 75	23.45
						150 x 150	99.55
						300 x 300	292.15
Alfa Aesar	Nickel Gauze		0.180	60	0.250	75 x 75	29.45
						150 x 150	59.75
						300 x 300	156.25
Alfa Aesar	Nickel : Chromium Gauze	80:20 wt%	0.250	40	0.420	75 x 75	67.10
						150 x 150	178.70
						300 x 300	536.10
Note: Sigma Aldrich and Alfa Aesar also do a range of foils							

Table B-5**: Nickel metallic catalyst suppliers**

Appendix C pICB Conference Paper

Presented at the 47th AIAA Joint Propulsion Conference, July 2011, AIAA 2011-5695 [76]

Experimental Assessment of Heterogeneous Catalysts for the Decomposition of Hydrogen Peroxide

Matthew J. Palmer, Antony J. Musker, Graham T. Roberts
School of Engineering Sciences, University of Southampton, SO17 1BJ, UK

With the increasingly stringent controls being placed on the use of hydrazine and its derivatives, "green" propellants such as hydrogen peroxide are receiving much interest from the space industry. This paper describes the development of an instrumented catalyst bed used to assess the performance and lifetime of catalysts used to promote the decomposition of hydrogen peroxide. The catalyst bed design and preliminary findings are described. Two catalysts have been tested with 87.5% concentration hydrogen peroxide: 0.5% platinum on alumina pellets and silver gauze. The preliminary results show that the 0.5% platinum pellets have a higher performance, achieving a steady state decomposition efficiency of 95.4%, with neither catalyst showing signs of exhaustion.

Introduction

IN recent years low toxicity (or "green") propellants have become increasingly attractive as possible substitutes for hydrazine and its derivatives[1]. Although highly reliable, these latter, toxic propellants have resulted in significant ground handling costs as regulations concerning their use become ever more stringent. Consequently a number of "green" propellants are being investigated as candidate replacements, particularly for small satellite applications where the handling of toxic propellants would be prohibitively expensive[2].

Hydrogen peroxide at high concentration (>80%) is one such low toxicity propellant, with high temperature steam and oxygen being generated upon decomposition. It was successfully used by Helmuth Walter in the 1930's to power both bipropellant and monopropellant rocket engines. In these early years decomposition of the peroxide was achieved using liquid, homogenous catalysts[3]. However, these were quickly replaced by heterogeneous catalyst beds which were identified as being both safer and higher performing than their liquid counterparts[4]. Modern research has therefore mostly focused on developing heterogeneous catalysts which are high performing, reliable and long-lived.

In order to assess catalysts various approaches can be used. Laboratory-based experiments can provide invaluable data on chemical properties and reaction kinetics[5,6].

However, only catalyst beds place the catalyst under realistic operating conditions, assessing both performance and susceptibility of the catalyst to mechanical and thermal shock. Significant testing has been carried out with catalyst beds; however, the location and quantity of instrumentation is often limited, resulting in general catalyst performance rather than specific degradation data[7,8]. One of the few exceptions to this is the work conducted at Purdue University which utilised a catalyst bed much more heavily laden with instrumentation[9].

This paper describes the on-going work to assess a range of viable heterogeneous catalysts within an instrumented catalyst bed using 87.5% concentration hydrogen peroxide. The assessment considers pressure and temperature performance as well as catalyst lifetime and is a continuation of previous laboratory-based assessments[10,11]. This work is one aspect of a wide-ranging study into low toxicity propellants referred to as the GRASP (GReen Advanced Space Propulsion) project[12], which is funded by the European Commission under the FP7 Program.

Instrumented Catalyst Bed Design

The aim of the instrumented catalyst bed (ICB) is to assess the decomposition of hydrogen peroxide on exposure to a range of candidate catalysts. The results will be used to estimate the location of the decomposition plane and the effect of channelling. Channelling is a term associated with the preferential flow of un-decomposed, liquid peroxide along the walls of the catalyst bed. This minimises the contact between the HTP and catalyst material and reduces performance. To test for this, thermocouples were placed near the wall of the catalyst bed, as well as on-axis, to identify radial temperature gradients.

The instrumented catalyst bed shown in Fig. 1 consists of an injection plate, catalyst bed (in which the decomposition occurs), retainer plate and nozzle. The bed is of modular design to facilitate catalyst insertion and extraction, with all major components being made from AISI 316 stainless steel. The flow of peroxide into the bed is controlled by a solenoid valve upstream of the injector plate, with the flow rate being measured by a volumetric flow meter connected to the propellant delivery rig.

The injector is designed to constrain the mass flow rate of peroxide to nominally 3.5 g/s at a delivery pressure of 15 bar. There is an estimated 3 bar drop across the injector plate to prevent unwanted pressure oscillations in the propellant feed system, which is energised by compressed nitrogen. The injector connects to the solenoid valve upstream and has a single 0.5 mm hole at its centre. Sealing between the injector and catalyst bed is provided via a Viton O-ring. The design operating temperature of the catalyst bed is significantly above the safe operating temperature of Viton (200°C); however the flow of liquid peroxide through the injector plate keeps the O-ring below this upper temperature limit. Due to the close proximity of the solenoid valve to the catalyst bed there is a concern that thermal soak-back at the end of the

run could damage the valve. Accordingly a heat sink has been incorporated into the injector design between the injector plate and valve.

The catalyst bed itself has a diameter of 16mm and a length of 104 mm, which leads to a length to diameter ratio (L/D) of 6.5 and a bed loading (based on the cross-sectional area of the bed) of 17.6 kg/s/m^2. This relatively low bed loading value reduces the likelihood of the catalyst becoming quenched as well as extending catalyst life. The L/D of the ICB is significantly larger than that initially required to decompose the incoming hydrogen peroxide. However with prolonged use catalyst performance can drop due to either poisoning or deactivation by some other means, causing the decomposition plane to move towards the chamber exit. The extended length therefore allows data to be collected over an extended period of time during which the catalyst performance might degrade. Nine standpipes are located along the catalyst bed; these can accept either thermocouples or pressure transducers. Details of the instrumentation are provided in the following section. Sealing between the catalyst bed, retainer plate and nozzle was achieved with metal O-rings.

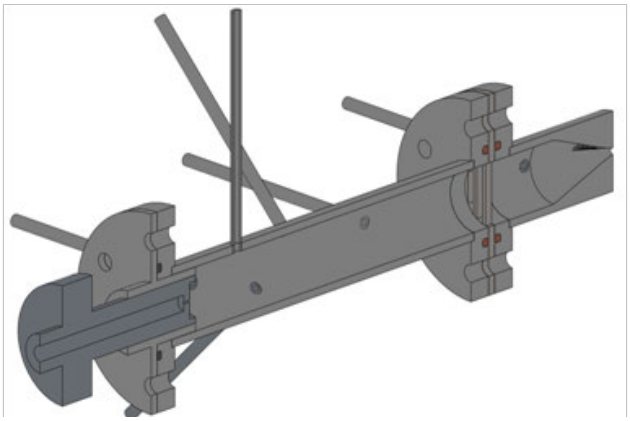

Figure 1. CAD diagram of the completed instrumented catalyst bed

A slot design has been adopted for the retainer plate that maximises the open area ratio whilst limiting the maximum open width to 2 mm. The nozzle for the instrumented catalyst bed is designed only to choke the flow and not to generate thrust. Accordingly the nozzle only contains a converging section culminating in a 1.6mm throat diameter. No attempt has been made to minimise the thermal mass of the catalyst bed and as a result the temperatures measured are expected to be lower than those in a real thruster.

Instrumented Catalyst Bed Instrumentation

In total there are nine standpipes (SP) located along the bed and two in the nozzle, however data are collected only from ten of these in total due to data acquisition limitations. Details of the locations of these standpipes and the instrumentation they contain are provided in Table 1. The temperature is measured both on axis and 2mm from the the bed wall, using 0.5mm stainless steel sheathed k-type thermocouples. The near-wall measurements, assessed at

two points along the bed, are used to give a deeper insight into the effect of channelling by attaining a temperature profile along the wall. The pressure transducers (Gems Sensors 0-25bar) were calibrated prior to use to maximise accuracy. The test stand and the instrumented catalyst bed are shown in Fig. 2

All temperature measurements were acquired using a National Instruments data acquisition system at a sampling rate of 3 Hz. Pressure and mass flow-rate were sampled at either 400 or 500 Hz. The results were recorded using LabVIEW software. This software also controlled the propellant delivery solenoid valve, which was initially pulsed open and closed with a pulse profile of 0.2 seconds open followed by 1.8 seconds closed. This pulsing sequence pre-heated the catalyst bed and was continued until the decomposition was judged to be nearly established, at which time the solenoid valve was left fully open. The criterion used to decide when to stop the pulsing and to open the propellant delivery valve fully was that the maximum observed temperature was greater than 400°C.

Table 1. Standpipe locations

Standpipe #	Instrument	Distance from Injector (mm)
SP1	Pressure transducer	10
SP2	Thermocouple	14
SP3	Thermocouple	21
SP4	Thermocouple	24
SP5	Thermocouple	33
SP6a	Thermocouple	43 (Channelling)
SP6b	Thermocouple	43
SP7	Thermocouple	68 (Channelling)
SP8	Pressure transducer	72
SP9a	Thermocouple	124 (located in the nozzle)

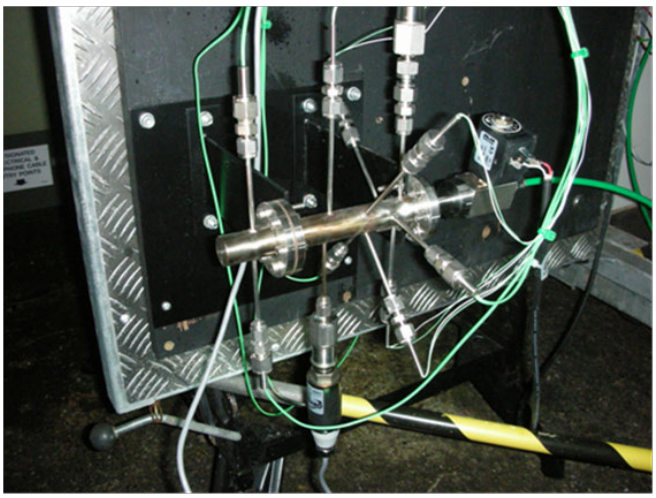

Figure 2. Test stand and instrumented catalyst bed

Results

To date two catalysts have been assessed using the ICB; these are 0.5% platinum on alumina pellets and metallic silver gauze (20 mesh with a wire diameter of 0.356mm). Both of these catalysts have been assessed within laboratory-based test programs and found to possess good catalytic properties[10,11]. The platinum pellets have a 3.2mm diameter and a length between 3.5 and 4mm. In all 401 pellets were placed within the catalyst bed with a single disc of nickel foam being positioned against the injector to help disperse the peroxide. The nickel foam served a secondary role and this was to cushion the pellets as they thermally expanded. This reduced the chance of the pellets structurally failing within the bed. In the case of silver gauze 157 discs were packed into the bed. This resulted in a compression ratio (available space / space required by uncompressed gauzes) of 1.0, i.e. no measurable compression. This was done to avoid damaging the thermocouples; however it is understood that high compression helps to alleviate some of the problems of channelling flows[13]. As a result there is an increased risk of channelling within the bed.

In the case of pellets, four runs were performed; however, due to instrumentation failure and subsequent replacement one of these runs had to be disregarded. The typical results for 0.5% platinum on alumina are presented in Figs. 3 - 5 and demonstrate that satisfactory steady state pressures and temperatures were achieved. The initial heating pulses are clearly identifiable on the pressure trace (Fig. 3), with 8 pulses being required to reach the 400°C target temperature. This amounts to a cumulative mass of peroxide of about 20 grams during the pulsing phase. The pulsing sequence is mirrored in the signal from the mass flow meter (Fig. 4). The mass flow rate associated with the pulses is seen to rise substantially above the final steady-state value. This is undoubtedly due to the fact that the chamber pressure during pulsing is lower than that in steady-state and hence the pressure drop across the injector plate is larger than the design value.

The thermocouple temperatures are plotted in Fig.5. As with the all the thermocouples the temperature closest to the injector (SP2) is seen to rise during the pulsing phase; this is a result of stopping the flow of liquid peroxide into the bed which would otherwise cool the upstream portion of the bed. Once the delivery valve is left open the temperature at SP2 is seen to fall with SP3 and SP4 also showing relatively low temperatures. However the temperature at SP5, located 33mm from the injector, is seen to rise rapidly reaching a steady-state temperature of 633°C, corresponding to a decomposition efficiency of 95.4% when corrected for ambient conditions. This indicates the change to a fully decomposed flow occurs at or just upstream of location SP5 and was a consistent observation with all the pellet runs conducted. Further downstream the temperature is seen to decrease, with SP6b and SP9a recording temperatures of only 500°C .This is most likely due to heat losses to the wall. Meanwhile, the temperatures at locations SP6a and SP7 (both located at the bed wall) are significantly below the asymptotic

value for SP5, indicating either channelling is taking place or, more likely, the effect of wall cooling.

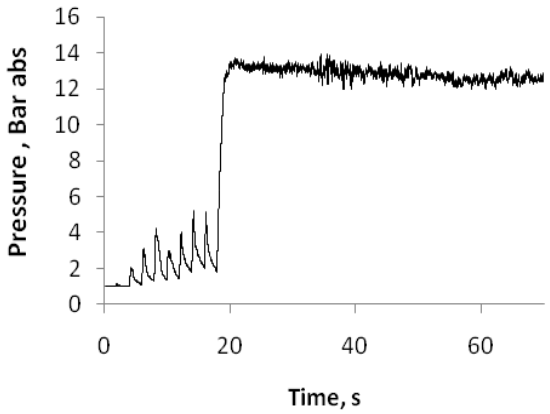

Figure 3. Downstream pressure for 0.5% Pt

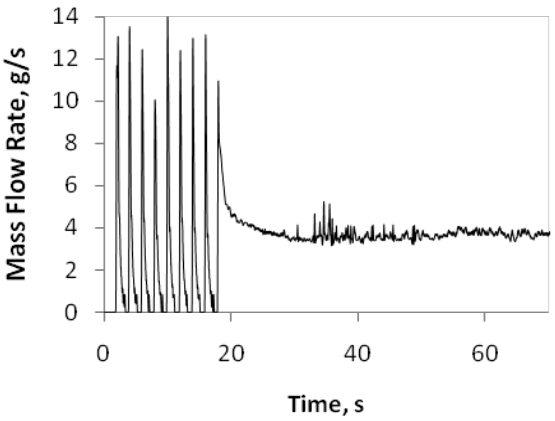

Figure 4. HTP Mass flow rate for 0.5% Pt

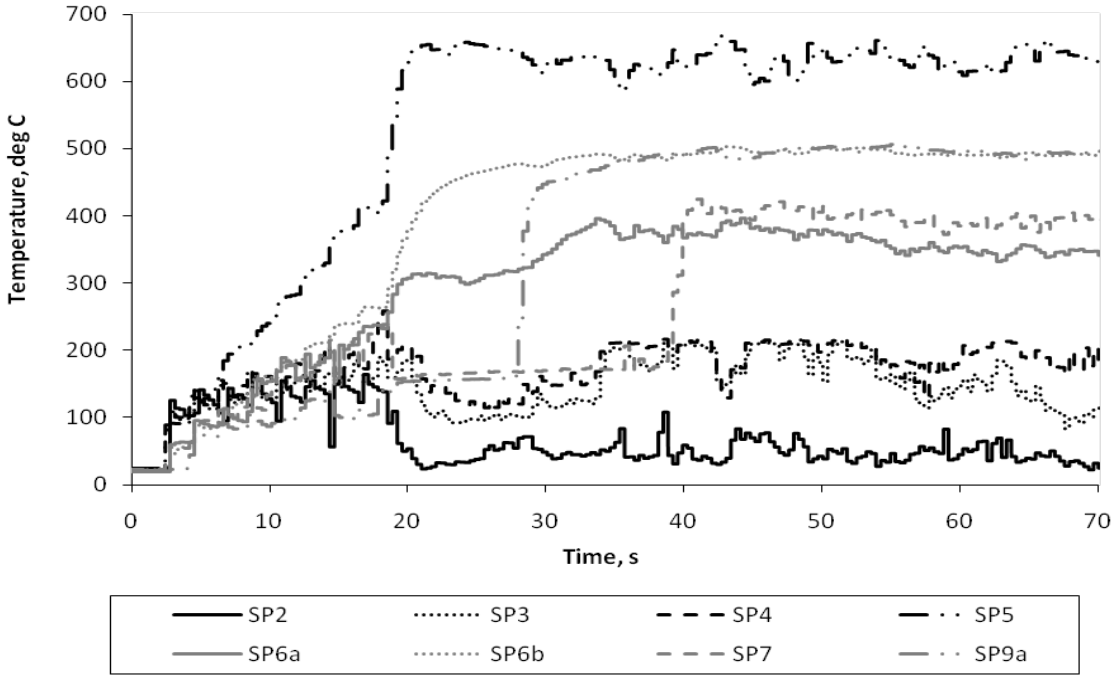

Figure 5. Temperature profiles for 0.5% platinum on alumina

The equivalent results obtained when using the silver gauze catalyst can be found in Figs. 6 - 8; although several runs were conducted, only two runs produced valid data. A low-frequency instability within the bed, typically at about 2 Hz, was observed in the initial runs. Several other authors have detected similar pressure oscillations in their work[14,15]. These runs have not been reported since the significant oscillatory variation in mass flow rate into the bed limited the output of useful data. In an attempt to overcome these oscillations the first fully analysed run, Run 12, was performed with a nitrogen delivery pressure of 19 bar absolute, significantly higher than the design pressure of 15 bar absolute. For this run no pressure oscillations were observed. Run 13 was then conducted at the design delivery pressure and

again no pressure oscillations were detected. The source of these oscillations is under investigation; however. previous authors have attributed the oscillations to the phenomenon of chugging. This is where pressure oscillations build up due to an insufficient pressure drop over the injector, which is not high enough to decouple transient effects in the bed from the upstream propellant supply.

The pressure profiles and peroxide mass flow rate, shown in Fig. 6 and Fig. 7 respectively for Run 13, are very similar to the results gathered for 0.5% platinum on alumina, but with 10 pulses being required to achieve the 400°C start temperature. Compared with the pellet runs, the mass flow rate and pressure signals appear to be significantly less noisy. This is thought to be due to the more homogeneous distribution of silver within the bed compared with the pellets, which adopt an irregular disposition due to the length of each pellet in relation to the bed's diameter. However, the mean steady-state values are similar for both measurements.

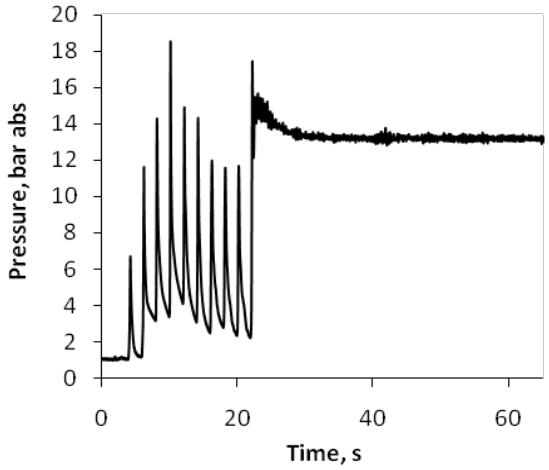

Figure 6. Downstream pressure for silver gauze

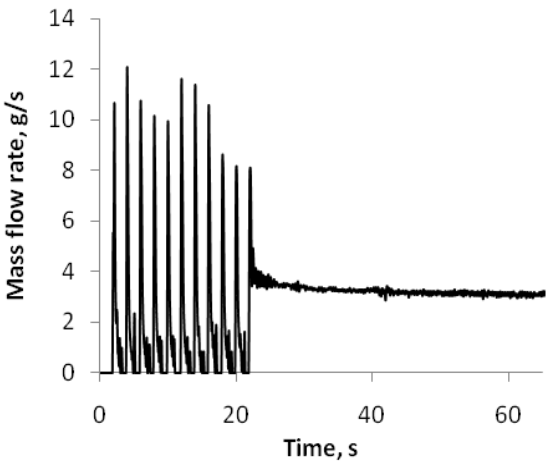

Figure 7. HTP Mass flow rate for silver gauze

The temperature profiles for Run 13 are shown in Fig. 8. As with platinum pellets there is a rise in temperature between SP2 and SP4 after the pulsing phase is completed. However, the temperatures recorded at SP5, SP6a and SP6b are almost 100°C lower than that detected at SP4. Subsequently the temperature rises rapidly, resulting in the thermocouple located at SP7 detecting the peak temperatures of the run before thermal losses lead to a lower temperature at SP9a. This trend was observed in both the silver gauze runs that produced steady-state conditions. Although the reasons for this temperature variation are still not fully understood, it is hypothesised that the thermocouples located at SP4 – 6b are detecting the boiling point of hydrogen peroxide. The decreasing temperature between these points maybe attributed to a reduction in the concentration of the hydrogen peroxide liquid, which would reduce the boiling point of the solution. Currently a mathematical model is being developed which will be used alongside further experiments to validate this hypothesis.

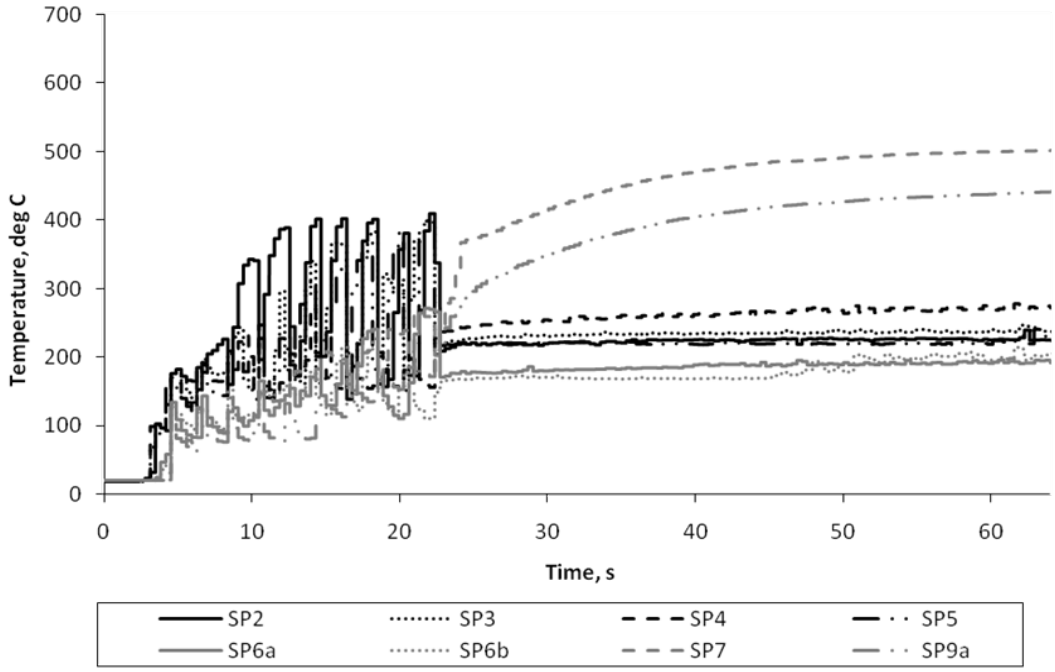

Figure 8. Temperature profiles for silver gauze

Analysis

A summary table of the five successful runs completed to date can be found in Table 2. The table indicates the variable starting conditions, which were unavoidable due to testing in an outdoors environment. These would have had some influence on the peak steady-state temperatures recorded. All steady-state readings were averaged over a four second period. The temperature data were based on the thermocouple showing the highest reading. Although the results have shown some variations in the data collected the summary table shows a good level of consistency between runs. Note that Run 12 was conducted with a higher propellant delivery pressure than the other runs, which resulted in a correspondingly higher propellant mass flow rate and nozzle plenum pressure. From the raw data provided the decomposition efficiency has been calculated. This is defined as the measured steady-state temperature rise in the catalyst bed divided by that predicted by the NASA CEA Code[16].

Table 2. Analysis of instrumented bed results

	0.5% Platinum Pellets			Silver Gauze	
	Run 0	**Run 1**	**Run 3**	**Run 12**	**Run 13**
HTP temperature at start (°C)	5.0	5.0	5.0	17	18
Catalyst nominal start temperature (°C)	7	15	25	18	18
HTP consumed this run (kg)	0.15	0.52	0.26	0.15	0.15
Total HTP consumed prior to this run (kg)	1.0	1.15	1.74	0.45	0.6
Delivery pressure (bar absolute)	15.0	15.3	15.2	19	15
Number of starting pulses	19	11	8	9	10
Number of pulses required to reach 300°C	14	7	6	6	4
Steady-state chamber pressure (bar abs)	12.27	12.54	13.03	16.67	13.21
Steady-state mean temperature (°C)	624	626	633	502	510
Corrected decomposition efficiency % *	94.0	94.3	95.4	73.5	74.5
Steady-state mean flow rate (g/s)	3.62	3.83	3.51	4.14	3.32

* *Ideal performance adjusted for HTP initial temperature*

One parameter the table does not address is the location of the decomposition plane, which can be inferred from the results. A comparison of the two catalysts has been made in Fig. 9, which shows the temperature distribution along the length of the catalyst bed. The measurements indicated with filled points refer to near-wall and not axial measurements. This was done to detect any tendency of the peroxide to channel along the walls of the bed. It can be seen that the peak temperature for pellets is recorded at distance of 33mm from the injector. Meanwhile the peak temperature for the silver gauze is located at 72mm on the wall of the bed in both cases. This suggests that peak activity occurs at an L/D of approximately 2 for pellets but a much greater 4.5 for gauzes; this observation, together with the higher peak temperatures recorded, suggests that the pellet-based catalyst was more effective than the silver gauze, even though the pellets had decomposed almost three times as much peroxide (Run 3) compared to silver gauze (Run 13). However, it is important to note that the Euclidian surface area (that is, excluding the effects of micro-roughness) of the pellets is many times greater than that of the silver gauze, which may partially account for the improved performance.

The graph also provides an indication of how the peroxide is distributed within the bed. Areas of high liquid peroxide loading can be subject to catalyst flooding, thereby limiting the decomposition temperature. Low temperatures can be identified with the pellets near the bed wall at a distance of 43 and 72mm from the injector. This is indicative of either channelling or the cooling effect of the relatively cold chamber wall. As already discussed the results of the silver gauze indicate decomposition is occurring between SP6b and SP 7, with the earlier thermocouples possibly recording the boiling point of the hydrogen peroxide.

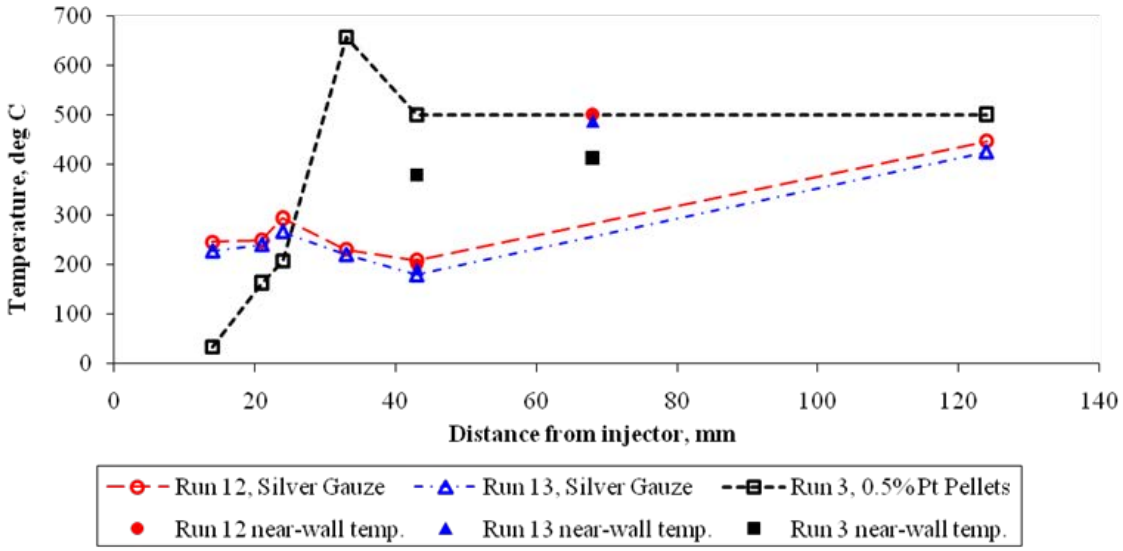

Figure 9. Catalyst bed temperature distributions at t=49s

The peak temperatures and decomposition efficiencies are significantly higher in the case of pellets, being in excess of 620°C and 95%, respectively. This indicates that they had a much greater ability to decompose the peroxide; however they also required more pulses to reach 300°C. During the firings the decision concerning when to leave the solenoid valve open was at the discretion of the operator. The target temperature for opening the valve fully was 400°C; however this varied on a run by run basis. As a result the total number of starting pulses is not considered an appropriate assessment parameter. From the results the number of pulses to reach 300°C provides much more insight. In the case of pellets it can be seen that this number decreased significantly as the bed temperature increased. The variation in pulse number between pellets and gauzes can be partially attributed to the difference in HTP temperature. For this reason care must be taken when drawing conclusions from these results.

Overall Table 2 and Fig. 9 both show pellets have outperformed gauzes under steady-state conditions. Due to the notable differences in the starting conditions it is difficult to make an assessment on the start-up characteristics of the two catalysts. Repeat testing has allowed some conclusions to be drawn on the re-start capability of the catalyst. Both catalysts have shown improved characteristics at re-start which may indicate that their peak performance has yet to be reached.

Conclusions

An instrumented catalyst bed has been developed and used to assess the performance of heterogeneous catalysts for the decomposition of high concentration (87.5%) hydrogen peroxide. The aim of the instrumented catalyst bed is to assess catalysts under realistic operating conditions, to provide data on catalyst lifetime as well as performance. To date two catalysts have been tested, the first of these is 0.5% platinum on alumina pellets and the second, silver

gauze. The preliminary findings have shown that the platinum coated pellets have outperformed the silver gauze, achieving higher decomposition efficiencies in a shorter bed length even after being exposed to almost three times the quantity of peroxide. At this early stage it is difficult to make an assessment of lifetime, but the runs conducted to date indicate an improving performance for both catalysts with total throughput of peroxide, suggesting they may have not yet attained their peak performance.

The next phase of testing will consist of a more structured test program in an attempt to provide quantitative data on catalyst lifetime. To that end a series of short runs will be conducted to assess start up characteristics at near ambient conditions. We consider this to be the most challenging operating regime for any catalyst and is most likely to provide clear evidence of catalyst exhaustion. This should manifest itself as a gradual progression of the location of the peak temperature, corresponding to the phase-change plane, downstream towards the nozzle. This work will be used to provide supplementary data for the design of a monopropellant hydrogen peroxide thruster.

Acknowledgements

The research leading to these results has received funding from the European Community's Seventh Framework Programme (FP7/2007-2013) under grant agreement number 218819.

References

[1]Kappenstein, C. "Contribution to the Green Propulsion Workshop" *Space Propulsion 2008 – Green Propulsion Workshop*, Crete, May 2008.

[2]Wallbank, J.R., Sermon, P.A., Baker, A.M., Courtney, L. and Sambrook, R.M. "Nitrous oxide as a green propellant for small satellites" *2nd International Conference on Green Propellants for Space Propulsion*, Sardinia, June 2004. ESA SP-557.

[3]Development of Hydrogen Peroxide Rockets in Germany, H. Walter found in History Of German Guided Missiles Development Edited by TH. Benecke and A.W. Quick, 1956, The Advisory Group for Aeronautical Research and Development, NATO

[4]Wernimont E.J., "Hydrogen Peroxide Catalyst Beds: Lighter and Better Than Liquid Injectors", *41st AIAA Joint Propulsion Conference*, Arizona, July 2005, AIAA 2005-4455

[5]Russo Sorge, A., Pilone, G., Bagnasco, G., Turco, M. "Decomposition of Hydrogen Peroxide on MnO2/TiO2 Catalysts", *Journal of Propulsion and Power*, Volume 20, Issue 6, pp.1069-1075, 2004

[6]Pirault-Roy, L., Kappenstein, C., Guerin, M., Eloirdi R., Pillet, N., "Hydrogen Peroxide Decomposition on Various Supported Catalysts Effect of Stabilizers" *Journal of Propulsion and Power*, Volume 18, Issue 6, pp.1235-1241, 2002

[7]Tian, H., Zhang, T., Sun, X., Liang, D., Lin. L., "Performance and deactivation of Ir/γ-Al2O3 catalyst in the hydrogen peroxide monopropellant thruster", *Applied Catalysis A: General* 210, 2001, pp.55–62

[8]Pasini, A., Torre, L., Cervone, A., Musker, A., Saccoccia, G., et al "Experimental Characterization of a 5 N Hydrogen Peroxide Monopropellant Thruster Prototype" *43rd AIAA Joint Propulsion Conference*, Cincinnati, July 2007, AIAA 2007-5465

[9]Blank, R.A., Pourpoint, T.L., Meyer, S.E., "Experimental Study of Flow Processes and Performance of a High Pressure Hydrogen Peroxide Catalyst Bed" *43rd AIAA Joint Propulsion Conference*, Cincinnati, July 2007, AIAA 2007-5469

[10]Palmer M.J., Musker A.J., Roberts G.T., Ponce-de-Leon C., "A Method of Ranking Candidate Catalysts for the Decomposition of Hydrogen Peroxide", *Space Propulsion 2010*, San Sebastian, May 2010

[11]Palmer M.J., Musker A.J., Roberts G.T., Ponce-de-Leon C., "A Manufacture, Assessment and Down-Selection of Catalysts for the Decomposition of Hydrogen Peroxide", *EUCASS Conference 2011*, St. Petersburg, July 2011

[12]GRASP - 'Green Advanced Space Propulsion', European Commission 7th Framework Programme, Theme 9, Grant Agreement Number 218819, 2008.

[13]Ponzo, J. "Small Envelope, High Flux 90% Hydrogen Peroxide Catalyst Bed" *39th AIAA Joint Propulsion Conference*, Alabama, July 2003, AIAA 2003-4622

[14]Jonker, W., Mayer, A., Zandbergen, B., "Development of a Rocket Engine Igniter Using the Catalytic Decomposition of Hydrogen Peroxide" *3rd Int. Conf. on Green Propellant for Space Propulsion, 9th Int. Hydrogen Peroxide Propulsion Conference*, Poitiers, 2006, ESA SP-635

[15]Lee, S.-L., Lee, C.-W., "Performance characteristics of silver catalyst bed for hydrogen peroxide" *Aerospace Science and Technology*, volume 13, pp. 12–17, 2009

[16] Gordon, S., McBride, B.J., Computer program for calculation of complex chemical equilibrium compositions, rocket performance, incident and reflected shocks, and Chapman–Jouguet detonations, NASA SP-273, 1971

Appendix D Mathematical Model for the EBB Design

Input variables:

T_{amb}	Ambient temperature	293 K
P_{amb}	Ambient pressure	100000 Pa
P_{tank}	Tank pressure	1700000 Pa
ΔP_i	Pressure drop across the injector	400000 Pa
ΔP_{cat}	Pressure drop across the catalyst bed	100000 Pa
C_{di}	Injector discharge coefficient	0.7
C_{dn}	Nozzle discharge coefficient	0.9
η_{TH}	Catalytic thermal efficiency	0.95
F	Thrust	20 N
$Conc_{HTP}$	HTP concentration	87.5 wt.%
No_i	Number of injector holes	4

Constants:

ρ_{HTP}	Density of HTP	1340 kg/m^3
R	Universal gas constant	8314 J/Kmol*K
g_0	Gravity	9.81 m/s^2

1) Output from NASA CEA code:

T_{ideal}	960.54 K
γ	1.2704
M	21.966 kg/kmol

The change in ideal temperature from ambient conditions can then be calculated as:

$$\Delta T_{ideal} = T_{ideal} - T_{\infty} = 667.390 \text{ K} \quad \text{(Eq. D-1)}$$

With the average molecular mass **M** given the specific gas constant can be calculated:

$$R = \frac{\mathbf{R}}{\mathbf{M}} = 378.49\,\mathrm{J/kg*K} \quad \text{(Eq. D-2)}$$

2) Calculating the chamber conditions at the inlet to the nozzle:

$$T_c = [\Delta T_{ideal} \times \eta_{cat}] + T_\infty = 927.17\ \mathrm{K} \quad \text{(Eq. D-3)}$$

$$P_c = P_{tank} - \Delta P_i - \Delta P_{cat} = 120000\ \mathrm{Pa} \quad \text{(Eq. D-4)}$$

3) Calculating the exit conditions:

- *Assuming the velocity within the decomposition chamber is negligible (*$\mathbf{V}_c \approx 0$*), i.e. the chamber pressure is equal to the total stagnation pressure*
- *Assuming a perfectly expanded nozzle, i.e.* $P_e = P_\infty = 100000$ Pa

Exhaust Mach number:

$$P_c = P_\infty \left[1 + \frac{1}{2}(\gamma - 1){M_e}^2\right]^{\gamma/\gamma-1} \quad \text{(Eq. D-5)}$$

Re-arrange:

$$M_e = \sqrt{\left(\left[\frac{P_c}{P_\infty}\right]^{\frac{\gamma-1}{\gamma}} \times \frac{1}{\frac{1}{2}(\gamma-1)} - 1\right)} = 2.271 \quad \text{(Eq. D-6)}$$

Exhaust velocity:

$$\mathbf{V}_e = \sqrt{\left(\frac{2\gamma}{\gamma-1} \times R \times T_c\left[1 - \left(\frac{P_c}{P_\infty}\right)^{\frac{\gamma-1}{\gamma}}\right]\right)} = 1163.80\ \mathrm{m/s} \quad \text{(Eq. D-7)}$$

Exhaust Temperature:

$$M_e = \frac{\mathbf{V}_e}{\sqrt{\gamma R T_e}} \quad \text{(Eq. D-8)}$$

Re-arrange:

$$T_e = \left[\frac{\mathbf{V}_e}{M_e}\right]^2 \times \frac{1}{\gamma R} = 546.37\ \mathrm{K} \quad \text{(Eq. D-9)}$$

4) Calculate the conditions at the throat

Mass flow rate:

$$\dot{m} = \frac{\mathbf{F}}{\mathbf{V_e}} = 0.01719 \text{ kg/s} \quad \text{(Eq. D-10)}$$

Throat area:

$$A_t = \frac{\dot{m}}{P_c} \times \frac{1}{C_{dn}} \times \sqrt{\frac{RT_c}{\gamma \left(\frac{2}{\gamma+1}\right)^{\gamma+1/\gamma-1}}} = 1.42420x10^{-5} \text{ m}^2 \quad \text{(Eq. D-11)}$$

Throat diameter:

$$d_t = \sqrt{\frac{A_t}{\pi}} \times 2 = 0.004259 \text{ m} \quad \text{(Eq. D-12)}$$

Exit/throat area ratio:

$$\frac{A_t}{A_e} = \left(\frac{\gamma+1}{2}\right)^{\frac{1}{\gamma-1}} \times \left(\frac{P_e}{P_c}\right)^{\frac{1}{\gamma}} \times \sqrt{\left[\frac{\gamma+1}{\gamma-1}\left(1 - \left(\frac{P_e}{P_c}\right)^{\frac{\gamma-1}{\gamma}}\right)\right]} \quad \text{(Eq. D-13)}$$

Therefore

$$\frac{A_e}{A_t} = \frac{1}{A_t/A_e} = 2.3822 \quad \text{(Eq. D-14)}$$

Exit diameter:

$$d_e = \sqrt{\frac{\pi}{A_e}} \times 2 = 0.006572 \text{ m} \quad \text{(Eq. D-15)}$$

Sonic temperature:

$$T_t = \frac{2T_c}{\gamma+1} = 812.60 \text{ K} \quad \text{(Eq. D-16)}$$

Sonic pressure:

$$P_t = \left[\frac{2}{\gamma+1}\right]^{\frac{\gamma}{\gamma-1}} \times P_c = 658802 \text{ Pa} \quad \text{(Eq. D-17)}$$

Sonic velocity:

$$\mathbf{V}_t = \left[\frac{2\gamma}{\gamma+1}\right] \times R \times T_c = 627.92 \text{ m/s} \quad \text{(Eq. D-18)}$$

5) Calculating the injector conditions:

Injector area:

$$\mathrm{Q} = C_{di} \times A_i \times \sqrt{\frac{2\Delta P_i}{\rho_{HTP}}} \quad \text{(Eq. D-19)}$$

Therefore

$$A_i = \frac{\mathrm{Q}}{\mathrm{C_{di}} \times \sqrt{2\Delta P_i / \rho_{HTP}}} \quad \text{(Eq. D-20)}$$

$$\left(\mathrm{Q} = \frac{\dot{\mathrm{m}}}{\rho_{\mathrm{HTP}}}\right) \qquad A_i = \frac{\dot{m}/\rho_{HTP}}{C_{di} \times \sqrt{2\Delta P_i / \rho_{HTP}}} = 7.49817x10^{-7} \text{ m}^2 \quad \text{(Eq. D-21)}$$

Injector diameter:

$$d_i = \sqrt{\frac{A_i}{No_i \text{ x } \pi}} \times 2 = 0.000489 \text{ m} \quad \text{(Eq. D-22)}$$

6) Thruster Performance:

Calculated specific impulse:

$$I_{SP} = \frac{\mathbf{F}}{\dot{m} \times g_0} = 118.63 \text{ s} \quad \text{(Eq. D-23)}$$

7) Model outputs:

Mass flow rate	17.5 g/s
Specific impulse	109.67 s
Chamber temperature	893.3 K
Injector throat diameter	0.49 mm
Nozzle throat diameter	4.26 mm
Nozzle exit diameter	6.58 mm

Bibliography

[1] Jones, C.W., Clark, J. H., *"Applications of Hydrogen Peroxide and Derivatives"*, Royal Society of Chemistry Clean technology Monographs, 1999, ISBN: 0-85404-536-8.

[2] Walter, H., *"Development of Hydrogen Peroxide Rockets in Germany"* found in *"History Of German Guided Missiles Development"* Edited by Benecke, T.H., and Quick, A.W., 1956, The Advisory Group for Aeronautical Research and Development, NATO

[3] http://www.fighter-planes.com/info/me163.htm - last accessed 17/08/10

[4] Baker, D., *"The rocket: The history and development of rocket & missile technology"* Published by: Crown; First Edition, 1978, ISBN-13: 978-0517534045

[5] Becklake, J., *"The British Black Knight Rocket"* Journal of the British Interplanetary Society, Vol. 43, No.7, p.p.283-290, 1990

[6] Ventura, M., Mullens, P., *"The Use of Hydrogen Peroxide for Propulsion and Power"* 35th AIAA Joint Propulsion Conference, Los Angeles, June 1999, AIAA-1999-2880

[7] Andrews, D., *"Advantages of Hydrogen Peroxide as a Rocket Oxidant"* Journal of the British Interplanetary Society, Vol. 43, No.7, p.p.319-328, 1990

[8] Wernimont, E., Ventura, M., Garboden, G., Mullens, P., *"Past and Present Uses of Rocket Grade Hydrogen Peroxide"* 2nd International Hydrogen Peroxide Propulsion Conference, 1999

[9] Hill, N., Wright, D., *"Derivatives of the Black Knight Technology"*, 2000 found at http://www.spaceuk.org/hill.pdf

[10] Encyclopaedia Britannica entry for Prospero (satellite) found at: http://www.britannica.com/EBchecked/topic/479463/Prospero

[11] Hill, N.C., *"A Vertical Empire: The History of the UK Rocket and Space Programme, 1950-1971"*, Imperial College Press, 2001, ISBN-13: 978-1860942686

[12] Love, J.E., Stillwell, W.H., *"The Hydrogen-Peroxide Rocket Reaction-Control System for the X-1B Research Plane"* Dryden Flight Research Centre, Edwards, California. Reported in NASA Technical Note D-185

[13] Musker, A. J., Roberts, G. T., Rusek J.J., Kappenstein, C., *"Hydrogen Peroxide – From Bridesmaid to Bride"* 3rd International Conference on Green Propellants, Poitiers, 2006

[14] Schmidt, E.W., Wucherer, E.J., *"Hydrazine(s) vs. Nontoxic Propellants - Where Do We Stand Now?"* 2nd International Conference on Green Propellants for Space Propulsion, Sardinia, June 2004. ESA SP-557.

[15] Clark, J., *"Ignition - An Informal History of Liquid Rocket Propellants"*, Rutgers University Press, New Brunswick, 1972.

[16] Sutton, G.P. *"Rocket Propulsion Elements, An Introduction to the Engineering of Rockets"*, 2nd Ed., John Wiley & Sons, 1956.

[17] GRASP team. General assessment of green propellants, seventh framework program, 2008

[18] Caramelli, F. *"Green propulsion activities overview"* Space Propulsion 2008, Green Propulsion Workshop, Crete, 2008.

[19] Gordon, S and McBride, B.J. *"Computer program for calculation of complex chemical equilibrium compositions, rocket performance, incident and reflected shocks and Chapman-Jouget detonations"* NASA SP-273, 1971. *See Also:* http://www.grc.nasa.gov/WWW/CEAWeb/

[20] Mungus, G. *"NOFBX™ single stage to Orbit Mars Ascent Vehicle"* Aerospace Conference 2012, Montana, March 2012

[21] Synder, J., Goebel, D., Hofer, R., Polk, J., Wallace, N., and Simpson, H. *"Performance Evaluation of the T6 Ion Engine"* Journal of Propulsion and Power, Vol. 28, No. 2, pp. 371-379, 2012

[22] European Commission website: http://ec.europa.eu/environment/archives/dansub/pdfs/annex3_en.pdf - last accessed 28/05/13

[23] *Chronic Toxicity Summery – Hydrazine* Determination of Noncancer Chronic Reference Exposure Levels Batch 2A, 2000, Office of Environmental Health Hazard Assessment – Canada

[24] http://news.bbc.co.uk/1/hi/world/americas/7245578.stm - last accessed 18/08/10

[25] Wallbank, J.R., Sermon, P.A., Baker, A.M., Courtney, L. and Sambrook, R.M. *"Nitrous oxide as a green propellant for small satellites"* 2nd International Conference on Green Propellants for Space Propulsion, Sardinia, June 2004. ESA SP-557.

[26] Bombelli, V., Simon. D., Marée, T., Moerel, J.*"Economic Benefits of the Use of Non-toxic Mono-Propellants for Spacecraft Applications"* Proceedings of the 39th AIAA Joint propulsion conference, Huntsville, July 2003, AIAA-2003-4783

[27] Kappenstein, C. *"Contribution to the Green Propulsion Workshop"* Space Propulsion 2008 – Green Propulsion Workshop, Crete, May 2008

[28] Lawrence, T.J. *"Possible applications of green and non-toxic propellants"* 1st International Conference on Green Propellants for Space Propulsion, ESTEC, Noordwijk, June 2001. ESA SP-484.

[29] http://www.lanl.gov/orgs/tt/arpa-e/pdf/TRL_definitions.pdf - last accessed 15/09/2013

[30] Wertz J.R., Larson W.J. *"Space mission analysis and design"*, Microcosm Press & Kluwer Academic Publishers, 3rd Edition, 1999, ISBN: 1-881883-10-8.

[31] Honse, J.P., Bangasser, C.T., Wilson, M.J. *"Delta-Qualification Test of Aerojet 6 and 9 lbf MR-106 Monopropellant Hydrazine Thrusters for Use on the Atlas Centaur Upper Stage During the Lunar Reconnaissance Orbiter (LRO) and Lunar Crater Observation and Sensing Satellite (LCROSS) Missions"* 45th AIAA Joint Propulsion Conference, Denver, August 2009, AIAA-2009-5481

[32] Wilson, M.J. *"Demonstration Testing of a Long-life 5-Lbf (22-N) MR-106L Monopropellant Hydrazine Rocket Engine Assembly"* 41st AIAA Joint Propulsion Conference, Tucson, July 2005, AIAA 2005-3954

[33] Airbus Defence and Space 1N Mono-propellant thruster promotional brochure, http://cs.astrium.eads.net/sp/brochures/thrusters/1N%20Thruster.pdf last accessed 02/08/14

[34] Young, R.A., Akhtar, M. *"Environmentally Friendly Technologies for the Pulp and Paper Industry"* Wiley, 1998, ISBN-13 9780471157700

[35] http://www.essentialchemicalindustry.org/chemicals/hydrogen-peroxide.html – Last accessed 01/09/2014

[36] Musker, A., Roberts, G., Chandler, P., Grayson, J., Holdsworth, J. *"Optimisation study of a homogeneously-catalysed HTP rocket engine"* 2nd International Conference on Green Propellants for Space Propulsion, Sardinia, June 2004. ESA SP-557.

[37] Musker, A., Roberts, G., *"An Exploratory Study of Some Liquid Catalysts for Use with Hydrogen Peroxide"*, 3rd Int. Conf. On Green Propellant for Space Propulsion / 9th Int. Hydrogen Peroxide Propulsion Conference, Poitiers, September 2006, ESA SP-635

[38] Musker, A. *"Highly stabilised hydrogen peroxide as a rocket propellant"* 39th AIAA Joint Propulsion Conference, Alabama, July 2003, AIAA 2003-4619

[39] http://www.sigmaaldrich.com/catalog/product/sial/31642?lang=en&region=GB – Last accessed 01/09/2014

[40] Ventura, M.C., Wernimont, E., Heister, S., Yuan. S, *"Rocket grade hydrogen peroxide (RGHP) for use in propulsion and power devices-historical discussion of hazards"* 43th AIAA Joint Propulsion Conference, Cincinnati July 2006, AIAA 2007-5468

[41] Ventura, M.C. *"Long term storability of hydrogen peroxide"* 41st AIAA Joint Propulsion Conference, Arizona, July 2005, AIAA 2005-4551

[42] http://webbook.nist.gov/cgi/cbook.cgi?ID=C7722841&Mask=1 – last accessed 15/08/14

[43] Connors, K.A. *"Chemical Kinetics: The Study of Reaction Rates in Solution"* John Wiley & Sons, 1990, ISBN-13 9781560810063

[44] Giguere, P.A., Liu, I.D. *"Kinetics of the Thermal Decomposition of Hydrogen Peroxide Vapor"* Canadian Journal of Chemistry, Vol. 35, No. 4, pp.283-293, 1957

[45] Hoare, D.E., Protheroe, J.B., Walsh, A.D. *"The Thermal Decomposition of Hydrogen Peroxide Vapour"* Transaction of Faraday Society, Vol. 55, pp.548-557, 1959.

[46] Pearson, N., Pourpoint,T., Anderson, W.E., *"Vaporization and decomposition of hydrogen peroxide drops"* 39th AIAA Joint Propulsion Conference, Alabama, July 2003, AIAA 2003-4642

[47] Levenspiel, O., *"Chemical Reaction Engineering"* 3rd Edition, Wiley, 1999, ISBN: 0-471-25424-X

[48] Bonifacio, S., Russo Sorge, A., *"Modelling hydrogen peroxide decomposition in monolithic beds"* 3rd Int. Conf. on Green Propellant for Space Propulsion, 9th Int. Hydrogen Peroxide Propulsion Conference, Poitiers, 2006, ESA SP-635

[49] Koopmans, R-J. *"Modelling of Multiphase Multicomponent Chemically Reacting Flows through Packed Beds"* PhD thesis, University of Southampton, May 2014

[50] Oehmichen, T., Datsevich, L., Jess, A. "Influence of bubble evolution on the effective kinetics of heterogeneously catalyzed gas/liquid reactions. part i: Reactions with gaseous products" Chemical Engineering & Technology, Vol. 33, No.6, pp.911–920, 2010

[51] Musker, A., Roberts, G., Ford, S., Reakes, E., Westbury, T. *"Auto-ignition of fuels using highly stabilised hydrogen peroxide"* 41st AIAA Joint Propulsion Conference, Arizona, July 2005, AIAA 2005-4454

[52] Beaumont, A., Beel, M., Beveridge, N., Horabin, E., *"Catalysis of Hydrogen Peroxide using Metal Compounds"* University of Southampton GDP report, 2007

[53] Kappenstein, C., Brahmi, R., Amariei, D., *et al "Catalytic decomposition of energetic compounds – Influence of catalyst shape and ceramic substrate"* 42nd AIAA Joint Propulsion Conference, Sacramento, July 2006, AIAA 2006-4546

[54] Scharlemann, C., Schiebl, M., Amsüss, R., *et al "Monopropellant thruster development: investigation of decomposition efficiencies"* 3rd Int. Conf. On Green Propellant for Space Propulsion / 9th Int. Hydrogen Peroxide Propulsion Conference, Poitiers, September 2006, ESA SP-635

[55] Bonifacio, S., Festa, G., Russo Sorge, A., *"Novel Structured Catalysts for Hydrogen Peroxide Decomposition in Monopropellant and Hybrid Rockets"* Journal of Propulsion and Power, Vol. 29, No. 5, 2013, pp. 1130-1137

[56] Wernimont, E.J., Durant, D. *"State of the Art High Performance Hydrogen Peroxide Catalyst Beds"* 43th AIAA Joint Propulsion Conference, Fort Lauderdale, July 2004, AIAA 2004-4147

[57] Rusek, J.J., *"New Decomposition Catalysts and Characterization Techniques for Rocket-Grade Hydrogen Peroxide"*, Journal of Propulsion and Power, Vol. 12, No. 3, pp. 574-579, 1996

[58] Romeo, L., Torre, L., Cervone, A., *et al "Performance of Different Catalysts Supported on Alumina Spheres for Hydrogen Peroxide Decomposition"* 43rd AIAA Joint Propulsion Conference, Cincinnati, July 2007, AIAA 2007-5466

[59] Eloirdi, R., Kappenstein, C., Gibbon, D., et al, *"An Investigation of Various Catalysts in a Small Hydrogen Peroxide Thruster"*, 1st Int. Conf. on Green Propellant for Space Propulsion, Noordwijk, June 2001, SP-484

[60] Tian, H., Zhang, T., Sun, X., Liang, D., Lin. L., *"Performance and deactivation of Ir/γ-Al2O3 catalyst in the hydrogen peroxide monopropellant thruster"*, Applied Catalysis A: General 210, 2001, pp.55–62

[61] http://www.averinox.nl/mesh_tables - last accessed 20/08/10

[62] Kuan, C-K., Chen, G-B., Chao, Y-C. "The Effects of Preheating and pH Value on the Performance of Hydrogen Peroxide Monopropellant Microthrusters" 42nd AIAA Joint Propulsion Conference, Sacramento, July 2006, AIAA 2006-5240

[63] Lee, S.-L., Lee, C.-W., *"Performance characteristics of silver catalyst bed for hydrogen peroxide"* Aerospace Science and Technology, volume 13, pp. 12–17, 2009

[64] Wanhainen, J.P., Ross, P.S., De Witt, R.L., *"Effect Of Propellant And Catalyst Bed Temperatures On Thrust Buildup In Several Hydrogen Peroxide Reaction Control Rockets"* Lewis Research Centre, NASA Technical Note D-480, 1960

[65] Runckel, J.F., Willis, C.M., Salters Jr, L.B., *"Investigation of catalyst beds for 98-percent-concentration Hydrogen Peroxide"* Langley research Centre, NASA Technical Note D-1808, 1963

[66] Palmer, M.J., Westcott, R.M.T., Harmer, P., Caley, S., *"Development of a Catalyst Bed for a Monopropellant Thruster"*, University of Southampton GDP report, 2008

[67] Iarochenko, N., Dedie, V., *"Hydrogen Peroxide as Monopropellant Catalysts and Catalyst Beds: Experience from More than 30 Years of Exploitation"* 1st International Conference on Green Propellants for Space Propulsion, Noordwijk, June 2001, SP-484

[68] Yang, W., Yang, S., Suna, W., Suna, G., Xin, Q., *"Nanostructured silver catalyzed nickel foam cathode for an aluminium–hydrogen peroxide fuel cell"* Journal of Power Sources 160, 2006, pp. 1420–1424

[69] Russo Sorge, A., Pilone, G., Bagnasco, G., Turco, M. *"Decomposition of Hydrogen Peroxide on MnO2/TiO2 Catalysts"*, Journal of Propulsion and Power, Volume 20, Issue 6, pp.1069-1075, 2004

[70] Pirault-Roy, L., Kappenstein, C., Guérin, M., Eloirdi R., Pillet, N. *"Hydrogen Peroxide Decomposition on Various Supported Catalysts Effect of Stabilizers"* Journal of Propulsion and Power, Volume 18, Issue 6, pp.1235-1241, 2002

[71] Lim, H., An, S., Kwon, S. *"Hydrogen Peroxide Gas Generator with Dual Catlaytic Beds for Nonpreheating Startup"* Journal of Propulsion and Power, Volume 23, Issue 5, pp. 1147-1150, 2007

[72] Cervone, A., Romeo, L., Torre, L., Musker, A., Roberts, G. *et al "Development of Green Hydrogen Peroxide Monopropellant Rocket Engines and Testing of Advanced Catalytic Beds"* 3rd Int. Conf. on Green Propellant for Space Propulsion, 9th Int. Hydrogen Peroxide Propulsion Conference, Poitiers, 2006, ESA SP-635

[73] Bramanti, C., Cervone, A., Romeo, L., Musker, A. *et al "Experimental Characterization of Advanced Materials for the Catalytic Decomposition of Hydrogen Peroxide"* 42nd AIAA Joint Propulsion Conference, Sacramento, July 2006, AIAA 2006-5238

[74] Pasini, A., Torre, L., Cervone, A., Musker, A., Saccoccia, G., *et al "Experimental Characterization of a 5 N Hydrogen Peroxide Monopropellant Thruster Prototype"* 43rd AIAA Joint Propulsion Conference, Cincinnati, July 2007, AIAA 2007-5465

[75] Blank, R.A., Pourpoint, T.L., Meyer, S.E., *"Experimental Study of Flow Processes and Performance of a High Pressure Hydrogen Peroxide Catalyst Bed"* 43rd AIAA Joint Propulsion Conference, Cincinnati, July 2007, AIAA 2007-5469

[76] Palmer, M., Musker, A., Roberts, G. *"Experimental Assessment of Heterogeneous Catalysts for the Decomposition of Hydrogen Peroxide"* 47th AIAA Joint Propulsion Conference, San Diego, July 2011, AIAA 2011-5695

[77] Jonker, W., Mayer, A., Zandbergen, B., *"Development of a Rocket Engine Igniter Using the Catalytic Decomposition of Hydrogen Peroxide"* 3rd Int. Conf. on Green Propellant for Space Propulsion, 9th Int. Hydrogen Peroxide Propulsion Conference, Poitiers, 2006, ESA SP-635

[78] Dines, T.J., Rochester, C.H., Thomson, J., *"Catalysis and surface characterisation"* Royal society of Chemistry, Special Publication Vol. 144, ISBN: 0851863353

[79] Peraldi, R., Monceau, D., Pieraggi, B. *"Correlations between Growth Kinetics and Microstructures for Scales Formed by High-Temperature Oxidation of Pure Nickel. I. Morphologies and Microstructures"*, Oxidation of Metals, Volume 58, Issue 3-4, pp.249-273, 2002

[80] Peraldi, R., Monceau, D., Pieraggi, B. *"Correlations between Growth Kinetics and Microstructures for Scales Formed by High-Temperature Oxidation of Pure Nickel. II. Growth Kinetics"*, Oxidation of Metals, Volume 58, Issue 3-4, pp.275-295, 2002

[81] Tsybukh, R. *"A comparative study of platinum nanodeposits on HOPG (0001), MnO (100) and MnOx/MnO (100) surfaces by STM and AFM after heat treatment in UHV, O2, CO and H2"* Leiden Institute of Chemistry, CASC, Faculty of Science, Leiden University, 2010.

[82] Xu, D., Yang, H., Zhou, X., Li, T., Cong, J., Zhang, T., *"An investigation in the catalytic decomposition of hydrogen peroxide for gas generation"* 5th International Hydrogen Peroxide Propulsion Conference, Purdue University, Sept 15-19, 2002

[83] Ponzo, J. *"Small Envelope, High Flux 90% Hydrogen Peroxide Catalyst Bed"* 39th AIAA Joint Propulsion Conference, Alabama, July 2003, AIAA 2003-4622

[84] Goto, D., Shinozaki, N., Yabuhara, E. "Experimental investigation of 1N monopropellant thruster catalyst damage mitigation" Space Propulsion 2010, San Sebastian, May 2010

[85] Musker, A.J. *"Development of a 200 Newton Bipropellant Thruster Using Heterogeneous Catalytic Reduction of Hydrogen Peroxide"* 4th European Conference For Aerospace Sciences, St. Petersburg, 2011

[86] Jo, S., Jang, D., Kim, J., Yoon, H., Kwon, S., *"Chugging Instability of H2O2 Monopropellant Thrusters with Catalyst Reactivity and Support Sizes"* 47th AIAA Joint Propulsion Conference, San Diego, July 2011, AIAA 2011-5694

[87] Douglass, H.W., Schmidt, H.W., Levinson, L., *"Liquid Propellant Gas Generators"*, Glenn Research Centre, NASA Special Publication SP-8081, 1972

[88] Scharlemann, C., Schiebl, M., Kappenstein, C., Batonneau, Y, *et al "Development and test of a miniature hydrogen peroxide monopropellant thruster"*, AIAA 42nd Joint Propulsion Conference, 2006, AIAA 2006-4550

[89] Miller, K.J., Sisco, J.C., Austin, B.L., Martin III, T.N., Anderson, W.E., *"Design and ground testing of a hydrogen peroxide/kerosene combustor for RBCC application"*, AIAA 39th Joint Propulsion Conference, 2003, AIAA 2003-4477

[90] Sisco, J.C., Austin, B.L., Mok, J.S., Anderson, W.E., *"Autoignition of kerosene by decomposed hydrogen peroxide in a dump-combustor configuration"*, Journal of Propulsion and Power, Vol. 21, No. 3, 2005, pp. 450-459

[91] Ponzo, J.B., *"Monolithic Hydrogen Peroxide Catalyst Bed Development"* Advanced Development Engineering, Aerojet, 2003

[92] Whitehead, J.C., *"Hydrogen peroxide propulsion for smaller satellites"*, 12th AIAA Annual Conference on Small Satellites, 1998, SSC98-VIII-1

[93] Wu, P.K., Fuller, R.P., Morlan, P.W., Ruttle, D.W., Nejad, A.S., Anderson, W.E., *"Development of a Pressure-Fed Rocket Engine Using Hydrogen Peroxide and JP-8"*, AIAA 35th Joint Propulsion Conference, 1999, AIAA 99-2877

[94] Unknown author, *"Development of Design and Scaling Criteria for Monopropellant Hydrazine Reactors Employing Shell 405 Spontaneous Catalyst"* Rocket Research Corporation, Seattle, Washington, 1967, NASA-CR-82457, RRC-66-R-76- VOL. I

[95] An, S., Brahmi, R., Kappenstein, C., Kwon, S., *"Transient Behavior of H2O2 Thruster: Effect of Injector Type and Ullage Volume"*, Journal of Propulsion and Power, Vol. 25, No. 6, 2009, pp. 1357-1360

[96] Huzel, D.K., Huang, D.H., *"Modern Engineering for Design of Liquid-Propellant Rocket Engines"*, AIAA, Vol. 147 Progress in Astronautics and Aeronautics, ISBN 1-56347-013-6

[97] Graham, R.L., Lubachevsky, B.D., Nurmela, K.J., Ostergglrd, P.R.J., *"Dense packings of congruent circles in a circle"*, Discrete Mathematics, Volume 181, 1998, pp. 139-154

[98] Sutton, G.P., Biblarz, O., *"Rocket Propulsion Elements"*, Wiley, 8th Edition, 2010, ISBN-13: 9780470080245

[99] Image found at: http://www.parabolicarc.com/2010/03/17/esa-developing-green-thruster-fuel/, last accessed 02/08/14

[100] Hazlett, R.N. "*Effect of Additives on the catalytic decomposition of hydrogen peroxide*", Chemistry Division, Naval Research Laboratory, Washington D.C., AD665294, 1955

[101] McRight, P., Popp, C., Pierce, C., Turpi, A., Urbanchock, W., Wilson, M. "*Confidence testing of Shell 405 and S-405 Catalysts in a Monopropellant Hydrazine Thruster*" 41st AIAA Joint Propulsion Conference, Tucson, July 2005, AIAA 2005-3952

[102] Wynn, J., "Development of a 10N TRL5 Monopropellant Thruster Using Hydrogen Peroxide" Space Propulsion 2014, Cologne, May 2014

[103] Palmer, M., "Design, Build and Test of a 1N Hydrogen Peroxide Monopropellant Thruster" Space Propulsion 2014, Cologne, May 2014

[104] An, S., Jin, J., Lee, J., Jo, S., Park, D., and Kwon, S., "Chugging Instability of H2O2 Monopropellant Thrusters with Reactor Aspect Ratio and Pressure," Journal of Propulsion and Power, Vol. 27, No. 2, 2011, pp. 422–427.